CONF-770686

SOLAR CROP DRYING CONFERENCE

Proceedings

By
J. L. Butler

June 30, 1977

Work Performed Under Contract No. EX-76-A-29-1021

Weaver Laboratories
North Carolina State University at Raleigh
Raleigh, North Carolina

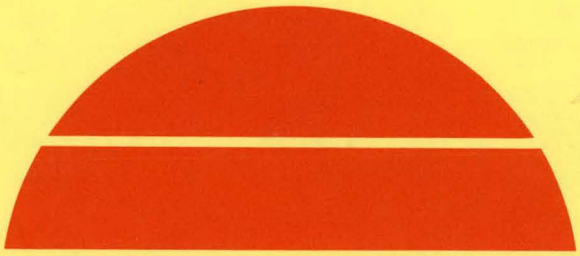

U.S. Department of Energy

Solar Energy

DISCLAIMER

NOTICE

CONF-770686
Distribution Category UC-59b

SOLAR CROP DRYING CONFERENCE

PROCEEDINGS

J. L. Butler

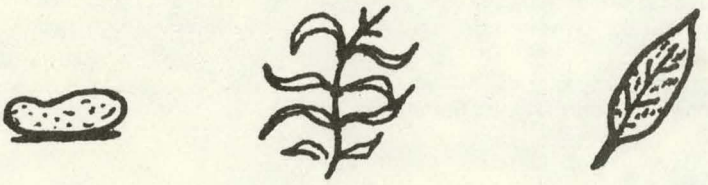

Peanuts — Forage — Tobacco

USDA, ARS
Coastal Plain Experiment Station
Tifton, Georgia 31794

June 30, 1977

Weaver Laboratories

North Carolina State University at Raleigh

Sponsored By:

Agricultural Research Service, USDA
American Society of Agricultural Engineers
Energy Research and Development Administration
Department of Biological and Agricultural Engineering, North Carolina State University at Raleigh

TABLE OF CONTENTS

AGRICULTURAL PROGRAMS FOR SOLAR ENERGY

by

Landy B. Altman
Energy Research Coordinator
USDA, ARS
Beltsville, Maryland

The U. S. agricultural system was developed with abundant supplies of low-cost energy which accounted for only a small fraction of the cost of supplying food, fiber, and wood products. Demands for energy are rapidly outstripping supply, and we can expect energy costs and availability to be significant factors in the future. About 20 percent of the total energy used in the United States is related to the production, processing, marketing, distribution, and utilization of food, natural fiber, and forest products. As population increases both in the U.S. and abroad, the demand for these products will increase and hence increase the demand for energy.

The Congress established the Energy Research and Development Administration (ERDA) as the lead Federal agency responsible for energy research, development and demonstration. Arrangements were made with ERDA for the Department of Agriculture to manage research on agricultural applications of solar energy. The Agricultural Research Service (ARS) was selected to be the agency primarily responsible for the program but with cooperation from the Cooperative State Research Service and, through them, with State Agricultural Experiment Stations. The conference today is to report the results from one of the five areas of research supported by this program. Table 1 lists the five areas and the number of projects funded in each area in 1977.

Table 1. Research on Agricultural Applications of Solar Energy

Research Area	Number of Projects
Solar Grain Drying	15
Application of Solar Energy for the Drying of Crops Other than Grain	8
Use of Solar Energy in Livestock Production	11
Solar Heating and Cooling of Greenhouses and Rural Residences	10
Solar Energy in Food Processing	6
Total	50

Of the above projects, 36 are at State Agricultural Experiment Stations, 11 in ARS laboratories, 2 in university laboratories, and 1 in an industry laboratory.

Other solar energy research with agricultural implications is underway but is not part of this program. ERDA has passed through to ARS funds to support research on rural and remote applications of wind energy. Agricultural and forest products and residues are solar in origin and research on their use for the production of energy is underway. Three experimental irrigation systems, one

uses photovoltaic cells and an electric motor and two use concentrating collectors and heat engines, will be in operation this summer.

A film called "Sunpower for Farms" was made by the USDA Film Production Unit in cooperation with ERDA. It gives a quick overview of the research on agricultural applications of solar energy and should set the stage for the Solar Crop Drying Conference.

SOLAR ENERGY RESEARCH FOR PEANUTS, FORAGE AND TOBACCO

by

James L. Butler
Principal Investigator, Crop Drying
USDA, ARS
Coastal Plain Experiment Station
Tifton, Georgia

The drying of peanuts, forage and tobacco requires substantial amounts of fossil fuel energy. Tobacco is second only to grain in the total energy required for drying and curing. Even though tobacco is a non-food crop, it is a high value crop and an important export crop. Peanuts are a valuable source of protein and oil. They require that the moisture be removed at the rate of about one-half percentage point per hour, from the time of digging, until a moisture content of 10 percent or less is reached. After a short exposure time in the windrow, the peanuts are harvested and the drying and curing is completed mechanically, using large quantities of LP gas. The increasing demand for a high quality forage, coupled with large round bales and small stacks of hay, has re-kindled interest in controlled drying of hay. The forage dehydration industry is also faced with the non-availability of fuel for producing the dehydrated product widely used as a feed additive.

It is estimated that the three crops mentioned above require the equivalent of more than 400 million gallons of LP gas annually. Fortunately, from the viewpoint of solar energy application, they require drying energy either in the summer or very early fall. Collectors used to supply heat energy to the crops for drying would thus be available to supply heat for heating for human or animal comfort, or for greenhouse production during the winter months.

The ERDA-ARS sponsored research on the application of solar energy to the drying of peanuts, forage and tobacco was initiated July 1, 1975.

Currently research is being conducted at eight locations. One of these is new this year, replacing the research on dessicants which is now funded directly by ERDA. Three projects are conducting research on tobacco, two on peanuts, two on forage and one on the development of solar energy collectors and storage units for agricultural applications. State Agricultural Experiment Stations are conducting five projects, USDA laboratories two projects and a state engineering experiment station is conducting one.

DESICCANT AS DRYING AGENT/HEAT STORAGE MEDIA FOR CROP DRYING BY SOLAR ENERGY*

by

S.M. Ko and P. O. McCormick
Lockheed Missiles & Space Company, Inc.
Huntsville, Alabama 35807

ABSTRACT

This paper reviews candidate desiccants that may be used in crop drying facilities, discusses concepts for drying crops with the desiccants and presents process flow diagrams for promising concepts. Both solid and liquid desiccants were considered for use in crop drying systems. Desiccants were reviewed relative to their thermal properties, affinity for water vapor, regeneration temperatures, toxicity, corrosion properties, stability, and costs. Solar energy was considered as the prime energy source for regenerating the desiccants. The investigation revealed that liquid desiccants are particularly applicable to solar systems since they can be pumped through the collector and can be regenerated at lower temperatures than the solid desiccants. In addition, the use of liquid desiccants allows the adaption of an efficient energy recovery and use methods that are capable of achieving energy savings of up to 50% over a conventional heated-air drying system.

INTRODUCTION

The United States produces large volumes of crops for food and livestock feed every year. The estimated total production of major agricultural crops in 1974 is over 10 billion bushels (Ref. 1). Drying these crops requires an annual energy expenditure of over 10^{14} Btu (Ref. 2).

The energy requirements for crop drying is substantial and, in view of dwindling fossil fuel energy sources, concepts for conserving energy expenditures for crop drying are desirable. A review of the manner in which conventional crop drying equipment operates reveals a way in which energy savings may be achieved. Conventional crop drying equipment dries crops in an open loop cycle wherein air is heated to decrease the relative humidity of the air and then drives the heated, low humidity air through the crop where moisture is absorbed from the crop. The air is then expended to the atmosphere and carries with it the energy used to vaporize moisture in the crop and that used to increase air temperature. Problems associated with this conventional approach are: (1) it is very difficult to control both temperature and relative humidity of the drying air, and (2) a significant amount of energy is lost from the system in the hot air that carries the moisture from the system.

One approach to solving these problems is to use desiccants for removing the moisture from the drying air in a closed system. The crop drying scheme presented in this paper uses desiccants in conjunction with a closed loop drying cycle to reclaim the energy expended in vaporizing moisture in harvested crops. In the closed loop cycle, the drying air is brought into contact with a desiccant after it exits the crop drying bin. Water vapor in the moist air is absorbed by the desiccant, thus reducing the relative humidity of the air. The air is then heated and returned to the crop bin. The used desiccant is heated (either fossil or solar energy heat sources may be used) and regenerated at high

* Sponsored by USDA/ERDA under Contract USDA-12-14-7001-817.

temperature, driving water vapor from the desiccant. This water vapor is condensed and used to preheat the dilute (wet) desiccant before heat is added from the external source (fossil or solar). The latent heat of vaporization of the moisture removed from the desiccant is "reclaimed" in this manner. Also, closed cycle operation implies that no net energy is expended in heating drying air. Another advantage of the desiccant crop drying is that the relative humidity of drying air can be controlled independently as required for specific applications.

In practice, all of the energy used in regeneration cannot be reclaimed by the desiccant without an eventual increase in temperature of the regenerated desiccant and a corresponding increase in sensible energy stored. This sensible energy can be put to use in crop drying quite easily since it is available at a temperature well above the drying temperature.

DRYING REQUIREMENTS

Moisture is removed from crops in order to achieve safe storage. Excessive moisture content in crops causes the growth of molds and attracts insects. Approximately 5 to 8 % loss occurs from the spoilage (Ref. 3). The moisture content of crops during harvest is typically 20 to 35% and the moisture content for safe storage is in the range of 10 to 13% (Ref. 4) for several selected crops. This means that typically 50% of the moisture contained in the crop when harvested must be removed to meet the safe storage requirement.

Various parameters influence the drying process. These include air relative humidity, air temperature, air flow rate, initial moisture content, and final moisture content. Among these parameters, the most important is the relative humidity of air used in the drying process. The relative humidity of the inlet air to the drying bin must be lower than the equilibrium relative humidity of the crop at its final moisture content (required safe storage moisture content) to be achieved by the process. In other words, the equilibrium moisture content (EMC) of the crop at the inlet air condition must be lower than the desired final moisture content of the crop. EMC is defined as the moisture content of a crop after it has been exposed to a particular environment for an infinitely long period of time (Ref. 5). For most crops, the EMC is lower than the safe storage moisture content for 35 to 45% relative humidity air. Therefore, a drying system must be capable of delivering 35 to 45% relative humidity to dry a crop to a safe storage moisture content.

The drying temperature is also an important parameter. In a conventional system, ambient air is heated to suppress the relative humidity to the required level. However, the drying air temperature must be kept below a certain maximum depending on the type of crop and the intended uses of the crop to prevent the crop from quality deterioration due to breakage, stress cracking, and possible discoloration (Ref. 4). At higher temperature (lower relative humidity), the drying time required is shorter, and this is the reason for using high temperature when the intended use of the crop is for animal feed. The drying temperature range for conventional crop drying is 90 to 180 F (Ref. 3), and this corresponds to relative humidity of 60 to 10%. High drying temperature is neither required nor desirable when the relative humidity and the temperature of drying air can be independently controlled. The effect of the drying temperature on the drying rate is relatively small. The reason for this is drying temperature has only a small effect on EMC.

Heating air in conventional crop drying systems assures that the relative humidity of the air will be low enough to remove the moisture from the crop. However, the energy required to remove the moisture from the crop is usually about half the total energy required for drying. Based on theoretical estimates, the heat of desorption of moisture from a crop ranges from 1030 to 1400 Btu/lb of moisture dried depending on the type and the moisture content of the crop. This is 30 to 400 Btu/lb of moisture higher than the heat vaporization pure water. In actual field use, conventional crop drying equipment requires 2200 Btu to remove 1 lb of water from a crop (Refs. 6 and 7).

The closed cycle dehumidification system using desiccants presented in this paper is operated at lower drying temperature than that of conventional open

cycle driers because heating is not necessary to control the relative humidity. Drying crops at low temperature has a number of inherent advantages. It is desirable to avoid damage to the crop as a result of thermal stresses both during the drying process as well as during cooling of the crop at the conclusion of drying. Also, the thermal losses are reduced when the temperatures throughout the drying equipment are maintained at low temperature. Furthermore, low temperature drying is mandatory for more delicate crops such as peanuts, rice, tobacco and various seed crops to preserve quality of the dried product. These crops are considered relatively difficult and expensive to dry in a conventional dryer, and thus are particularly suited for the regenerated desiccant crop drying system discussed in this paper.

DESICCANTS

Desiccants are hygroscopic chemical substances that have large affinity for water. Although desiccants remove water by a variety of mechanisms, the action of many desiccants may be understood in terms of water vapor partial pressure. Due to the difference in the partial pressure of water vapor in the desiccant and the material to be dried, water will diffuse from the material being dried to the desiccant until a dynamic equilibrium is reached. This occurs when the two substances attain the same partial pressure of water. At this point no net transfer of water takes place. The performance of the desiccant may be evaluated in terms of efficiency and capacity that are defined as follows. Drying efficiency is the fraction of total water input that the desiccant removes. Drying capacity is the quantity of water that a unit mass of desiccant can take up before losing drying efficiency (Ref. 8).

A typical isothermal regenerative desiccant drying cycle is illustrated in Fig. 1. The figure shows the basic relationships of the water vapor partial pressures in the desiccant at various points in the drying cycle.

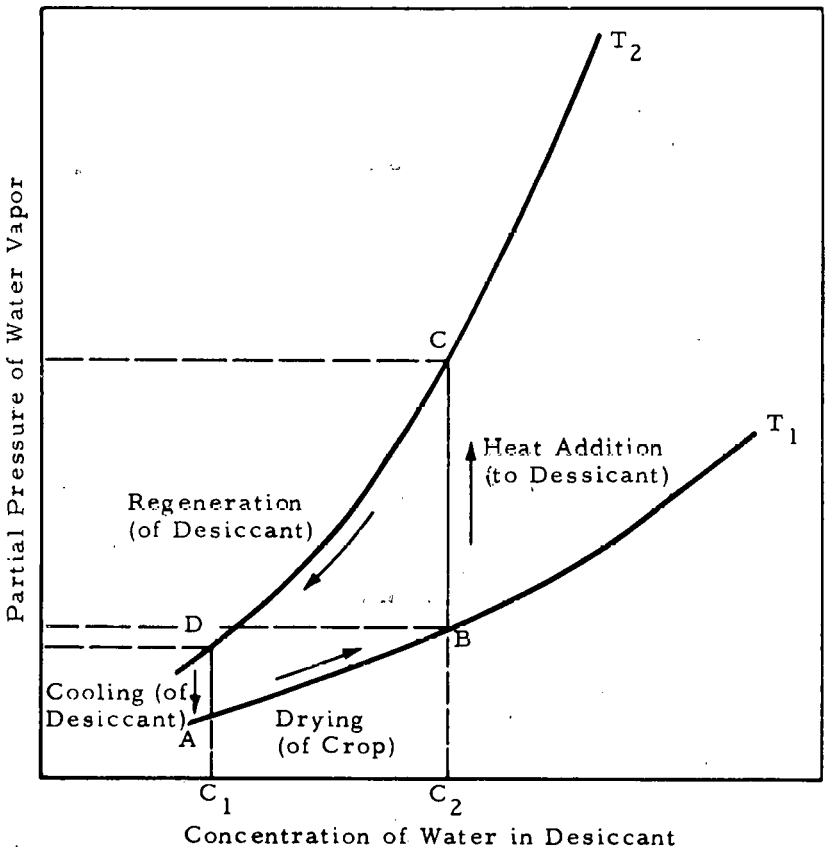

Fig. 1 - Partial Pressure of Water Vapor vs Concentration of Water Vapor in the Desiccant (Isothermal Operation)

Four unit processes are shown on the vapor pressure versus desiccant concentration diagram. Process A-B represents the drying process in which concentration of water in the desiccant and the vapor pressure of water increase as the drying capacity of the desiccant is used. Heat is added in process B-C to increase the vapor pressure in the desiccant. Process C-D represents the regeneration process in which water is driven out of the desiccant. The desiccant is cooled in process D-A to suppress the equilibrium vapor pressure of the desiccant in order to restore drying capacity.

Drying rate cannot be determined from the figure, which presents equilibrium data only. Drying rate is too complex for exact and concise quantitative treatment. However, existing commercial practice in the design of absorption towers, solid desiccant beds, and crop drying equipment may be relied upon to furnish estimates of drying rates.

Classification

Desiccants may be classified in two groups: soluble liquid or solid desiccants, and insoluble solid desiccants. Desiccants may also be classified into five classes by chemical reactions involved in the drying process (Ref. 9) as shown in Table 1:

TABLE 1. CLASSIFICATION OF DESICCANTS

Class	Reactions Involved
A	D^{*} (pure or concentrated solution) + H_2O = dilute solution
B	D (solid) + H_2O = physical adsorption
C	D (solid) + H_2O = saturated solution
D	$D\ (H_2O)_y$ (solid) + xH_2O = $D\ (H_2O)_{x+y}$ (solid)
E	M^{**} + $(H_2O)_x$ = $M(OH)_x$ + $x/2H_2$

*Desiccant **Metal

Among the five classes of desiccants, class A liquid (solution) desiccants and class B and D solid (adsorptive) desiccants are of interest in solar crop drying application.

Liquid Desiccant Characteristics

Liquid desiccants include deliquescent salt solutions such as calcium chloride in water as well as organic compounds like glycol and sulfuric acid. These are all liquid at all ordinary ranges of temperatures and dilution. When in solution, deliquescent componds will obviously have lower drying efficiency and capacity than the same anhydrous salt, but the much greater ease of handling the liquid solution makes the solutions preferable where very low humidities are not required as is the case in crop drying. The anhydrous liquids (glycol for example) can produce nearly complete dehydration, but large quantities of the drying agent must be used due to low drying capacity, and complete regeneration is usually difficult. One of the greatest advantages of the liquids is that a desired relative humidity of the drying air can be maintained with very close control regardless of inlet moisture conditions. This is accomplished by simply maintaining the dehydration solution at the proper concentration and temperature or by varying the flow rate of the desiccant.

Properties of candidate liquid desiccants are summarized in Table 2. The suitability of these chemicals are compared in terms of the following properties (Refs. 8 through 15):

1. Specific heat is an important measure of thermal storage capacity. It ranges from 0.4 to 0.9 and varies with the concentration, temperature and type of desiccant.

TABLE 2. SUMMARY OF LIQUID DESICCANT PROPERTIES

Liquid Desiccant	C_p (Btu/lb-F)	R.H. at 90F for Sat. Solu. (%)	Useful Concen. Range (%)	Range of Regen. Temp. (F)	Chemical Stability	Heat of Dilution (Btu/lb)	Corrosion	Toxicity	$/lb
Lithium Chloride	0.68 (70 F, 40%)	11	23-45	200-250	Stable	~200	Rela. Non-Corrosive	Rela. Non-Toxic	1.26
Calcium Chloride	0.60	21	32-40	200-250	Sat. Solu. Solidifies Below 86 F	~200	Rela. Non-Corrosive	None	0.04
Sulfuric Acid	0.4-0.6	0	35-100	250-300	Relatively Stable	~200	Bad	Toxic	0.03
Glycerine (Glycerol)	0.6-0.9	0	50-100	200-250	Heat Sens. Oxidize	Low	None	None	0.50
Tri-ethylene Glycol	0.6-0.9	0	96-100	250-300	Heat Sensitive	Low	Noncorr. with Inhibitor	Rela. Non-Toxic	0.30

2. Relative humidity of the air that can be obtained using a saturated solution at 90 F is a relative measure of comparing the drying efficiency. Lithium chloride is the best among the salt solutions, although it is not as powerful as sulfuric acid or organic desiccants which are capable of complete dehydration. This is not a critical factor in drying crops since complete dehydration of the drying air is not necessary.

3. Useful concentration range for crop drying application. Lower limits in the table represent equilibrium concentration for 60% relative humidity air which is the maximum relative humidity at which most crops can be dried. Wider useful concentration range is desirable since it assures higher drying capacity and flexible operation of the drying system.

4. Range of Regeneration Temperature. Sulfuric acid and glycol require rather higher regeneration temperature than salt solutions and glycerine. This property heavily impacts the suitability for regeneration and the thermal efficiency of the system.

5. Chemical Stability. Calcium chloride solution at saturation solidifies below 86 F to form the solid hexahydrate. Lithium chloride, on the other hand, has no danger of solidifying if kept above -90 F, which makes lithium chloride markedly superior to calcium chloride with regard to maintenance of stripping and absorption packed columns. Glycerine is sensitive to thermal decomposition and must be regenerated in vacuum. Glycol is less sensitive to thermal decomposition than glycerine.

6. The heat of dilution of the solution is approximately the same for all salt solutions and sulfuric acid. Glycerine and glycol have relatively low heat of dilution (less than 20 Btu/lb). High heat of dilution is desirable in terms of thermal efficiency of the system. However, it has slightly negative effect on the efficiency of dehumidification operation.

7. Corrosion. Sulfuric acid is very corrosive. Salt solution often causes electrolytic corrosion. However, when properly used with corrosion inhibitors they are relatively noncorrosive. The most often used inhibitors are sodium chromate or dichromate.

8. Toxicity. Lithium chloride may become toxic at continuous daily dose of over 100 mg/day. However, since the vapor pressure of lithium chloride over the solution is zero, the drying air will not be contaminated if a demister is properly installed in the dehumidification (absorption) column. Sulfuric acid and triethylene glycol have vapor pressures of over 1 mm

Hg at operating temperature range for crop drying. These desiccants are toxic and must be avoided.

9. Cost. Lithium chloride is relatively expensive. Calcium chloride and sulfuric acid are inexpensive while organic dessicants are in the moderate price range. Note that the cost for lithium chloride is based on solid lithium chloride and the cost for 40% solution is comparable with that of glycerine.

It is evident from the above comparison that the most promising liquid desiccant is lithium chloride although it is relatively expensive. Calcium chloride can be used depending on the requirements of specific application. However, the operating range of calcium chloride is limited compared to lithium chloride as shown in Fig. 2. This figure gives values of equilibrium relative humidity and temperature for air and desiccants.

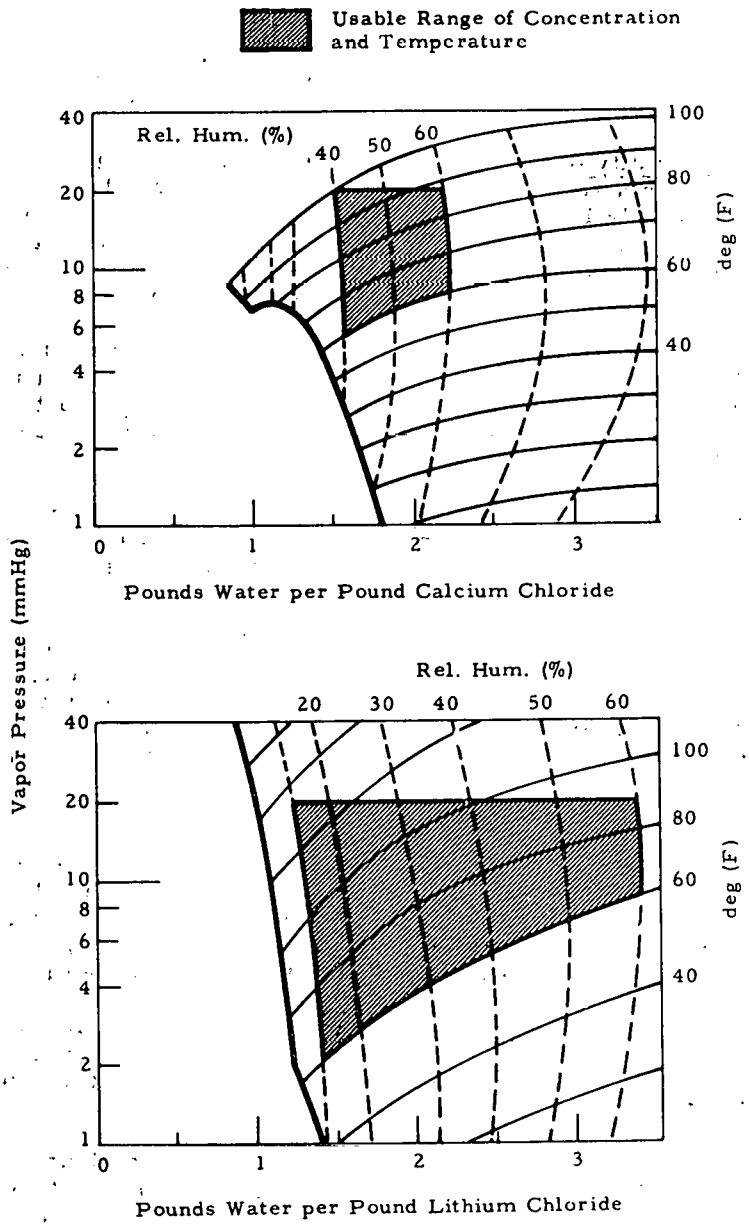

Fig. 2 - Operating Range of Two Liquid Desiccants for Crop Drying

Solid Desiccant Characteristics

Both adsorptive and reactive types of solid desiccants which do not become wet or sticky in normal service are considered in this section. These solid desiccants are widely used in applications where nearly complete drying is required. Since it is not generally possible to move the used desiccant from the drying chamber to a regeneration chamber, solid desiccants are usually regenerated in a stationary container at the end of a drying cycle. This necessitates the use of several beds of solids where continuous drying is necessary. In addition to drying efficiency, capacity and activity, the size of the desiccant pellets is an important factor in considering a solid desiccant. Size is important because of its effect on the pressure drop of air passing through the bed and the area for mass transfer (of water vapor) from the desiccant pellet to the air.

Properties of common solid desiccants are summarized in Table 3, and the suitability of these chemicals is compared in terms of the following properties (Refs. 8, 9, and 16 through 25):

TABLE 3. SUMMARY OF SOLID DESICCANT PROPERTIES

Solid Desiccant	C_p (Btu/lb-F)	Adsorption Capacity $\left(\frac{\text{lb } H_2O}{\text{Lb Desiccant}}\right)$	Range of Regeneration Temperature (F)	Number of Regeneration Cycles	Average Heat of Wetting	$/lb
Selica Gel	0.20-0.22	0.4-0.5	200-350	Unlimited	~200	0.60
Activated Alumina	0.24	0.14	300-600	Unlimited	~200	0.32
Anhydrous Calcium Sulfate	0.17	0.12	400-500	Limited (~200 Reg.)	540	0.55
Anhydrous Magnesium Perchlorate	—	0.48	400-500	Limited	264	2.10
Activated Carbon	0.20	~0.4	220-240*	Unlimited	~200	1.40

* For embedded heater (steam or electric).

— Data not available.

1. Specific Heat. Specific heats of solid desiccants range from 0.20 to 0.24 which is considerably lower than liquid desiccants.

2. Adsorption Capacity. Silica gel and activated carbon have considerably higher drying capacity than activated alumina or anhydrous calcium sulfate. Anhydrous magnesium perchlorate also has high drying capacity.

3. Range of Regeneration Temperature. The range of regeneration temperature for solid desiccants is generally higher than liquid desiccants, which is not preferable when the solar regeneration method is employed. For complete regeneration, temperature ranges higher than those listed in the table must be used. The temperature ranges listed in the table include partial regeneration ranges. For example, the recommended range for complete regeneration of silica gel is 300 to 350 F, although it can be partially regenerated as low as 200 F where extremely dry air is not necessary, such as in crop drying applications. Considerably higher regeneration temperature must be used for activated alumina, anhydrous calcium sulfate and magnesium perchlorate.

4. Number of Regeneration Cycles. Anhydrous solid desiccants have relatively short length of service life due to the limited regenerability. Anhydrous calcium sulfate can only be subjected to about 200 drying and regeneration cycles, after which its drying power deteriorates.

5. Heat of Wetting. Adsorptive solid desiccants have comparable heat of wetting with the heat of solution of saline liquid desiccants. Heat of reaction is responsible for higher heat of wetting for anhydrous desiccants High heat of wetting is not favorable in adiabatic drying operations since it may require additional cooling of the dried air stream.

6. Cost. In general solid desiccants are more expensive than liquid desiccants. Silica gel, activated alumina and anhydrous calcium sulfate are the less expensive solid desiccants.

Among the solid desiccants compared in the table, silica gel is the most favorable one when the solar regeneration method is employed. Activated alumina can be attractive when a high temperature solar collector or auxillary heating device is used.

CONCEPTUAL DESIGNS

Apparatus required to utilize desiccants and solar energy for crop drying include several heat exchangers, pumps, blowers, packed columns, storage tanks for the desiccant, a solar collector and an auxiliary heat source. These units may be combined in different ways to perform the crop drying operation. The optimum configuration of the crop drying apparatus is subject to an extensive analytical study in which the capability to conserve energy and capital cost of the apparatus are compared. Concepts using liquid desiccants are presented and system energy requirements are compared. Solid desiccant systems are not presented because of the difficulties in regeneration and energy recovery discussed in the previous section.

A schematic of a system using liquid desiccants (lithium chloride solution, for example) to dry crops in two separate bins is shown in Fig. 3. Solar energy is

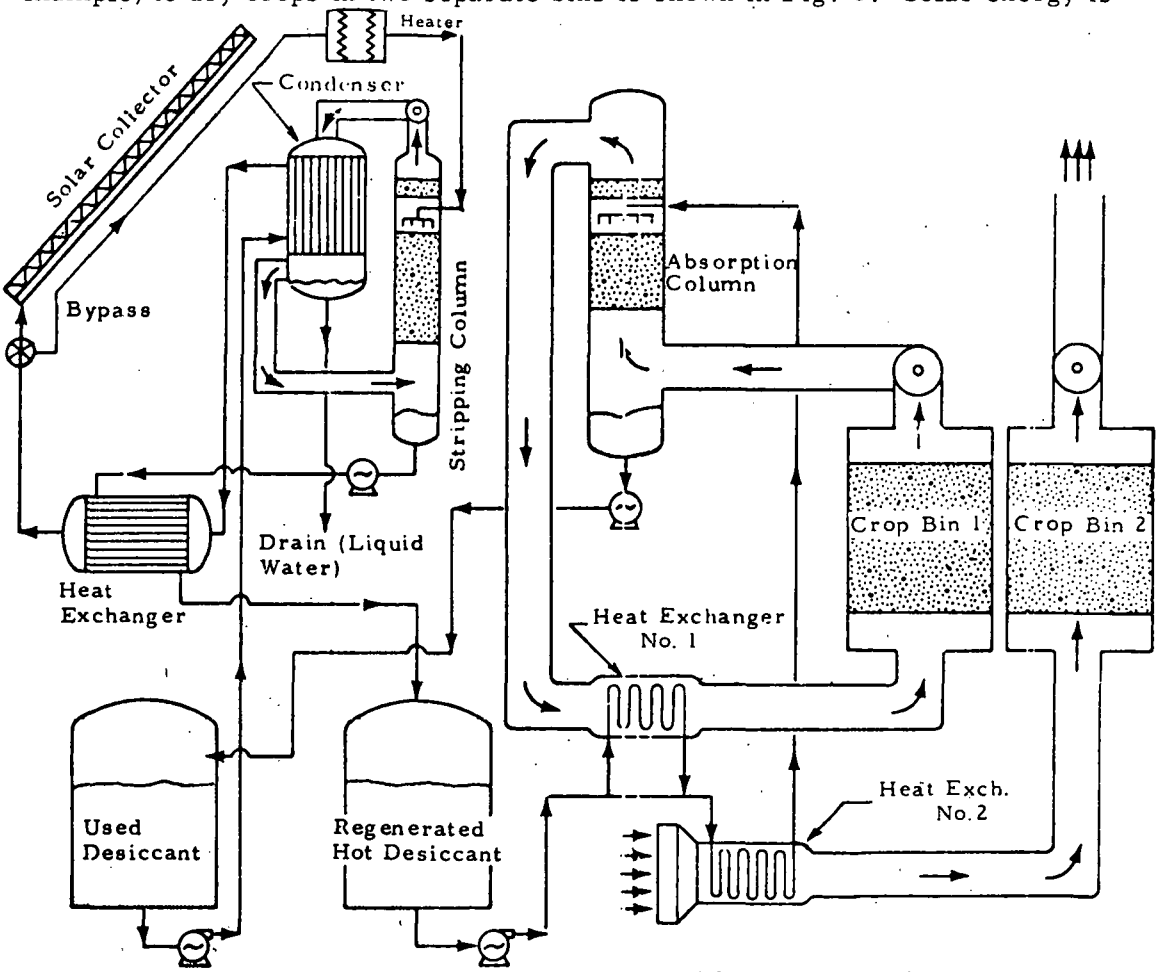

Fig. 3 - Desiccant Drying Concept with Two Crop Bins

used to regenerate the dilute (wet) desiccant solution which is used to dehumidify the air passing through the closed loop drying cycle. Water vapor is fed into a condenser where the dilute cool desiccant is preheated before passing through the solar collector. The dilute desiccant is also preheated by the hot regenerated desiccant in a liquid-liquid heat exchanger "downstream" from the condenser. The hot, regenerated desiccant is returned to a storage tank. The regenerated desiccant is used to heat the air in the closed loop cycle at Heat Exchanger 1 before passing the air through Crop Bin 1. Moist air from Crop Bin 1 is dehumidified in a packed absorption column where the air in the closed loop cycle and the regenerated desiccant make contact.

The temperature of the regenerated desiccant must be suppressed in order to achieve drying potential before bringing it into contact with the moist air in the closed cycle drying loop. This is done in Heat Exchanger 2. The heat rejected by the hot, regenerated desiccant is supplied to another crop bin (Crop Bin 2) which operates in the conventional open loop fashion.

Figure 4 shows a similar concept which uses a two stage column dryer where grain is initially dried and preheated in conventional open loop fashion using heat rejected in cooling the hot, regenerated desiccant. The grain then passes into the closed loop portion of the drying scheme. The total system operates in a similar fashion to the apparatus shown in Fig. 3. However, additional energy

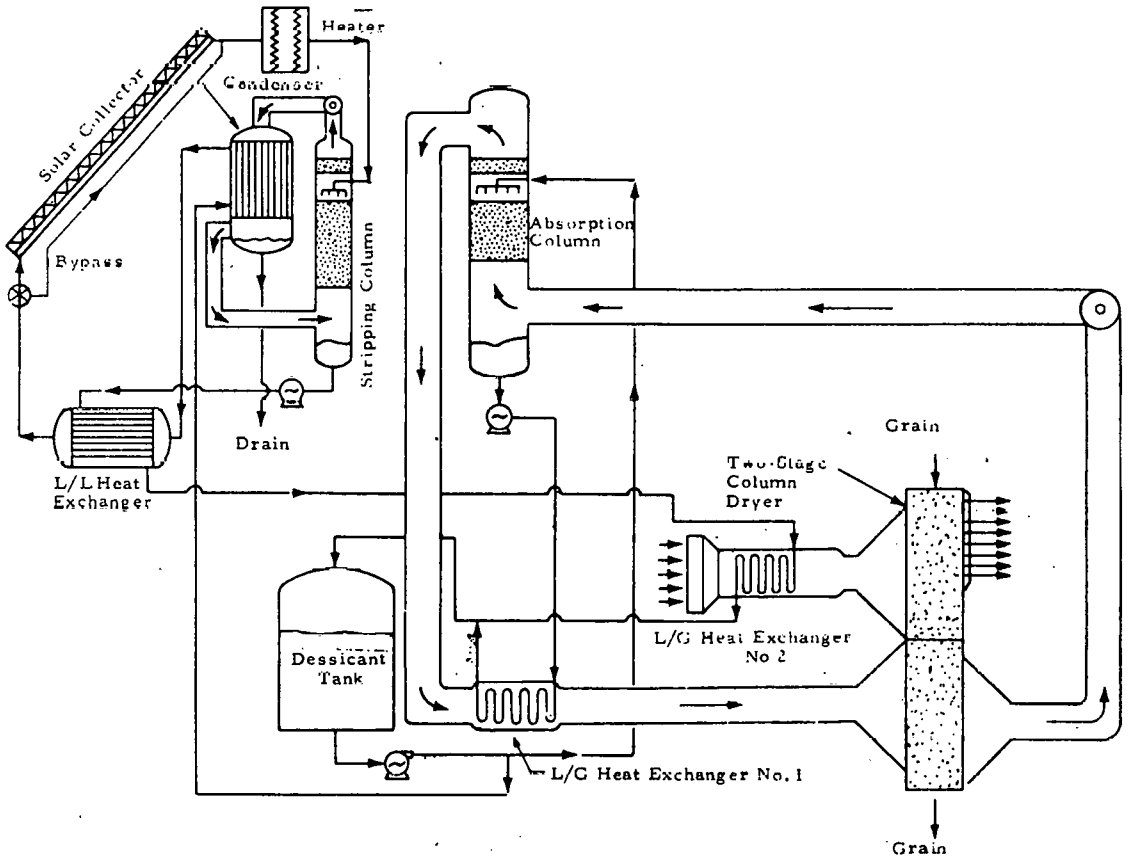

Fig. 4 - Desiccant Drying Concept with Continuous Column Dryer (Two-Stage Drying)

savings is expected because the thermal energy required to preheat the grain in open loop drying is retained in the closed loop portion as the grain moves continuously from one stage to the next. Figure 5 shows a two mode drying concept with one bin where the crop is initially dried in an open cycle drying mode while the desiccant is regenerated and then dried in a closed cycle mode using regenerated, stored, desiccant to a desired crop moisture content level. This two-mode concept is similar to the two-stage concept except that it is a batch drying process.

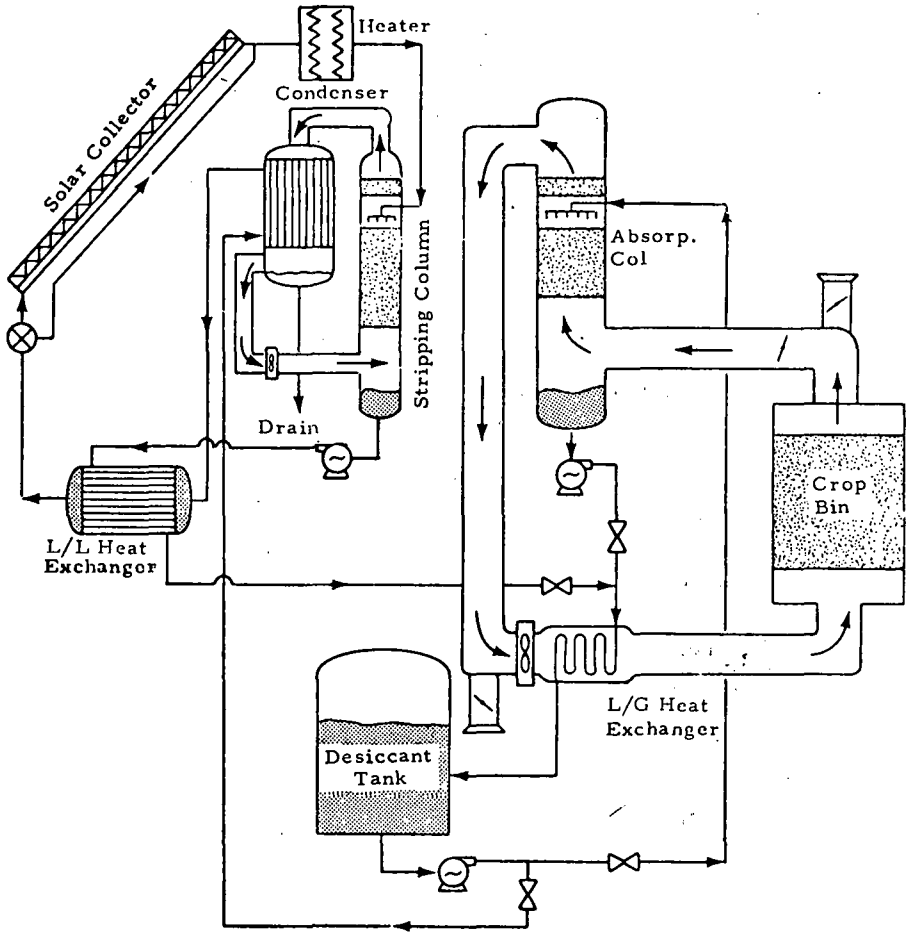

Fig. 5 - Desiccant Crop Drying Concept with One Crop Bin (Two-Mode Drying)

Figures 3, 4 and 5 display concepts in which some thermal energy must be rejected from the system. Although this thermal energy is used in open cycle crop drying, energy is still used relatively inefficiently in heating ambient air in vaporizing water from the crop. This energy cannot be reclaimed as is possible in the closed cycle drying portion of the crop drying configuration. A third concept for using liquid desiccants combines crop drying with some other thermal energy use. A good example is soybean processing. Soybean processing facilities currently use large amounts of energy both for drying and processing the beans into oil and high protein meal. In this third concept, the process thermal energy used for tempering, cooking and evaporating hexane (used to separate the oil from the meal) could be obtained from the thermal energy available in the regeneration of the desiccant. The net result of this arrangement is that drying and processing of the soybeans is accomplished with about 14% of the conventional energy requirements for soybean drying.

The results of three process analyses using liquid desiccants ($CaCl_2$ or $LiCl$ solutions) are shown in Table 4 compared with conventional open cycle dryers. The three desiccant cases represent three different ways of using the energy recovered during the regeneration cycle, namely: 2 crop bin mode (Fig. 3), two-stage drying (Fig. 4) or two-mode drying (Fig. 5) and alternate nondrying energy use for rejected thermal energy. The results shown are in the form of the total energy required to remove one pound of water from a crop (peanuts in this case). Both thermal energy and electrical energy (for pumps and blowers) are included in this total.

TABLE 4. COMPARISON OF DIFFERENT DRYING SCHEMES

Case/Description	Btu/lb H_2O Removed	Frac. of Energy Used Compared with Conventional
1. Desiccant — 2 crop drying bins	1100	0.50
2. Desiccant — 2 stage drying or 2 mode drying	1000	0.46
3. Desiccant — 1 stage drying with non-drying energy use	300	0.14
4. Conventional, open cycle crop drying	2200	1.00

SUMMARY

The chemical and physical properties of solid and liquid desiccants have been studied to identify desiccants that can be used in crop drying applications. The desiccant can be used as an active drying agent as well as serving as an energy storage media for collected solar energy. The crop drying apparatus is configured such that continous or batch drying of the crop can be accomplished. Regeneration of the desiccant is performed in such a manner that virtually all the energy expended in evaporation of the moisture from the desiccant is recovered and used within the drying process which results in a significant energy savings over a conventional heated air drying system. The absorption column (dehumidifiers) is configured such that the relative humidity of drying air can be controlled independent of temperature.

Conceptual designs and process flow diagrams for using solar energy for regeneration of solid and liquid desiccants have been identified. Liquid desiccants are more attractive than solid desiccants because of easier controllability and relatively low regeneration temperatures.

Analysis of the chemical and physical properties of desiccants indicate that calcium chloride and lithium chloride salt solutions have the best application in solar regenerated desiccant crop drying apparatus. Calcium chloride and lithium chloride solutions can be regenerated at lower temperatures than other desiccants (which relaxes constraints on the choice of solar collector hardware), have high specific heats (which augments thermal storage capacity), and are stable, relatively nontoxic chemicals. These salt solutions can cause corrosion but use of proper materials in fabricating crop drying equipment can overcome this problem.

The desiccant drying concepts offer three advantages: (1) energy savings of up to 50% over a conventional heated-air concept; (2) independent controllability of relative humidity of drying air; and (3) use of solar energy.

ACKNOWLEDGEMENTS

The authors are grateful to Dr. P.G. Grodzka of Lockheed-Huntsville for her initial suggestion of the use of desiccant as drying agent/heat storage media. The contributions made by Dr. G.H. Watson of Oak Ridge National Laboratories, during his tenure at Lockheed-Huntsville, are also acknowledged.

REFERENCES

1. United States Department of Agricluture, "Agricultural Statistics, 1974," U.S. Government Printing Office, Washington, D.C., 1974.

2. Reding, J.T., and B.P. Sheperd, "Energy Conservation: Fuel Utilization and Conservation in Industry," Dow Chemical Company, Contract 68-62-1329, for U.S. Environmental Protection Agency, August 1975.

3. Hall, Carl T., Drying Farm Crops, Agricultural Consulting Associates, Inc., Reynoldsburg, Ohio, 1957.

4. Brooker, D.B., F.W. Bakker-Arkema, and C.W. Hall, Drying Cereal Grains, AVI Publishing Co., Inc., Westport, Conn., 1974.

5. Henderson, S.M., and R.L. Perry, Agricultural Process Engineering, Second Edition, University of California, 1974.

6. Foster, G.H., "Heated-Air Grain Drying," in Grain Storage: Part of a System, AVI Publishing Co., Westport, Conn., 1973.

7. Harris, W. L. et al., "Solar Energy Applications in Agriculture Potential, Research Needs and Adoption Strategies," prepared for USDA under NSF grant PTP 75-10573, January 1976.

8. Hougen, O.A., and F.W. Dodge, The Drying of Gases, Edwards Brothers, Inc., Ann Arbor, Mich., 1947.

9. Bower, J.H., "Comparative Efficiencies of Various Dehydrating Agents Used for Drying Gases," Bureau of Standards Journal of Research, Vol. 12, 1934.

10. Johnson, F.M., "Moisture Control by Liquid Absorption," Heating, Piping, Air Conditioning, December 1968.

11. Knowles, A.F.H., "The Glycerol Gas drying Process," Gas World, Vol. 94, 382-3, 1931, pp. 482-483.

12. Hollands, K.G.T., "The Regeneration of Lithium Chloride Brine in a Solar Still," Solar Energy, Vol. 7, No. 2, 1963.

13. Mullick, S.C., and M.C. Gupta, "Solar Desorption of Absorbent Solutions," Solar Energy, Vol. 16, No. 1, 1974

14. Lof, G.O.S., "Recent Investigations in the Use of Solar Energy for the Drying of Solids," Sol. Energy, Vol.6, No.4, 1962, pp. 122-128.

15. Glicksman, L.R., and J.W. Meyer, "Solar Energy Dehumidification Experiment on the Citicorp Center Building Interim Report," Energy Laboratory, MIT, Cambridge, Mass., 1975.

16. Hubard, S.S., "Equilibrium Data for Silica Gel and Water Vapor," I.E.C., Vol. 46, No. 2, 1954.

17. Hammond, W.A., "Use and Regeneration of Drierite," J. Chem Education, Vol. 12, 1935, pp. 445-446.

18. Chaney, N.K., "The Properties of Activated Carbon," Ind. Eng. Chem., Vol. 15, 1923, p. 124.

19. Derr, R.B., "Drying Air and Commercial Gases with Activated Alumina," Ind. Eng. Chem., Vol.30, 1938, pp 384-388.

20. Druce, J.G.F., "Magnesium Perchlorate as a Drying Agent," Chem. and Ind., Vol. 54, 1935, p. 133.

21. Mantell, C.L., Adsorption, McGraw-Hill, New York, 1951.

22. Getty, R.J., and W.P. Armstrong, "Drying Air with Activated Alumina Under Adiabatic Conditions," I&EC Process Design and Development, Vol. 3, No. 1, 1964.

23. Buelow, F.H., "Drying Crops with Solar Heated Air," Proceedings of the United Nations Conference on New Sources of Energy, Vol. 5, Rome, 1961.

24. Satcunanathan, S., "Crop Drier Utilizing a Two Pass Solar Air Heater," from International Congress on the Sun in the Service of Mankind, Unesco House, Paris, 1973.

25. Davis, C. P., and P. I. Lipper, "Solar Energy Utilization for Crop Drying," Proceedings of the United Nations Conference on New Sources of Energy, Vol. 5, Rome, 1961.

ANALYSIS AND DEVELOPMENT OF A SOLAR ENERGY REGENERATED DESICCANT CROP DRYING FACILITY*

by

S. M. Ko and D. V. Merrifield
Lockheed Missiles and Space Company, Inc.
Huntsville, Alabama 35807

A study was conducted to investigate the technical and economic feasibility of a solar energy regenerated desiccant crop drying concept. The study was sponsored by ERDA under Contract E (40-1) 5157 and includes design concepts and data developed under Contract USDA-12-14-7001-817 for the US Department of Agriculture, Agricultural Research Service.

As an integral part of the work, a bench scale electrically heated drying system was built and experimentally tested. Close agreement was obtained between analytical simulation and measured performance. The thermal energy required to remove each pound of water from the test crop was found to be less than 1150 Btu.

The principal conclusion of the study was that the regenerated desiccant crop drying concept is technically feasible and has the capability to achieve a drying efficiency of approximately twice that of conventional crop drying systems. When using a fossil fuel energy source, energy savings will be approximately 40 to 50%. With solar energy input, the total energy savings could be 70 to 90%. The economic feasibility of the system appears promising. As with other new energy conserving systems that are presently capital-intensive, the economic viability of the system will be dependent on future capital cost reductions, on the future price of fossil fuels, and on the specific application of the system. Regarding system applications, it was concluded that the regenerated desiccant drying system, with or without the use of solar energy, will be economically best suited for a large central processing application, where it can receive a maximum amount of use and will benefit from economy-of-scale cost considerations.

The basic study recommendations are: (1) additional R&D activities should be conducted to identify and evaluate means for achieving system cost reductions; and (2) a mobile pilot drying facility program should be initiated.

*Abstract of a paper entitled "Energy-Efficient Desiccant Drying/Dehumidification Using Solar or Fossil Fuel Energy," to be published in the proceedings of the 12th Intersociety Energy Conversion Engineering Conference, to be held in Washington, D.C., August 28 through September 2, 1977.

A LOW COST SOLAR COLLECTOR SUITABLE FOR USE IN PEANUT DRYING APPLICATIONS

by

J. H. Schlag, A. P. Sheppard, and J. M. Wood
Georgia Institute of Technology
Atlanta, Georgia 30332

INTRODUCTION

Over the past two years, three types of low cost solar collectors have been tested to determine their applicability as energy sources for peanut drying. They are a black film hot air collector, an integral rock storage and collection system, and a shallow solar pond collector. The results to date indicate that the first two systems are the most promising and that the most effective method of utilizing them is to combine them in a series installation which we refer to as the Augmented Integrated Rock System or AIRS.

Two overriding considerations dictated the design of the collectors discussed in this paper. One was that they must be constructed of inexpensive materials and the other was that a farmer should be able to construct them on-site from a set of simple plans. It is felt that a solar system will have to meet these criteria if it is to receive widespread acceptance in the agricultural community.

INTEGRATED ROCK-STORAGE AND COLLECTION SYSTEM

By blackening the top layer of a rock bed and covering it with an appropriate glazing material, one can construct both an efficient collector of solar radiation and an inexpensive storage system as shown in Figure 1. The heat, however, tends to be concentrated near the surface of the rock bed. Tests have shown that without air circulation, the heat will penetrate only about 6 inches into the bed. Figure 2 illustrates the temperature profile within a test system during a period of 11 hours without air circulation.

Circulating air through the rock bed in a downward direction during the collecting period is desirable because surface heat is thus conveyed to the lower rock layers creating a more uniform temperature distribution. The more uniform distribution of heat will lower the rate at which heat is radiated from the system.

It has been determined that in order to achieve an average rock temperature of 60°C (with air circulation), the rock bed thickness should be no more than 0.3 meters. As the rock depth is increased beyond this figure, the collecting surface is not large enough to raise the temperature of the rock to a sufficiently high temperature for crop drying. In order to obtain more storage without increasing the surface area of the rock it is desirable to supplement this system by using the black film hot air collector described in the following section.

One potential problem in evaluating the performance of this system is that the interior temperatures of each rock lags behind the surface temperature as the rocks are heated. In order to determine the lag time in temperature response a 10 cm. diameter rock was equipped with 3 thermocouplers. A hole was drilled in the rock and a thermocouple was sealed inside the rock to measure the temperature of the center of the rock. The other two where placed on the top and bottom of the rock. The rock was then placed in the sun and the temperatures of the top, center and bottom of the rock were measured. It was found that five minutes were required for the temperature of the center and bottom of the rock to equal the temperature of the top of the rock. Thus, it was concluded that the temperature gradient in the individual rocks can be ignored for most practical purposes.

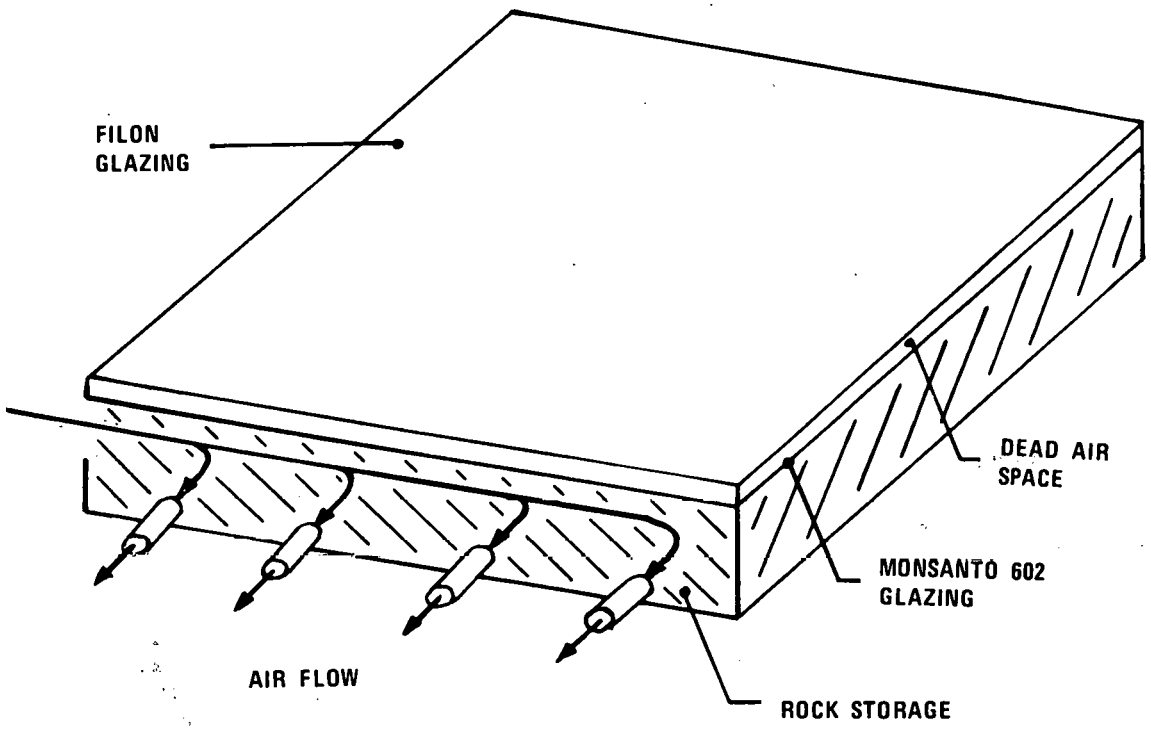

FIGURE 1, INTEGRATED ROCK STORAGE AND COLLECTION SYSTEM

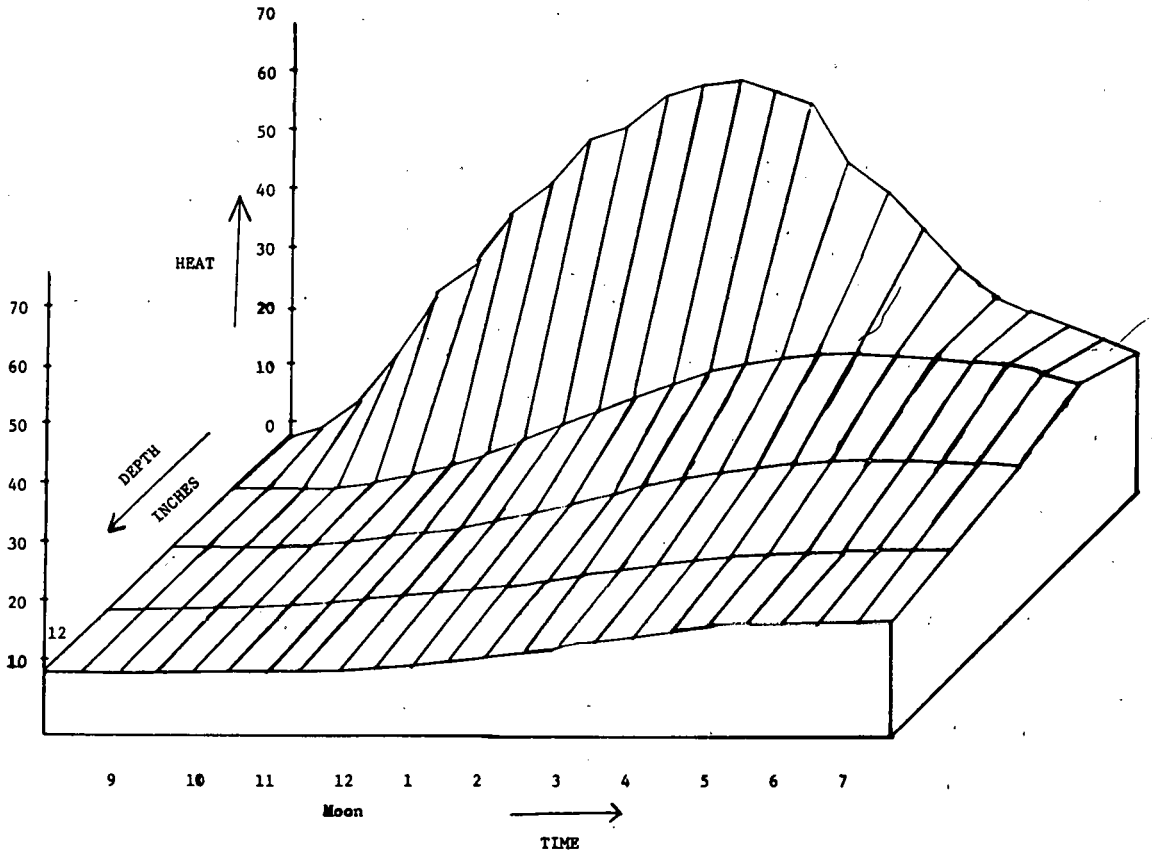

FIGURE 2 TEMPERATURE PROFILE OF ROCKS WITH NO AIR FLOW

Double glazing is used for the rock bed system because it becomes imperative to have the rocks well insulated in order to preserve the built-in storage capability. The upper layer of glazing is fiberglass coated with Tedlar. This material is used because it is more opaque to infrared radiation than plain plastic and has an expected life span of 15 years. The lower layer of glazing is Monsanto 602 plastic. The Monsanto 602 is much less expensive than the fiberglass and since this layer will not be exposed to the elements or U.V. radiation its lifespan should exceed two years. The spacing between the two layers is about 2.5 cm, the spacing required to minimize heat transfer between the two surfaces. A smaller spacing results in smaller convective heat losses, but larger conductive heat losses. Increasing the spacing does not significantly change the amount of heat loss because as the conductive heat losses are lowered, the convective heat losses increase.

The rocks used in the system are granite and average 10 cm. in diameter. This size provides relatively good heat transfer properties because the rocks present a large surface area to the air stream and yet they do not unduley impede the air flow. It is important that the rocks be of uniform size to avoid impeding the air flow.

BLACK FILM HOT AIR COLLECTOR

Two designs have been tested for the Black Film Hot Air Collector. They are shown in Figures 3 and 4.

The design shown in Figure 3 consists of a layer of glazing and a layer of blackened Fesco insulation. Air is drawn in between the glazing and the insulation and heated as it passes through the collector. The air is forced through the collector by a fan located at the base of the unit.

The design shown in Figure 4 consists of a layer of clear glazing, a 2.5 cm stagnant air gap, a layer of black Typar, a 5 cm space for hot air, and a layer of Fesco board insulation. Air enters at the top of the collector and is heated as it passes behind the Typar. The heat can then be stored in a rock storage bin. The air is moved through the collector by a fan located at the base of the unit. Typar was chosen as the absorbing material over black polyethylene, tar paper, black painted paper, and black painted aluminum foil. The Typar and the black polyethylene both have superior absorbing characteristics, but the polyethylene was ruled out because it melted at the temperatures encountered in the system.

The graph in Figure 5 plots the temperature at the top of the collector design shown in Figure 3 over a 17 hour period along with the air temperature and the incident radiation. By comparing this with the performance of the other collector design, shown in Figure 6, it can be seen that the second design has a significantly higher temperature rise. In actuality, the temperature curve for the second design is flattened at the top because the thermocouples which measured the temperature became saturated at 100°C.

The temperature within both collectors varied and Figure 7 illustrates this variation for several heights within the collector which has Typar as the absorber at different times of the day. Once again, the saturation of the thermocouples is apparent in this graph.

AUGUMENTED INTEGRATED ROCK SYSTEM (A.I.R.S.)

Combining the two solar collectors previously discussed provides a very inexpensive system with the advantages of both systems. The rock bed system can not be placed at the proper angle to the sum without incurring the expense of grading the earth. It will also radiate energy from its entire surface area. By combining the two units as shown in Figure 8, you can have as much surface area as the system shown in Figure 9 but more radiation will be intercepted because the black film hot air collector is at a high enough angle to intercept the maximum amount

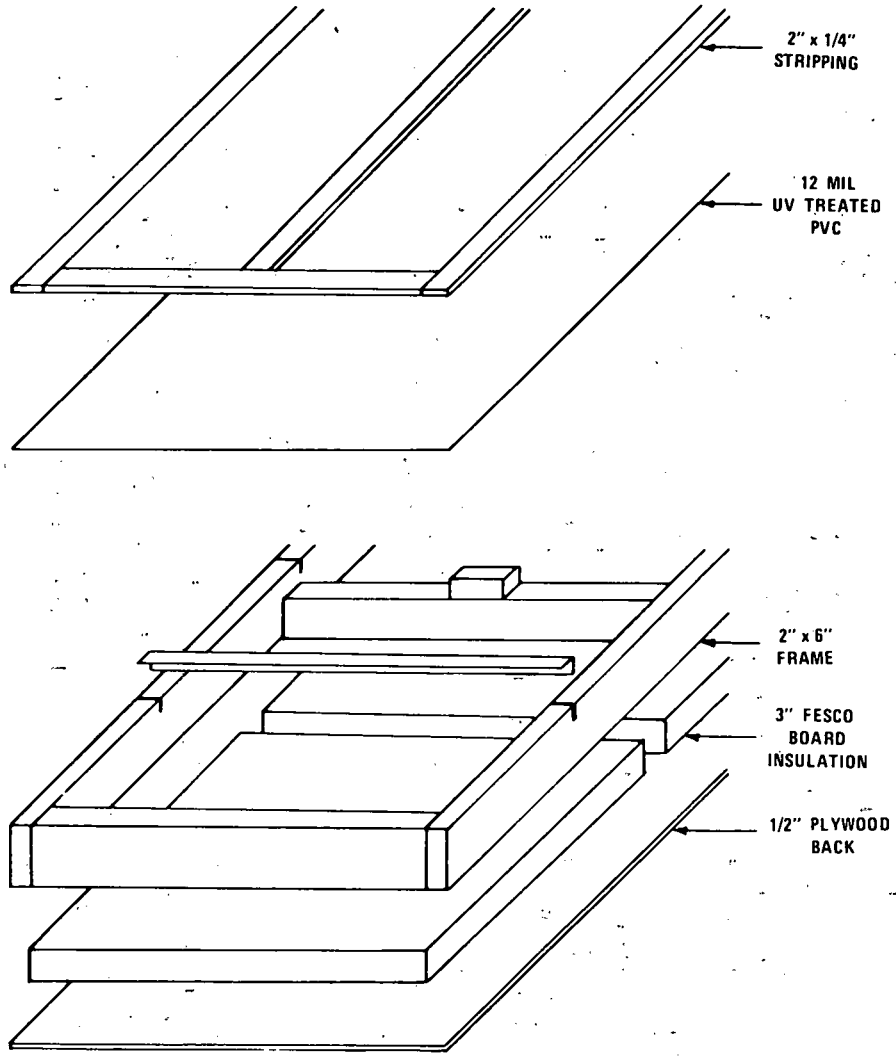

FIGURE 3. AIR DRYER CONSTRUCTION WITH BLACKENED FESCO AS THE ABSORBER.

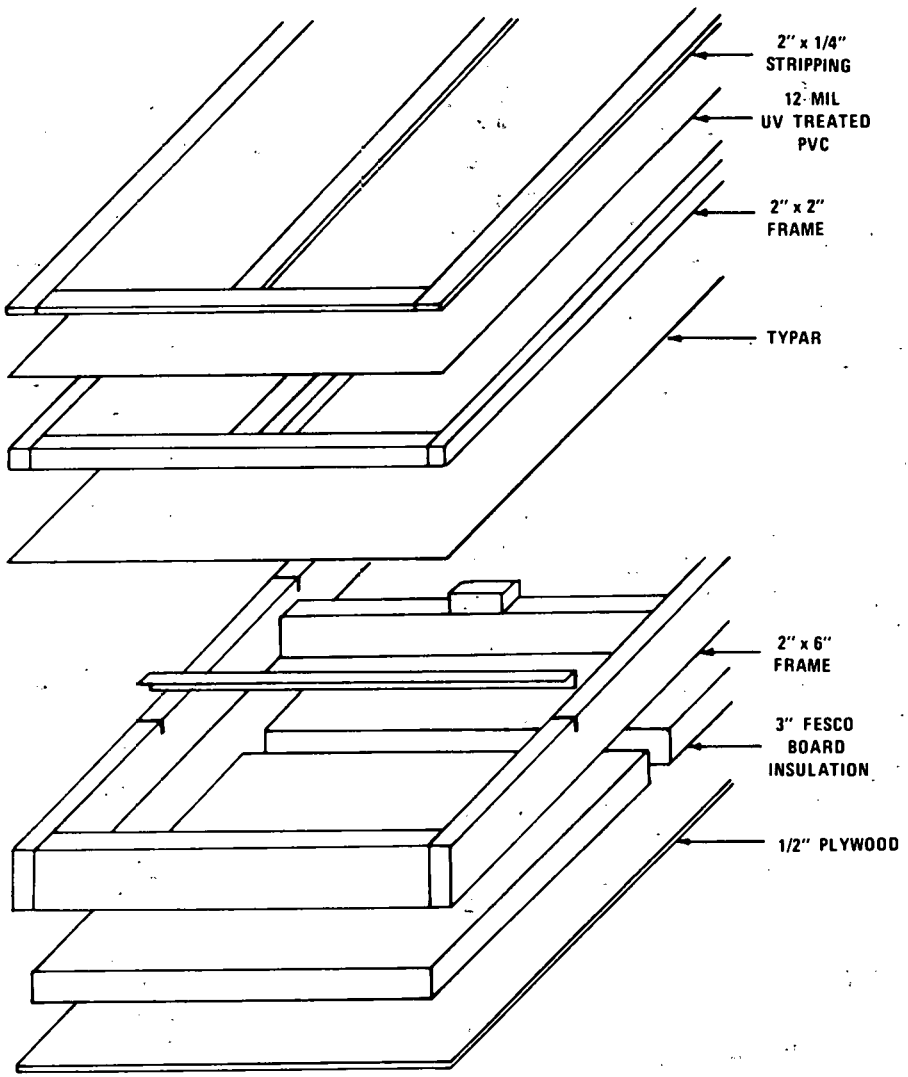

FIGURE 4. AIR DRYER CONSTRUCTION WITH TYPAR AS THE ABSORBER.

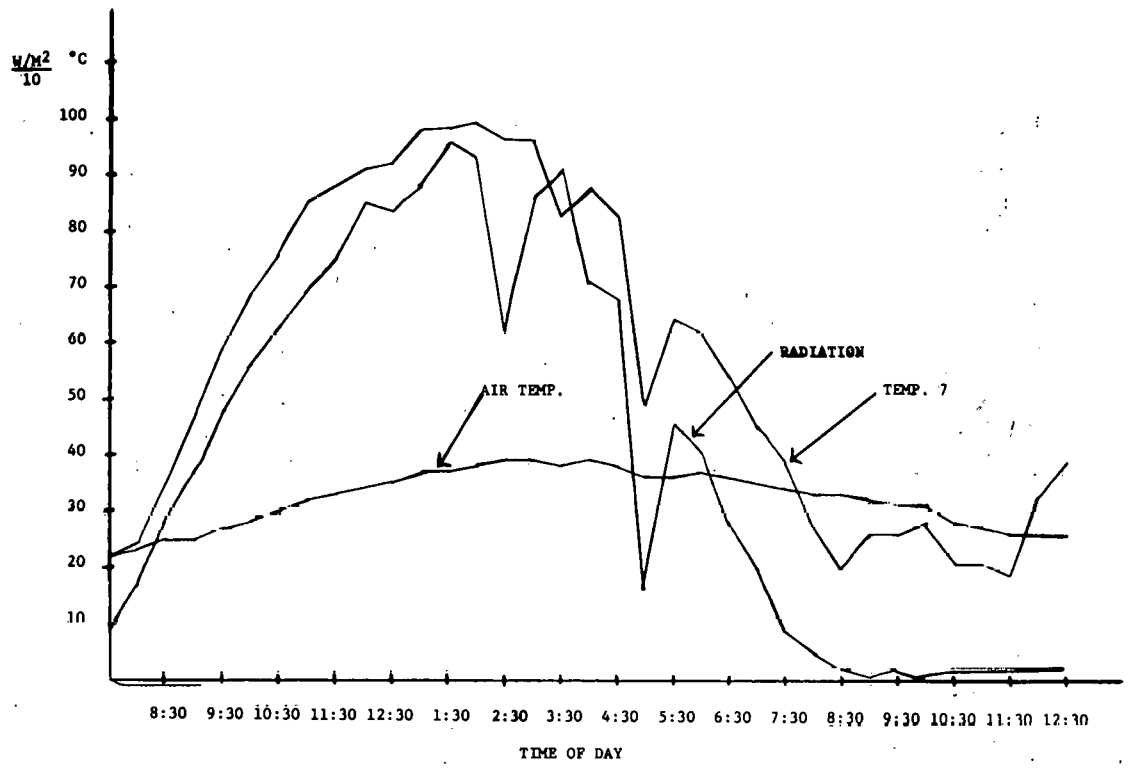

FIGURE 5 TEMPERATURE AND RADIATION CURVES OF AIR DRYER WITH BLACKENED FESCO

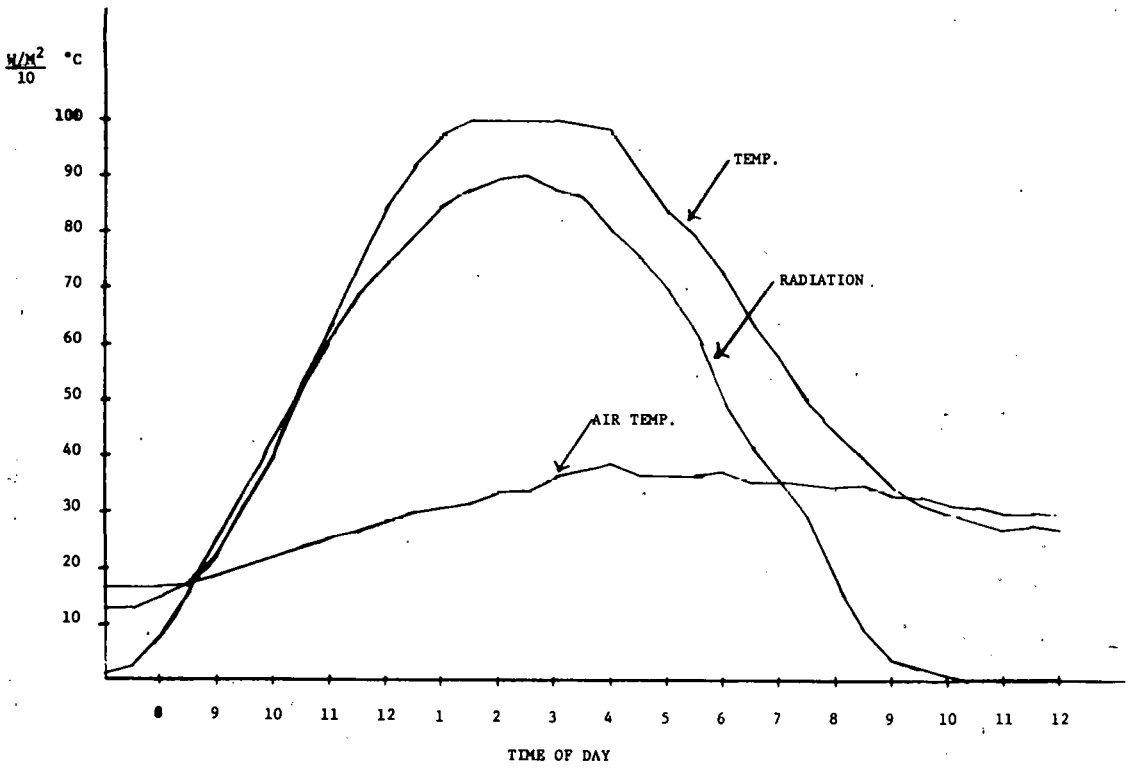

FIGURE 6 TEMPERATURE AND RADIATION CURVES OF AIR DRYER WITH TYPER AS THE ABSORBER

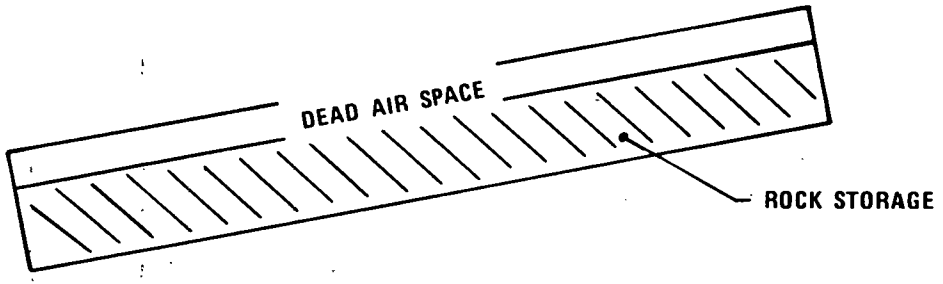

FIGURE 9 INTEGRATED ROCK STORAGE

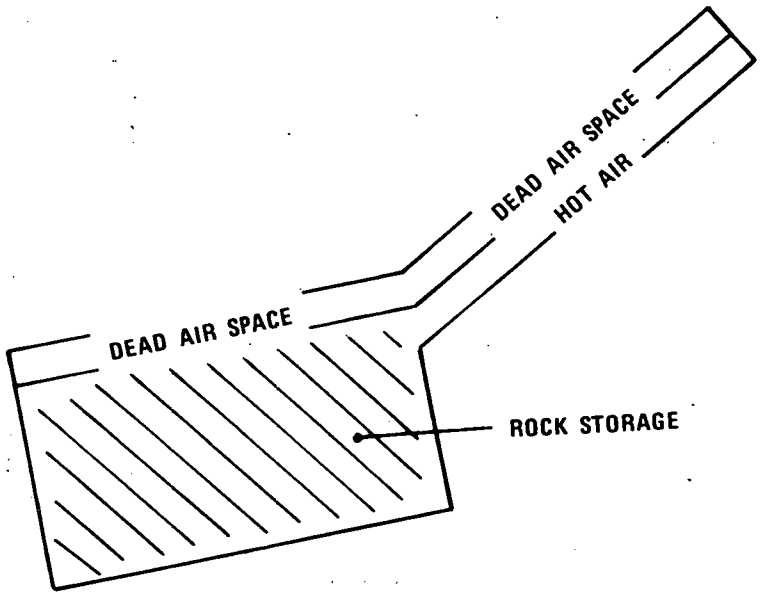

FIGURE 8 AUGMENTED INTEGRATED ROCK SYSTEM (A.I.R.S.)

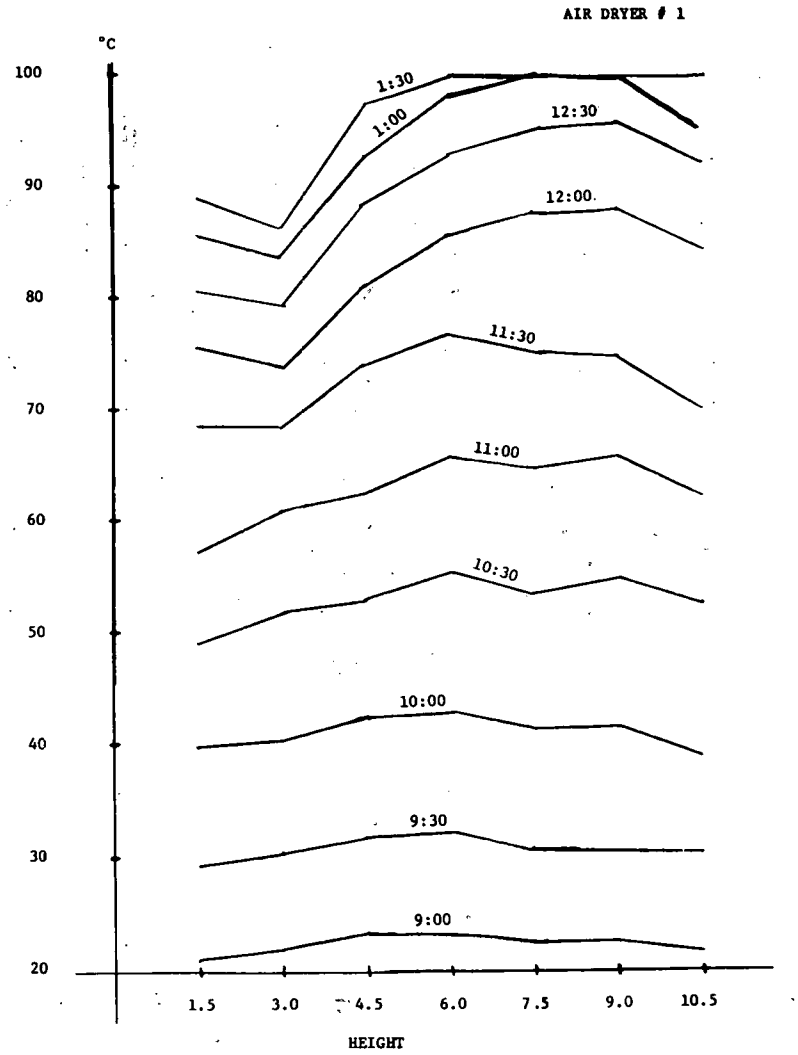

FIGURE 7 TEMPERATURE VS. HEIGHT FOR THE AIR COLLECTOR WITH TYPAR AS THE ABSORBER

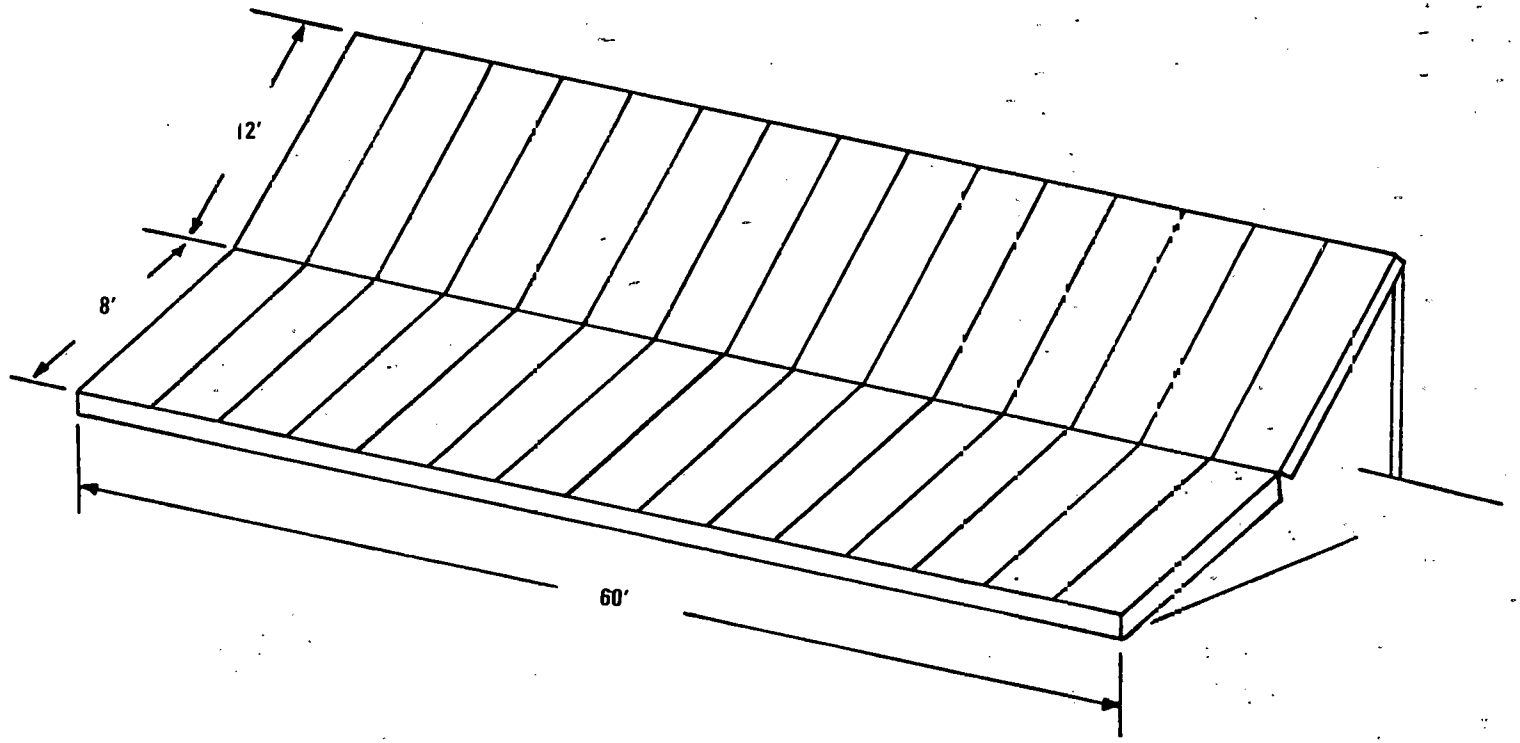

FIGURE 10 LAYOUT OF A.I.R.S. TO BE BUILT ON GEORGIA TECH CAMPUS

of the sun's radiation. In addition, the storage area has half of the surface area of the system in Figure 9. On the other hand, if the black film hot air collector were used alone it would still require a storage unit and a convential storage unit would not be acting as a collector.

A 1200 square foot AIRS, as illustrated in Figure 10, will be constructed this summer. It will have a 720 square foot (60 x 12) black film hot air collector connected in series with a 480 square foot (60 x 8) integrated rock storage and collection system. The rocks will be 12 inches deep and will be able to store about one million BTU's at a ΔT of 100°F. The ground will be graded so that the rock storage and collection system will face south at a 5 degree slope. The black film hot air collector will be placed at a 35° angle.

Figure 11 shows the air flow in the AIRS when it is operating in the energy storage mode. Air is forced by the fan into the top of the black film hot air collector where it is heated as it travels down the collector beneath the black Typar absorber. Upon entering the rock storage and collection system, it is heated further and forced down through the rocks. The air heats the rocks and then returns to the black film hot air collector. The second fan in the unit will force air into the drying wagon or shed.

The materials cost of the AIRS unit is under \$2.00/foot^2 for the black film hot air collector and under \$1.00/foot^2 for the integrated rock-storage and collection system. It is felt that at this price the AIRS unit will provide a practical low-cost alternative to drying crops using fossil fuels.

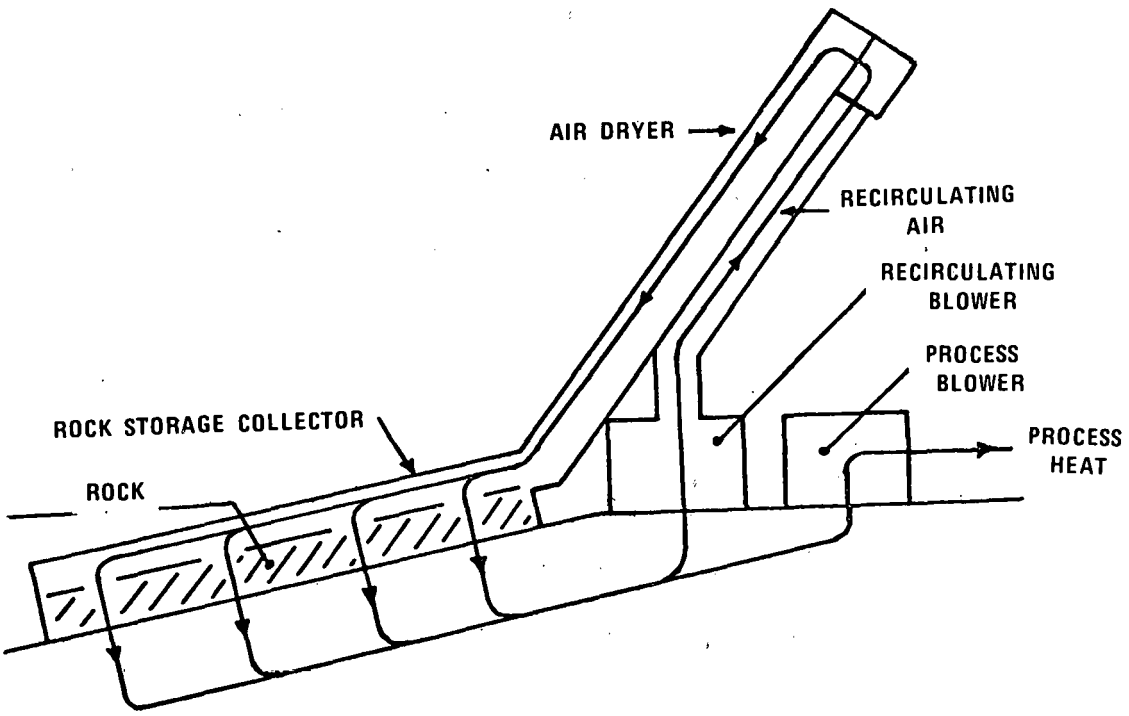

FIGURE II AIR FLOW IN THE A.I.R.S. SYSTEM

MATERIAL SELECTION FOR AGRICULTURAL SOLAR SYSTEMS

by

J. H. Schlag, A. P. Sheppard and J. M. Wood
Georgia Institute of Technology
Atlanta, Georgia 30332

Introduction

When selecting materials for use in constructing solar systems for agricultural uses it is often necessary to make trade offs, i.e. durability vs low cost. This article compares the attributes of common materials which can be used as glazings, absorbers and insulation. It does not attempt to select the best material in any category as the best material may well vary between systems and applications.

This paper will also compare water and rocks as storage mediums.

Glazing

In choosing a glazing material for a solar collector, the most important items to consider are cost, transmissivity, durability and heat retention.

The costs of several candidate materials are shown in Figure 1.

FIGURE 1

Material	Cost Per Square Foot
Glass	$1.00
Low Iron Glass "Waterwhite"	2.00
PVC (10 Mill)	.30
Monsanto 602	.02
Fiberglass Reinforced Plastic	.45
Tenite (Cellulose Acetate Butyrate)	.03
Tedlar	.35

Transmissivity tests on candidate materials were performed according to the National Bureau of Standards Specifications 21387-1973. A typical plot of the data from one transmissivity test run is shown in Figure 2 and a table of the test results is shown in Figure 3.

The ideal glazing material would be perfectly transparent to radiation in the solar spectrum (wavelengths .2 - 2.6 um) and opaque to all radiation with longer wavelengths. Two tests were used to test for these properties, the spectral density of the materials was evaluated using a Perkin-Elmer Model 700 Spectrophotometer. Results of one of these tests on M602 are shown in Figure 4. In addition, a test chamber was constructed with four compartments so that four samples can be exposed to identical radiation. The rise and fall of temperatures inside the absorption chambers over 30 minutes is shown in Figure 5.

The expected life-span of various glazings when exposed to U.V. radiation and normal weather conditions is shown in Figure 6. It should be recalled that when

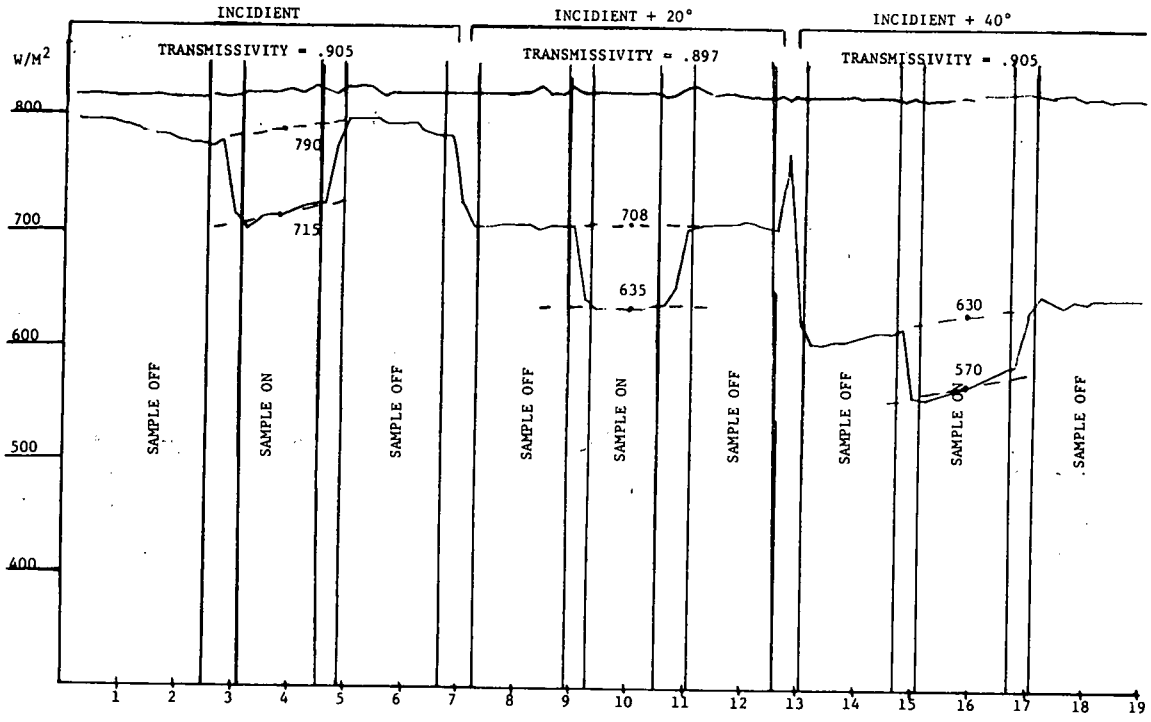

FIGURE 2 TRANSMISSIVITY OF CLEAR 10 MIL TENITE BUTYRATE

FIGURE 3

MATERIAL	TRANSMISSIVITY		
	DIRECT RADIATION	20° RADIATION	40° RADIATION
KALWALL	.881	.875	
PVC	.937	.862	
TEDLAR	.919	.826	
MONSANTO 602	.903	.841	
FIBERGLASS	.815	.813	.781
FIBERGLASS (CROSS GRAIN)	.815	.796	.878
TENITE PTMT	.907	.898	.884
TENITE BUTYRATE	.905	.897	.905

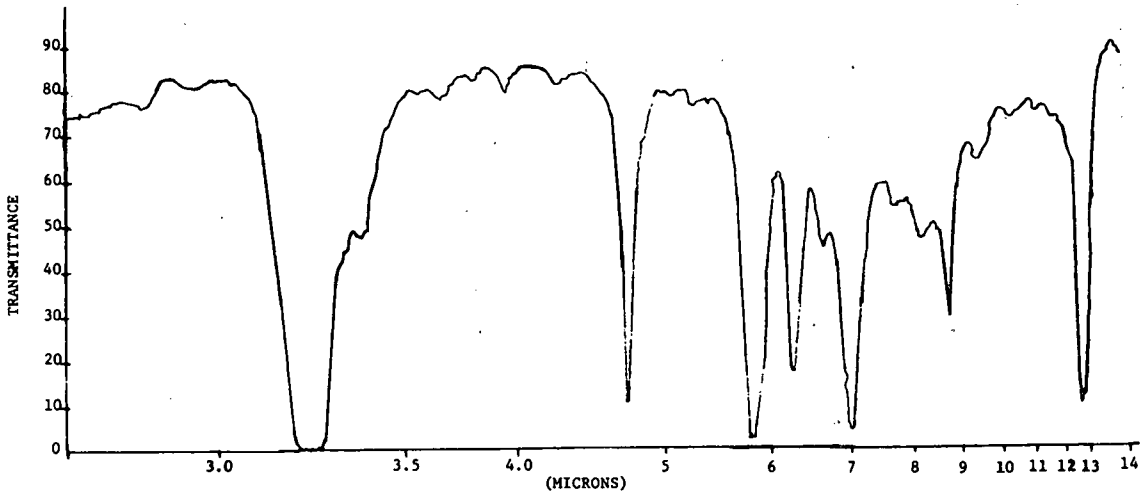

FIGURE 4 TRANSMITTANCE OF MONSANTO – 602 UV RESISTANT POLYETHYLENE

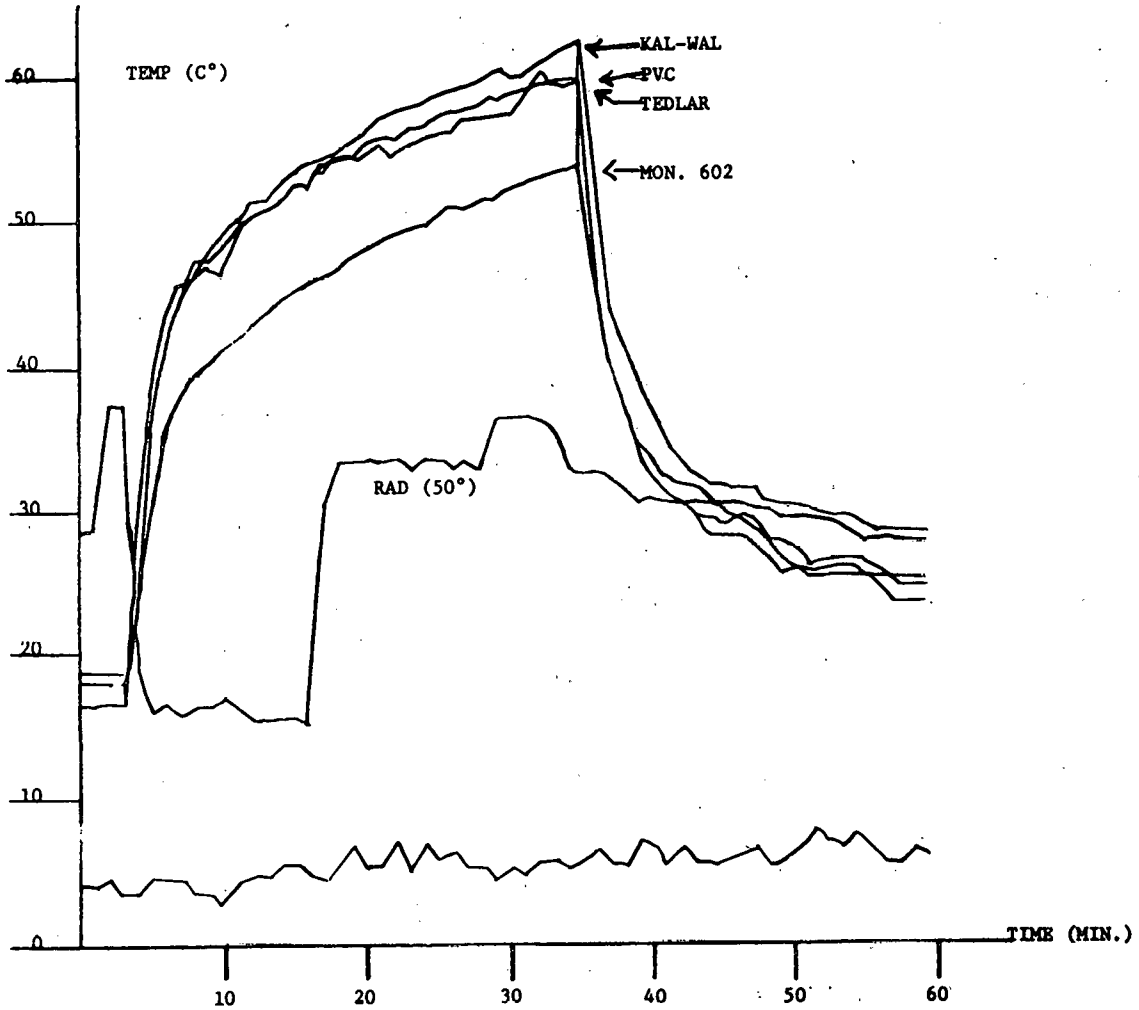

FIGURE 5 TEMPERATURE RISE IN AN ABSORPTION CHAMBER WITH FOUR GLAZING MATERIALS

using double glazing the lower glazing is exposed to less severe conditions and would therefore have a longer expected life span than shown in Figure 6. It should be noted, however, that the tenite will degrade in about one month if exposed to high temperatures. It could therefore be used as the top glazing in a double glazed system.

FIGURE 6

Material	Expected Life in Years
Glass	20+
PVC (10 Mill)	1
Monsanto 602	2
Fiberglass Reinforced Plastic	10
Tenite	10
Tedlar	20

Insulators

The most important properties of insulating materials are cost, durability and thermal resistance. Thermal resistance is expressed in "degrees per BTUh per square foot." It is the temperature drop expressed in degrees Fahrenheit through the insulating material when heat is passing through it at the rate of 1.0 BTU per square foot of surface per hour. The total thermal resistance of any heat barrier is the sum of the thermal resistance of its parts.

The conductance of a material or its U value is the inverse of its thermal resistance.

$$U = \frac{1}{R}$$

The U value is measured in BTU's of heat flow per hour per square foot per degree F temperature difference. Therefore, the smaller the U value of a material the better it is as an insulator.

The durability of an insulating material depends on the conditions to which it is exposed. Most materials lose their insulating value when wet. Some are protected with a moisture barrier to prevent them from becoming wet. An insulating material should not lose its thermal resistance or deform under the greatest temperature range to which it might be subjected. (-30°F - 300°F is a possible range for non-focusing solar collectors.) The degree of structural strength and the resistance to abrasion required are also function of the application.

Figure 7 compares the cost per square foot and R value of some common insulators.

FIGURE 7

Wood	Cost/ft^2	R
6" Fiberglass Craft Back	.13	19
1" Fesco Board	.20	2.78
3/4" Styrofoam (Technofoam by Celotex)	.35	8
3/4" Styrofoam (Dow)	.35	5.4
5/8" Polystyrene	.20	4

Absorbing Materials

A good absorbing material should have a high absorbtivity, a high melting point and a high thermal conductivity. It should also present a large surface area to the heat transfer fluid (i.e. air or water). This would imply that in general it is preferable to have a rough surface or corrugated surface to a flat surface. As with all materials, cost plays an important role in material selection.

The materials that have so far been tested as possible absorbing materials are black polyethylene, tar paper, black painted paper, black painted aluminum foil, and various formulations of a Dupont material called Typar. Of these materials, the Typar and the black polyethylene had the best absorbing characteristics, as shown in Figures 8 and 9. The black polyethylene was found to melt when exposed to high temperatures for a long period of time, and therefore the Typar appears to be the best available absorber.

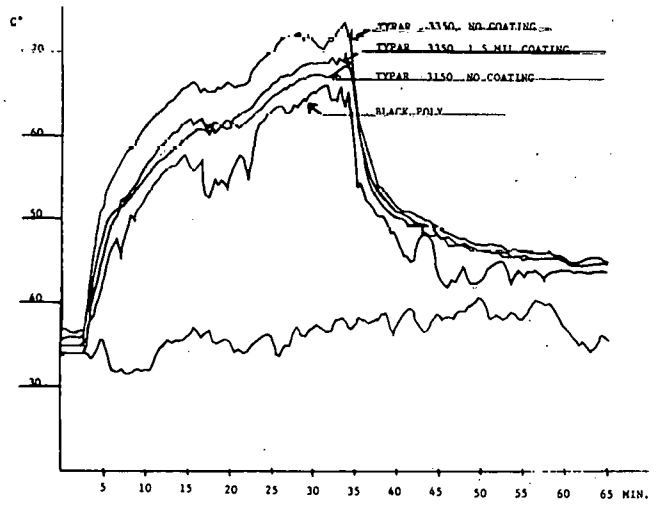

FIGURE 8 TEMPERATURE RISE IN AN ABSORPTION CHAMBER WITH FOUR ABSORBING MATERIALS

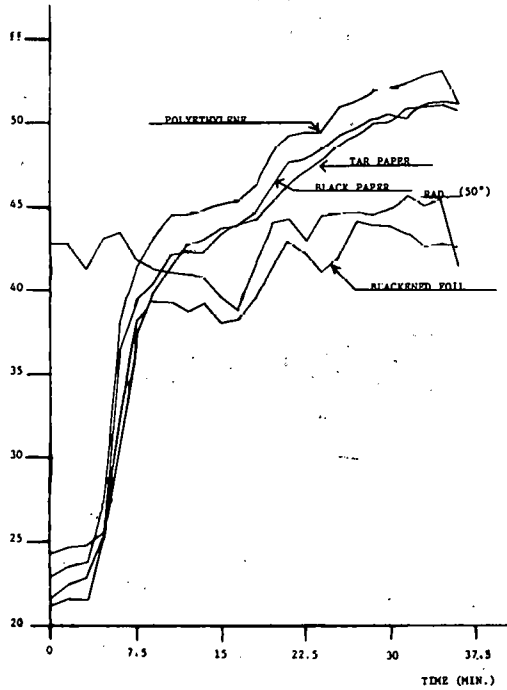

FIGURE 9 TEMPERATURE RISE IN AN ABSORPTION CHAMBER WITH FOUR ABSORBING MATERIALS

Storage Mediums

Since agricultural drying must usually proceed for 24 hours a day and solar radiation is available only 8-10 hours per day, some method of energy storage must be employed. The choice of storage media is usually between storing sensible heat in either water or rock.

In general, the choice of a storage media is dependent upon the characteristics of the solar system, the amount of energy to be stored and the costs of implementing the storage. Figure 10 compares the heat capacity and density of water, rock and iron.

FIGURE 10.

	C_p	Density
	KJ/Kg°C	Kg/m^3
Water	4.19	1000
Rock	.88	2500-3500
Iron	.50	7860

From this table it can be seen that in a given cubic foot of space about twice as much heat can be stored in water than in rock. Iron can store about 3/4 as much heat as water in the same volume. Thus, if space is the primary consideration, water is the storage media of choice.

However, the costs of using a water storage system usually exceed the costs of using a rock storage system. In addition to their low pice, rock storage units have the desirable characteristic that the heat transfer coefficient between circulating air and the rocks is high, and the conductivity of the bed is low when there is no air flow.

In constructing a rock bed, rocks from 1 to 5 cm have been used. The rocks should be uniform in size so that pressure drops will be minimized.

SOLAR DRYING OF PEANUTS IN GEORGIA

by

J. M. Troeger and J. L. Butler
Agricultural Engineers
USDA, ARS
Coastal Plain Experiment Station
Tifton, Georgia 31794

Introduction

Most peanuts grown in Georgia are normally harvested in September or early October. The plants are removed from the soil, inverted to expose the pods to the sun, and combined after 3 to 7 days of windrow curing. After they are combined, the partially cured peanuts (20-30% wet basis) are placed in a bin or wagon and dried to 10% moisture content or less with heated air. Liquified petroleum gas (LPG) is commonly used to heat the drying air, but as fossil fuel supplies dwindle alternative forms of energy become more desirable.

Production of edible peanuts requires careful drying procedures. Peanuts dried continuously at temperatures above 35°C develop an off flavor (Beasley and Dickens, 1963)[1/]. Peanut temperatures in the field, however, may reach 50°C for several hours with no loss of flavor (Butler, Pearman and Williams, 1969). Peanuts dried in the laboratory, with drying air temperatures programmed to maintain 50°C for 3 hours in a 12 hour period, developed no off-flavor (Troeger and Butler, 1972).

Split kernels, a measure of milling quality, increase when the drying air temperature exceeds 35°C. Likewise, low relative humidity may cause excessive splits. (Beasley and Dickens, 1963).

Peanuts must be dried promptly after they are removed from the soil. Interruption or delay of the drying process may encourage mold growth and increase the potential for mycotoxin development (Troeger, Williams and Holaday, 1969).

General recommendations for peanut drying include: limiting the drying air temperature to 35°C, limiting the temperature rise of the drying air above ambient to 8°C and maintaining a minimum air flow rate of 12.5 m^3/min. per m^3 of peanuts.

This paper reports the results of 2 years of research by the Agricultural Research Service, U.S. Department of Agriculture in cooperation with the Energy Research and Development Administration and the Georgia Coastal Plain Experiment Station at Tifton, The purpose of the research was to determine and demonstrate the feasibility of using solar energy for drying peanuts.

Facilities and Equipment

Facilities were constructed for comparing three methods of heating the air for drying peanuts.

1. Water was heated by solar collectors and stored in tanks, then used to heat the drying air (Figure 1). Supplementary LPG heated the air when solar heating was inadequate.

1/ Refers to appended references.

2. Air was heated by a solar collector and used directly for drying with no energy storage (Figure 2).

3. Air was heated with a conventional LPG burner.

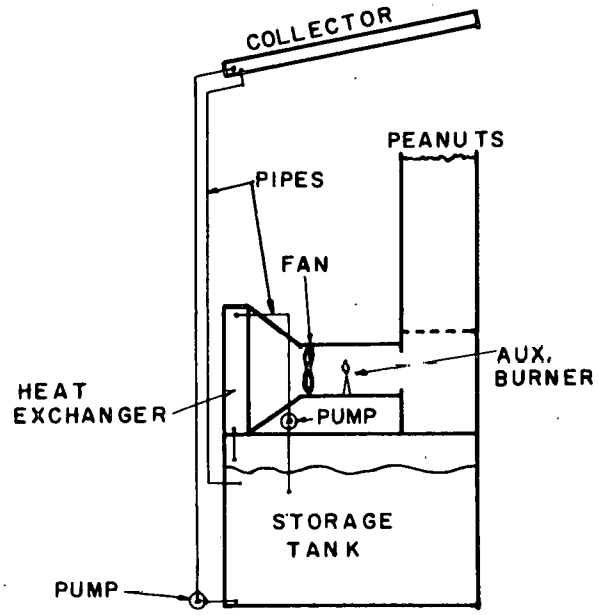

Figure 1. Schematic drawing of solar-heated-water system.

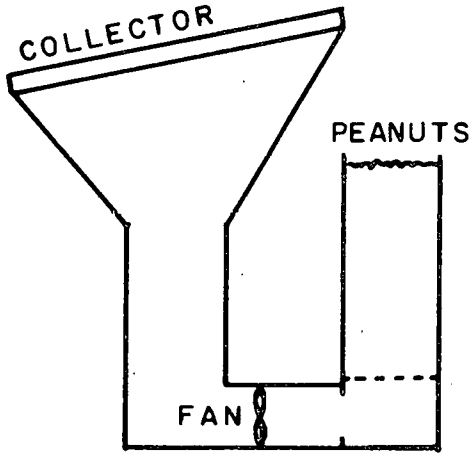

Figure 2. Schematic drawing of solar-heated-air system.

All three systems dried the peanuts in plywood model bins (0.6 x 0.6 x 1.2 m deep). Air flow through the dryers was a nominal 340 m^3/hr. Pipes and ducts connecting the components of the systems were insulated.

Solar Heated Water System

Collectors - 1975. Several types of solar collectors were constructed between the Z-bars of a steel frame building (Figure 3). Table 1 describes the components used in the collectors and gives the relative effectiveness of the collectors. All collectors, except the Roll-bond, were 11.6 m long by 1.2 m wide. The Roll-bond collector had four plates (2.4 by 0.5 m) connected in series.

Relative effectiveness was determined by running the group of collectors simultaneously on a cloudless day. The total heat gain of the water flowing through the collectors, per unit area, was measured. Temperature of the entering water was the same for all collectors.

Thermal bonding with a high-temperature grease increased the effectiveness of the galvanized pipe collector by 15%. The grease was specified to withstand temperatures to 230°C but it melted with temperatures up to 140°C when no water circulated through the collector.

Rigid styrofoam (2.5 cm thick) insulated the underside of the collectors. Without circulation, however, the styrofoam partially melted at the higher temperatures.

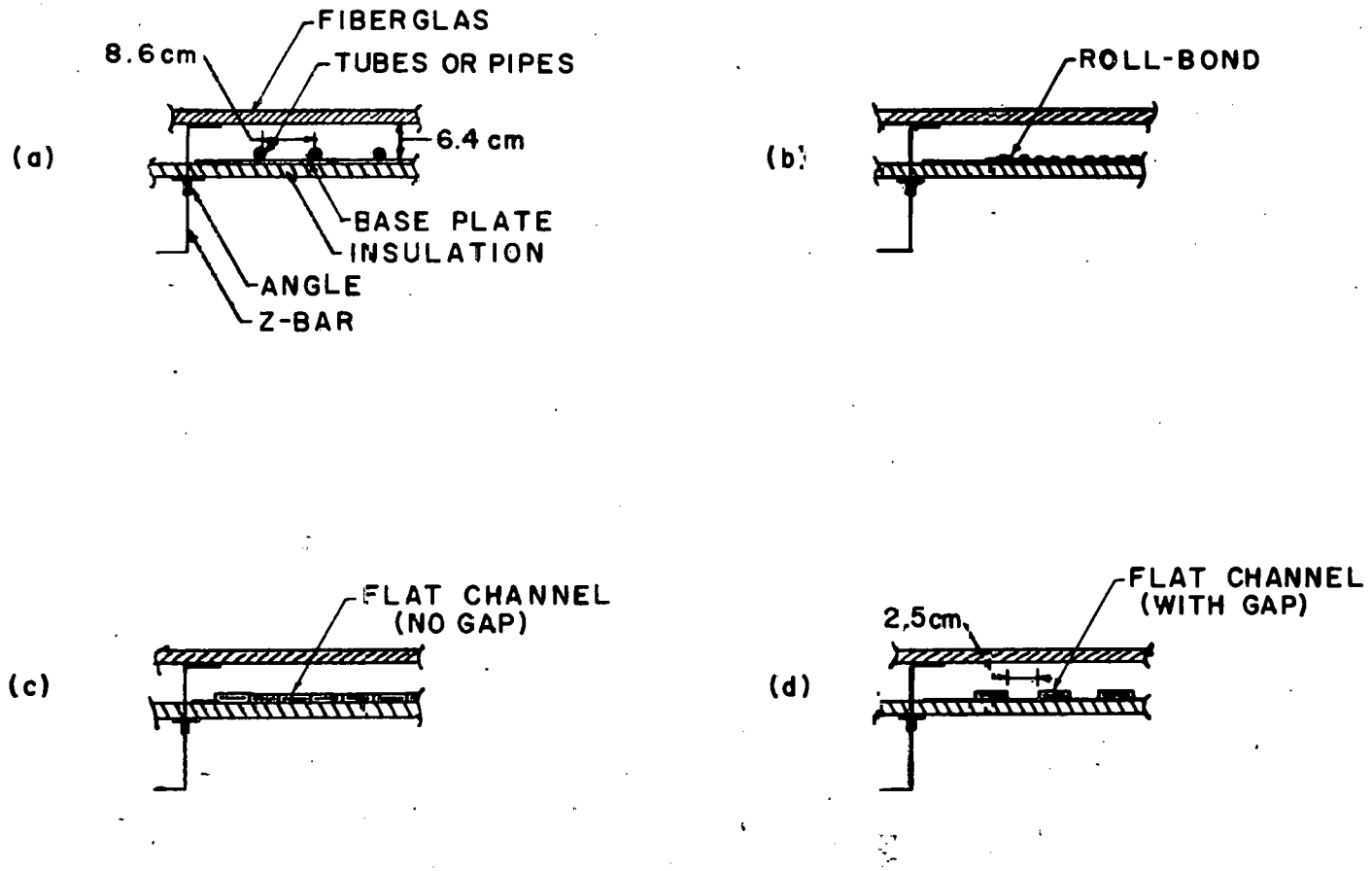

Figure 3. Schematic drawing of 1975 solar-heated-water collectors.

Table 1. Description of collector components and relative effectivness of the collectors.

Material	Dimensions (cm) Inside Tube	Spacing on Centers	Relative Effectiveness[1/]
1975			
Galvanized pipe[2/]	1.58	8.6	.73
Black pipe[2/]	1.58	8.6	.75
Copper tubing[2/]	1.12	8.6	.34
Copper Roll-bond[3/]	1.17 x .40	2.5	1.00
Flat aluminum (no gap)[4/]	4.65 x .64	5.1	.69
Flat aluminum (with gap)[4/]	4.65 x .64	10.1	1.35
1976			
Copper Roll-bond[3/]	1.17 x .40	2.5	1.00
Pipe above plate[5/]	1.58	15	.72
Pipe below plate[5/]	1.58	15	.54

1/ Effectiveness determined by measuring heat gain across collector. Roll-bond = 1.00.

2/ 1975 collectors were placed on unpainted black-iron sheet metal base (18 gage (0.12 cm)). Unpainted tubes were thermally bonded to plate with a high-temperature grease. (Figure 3a)

3/ Roll-bond plates are commercially available as an integral tube within a sheet heat exchanger (Figures 3b and 4c). Plates were painted with flat black paint.

4/ The flat aluminum channels were placed in two configurations (a) channels adjacent to one another with no gap (Figure 3c) and, (b) channels separated by a gap of 5 cm. (Figure 3d). Channels had a dull, smooth, black, painted surface. The black-iron base was unpainted.

5/ 1976 collectors were painted with smooth flat-black finish. There was no thermal bonding (Figure 4a and 4b).

One layer of Tedlar-coated, corrugated, translucent fiberglas covered the collectors. The Tedlar filtered out the ultraviolet radiation which may degrade the fiberglas over a period of time. The fiberglas, though clear when installed, became clouded after several months' exposure. The loss of translucency varied among sheets.

The roof of the building sloped 5° to the south and the collectors lay level in the east-west direction. Because of their orientation, the collector tubes could not be completely drained so several tubes burst during freezing weather.

The collector with copper tubing was less effective than the other collectors because the flexibility of the tubing prevented it from being properly spaced and from being kept in thermal contact with the base plate. The collector with gaps between the flat channels was more effective than the collector with flat channels adjacent to one another because the rough base plate surface in the gaps was a better radiation absorber than the smooth black surface of the channels.

Collectors - 1976. In 1976, the collectors were redesigned (Figure 4) and installed above the Z-bars in a north-south orientation. The slope between the ends of the collectors facilitated drainage. Collectors, except Roll-bond, were 6.6 m long by 0.9 m wide. The Roll-bond collectors contained two plates placed in series. Table 1 describes the components and the relative effectiveness of the collectors.

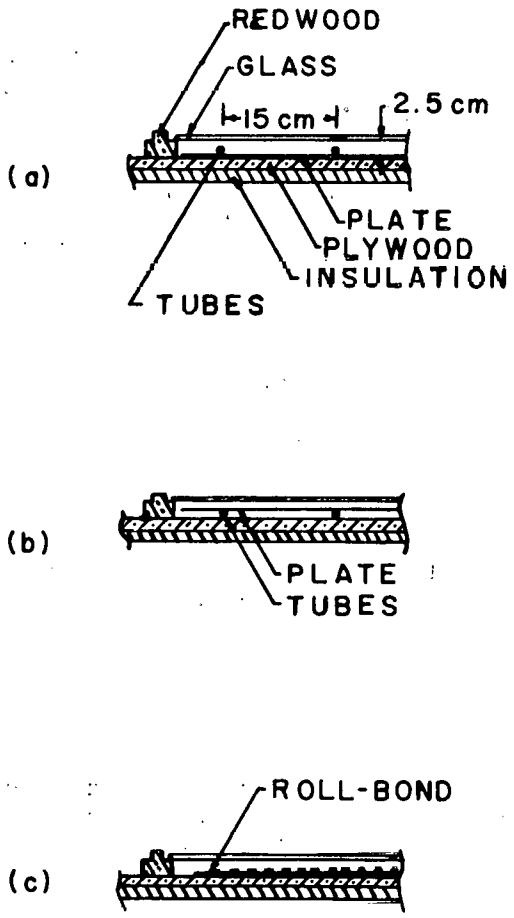

Figure 4. Schematic drawing of 1976 solar-heated-water collectors.

The collectors were insulated on the bottom by flexible fiberglas beneath a plywood base. Circulation tubes were in physical contact with the metal plate but were not thermally bonded to it. Collector surfaces were painted with a flat black paint and covered with one layer of a heat-treated, low-iron-content glass.

Energy Storage Tanks. Ten concrete septic tanks (5.3 m^3 volume) were installed for storing the solar-heated water. Six-mil (0.15 mm) polyethylene film sealed the interior of the tanks. The outsides of the tanks were insulated with 10 cm of rigid styrofoam. There was no insulation between adjacent tanks so there was considerable heat loss between adjacent tanks when there was a large temperature difference.

Controls. An on-off differential controller was used to control the circulating pumps for the collector. The pumps operated when the collector surface temperatures were 2°C or more above the temperature of the water in the bottom of the tanks.

A thermostat located after the water-air heat exchanger controlled the heat exchanger pump, limiting the heated air temperature to a maximum of 35°C. A second thermostat in the plenum beneath the drying bin limited the temperature from the LPG burner to a maximum of 35°C. Two thermostats were used because rapid cycling of the LPG burner when the temperature was near the set point would disable the heat exchanger pump if it also cycled rapidly. Temperature rise through the burner was limited to 8°C.

Solar-Heated-Air System

Galvanized sheet metal panels were riveted to the Z-bars supporting the roof of an existing building to form a duct 5 cm deep. Rigid styrofoam insulated the underside of the duct. The weathered galvanized steel roof, with no glazing, was the absorbing surface. Total collector area was 46 m^2.

Air was used directly for drying with no energy storage. Because previous studies (Troeger and Butler, 1972) have shown that short periods of high temperature do not adversely affect peanut quality, the entering air temperature was not regulated by automatic controls.

Conventional System

The conventional system used LPG to heat the drying air. The LPG burner was controlled by a thermostat in the plenum set to limit the air temperature to a maximum of 35°C. Temperature rise through the burner was limited to 8°C.

Procedure

Approximately 135 kg of partially field cured Florunner peanuts were placed in each bin at the beginning of a test. Tests of each of the three drying systems were replicated four times. A separate collector and storage tank were used for each bin in the solar-heated-water system. A single collector was used for the solar-heated-air system. Separate burners and LPG tanks were used for each bin in the solar-heated-water system and the conventional system. LPG tanks were weighed before and after each test.

Moisture samples were obtained from the top of each bin twice daily throughout each test. At the end of a test, moisture samples were obtained from both the top and bottom of the bin. Moisture content was determined by drying a 250-gram sample of whole pods at 130°C for 12 hours.

Temperatures were recorded hourly with a digital data acquisition system. Copper-constantan (Type T) thermocouples sensed temperatures throughout the system. Energy use was calculated from the temperature rise of the air and the rate of air flow. Air flow rate was measured with a hot wire anemometer.

At the end of each test the Federal-State grading procedure was used to determine the percentage of sound splits in 500 gram samples taken from the top and bottom of each bin. The percentage of sound splits is a measure of milling quality and of the harshness of the temperature treatment during drying.

Peanuts remained on the dryers of the solar-heated-water system and the conventional system until dry (40-60 hours). Peanuts remained on the solar-heated-air dryers for three days of solar radiation. Then, if they were not dry (<10%), they were placed on the conventional dryers to finish drying. Only one solar-heated-air test (76-5) was completed without using LPG.

Six tests were completed on the dryers, one in 1975 and five in 1976. Solar energy contributed a significant portion of the total energy used to heat the air.

Data were statistically analyzed with analysis of variance using a completely randomized design (Ostle, 1954). Comparison among individual systems was made by subdividing the treatment sum of squares into its component parts, each

representing a single degree of freedom. The F-test was used to determine significance.

Results

Energy Use

Solar-heated-water system. With energy storage, this system used about 60% solar energy to maintain the temperature of the drying air (Table 2). There was little variation in percentage of solar energy among the tests. The specific energy input (SEI) (kJ/gram water removed) varied with initial moisture content and with minimum ambient temperature (Figures 5 & 6). SEI for this system was significantly different (at 5% probability level) from that for the conventional drying system in all tests.

Table 2. Specific energy input (SEI) and drying conditions.

Test	Min. Amb. Temp. °C	In. Moist. % w.b.	Avg. Daily Rad. ly[1/]	SEI kJ/g			% Solar	
				Solar Water	Solar Air	Conven.	Solar Water	Solar Air
75-1	18	23	382	9.2a[2/]	4.4b	5.1b	70	86
76-1	18	21	323	-----	5.9a	8.6b	--	22
76-2	19	29	242	9.7a	6.0b	7.3c	61	30
76-3	14	28	434	7.0a	4.9b	---	59	63
76-4	19	19	271	12.0ab	13.0a	10.4b	64	45
76-5	11	29	420	5.5a	3.3b	4.9c	56	100

1/ Langley (ly) = gram calorie per square centimeter. Values are total radiation (direct + diffuse) measured on a horizontal surface by an Eppley pyranometer (Model 50).

2/ Numbers with the same letter horizontally are not significantly different at the 5% probability level. Vertical columns are not comparable.

Solar-heated-air system. Without energy stoage, this system could completely dry the peanuts only during periods of high solar radiation levels. Among all of the tests with the aolar-heated-air system, about 50% of the energy to heat the drying air came from solar energy (Table 2).

Except for test 76-4 (Table 2) the SEI (including LPG input) was significantly less (at 5% probability level) for the solar-heated-air system than for either the solar-heated-water system or the conventional system.

Effect of initial moisture and minimum temperature. SEI was higher with lower initial moisture content (Figure 5). The last molecules of water within the kernel are more tightly bound than the first molecules and require more energy to remove (Henderson and Pabis, 1961). The difference between the vapor pressure in the kernel and that of the surrounding air becomes less as the moisture decreases.

SEI was less with lower minimum ambient temperature (Figure 6). At a low minimum ambient temperature, the vapor pressure of the air is low. When the vapor pressure of the air is low, the difference between the vapor pressure of the kernel and the air is increased, therefore less energy is required to remove the moisture from the kernel than when the vapor pressure difference is low.

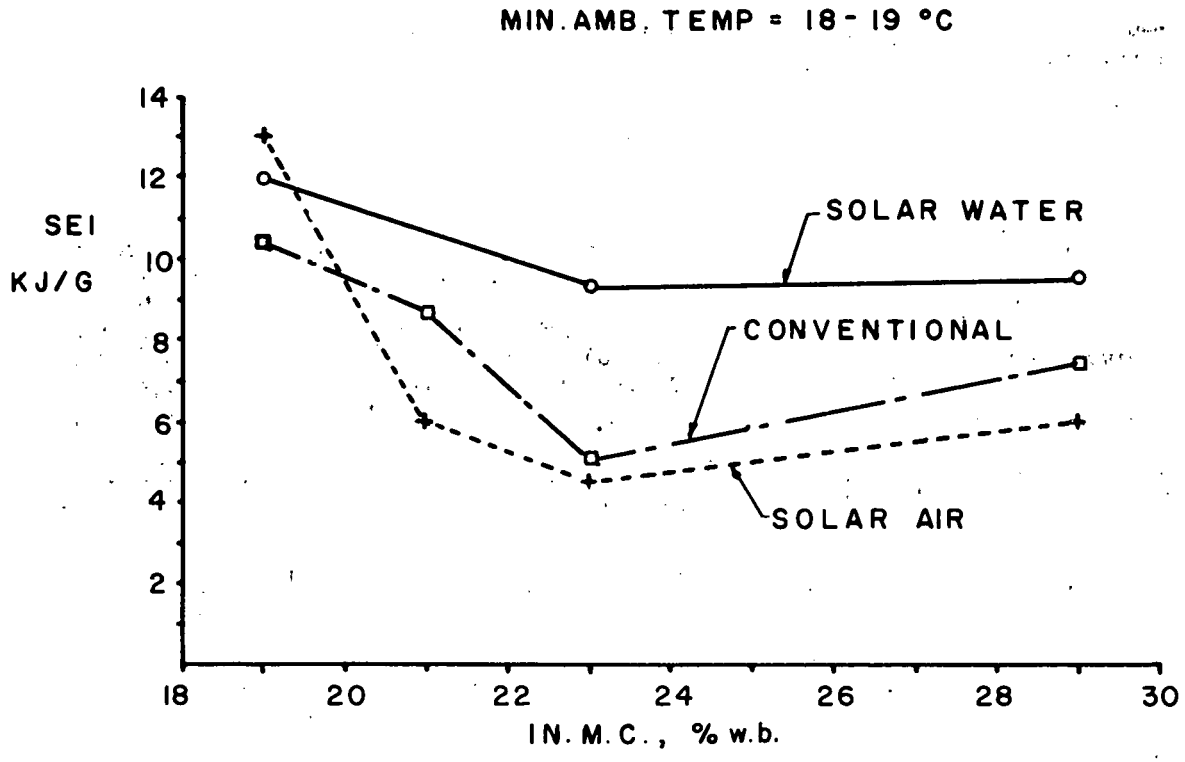

Figure 5. Effect of initial moisture on specific energy input.

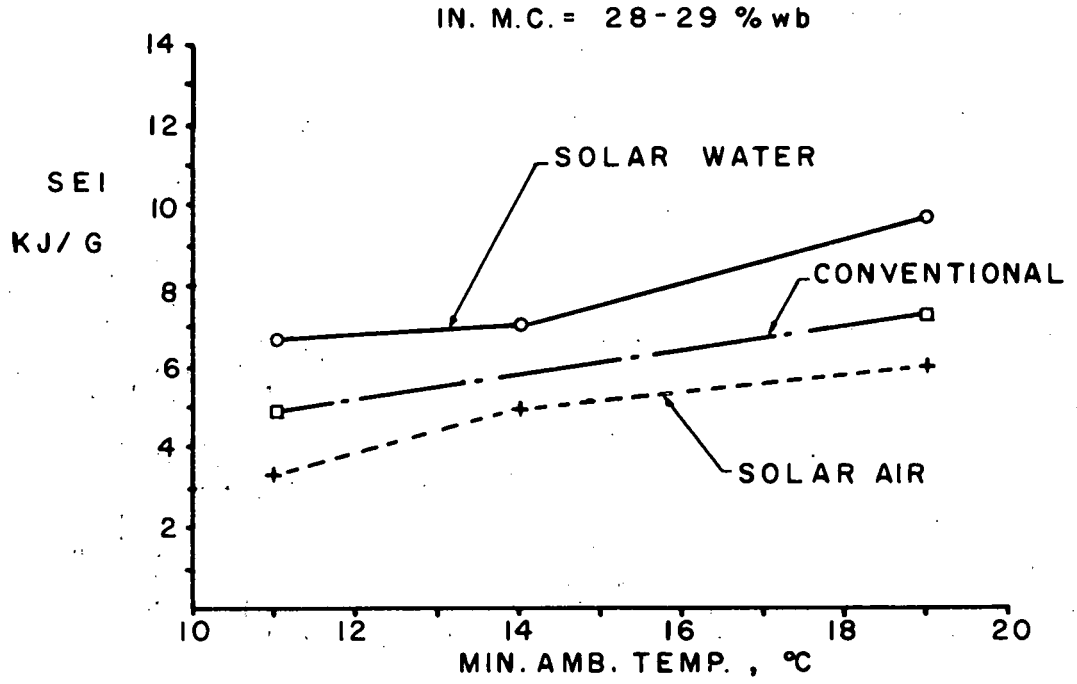

Figure 6. Effect of minimum ambient temperature on specific energy input.

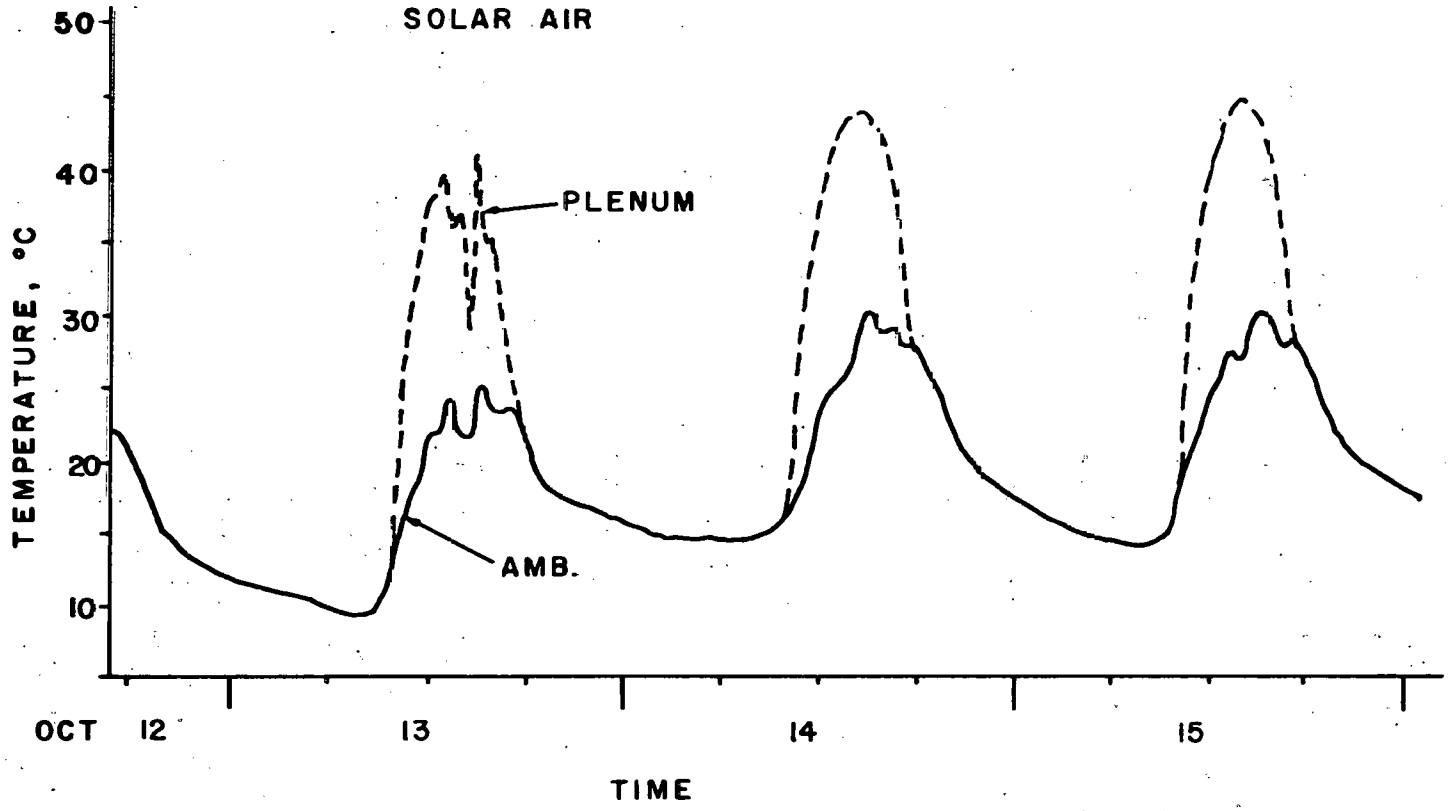

Figure 7. Typical temperature pattern for solar heated-air dryer.

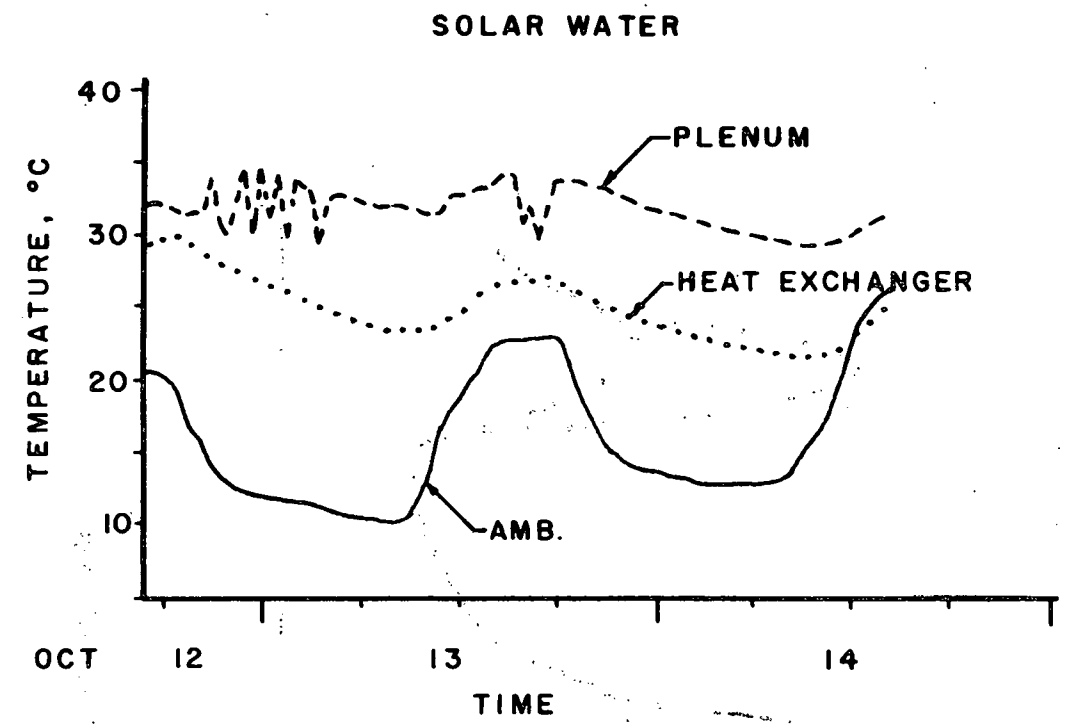

Figure 8. Typical temperature pattern for solar-heated-water dryer.

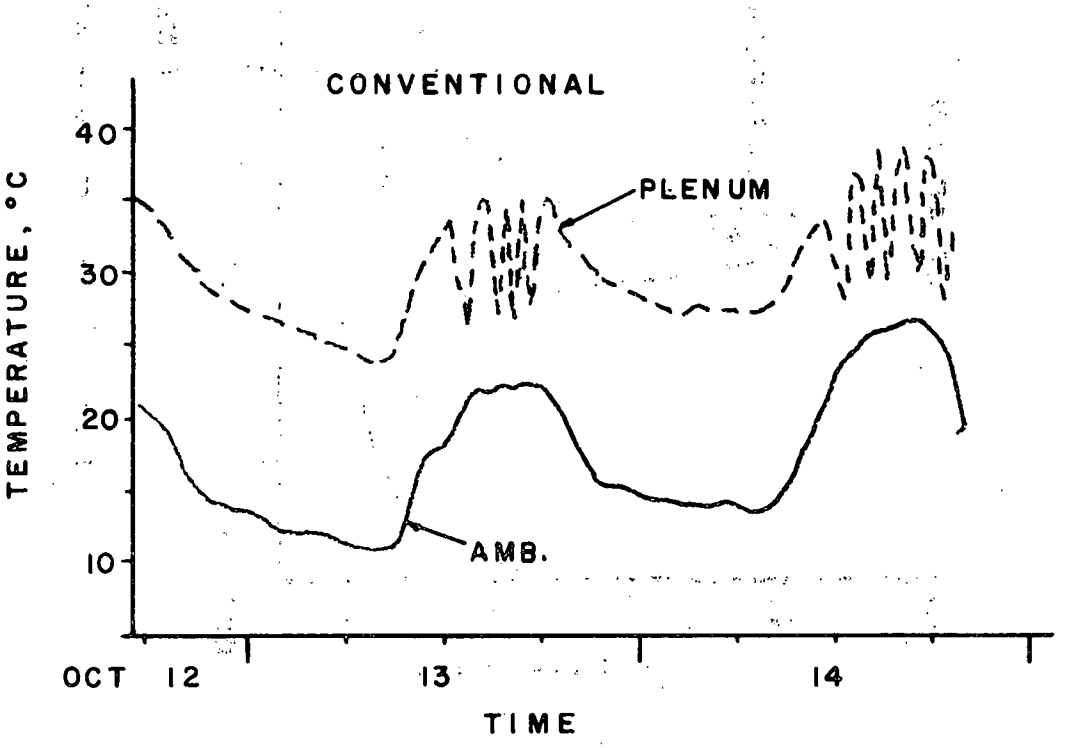

Figure 9. Typical temperature pattern for conventional dryer.

Equations predicting SEI from initial moisture and minimum ambient temperature were developed using multiple regression analysis for each system:

Solar-heated-air system

$$SEI = -.1006 + .0464\ M_o + .295\ T$$

Solar-heated-water system

$$SEI = 7.811 - .208\ M_o + .393\ T$$

Conventional system

$$SEI = 9.230 - .255\ M_o + .248\ T$$

where M_o = initial moisture content, % wet basis

T = minimum ambient temperature, ^{o}C

Drying Time

There was no significant difference (at 5% probability level) between the drying time with the solar-heated-water system and the conventional system. The solar-heated-air system required about twice as long to dry the peanuts as did either of the other systems.

Temperature

The solar-heated-air system with no controls recorded the highest drying air temperature ($44^{o}C$) (Figure 7). The high temperature, however, occurred for only a few hours each day, so the plenum temperature was near ambient most of the time.

The solar-heated-water system increased the temperature of the drying air by as much as $22^{o}C$, when the ambient temperature was low (Figure 8). The high temperature rise occurred because there was no limit on the temperature rise through the heat exchanger if the heated air temperature remained below $35^{o}C$. When the ambient temperature dropped to $10^{o}C$ and the water in the tank was $25^{o}C$, the temperature rise was nearly $15^{o}C$ from solar energy, plus an additional $8^{o}C$ from LPG, without exceeding the $35^{o}C$ maximum temperature.

A typical temperature pattern for the conventional system is given in Figure 9.

When the drying air temperature was near the set point of the thermostat, the LPG burner cycled every few minutes. Since temperatures were recorded only hourly, the plots in Figures 8 and 9 present a distorted picture of the drying air temperature record.

Milling Quality

There were no significant differences (at 5% probability level) within tests, among the percentages of split kernels, in peanuts dried by the three drying systems. However, the percentages of split kernels varied widely among tests because of windrow and harvest conditions (Table 3).

The difference between the percentages of split kernels in the top and bottom of the bin was significant (at 5% probability level) for all three drying systems. Peanuts in the top of the bin had about 25% less split kernels than the peanuts in the bottom of the bin. Harsh temperature conditions of the air entering the bin were moderated as the air moved up through the bin.

Table 3. Milling quality.

Test	Percent Sound Split Kernels					
	Solar Water		Solar Air		Conventional	
	Top	Bottom	Top	Bottom	Top	Bottom
75-1	2.5a[1/]	3.1a	2.1a	2.5a	2.3a	2.3a
76-1	---	---	1.1a	1.6b	1.5b	1.5b
76-2	2.1a	2.5a	3.1b	3.7c	2.3a	2.2a
76-3	2.2ab	3.7c	1.7a	2.6b	---	---
76-4	1.7a	2.5bc	2.1ab	2.8c	2.0a	2.6bc
76-5	2.7a	4.5c	2.5a	3.8b	2.4a	4.0bc

1/Samples with the same letter horizontally are not significantly different at the 5% probability level. Vertical columns are not comparable.

Summary and Conclusions

Tests showed that solar energy can be used to supply 50 to 60% of the energy needed for heating the air used for drying peanuts. If the energy is stored for use when the sun is not shining, the drying time can be comparable to that for conventional drying. Specific energy input varied widely, depending on initial moisture, ambient conditions and the drying time.

Although the peanuts dried by the solar drying systems were subjected to harsher temperature conditions than those dried by the conventional system, the milling quality, as measured by the Federal-State grading procedure, showed no significant differences.

Results of this study showed the importance of selecting materials and using design techniques such that a solar collector will operate efficiently and withstand adverse temperatures when not operating.

References

Beasley, E. O., J. W. Dickens. 1963. Engineering research in peanut curing. Tech. Bulletin No. 155. N. C. Agricultural Experiment Station, Raleigh, N.C.

Butler, J. L., G. E. Pearman, E. J. Williams. 1969. Effect of windrow configuration on temperature, drying rate and uniformity of moisture content of peanuts. Journal American Peanut Research and Education Association. 1:54-57.

Henderson, S. M., S. Pabis. 1961. Grain drying theory - temperature effect on drying coefficient. J. Ag. Engr. Res. 6(3):169-174.

Ostle, B. 1954. Statistics in research. Iowa State University Press. Ames, Iowa.

Troeger, J. M., E. J. Williams, C. E. Holaday. 1969. Aflatoxin incidence in peanuts as affected by harvesting and curing procedures. Journal American Peanut Research & Education Association. 1:62-67.

Troeger, J. M., J. L. Butler. 1972. Curing peanuts with periodic high temperatures. Journal American Peanut Research & Education Association. 4:82-88.

EVALUATION OF MATRIX SOLAR COLLECTOR FOR HEATING AIR

by

Bobby L. Clary, P.E., and Ronnie G. Morgan
Associate Professor and former Graduate Research Assistant
Agricultural Engineering Department
Oklahoma State University
Stillwater, Oklahoma 74074

Introduction

The results presented in this paper are part of an overall project on drying and curing peanut pods with solar energy. One paper titled "Drying and Curing Spanish Pods With Solar Energy" describes results of the peanut drying studies and was presented before the American Peanut Research and Education Association in Dallas, Texas, in June 1976.

Many solar collectors being promoted for their high efficiencies are either complex in construction and/or have moderate to high initial costs. Therefore, it is desirable to design a low-cost, efficient solar collector that may be easily constructed.

In most solar collectors for heating air, there is only one layer of absorbing material facing the sun and therefore heat transfer area is usually low. With air, heat transfer coefficients are low, thus requiring large plate temperatures for collection of substantial quantities of energy. These large plate temperatures increase collector heat losses to the atmosphere and therefore reduces the overall collector efficiency.

Utilization of porous matrices as an absorber for solar collectors offers several advantages. First, such matrices have high heat transfer area to volume ratios, usually accompanied by high heat transfer coefficients. Higher heat transfer rates, due to larger area to volume ratio, results in reduced operating temperatures. A collector operating with low temperature differences will have less heat loss and hence higher efficiency.

As implied above, an efficient low-cost collector design might be one in which a matrix of porous media is used as the absorber. One problem is to select a low-cost durable porous material that may be easily installed in solar collectors. Duralast filter material is a non-metallic, porous material that satisfies these requirements and has several additional advantages. It is lightweight, flexible, readily obtained in large quantities, and non-corrosive. The term matrix is used throughout this report to refer to a layer or bed of porous media having interconnecting voids.

Accurate theoretical analysis of a matrix solar collector design provides the means of evaluation and prevents costly construction and testing of additional models and prototypes. However, most available analytical solutions to heat transfer in matrix collectors have required complicated manipulations of differential and integral equations. Solutions to these equations are usually obtained by numerical analysis techniques with the aid of a digital computer. Thus, there is a need to develop a simplified method to theoretically evaluate the performance of a matrix solar collector for providing energy for drying peanut pods.

Therefore, this paper presents the results and validation of a simplified theoretical technique for predicting the performance of matrix absorbers for use in drying peanut pods. Validation of the results were obtained from experimental tests conducted on laboratory models while drying farmers' stock peanut pods and by comparing the simplified analysis with results of rigorous analyses available in the literature.

Development of Collector Theory

Several assumptions were made to reduce mathematical relationships governing flow and heat transfer characteristics of the matrix solar collector. It was assumed that axial and horizontal conduction through the non-metallic porous bed could be neglected. The bed was assumed to be a gray non-scattering body and to have a constant absorption coefficient. The bed was considered to have a one dimensional steady-state temperature distribution within an isotropic porous media. Only direct radiation effects were considered. However, diffuse radiation also contributes to solar radiation and can become significant in an overcast sky.

Because of low temperature differences between the matrix lower surface and the outlet air and between the outlet air and the front side of the collector back plate, heat transfer by radiation between these parts was neglected. Heat is transferred to air by convection as it makes contact with the top matrix surface. However, most of this air passes directly into the matrix where it is heated as it makes contact with the matrix interior. No attempt was made to separate convection heat transfer on the top of the matrix surface from that occurring within the matrix bed.

Absorption of radiation by a partially transparent media can be described by Bouger's Law (3), which is based on the assumption that absorbed radiation is proportional to local intensity in the media and distance radiation traveled through the media and is given by the equation:

$$dI = \beta I dx \qquad [1]$$

Integrating the above expressions between the bed depth limits of 0 and L yields

$$I_L/I_0 = e^{-\beta L} \qquad [2]$$

The ratio I_L/I_0 is used to determine the amount of solar radiation passing through the matrix layer unabsorbed.

Neglecting axial conduction, an energy balance on a fluid element within the bed becomes

$$G\, C_p \frac{\partial T_f}{\partial x} - h_{vx} (T_{bx} - T_{fx}) = 0 \qquad [3]$$

and neglecting diffuse radiation effects, an energy balance on the bed element (Figure 1) yields

$$\tau_c I_0 e^{-\beta x} - h_{vx} (T_{bx} - T_{f_x}) - \sigma E_{gx} (T_{bx}^4 - T_c^4) = 0 \qquad [4]$$

Equation 3 can be integrated from x = 0 to x = L yielding

$$G\, C_p (T_{fl} - T_{fo}) - L\, h_{va} (T_{ba} - T_{fa}) = 0 \qquad [5]$$

where T_{ba} and T_{fa} are average bed and fluid temperatures, respectively, and h_{va} is defined as $1/L \int_0^L h_{vx}dx$. Integrating equation 4 with the same limits of x yields

$$\tau_c I_0 \ (1 - e^{-\beta L}) - Lh_{va} \ (T_{ba} - T_{fa}) - \sigma \int_0^L E_{gx} \ (T_{bx}^4 - T_c^4) \ dx = 0 \quad [6]$$

The energy balance on the bed element is shown in Figure 1. Because of complexity and difficulty in determining E_{gx} for this type of matrix material, it was assumed that

$$\int_0^L E_{gx} \ (T_{bx}^4 - T_c^4) \ dx$$

may be approximated by

$$e_g \ (T_{ba}^4 - T_c^4)$$

where e_g is the radiant interchange factor between two parallel plates and T_{ba} is average bed temperature. This assumption means that reradiation from all points within the matrix layer to the cover was approximated by assuming the matrix a flat plate at average bed temperature. Recall that e_g is expressed as

$$e_g = \frac{1}{1/e_b + 1/e_c - 1} \quad [7]$$

Equation 3 and 4 must satisfy the boundary condition

$$T_{fx_{x=0}} = T_{fo} \quad [8]$$

where T_{fo} is temperature of fluid entering the matrix layer. The above boundary condition and use of the Stefan-Boltzmann constant introduces convenient parameters which lead to the following dimensionless terms.

T_{fo}^* = Dimensionless temperature ratio, $T_{fo}/T_{fo} = 1$

T_{fl}^* = Dimensionless temperature ratio, T_{fl}/T_{fo}

T_{ba}^* = Dimensionless temperature ratio, T_{ba}/T_{fo}

T_{fa}^* = Dimensionless temperature ratio, T_{fa}/T_{fo}

T_c^* = Dimensionless temperature ratio, T_c/T_{fo}

τ = Optical depth, βx

θ = Dimensionless volumetric heat transfer coefficient, $h_{va} \ T_{fo}/\beta\sigma T_{fo}^4$

Γ = Dimensionless mass flow rate, $G \ C_p \ T_{fo}/\sigma T_{fo}^4$

ψ = Dimensionless direct solar radiation, $I_0/\sigma T_{fo}^4$

Substituting the dimensionless term into equation 5 and 6 produces the dimensionless equations

$$\Gamma\ (T_{fl}^* - 1) - \tau\theta(T_{ba}^* - T_{fa}^*) = 0 \qquad [9]$$

$$\tau_c\psi\ (1 - e^{-\tau}) - \tau\theta(T_{ba}^* - T_{fa}^*) - e_g\ (T_{ba}^{*4} - T_c^{*4}) = 0 \qquad [10]$$

Values of G, C_p, I_o, T_c, e_g and τ are usually given or can be easily determined by measuring bed depth and the average matrix extinction coefficient. For this study, matrix inlet air temperature, T_{fo}, was assumed to be equal to temperature of atmospheric air, which is known for a given condition. This allows calculation of corresponding values of ψ. Values of the dimensionless volumetric heat transfer coefficient, θ, in equation 9 and 10 are usually unknown because of the difficulty of determining the volumetric heat transfer coefficient (h_{fva}). However, since dimensionless flow rate, Γ, is known, the term $\Gamma\ (T_{fl}^* - 1)$ in equation 9 can be substituted directly into equation 10 for $\tau\theta\ (T_{ba}^* - T_{fl}^*)$ yielding the following equation.

$$\tau_c\psi\ (1 - e^{-\tau}) - \Gamma\ (T_{fl}^* - 1) - e_g\ (T_{ba}^{*4} - T_c^{*4}) = 0 \qquad [11]$$

Equation 11 has three unknowns, T_{fl}^*, T_{ba}^*, and T_c^*. Assumptions must be made to reduce the number of unknowns to one, T_{fl}^*.

Because of the collector design to insure that cool incoming air is always in contact with the collector surface, temperature of the cover plate was assumed equal to temperature of the ambient air, $T_c = T_{fo}$. This yields a value of $T_c^* = 1$.

Preliminary experiments with the test model indicated that bed temperatures at depths of 0.0381m were usually within 1K of fluid leaving the matrix. Hamid and Beckman's (5) study of heat transfer in porous beds indicates that average theoretical bed temperature can be approximated to be equal to fluid temperature leaving the bed. This assumption contains an error of 3-5% for the range of flow rates and optical depths used in this study. From the above analogy, T_{ba} is approximated by T_{fl} and hence $T_{ba}^* = T_{fl}^*$.

Substituting these approximations into equation 11 yields an equation with only one unknown, T_{fl}^*, and can be implicitly solved by successive iterations.

$$\tau_c\psi\ (1 - e^{-\tau}) - \Gamma(T_{fl}^* - 1) - e_g\ (T_{fl}^{*4} - 1) = 0 \qquad [12]$$

Bed efficiency was calculated from the following equation and is designed as a ratio of actual temperature rise to maximum temperature rise.

$$\eta_b = \frac{\Gamma\ (T_{fl}^* - 1)}{\tau_c\psi} \qquad [13]$$

Assuming fluid properties can be evaluated at an average temperature of T_{fl}, the temperature of the air leaving the collector, and T_{fe}, the following energy balance yields a direct solution for T_{fe}.

$$\Gamma\,(T_{fe}^{*} - 1) = \Gamma\,(T_{f1}^{*} - 1) + \tau_c \psi e^{-\tau} - \left(\frac{T_{f1}^{*} + T_{fe}^{*}}{2} - 1\right) \qquad [14]$$

The term $\tau_c \psi e^{-\tau}$ in equation 14 represents the amount of radient energy passing through the matrix unabsorbed. For relatively thick layers of matrices with moderate extinction coefficients this term usually represents a small portion of total radiation available at the bed's top surface.

After solving equation 14 explicitly for T_{fe}^{*}, overall collector efficiency can be calculated using equation 15.

$$\eta_c = \Gamma \frac{(T_{fe}^{*} - 1)}{\psi} \qquad [15]$$

Collector efficiency is defined as the ratio of heat gained by air passing through the collector divided by total available insolation normal to the collector's surface.

Results of the Study

Matrix Porosity and Density

One of the important physical characteristics of a porous media (matrix) is porosity. Total porosity of a matrix is defined as the ratio of void volume to total volume. Effective porosity, however, is the ratio of the interconnected void volume to the total volume (9). The matrix used in this study, Duralast filter media, was unconsolidated (interconnected voids) and therefore assumed to have equal total and effective porosities.

Equation 16 was used to calculate matrix porosity from the experimental data in Table I.

$$\lambda = \frac{V_t - V_w}{V_t} \qquad [16]$$

Calculated values of porosity from the experimental data are also listed in Table I. The average porosity was found to be 0.955 and all experimental values are within 0.31% of the average. Also listed in Table I is the apparent or bulk density and the specific density of the matrix material. Porosity is the only matrix physical property used in theoretical evaluation of the solar collector.

Matrix Friction Loss Characteristics

In a matrix solar collector, friction loss through the absorber is usually a large percentage of the total friction loss through the collector. Therefore, in most cases, knowledge of matrix friction loss characteristics is adequate for collector evaluation.

Data for friction loss through Duralast filter media are shown in Table II. The Reynolds number, Re, and Fanning friction factor, f, listed in Table II were calculated using the hydraulic radius of the matrix as the length dimension. The average matrix filament diameter was measured to be 0.0284cm. This value was the average of ten random samples with diameters ranging from 0.0213cm to 0.0368cm.

A plot of Reynolds number versus friction factor is plotted in log-log space in Figure 2. A least squares regression analysis of the data in rectangular, semi-log and log-log coordinate systems indicated that log-log coordinates yielded the best fit. The friction factor is defined by the following equation.

$$f = 42.4\ Re^{-0.464} \qquad [17]$$

The regression correlation coefficient was 0.923 with a standard deviation of 1.10.

Chiou (1) studied the effects of Reynolds number on friction loss through slit-and-expanded aluminum-foil matrices. One type of matrix used in his study had a porosity of 0.962, very similar to that of Duralast filter media with the porosity of 0.955. Results of this study were compared with results from Chiou's study for Reynolds numbers between 3.0 and 30.0. Friction loss coefficients for Duralast filter media were found to be 2.0-4.0 times as high as those for Chiou's matrix material. Coppage and London (2) reported for wire-screen matrices, that St $Pr^{2/3}$ was of the order f/10 indicating the heat transfer capability of Duralast filter media is 2.0-4.0 times that of the aluminum-foil matrix used by Chiou (1).

Average Extinction Coefficient

The extinction coefficient, β, is defined as the slope of the curve of the logarithm ratio of emerging to incident energy versus thickness of the matrix. A least squares linear regression analysis on experimental data is plotted in Figure 3 and yields an average extinction coefficient of 187.8 m^{-1} with a regression correlation coefficient of 0.992 and standard deviation of 0.281. Theoretically, the intercept coefficient of 0.954 in Figure 3 should be 1.0; however, this difference is partially due to experimental error encountered in measuring bed depth and in the transient characteristics of the solar system. Bed thicknesses exceeding 0.038m absorbed over 99.9% of incident radiant energy.

Transmittance of the six mil polyethylene cover was measured and yielded an average value of 0.885. These data produced a standard deviation of 0.009. In their study of greenhouse covering materials, Duncan and Walker (4) list values of 0.85-0.88 for effective transmittance of six mil clear polyethylene. These values agree quite well with those measured in this study.

Matrix Solar Collector

Equations 11, 12, 13, 14 and 15 were solved simultaneously for atmospheric conditions similar to those encountered in actual experiments. Listed below are numerical values of environmental conditions and collector physical parameters used in the theoretical collector analysis.

$e_b = 0.95$

$e_c = 0.90$

$\tau_c = 0.885$

$T_{fo} = 305.2\ K$

$I_o = 916\ w/m^2$

$A_L = 1.58\ m^2/m^2$

$$U_L = 1.68 \text{ w/(m}^2\text{-K)}$$

$$\psi = I_o/\sigma T_{fo}^4 = 1.87$$

$$\phi = A_L\ U_L\ T_{fo}/\sigma T_{fo}^4 = 1.65$$

Results of the theoretical analysis showing effects of dimensionless flow rate on bed and collector efficiencies are shown in Figure 4. At a dimensionless flow rate of 31.2, bed efficiency is 13.3% higher than collector efficiency. Figure 4 illustrates that increasing dimensionless flow rate beyond 20 results in little increase in bed or collector efficiency.

A least squares regression analysis was used to fit experimental data on rectangular, semi-log, and log-log coordinates. Comparison of the regression correlation coefficient, coefficient of variance, standard error, and F statistic in analysis of variance of regression coefficients were used to select best fit equations to represent observed data.

Table III is a condensed record of experimental data recorded during prototype studies conducted in June 1976. Insolation during any test varied not more than 8% from its average value over the test period. Insolation for all tests ranged from 793 w/m^2 to 985 w/m^2 while ambient temperature varied from 25.8 °C to 33.9 °C. The average dimensionless insolation, ψ, in Table III, is 1.87 and equals the value used in the theoretical analysis. Average ambient temperature of observed data was 31.2 °C. This compares quite well to the value of 32.0 °C used for theoretical analysis.

A plot of observed data for collector efficiency as a function of dimensionless flow rate is shown in Figure 5. Equation 18 is the empirical equation selected to fit the data.

$$\eta_c = 57.7\ (1 - e^{-0.148\Gamma}) \qquad [18]$$

The above equation was selected because it satisfied the boundary condition, $\eta_c = 0$ at $\Gamma = 0$, and fit the data quite well. Analysis indicated a regression correlation coefficient of 0.971 and a standard deviation of 2.62.

Theoretical collector efficiencies are also plotted in Figure 5. Predicted collector efficiency fit the observed data for dimensionless flow rates less than 5.0. However, as dimensionless flow rates increase above 5, error in predicting collector efficiency increased. It appears that accuracy of predicting collector efficiency is related to collector flow rate. Before an attempt to identify sources of error, experimental data from another reference was used to further test accuracy of the analytical solution (5).

Hamid and Beckman's (5) study of performance of air-cooled radiatively heated screen matrices dealt with a similar design as the one used in this study. A small test box was constructed and two different specimens of stacked wire screens were subjected to collimated radiant flux and a normal flow of atmospheric air. They compared their experimental data with analytical results from previous research (6) on transpiration cooling of radiatively heated porous beds. Figure 6 illustrates the accuracy they obtained in analytically predicting matrix bed efficiency as a function of collector dimensionless flow rate.

Using the theoretical analysis developed earlier, bed efficiency of Hamid and Beckman's (5) matrix was calculated and is shown in Figure 6. The same boundary conditions were used in both studies. However, their analysis considered both direct and diffuse radiant flux and treated them separately. The solution developed in this study considered a total incident radiant flux equal to the

combined value of direct and diffuse radiation used by Hamid and Beckman (6).

Comparison of the curves in Figure 6 was used to verify the assumptions and approximations presented earlier for calculated bed efficiency. However, prediction of collector efficiency, as described earlier, using these assumptions results in considerable error, as much as 24%.

One source of error could arise from the assumption of one-dimensional steady flow normal to the matrix. Location and size of inlet ports around the collector parameter causes non-uniform air flow through the matrix bed. Turbulence of air at high velocities as it passes through inlet ports results in a three-dimensional flow regime through the matrix. This causes non-uniform horizontal temperature gradients and heat flow through the matrix by conduction and convection.

Another possible factor resulting in large prediction errors at high flow rate is that the triangular-shaped plenum inlet was designed for low to moderate flow rates. This results in non-uniform air flow when flow rate varies widely from its original design condition. Non-uniform air flow through the matrix will create "hot spots" or concentrated areas of high temperature, thus causing excess heat loss by reradiation and convection to the collector cover.

Another probable cause for prediction error could be the lack of air flow through the matrix in the corners and in narrow widths adjacent to collector side walls. No attempt was made in the analytical solution to account for the lack of air flow through portions of the matrix. In summary, non-uniformity of air flow through the matrix is probably the most important factor that affects accurate prediction of collector performance. As collector sizes increase to prototype size rather than experimental models, these errors will likely decrease.

Experimental data and the analytical solution showing effects of dimensionless flow rate on collector outlet temperature ratio are plotted in Figure 7. Data were transformed to log-log coordinates and least squares regression was used to determine the coefficients in equation 19.

$$T_{fe}^* = 1.18\Gamma^{-0.0382} \qquad [19]$$

The regression correlation coefficient and standard deviation are 0.945 and 0.007, respectively.

Figure 8 shows the effect of dimensionless temperature ratio, T_{fe}^*, on collector efficiency. A second degree polynomial was found to produce the best fit equation. However, one should use equation 20 with caution when extrapolating beyond the range of this study.

$$\eta_c = 4829\ T_{fe}^* - 2404\ (T_{fe}^*)^2 - 2367 \qquad [20]$$

The regression correlation coefficient and standard deviation for equation 20 are given in Figure 8.

Summary and Conclusions

A matrix solar collector for drying peanut pods was designed and constructed for an initial materials cost of $\$20.00/m^2$. A series of tests were conducted to evaluate physical properties of 1.91cm Duralast filter media being used as the absorber. Experiments were also conducted to obtain actual data on collector efficiency. Collector flow rates ranged from 0.30 to 2.52 $m^3/(min\text{-}m^2)$. These data were used to verify a theoretical analysis of the collector.

The following conclusions were based on interpretation of observed and analytical data analysis conducted during this study. Caution should be taken when extrapolating values beyond the scope of this study.

1. Bed efficiency was theoretically predicted with 94% accuracy.

2. Collector efficiency of the design used in this study was theoretically predicted with a maximum error of 24%. However, error in predicting collector efficiency decreased with flow rate.

3. The simplified theoretical analysis can be used to evaluate matrix solar collector performance for flow rates less than 0.15 $m^3/(min\text{-}m^2)$ with a maximum error of 16%.

4. The collector design utilizing a 1.91cm layer of Duralast filter media for a matrix absorber yielded a low-cost ($20/$m^2$) efficient (maximum efficiency of 60%) solar collector that may be used for drying agricultural crops.

5. A solar peanut drying system using matrix solar collectors can become economically feasible if other uses are found for the collector during the off-drying season.

6. The collector was successfully incorporated into a peanut drying operation and utilized over 50% of available insolation for eight hours each day.

7. A collector area three to five times that of dryer floor area provided sufficient temperature rises (greater than 10 °C) needed for adequate peanut drying in central Oklahoma.

8. Operating the collector above 1.5 $m^3/(min\text{-}m^2)$ did not result in any significant increase in efficiency.

References

1. Chiou, J. P., J. A. Duffie, and M. M. El-Wakil. "A Slit-and-Expanded Aluminum-Foil Matrix Solar Collector." ASME Paper No. 64-WA/Sol-10.

2. Coppage, J. E., and A. L. London. "Heat Transfer and Flow Friction Characteristics of Porous Media." Chemical Engineering Progress, No. 2, 52; 57-63F.

3. Duffie, J. A., and W. A. Beckman. Solar Energy Thermal Processes. John Wiley and Sons, Inc., New York, 1974.

4. Duncan, G. A., and J. N. Walker. "Selection of Greenhouse Covering Materials." Trans. of ASAE, 1975, 703-710.

5. Hamid, Y. H., and W. A. Beckman. "Performance of Air-Cooled Radiatively Heated Screen Matrices." ASME Paper No. 70-WA/Sol-1.

6. Hamid, Y. H., and W. A. Beckman. "Transpiration Cooling of Radiatively Heated Porous Bed." ASME Paper No. 69-WA/Sol-6.

7. Morgan, R. G. "Design, Construction and Evaluation of a Wedge-Shaped Matrix Solar Collector for Drying Peanuts". M. S. Thesis, Oklahoma State University, Stillwater, OK, 1976.

8. Morgan, R. G., R. Rogers, B. L. Clary and G. H. Brusewitz. Drying and Curing Spanish Peanut Pods With Solar Energy. Meeting of APREA, Dallas, TX, July, 1976.

9. Parker, J. D., J. H. Boggs and E. F. Blick. Introduction to Fluid Mechanics and Heat Transfer. Addison-Wesley Publishing Co., Inc., Reading, MA, 1970.

Nomenclature

A_L = Heat transfer area subject to conduction per unit of collector area, m^2/m^2

C_p = Specific heat of fluid, w-hr/(Kg-K)

D_f = Average diameter of matrix filaments, m

dp/dz = Pressure drop across matrix layer per unit depth, Pa/m

e_b = Emissivity of bed

e_c = Emissivity of cover

e_g = Radiant interchange factor between two parallel plates

F_{gx} = Radiant interchange factor between collector cover and point x in matrix layer, m^{-1}

f = Fanning friction factor, $2r_h\ (-dp/dz)/\rho_a u^2$

G = Mass flow rate per unit area, $Kg/(hr\text{-}m^2)$

h_{vx} = Volumetric heat transfer coefficient at point x in the bed, $w/(m^3\text{-}K)$

I_L = Emerging solar radiation normal to absorber, w/m^2

I_0 = Direct solar radiation normal to collector cover, w/m^2

L = Total matrix thickness, m

Re = Reynolds number, $4r_h\ (-dp/dz)/\rho_a u^2$

r_h = Hydraulic radius of matrix, $r_h = D_f\lambda/4\ (1\text{-}\lambda)$, m

T_{ba} = Average bed temperature, K

T_{ba}^* = Dimensionless temperature ratio, T_{ba}/T_{fo}

T_{bx} = Temperature of bed at x, K

T_c = Temperature of cover plate, K

T_c^* = Dimensionless temperature ratio, T_c/T_{fo}

T_f = Temperature of fluid, K

T_{fa} = Average fluid temperature, K

T_{fa}^* = Dimensionless temperature ratio, T_{fa}/T_{fo}

T_{fl}^* = Dimensionless temperature ratio, T_{fl}/T_{fo}

T_{fo} = Temperature of fluid entering matrix, k

T_{fo}^* = Dimensionless temperature ratio, $T_{fo}/T_{fo} = 1$

T_{fx} = Temperature of fluid at x, K

u = Velocity of air through matrix voids

U_L = Overall heat transfer coefficient for collector walls and back plate, $w/(m^2-K)$

V_i = Total sample volume, cm^3

V_w = Volume of water displaced by submerged sample, cm^3

x = Distance from top of bed surface, m

β = Average extinction coefficient of bed, m^{-1}

η_b = Matrix bed collection efficiency, %

η_c = Collector efficiency, %

Γ = Dimensionless mass flow rate, $G\ Cp\ T_{fo}/\sigma T_{fo}^4$

λ = Porosity, %

μ = Dynamic viscosity of air, kg/(m-sec)

ψ = Dimensionless direct solar radiation, $I_0/\sigma T_{fo}^4$

ρ_a = Density of air, kg/m^3

σ = Stefan-Boltzmann constant, $w/(m^2-K^4)$

τ = Optical depth, βx

τ_c = Effective transmittance of collector cover

θ = Dimensionless volumetric heat transfer coefficient, $h_{va}\ T_{fo}/\beta\sigma T_{fo}^4$

TABLE I

MATRIX POROSITY AND DENSITY

Sample I. D.	Sample Thickness cm	Total Sample Volume cm^3	Volume of Solid cm^3	Mass of Sample g	Porosity	Apparent Density g/cm^3	Specific Density g/cm^3
1	1.91	282.9	13.5	14.75	0.952	0.0521	1.09
2	1.91	284.8	12.5	14.75	0.956	0.0518	1.18
3	1.91	291.5	14.2	16.50	0.953	0.0535	1.09
1	1.27	170.4	7.2	8.88	0.958	0.0521	1.24
2	1.27	177.5	8.0	9.40	0.955	0.0530	1.18
3	1.27	174.4	7.7	9.53	0.956	0.0533	1.24

TABLE II

MATRIX FRICTION LOSS CHARACTERISTICS

Rep	Air Velocity u (m/sec)	Reynolds Number Re	Pressure Drop dp/dz (Pa/m)	Friction Factor (Fanning) f
1	0.0091	3.27	0.92	28.14
2	0.0098	3.52	1.15	30.13
3	0.0111	4.00	0.92	18.74
1	0.0117	4.22	1.27	23.20
2	0.0111	4.00	0.92	18.76
3	0.0128	4.61	1.15	20.14
1	0.0148	5.34	1.62	18.45
2	0.0148	5.33	1.73	19.78
3	0.0148	5.33	1.73	19.77
1	0.0216	7.78	3.23	17.38
2	0.0234	8.43	3.58	16.35
3	0.0227	8.21	2.77	13.32
1	0.0366	13.22	6.81	12.70
2	0.0369	13.25	6.23	11.51
3	0.0373	13.39	6.46	11.69
1	0.0392	14.13	7.62	12.43
2	0.0387	13.91	8.54	14.32
3	0.0389	13.97	7.16	11.89
1	0.0598	21.57	15.12	10.58
2	0.0598	21.48	13.85	9.73
3	0.0597	21.44	14.08	9.93
1	0.0626	22.58	16.28	10.40
2	0.0625	22.45	16.16	10.40
3	0.0625	22.44	15.81	10.17
1	0.0643	23.20	16.51	9.99
2	0.0641	23.04	16.97	10.37
3	0.0641	23.03	16.51	10.09

TABLE III

MATRIX EXTINCTION COEFFICIENT

Bed Thickness L (m)	Ratio of Emerging to Incident Energy I_L/I_0
0.000	1.000
0.0127	0.0870
0.0191	0.0322
0.0254	0.0054
0.0381	0.0009

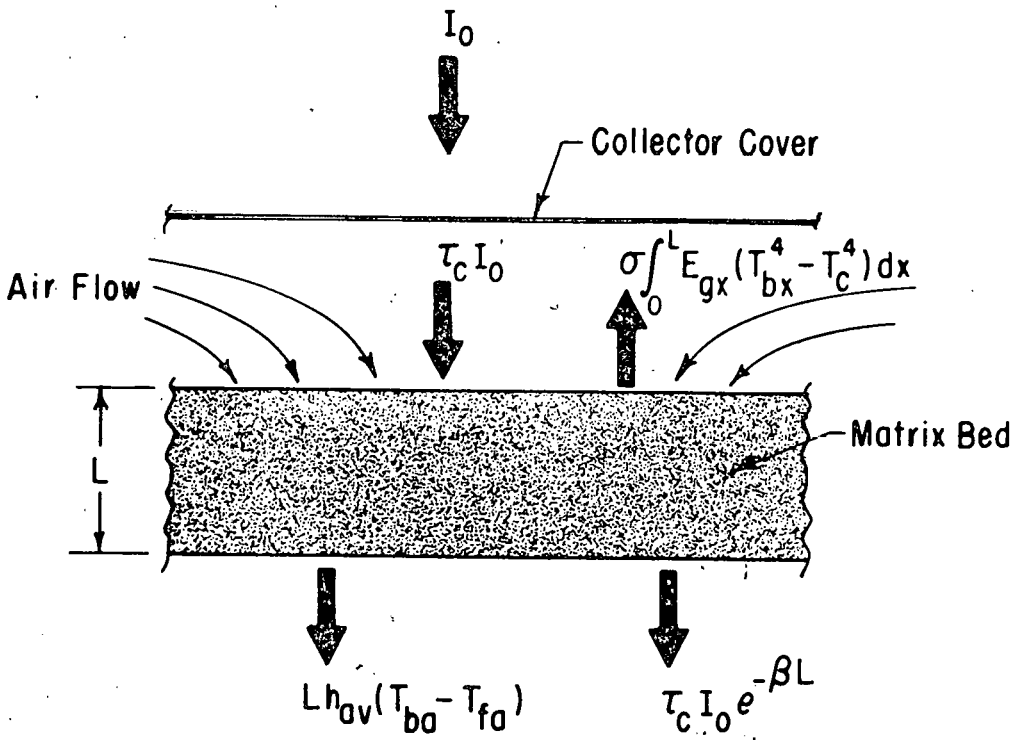

Figure 1. Energy Flow Terms for a Matrix Bed Element

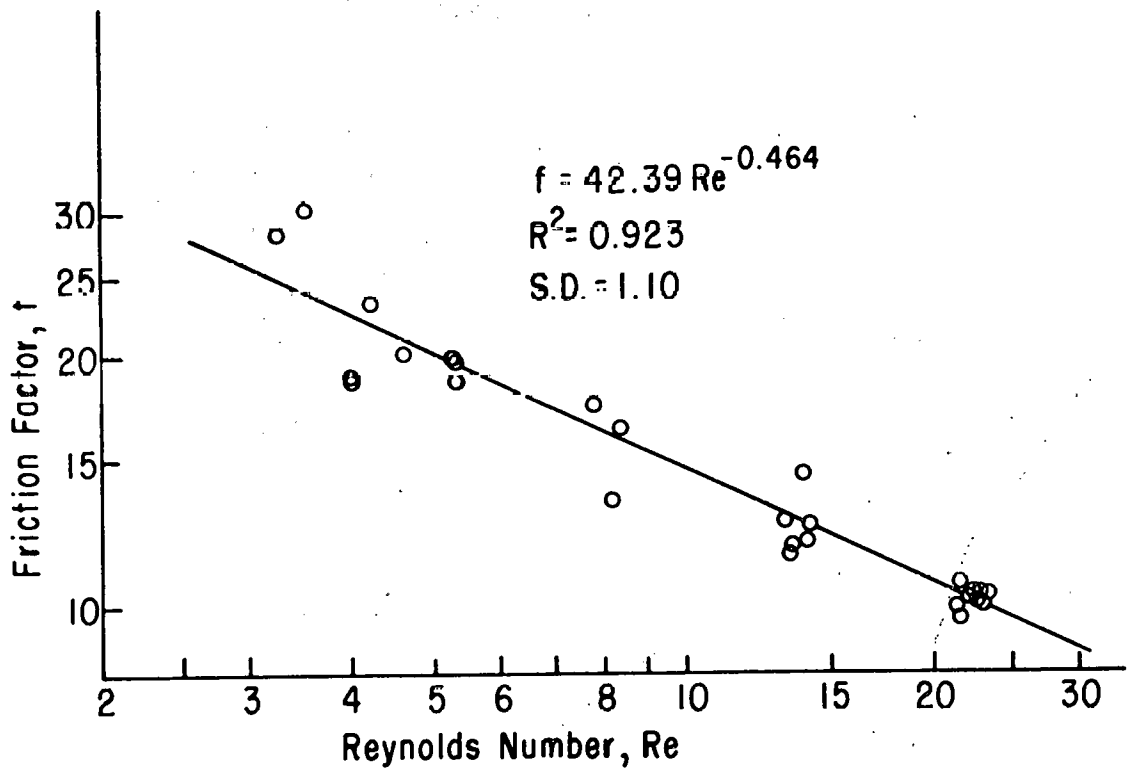

Figure 2. Fanning Friction Factor as a Function of Reynolds Number for Duralast Filter Media

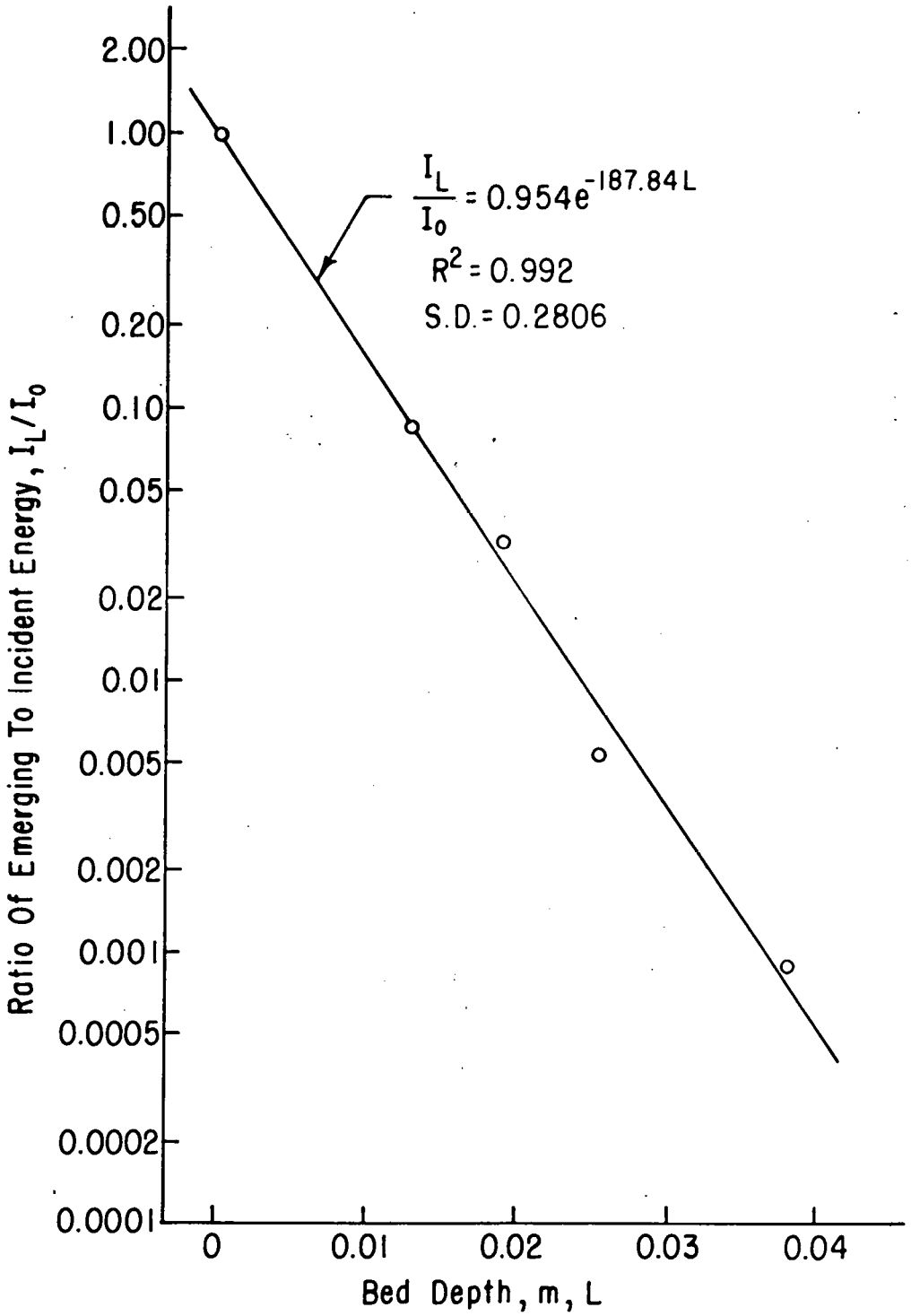

Figure 3. Ratio of Emerging to Incident Energy as a Function of Matrix Bed Depth for Duralast Filter Media

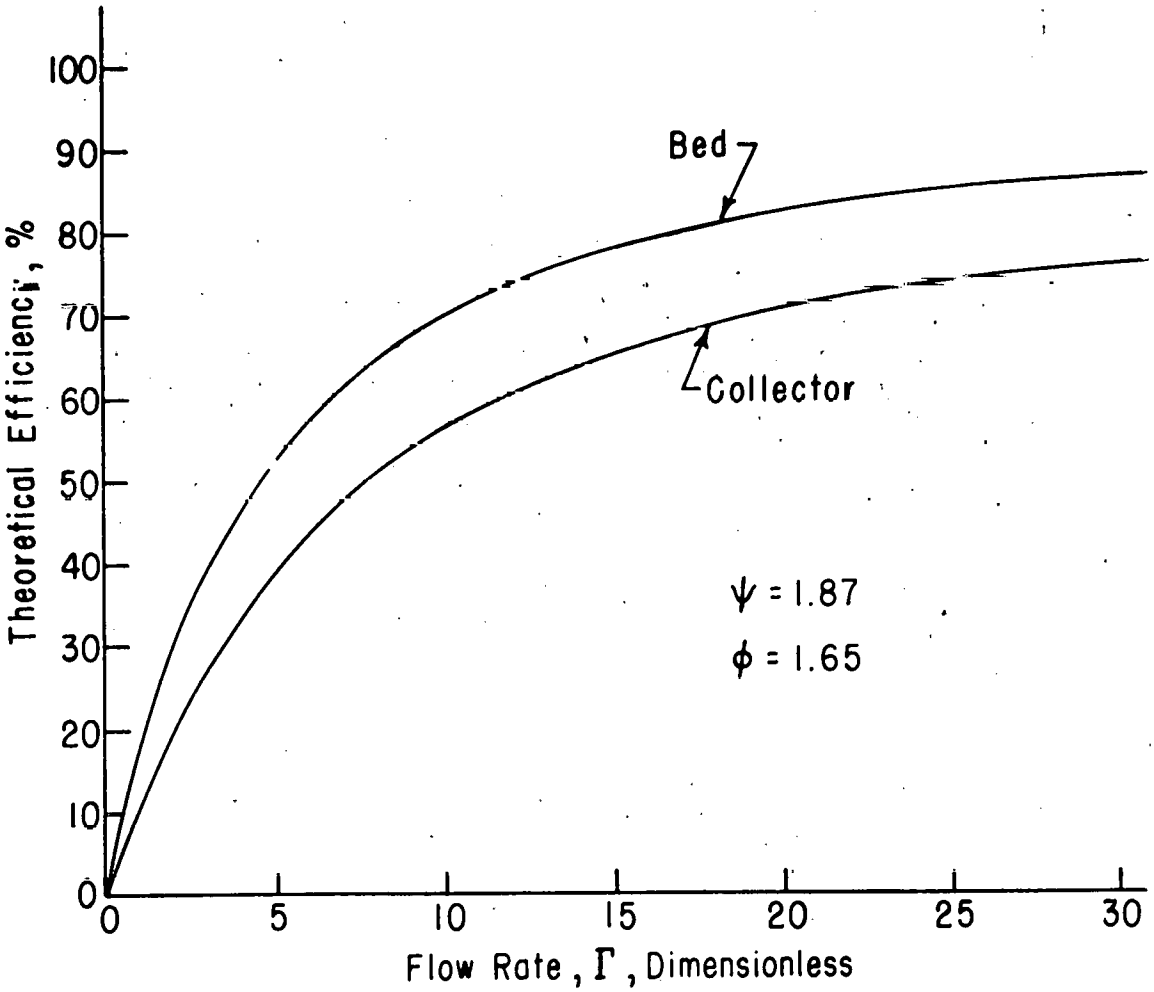

Figure 4. Theoretical Bed and Collector Efficiency as a Function of Dimensionless Flow Rate

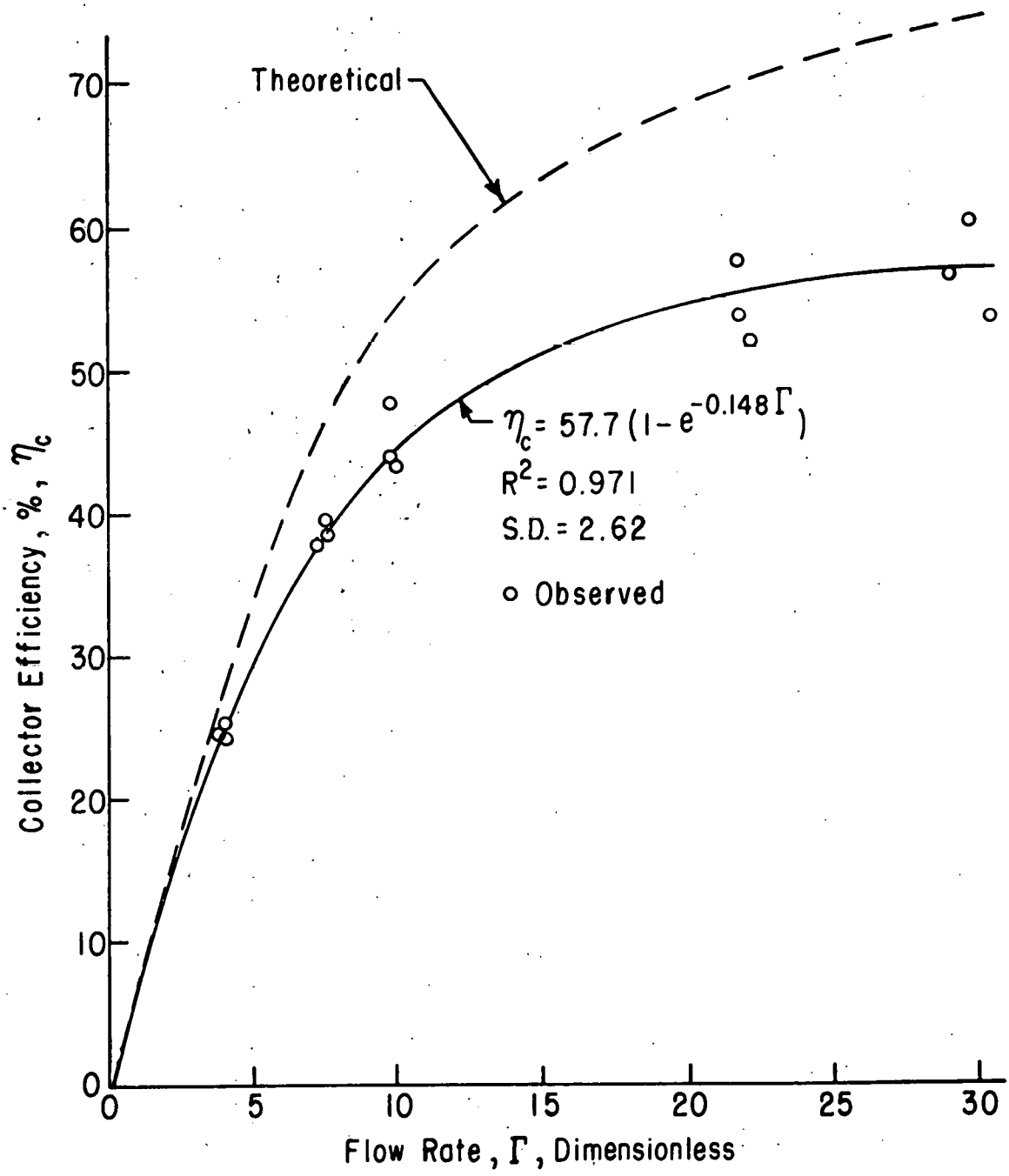

Figure 5. Observed and Theoretical Collector Efficiency as a Function of Dimensionless Flow Rate for Wedge-Shaped Matrix Solar Collector

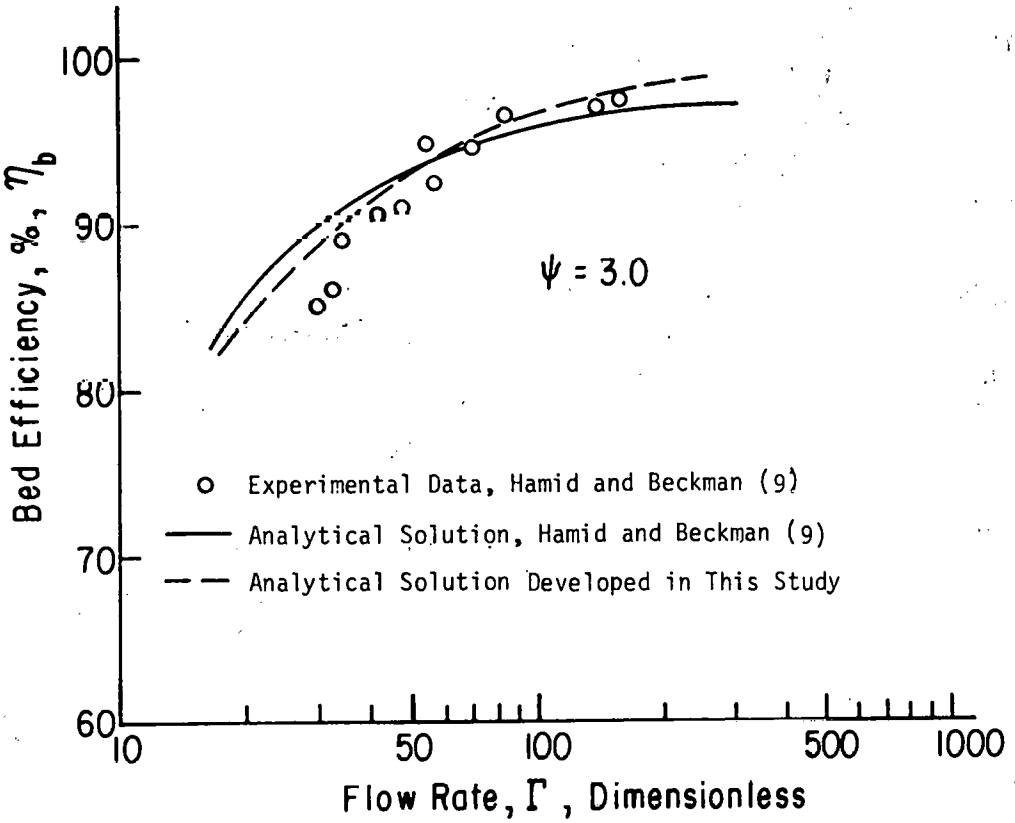

Figure 6. Bed Efficiency as a Function of Dimensionless Flow Rate for Experimental Data and Analytical Solution from Reference (6) and the Analytical Solution from This Study

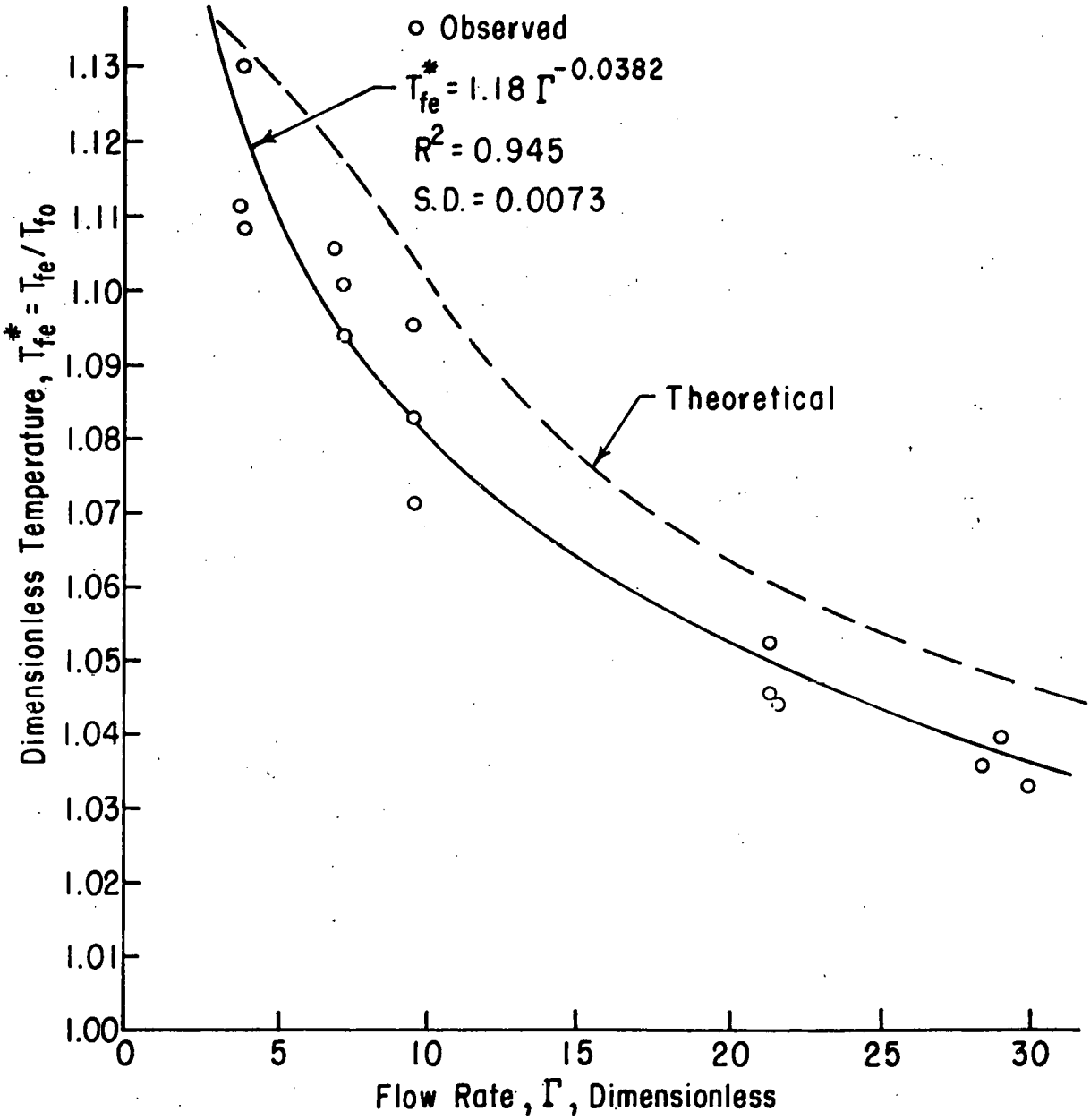

Figure 7. Effects of Dimensionless Flow Rate on Dimensionless Temperature Ratio for Observed Data and Theoretical Solution of Matrix Solar Collector

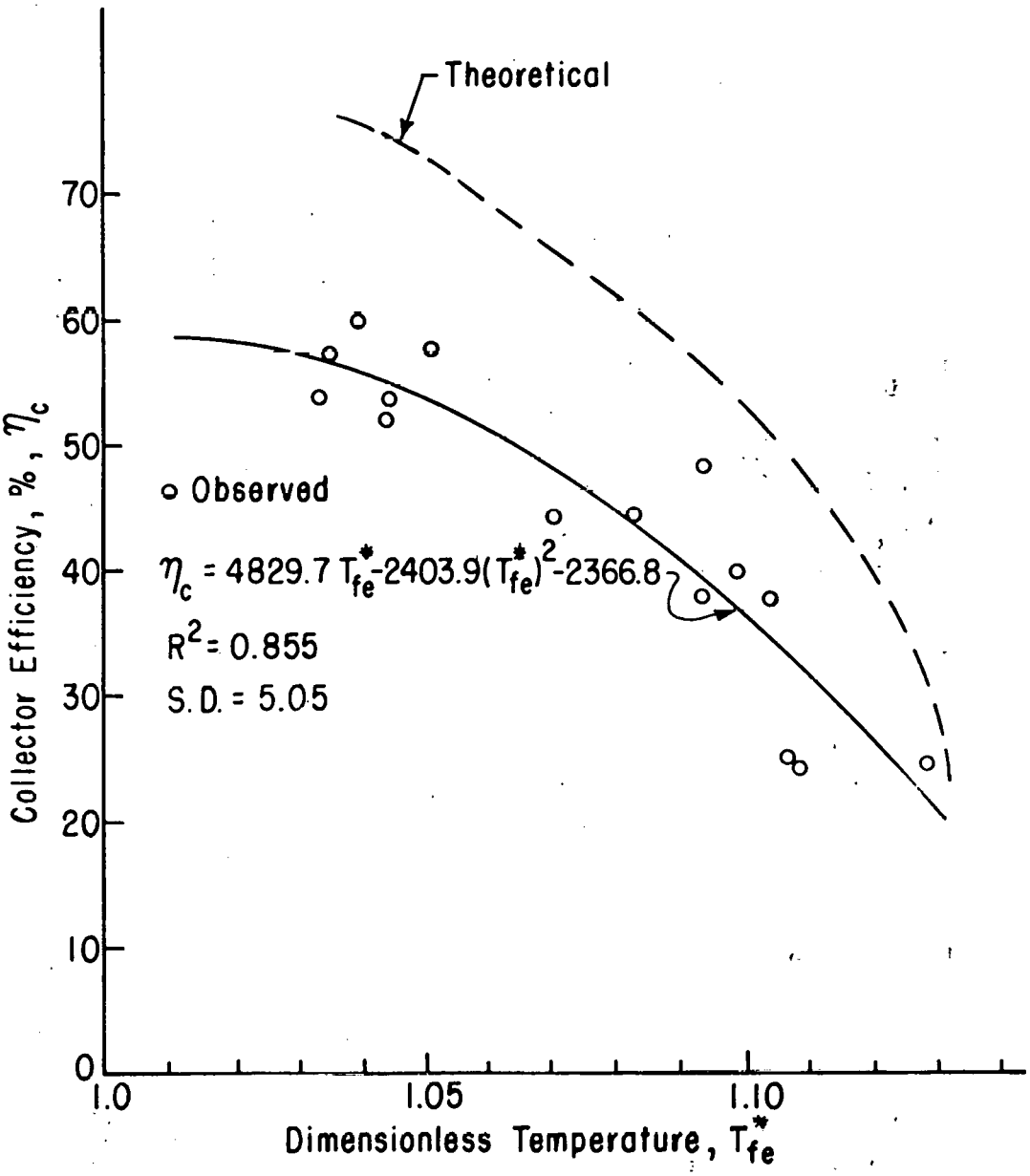

Figure 8. Observed and Theoretical Collector Efficiency as a Function of Outlet Dimensionless Temperature Ratio

CLOSED-AIR SYSTEM FOR DRYING PEANUTS

by

N. K. Person, Jr.
and
J. W. Sorenson, Jr.
Department of Agricultural Engineering
Texas Agricultural Experiment Station
Texas A&M University System
College Station, Texas
77843

INTRODUCTION

Even though solar radiation is considered to be an unlimited source of energy throughout the universe, specific quantities of this energy over any finite area are very limited. In fact, it is of such a limited quantity when considered for crop drying that if 100 percent of the solar radiation striking the earth's surface each day could be collected, it would still require approximately 0.52 square feet (sq. ft.) of collection area per cubic foot of natural gas replaced. This is a significant problem since present drying procedures require about 16.5 cubic feet of gas to dry each 100 pounds of peanuts.

Approximately 78 million cubic feet of natural gas are consumed in Texas each year to dry peanuts (1).* This quantity has been of little importance in the past since fossil fuels were considered an abundant source of cheap energy. This is no longer the case since our demand now exceeds the supply. The utilization of other available sources of energy for peanut drying is imperative if the industry is to continue to supply a high quality product to the consumer. Past accomplishments in solar-cooling technology indicate that cooling systems powered by solar energy could be available in the very near future. Results of research conducted on the use of cooling systems for drying peanuts are presented in this report.

STATE OF THE ART

Until recent years, radiation from the sun was the primary source of all energy being utilized on earth. Through the ages solar energy has been harnessed and stored by growing plants and then converted by nature into the fossil fuels of today. The solar energy received by the earth is estimated to be 100,000 times as great as the world's present electric generating power capacity.

The average solar energy incident upon a unit surface normal to the solar beam at the edge of the earth's atmosphere is 442 Btu per hour per sq. ft. Much of this energy is dissipated in the atmosphere while enroute to the earth. The average daily incidence of solar radiation at the earth's surface has been determined to be about 1500 Btu per day per sq. ft. This is equivalent to 44 kwh of energy per day for every 100 sq. ft. of area. Becker and Boyd (2) report that a maximum value of 2650 Btu per day per sq. ft. is reached during June and July for most areas in the United States. Incident solar radiation may vary with cloudiness, time of day, season of the year, and the latitude and altitude at which the measurement is being made. An everlasting supply of energy is thus available, and the challenge is to harness it in some way to serve man.

* Numbers in parentheses refer to references.

There is less information in the literature concerning the effective utilization of this energy. In order for solar energy to be utilized, it must first be collected and concentrated into a relatively high temperature or it must be converted into some other form of energy. The energy collection involves an accumulation process which is a function of the solar collector. Two kinds of solar collectors in use today are non-concentrating or the flat-plate type and the concentrating or focusing type. The former functions best for lower temperature applications (100 to 175°F) while the latter is more appropriate for higher temperature applications. Thermal efficiencies for flat-plate collectors have ranged from 40 to 60 percent (3). The plate collectors usually cost less to construct, need no tracking device and have the ability to collect both diffused and direct solar radiation. The collector efficiency reduces as the operating temperature is increased.

Hot water obtained from solar collectors can be converted into cold air by using conventional absorption refrigeration machines. Because of its compactness and vibrationless operation, it can be installed anywhere space and a heat source are available. It uses the cheapest, safest and most available of all refrigerants, ordinary tap water (4). Its absorbent is a simple salt. The use of absorption refrigeration systems powered by solar collectors has received some attention in the agricultural structures field. White and Isaacs (5) reported peak cooling rates of approximately 60 Btu per hr. per sq. ft. of collection area utilizing this solar cooling method. Peak energy available for storage ranged around 180 Btu per hr. per sq. ft.

Successful use of a cooling medium for drying agricultural products appears to center around a modified heat pump principle. This modified cycle would not only use the heat of the condensing refrigerant but also the evaporation of this same fluid. In a practical application, air leaving the drying product would be passed over the evaporator to extract moisture, then to the condenser unit to be heated before being moved back through the product. This system would result in a closed-air cycle with little dependence on the ambient conditions. Flikke, et al. (6) studied this principle many years ago for grain drying. They reported that 6 pounds of water could be removed per hr. from grain for each 10,000 Btu per hr. refrigeration capacity. The most recent efforts in use of a heat pump in a closed-air cycle have been reported by Ayers, et al. (7). Their analysis of the First-Law-of-Thermodynamics shows this to be the most energy-efficient dryer possible, as no energy losses to ambient are present.

MATERIALS AND METHODS

The materials and methods presented in this section of the report will describe only those used during the past field testing period. They were actually developed over a three-year research program conducted by the Texas Agricultural Experiment Station, of which the final year was supported by the Energy Research and Development Administration (ERDA). Several changes were made in the materials and methods used during the developmental period in order to accomplish the objectives of this research. Those given in this report represent the most advanced and suitable ones for actual practice.

A small-scale 4 ft. x 4 ft. x 8 ft. drying bin was constructed for these tests, Figure 1. It was made of plywood with a perforated metal floor installed 1 ft. from the bottom. The bin was loaded to a depth of 5 ft. with partially field-cured peanuts during each drying test. The approximate initial weight of wet peanuts was 1 ton. The schematic of the closed-air drying system is shown in Figure 2. The system was composed of the following components: fan, evaporator coil, condenser coil, auxiliary condenser coil, vapor-compression type refrigeration compressor, and related refrigerant components. Figure 3 shows a schematic of the refrigeration system.

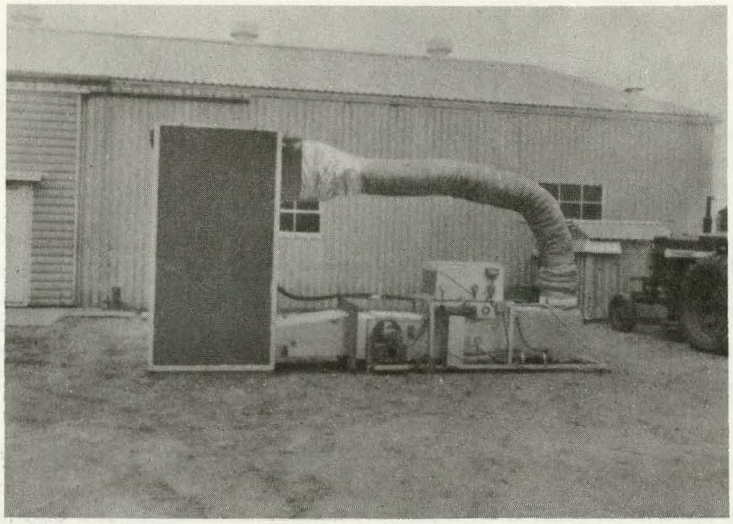

Figure 1. Experimental peanut dryer utilizing the closed-air principle.

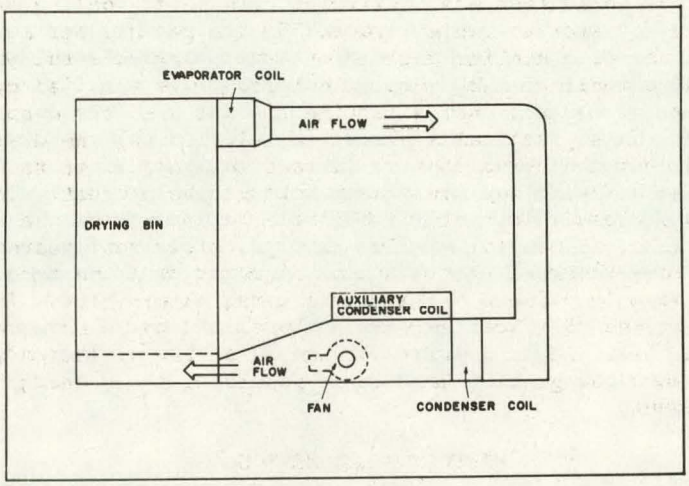

Figure 2. Schematic diagram of the closed-air system for drying peanuts.

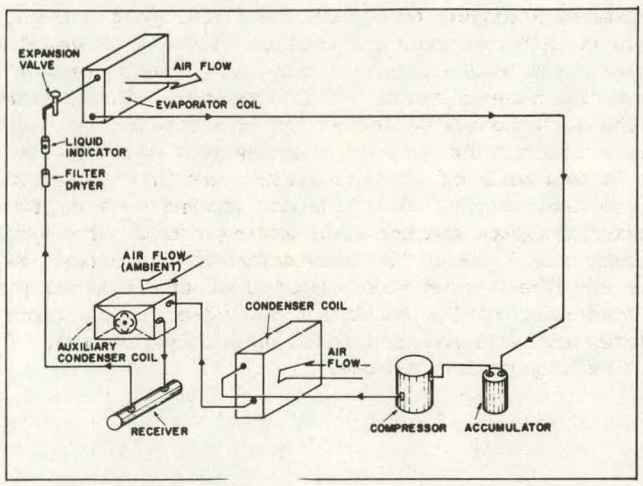

Figure 3. Schematic diagram of refrigeration system used in closed-air dryer.

Since the performance of the closed-air system depends to a great extent on the individual components, a brief description of each is necessary.

FAN: direct-drive, forward curved centrifugal blower capable of delivering approximately 1000 CFM under test conditions; blower driven by 1-1/2 hp motor

EVAPORATOR COIL: nominal 3-ton capacity

CONDENSER COIL: nominal 3-ton capacity

AUXILIARY CONDENSER COIL: nominal 5000 BTUH capacity with a shutter-mounted exhaust fan rated at 520 CFM free delivery

REFRIGERATION COMPRESSOR: high temperature, R-22, hermetic compressor with nominal capacity of 16,700 BTUH under standard rating conditions

It should be pointed out that the evaporator and condenser coils have a somewhat higher rating than the compressor. These coils were used during the first two years of the system development period, at which time a larger compressor was under test. When the above listed compressor was incorporated into the present system, the coils were retained in order to test the system under the most efficient operating conditions. These coils actually represent approximately 25 percent over design when the compressor was under test conditions.

Two drying test runs were conducted during the past harvest season at the Texas A&M University Research and Extension Center at Stephenville, Texas. This Center is located in the major peanut producing area of Texas and therefore the test conditions were similar to those which would be encountered on a full scale. The dryer was located under an open shed to simulate actual practice. Spanish variety peanuts were grown at the Center where they were dug and handled in the same manner as they would have been for conventional dryers. The only difference was the equipment used for drying.

Two drying test runs were conducted in early November during the 1976 harvest season. Peanuts used for both runs were partially field cured prior to combining and mechanical drying. When the peanuts reached a pod moisture content of approximately 23 and 26 percent for Runs 1 and 2, respectively, they were combined and loaded into the dryer. The drying tests were initiated within 1 hr. after the dryer was loaded.

RESULTS

The conditions under which the two test runs were conducted were not exactly the same; therefore, the runs are not treated as statistical replications. The peanuts used for the runs were harvested at different times and from different fields which caused several uncontrolled variables. The most important differences occurred in the condition of the peanuts and the ambient temperatures under which the tests were conducted. The peanuts used in Run 1 were extremely dirty while those used in Run 2 were more similar to those normally received at the buying stations. Also, the average ambient dry-bulb temperature during Run 1 was 54.8°F while the average during Run 2 was 60.5°F.

Even though the test conditions were somewhat different for the two test runs, test results were similar. The numerical numbers were not the same for both test runs but the same patterns and characteristics were followed. Since both runs exhibited similar results, all the test data will not be presented in this report. Some of the results will be illustrated with data collected during Run 1 while others will be shown with data obtained during Run 2.

Theoretical System Characteristics

The principle of the closed-air system is quite simple and the design is fairly straightforward once the system characteristics are understood. The basic psychrometric process for the closed-air system is shown in Figure 4.

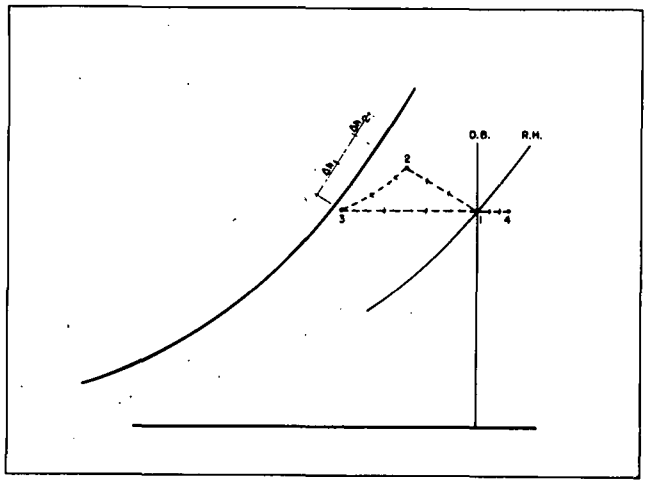

Figure 4. Basic psychrometric process for the closed-air system.

State 1 represents the design conditions for the system. In the case of a peanut dryer, these conditions are normally 90-95°F dry-bulb temperature with a relative humidity in the 40-50 percent range. Air conditions shown at State 1 are established by the heat pump equipment and represent the desired plenum conditions. State 2 is the point at which the air leaves the dryer. Since the drying process is considered to be adiabatic, the wet-bulb temperature at State 2 is normally within $\pm$ 1°F of the wet-bulb temperature at State 1. Theoretically it will be the same enthalpy at both states except for the water added to the system. It should be noted that the conditions represented at State 2 are continuously changing. At the beginning of the drying process the exhaust point will be near saturation while at the end it will approach State 1. Air leaving the wet product in a closed-air system will then enter the evaporator coil of the refrigeration system. The change in the air properties through the evaporator is shown from State 2 to State 3 in Figure 4. This causes the air to be cooled to below its dew point temperature and consequently lowers the specific humidity. After the air passes through the evaporator it then is heated sensibly by the condenser coil, State 3 to State 1 or 4, depending upon system design.

In theory, the main advantage of the closed-air system for drying peanuts is twofold. One advantage is that it allows the engineer to design the dryer for the optimum air conditions required for peanuts regardless of the ambient conditions. Second, it offers a simple method of maintaining the designed conditions. All that is required in this case is for the condenser coil to release the same quantity of heat to the air stream as the evaporator coil removed. This is illustrated in Figure 4 by Δh_1. If the system is designed properly then Δh_1 represents the change in enthalpy of the air across the evaporator as well as across the condenser. This being the case, State 1 must then represent the air leaving the condenser, which was the original design condition for the air entering the peanuts.

The principle theory of the closed-air system does not hold up in actual practice due to the heat of compression of the refrigeration machine. Consequently, the air leaving the condenser will not be at State 1 but will approach State 4. This causes the system to go out of control and results in a steady increase in the design dry-bulb temperature. To prevent this uncontrolled condition, some method must be employed to offset the Δh_2 in Figure 4 resulting

from the heat of compression. There are several methods at the disposal of the designer. The one found to be the most suitable for peanut dryers was the incorporation of an auxiliary condenser coil with a capacity of Δh_2.

The auxiliary condenser used in this research was piped in series with the main condenser coil so that there was full flow of refrigerant through it at all times. This auxiliary coil had a built-in shutter-mounted exhaust fan in order to pull outside air through it. This removed the excess heat caused by the work done on the refrigerant. Since it was difficult in the early stages of the research to design the auxiliary coil to remove the exact amount of excess heat, an over design was made. To maintain the proper design conditions with this oversized coil, the auxiliary condenser coil fan was cycled by a thermostat sensing the dry-bulb temperature in the dryer plenum. When the temperature of the air entering the peanuts reached the set point of the thermostat the fan would cycle on to remove heat from the closed-air system by exhausting it to the atmosphere. The resulting swing in the design temperature in the experimental dryer was 7°F. This figure can be reduced by reducing the size of the auxiliary coil, limiting the airflow across it, or redesigning the refrigerant piping system. The designer should not attempt to reach a perfect balance in this system since no control can be maintained over the temperature of the outside air passing through the auxiliary condenser.

Test System Characteristics

The psychrometric process of the closed-air system under test conditions is given in Figure 5. This instantaneous reading was taken 12.5 hours after the drying process was initiated and conforms very closely to the theoretical process. Data collected later on in the drying period did not conform as well because of the problems encountered with instantaneous readings. Factors such as changes in the air conditions leaving the peanuts, modulation of the expansion valve and cycling of the auxiliary condenser fan cause these readings to vary at different rates.

The performance of the condenser coil during Test Run 1 is shown in Figure 6. These curves were plotted as second order functions to illustrate the trends. The average temperature entering and leaving the condenser was 64.3°F and 87°F, respectively. It should be pointed out that a lot of the deviation of individual points away from the curves was due to the cycling of the auxiliary coil. These data were recorded periodically without regard to the auxiliary coil operation. If it is assumed that there was an equal probability of coil operation each time the data were collected, then there was a gradual decrease in the air temperature leaving the condenser coil.

It appears at the present time that the major cause for this decrease was related to the ambient conditions under which the system was operating. Ambient dry-bulb temperatures below approximately 50°F caused the air temperature entering the peanuts to drop below the design point. For example, the air temperature leaving the condenser coil in Run 1, Figure 6, was fairly constant for the first 30 hrs. of drying. The average leaving temperature up to this time was 91.3°F. However, as the ambient temperature decreased it caused the temperature of the air entering the condenser to decrease which resulted in a decrease in the leaving temperature. The effects of the ambient temperature on the condenser coil entering temperature are related to the evaporator coil performance and are discussed later in this section.

The air conditions entering the peanuts are shown in Figure 7. The gradual decrease in the air temperature leaving the condenser coil is reflected in this graph. The average dry-bulb temperature entering the peanuts during the drying period was 87.3°F with a maximum and minimum of 95°F and 78°F, respectively. The minimum temperature encountered was much lower than the design temperature;

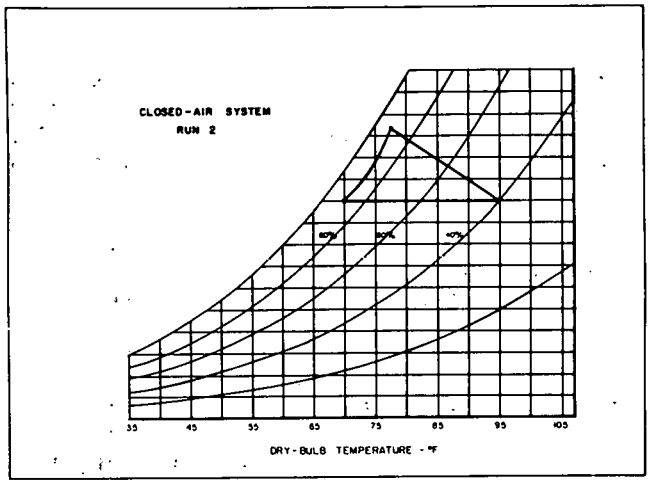

Figure 5. Typical psychrometric process of the closed-air system while drying peanuts.

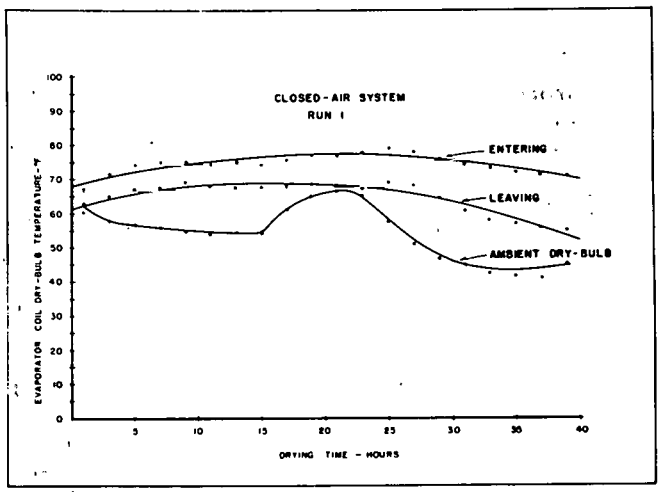

Figure 6. Entering and leaving dry-bulb temperatures of the condenser coil during the drying period.

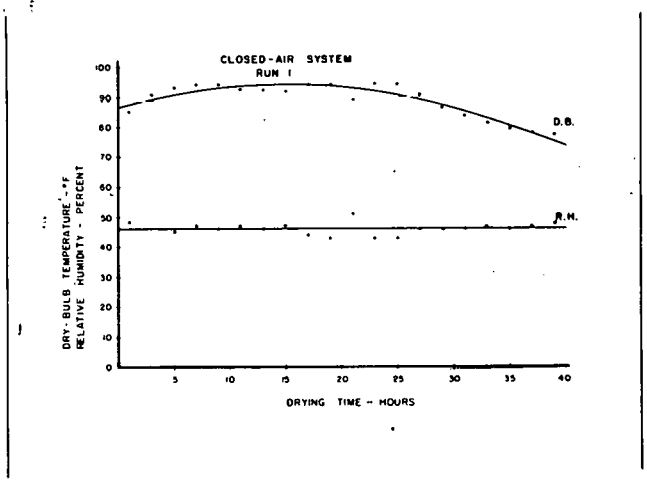

Figure 7. Air conditions entering the peanuts during the drying period.

however, the gradual decrease mentioned above occurred only during the last 9 hrs. of drying. The average temperature entering the peanuts up to the time the ambient temperature influenced the conditions was 91.6°F with a minimum of 87.5°F. The relative humidity of the drying air averaged 46 percent during this test run. The maximum and minimum were 51 and 43 percent, respectively.

The air conditions leaving the peanuts during the drying stages in the closed-air system are illustrated in Figure 8. Test Run 2 is shown in this case since this run was not significantly influenced by ambient conditions. The dry-bulb temperature of the air leaving the peanuts gradually increased as the peanuts became drier. This is normal because there is less moisture being evaporated in the dryer toward the end of the drying process. This is illustrated by the decrease in the exhaust air relative humidity.

The air conditions leaving the peanuts in a closed-air system are the conditions entering the evaporator coil. Typical conditions shown in Figure 8 are essential to maintain the design conditions entering the peanuts. During the early stages of the drying process the dry-bulb temperature is low due to the evaporative cooling which takes place in the drying bin. This is important because proper control of the entering air temperature to the peanuts depends upon a constant temperature leaving the evaporator, neglecting effects of the heat of compression. To maintain a constant temperature of the air leaving the evaporator during early stages of drying, it is necessary to have a reasonably low entering temperature because the major portion of the load on the coil is latent. As the drying process approaches the final desired moisture content, the load changes to sensible. This is significant from a control standpoint because as the load on the evaporator shifts to a sensible load, the temperature entering the coil increases at the same time. The overall result is a fairly uniform temperature leaving the evaporator coil.

The change of the latent and sensible loads on the evaporator coil in a closed-air system is shown in Figure 9. These curves represent the accumulated pounds of water condensed and drained from the evaporator coils during drying. It can be seen that during the final drying periods the slope of the curves were much less than at the beginning. This indicates a substantial reduction in the coil latent load with drying time. No correlation of the total amount of water removed from the system with pod moisture contents should be attempted because of the quantity of foreign material present.

In the case of Run 1 when the ambient temperatures decreased below 50°F during the later stages of drying, the temperature leaving the evaporator could not be held constant. Heat losses from the dryer to the atmosphere at these low temperatures prevented the dryer exhaust air temperature from rising, Figure 10. Consequently, when the load on the coil shifted to a sensible load there was not an accompanying increase in the entering temperature. This allowed the coil to pull the leaving air temperature down below that required to maintain the design temperature of the dryer.

The air temperature changes across the condenser and evaporator coils during Run 1 are shown in Figure 11. This again shows the increased sensible capacity of the evaporator coil as the drying process progresses. Since low ambient conditions prevented the evaporator coil entering air temperature from increasing, the lower entering conditions to the condenser coil influenced the temperature rise across the condenser because the head pressure was substantially lowered.

Drying Rate

The typical moisture loss versus drying time curves for different depths of peanuts in the closed-air system is given in Figure 12. The depths recorded on this graph represent the depth from the bottom of the drying bin. This graph shows that the peanuts located near the top of the dryer, 4-ft. depth, dried to 10 percent pod moisture content in approximately 39 hrs. Those located 1 ft. from the bottom required only 28.5 hrs. to reach 10 percent. This resulted in a 3 percentage point spread between the top and bottom of the dryer which is slightly above that of conventional dryers operating under an equivalent airflow rate of 16 cfm/bu. The difference in the other test run was only 2 percentage points.

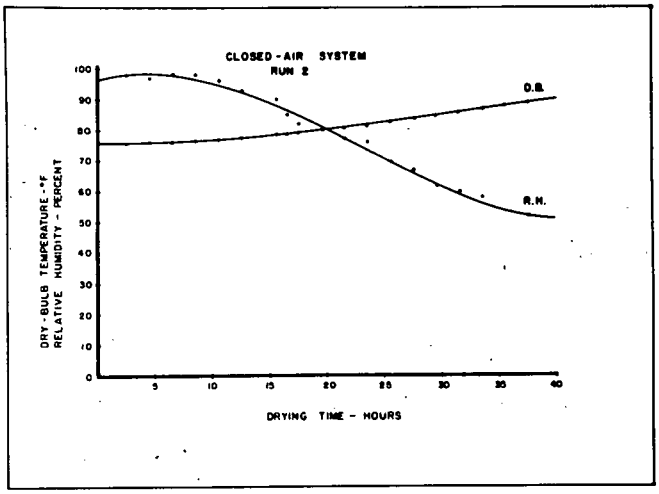

Figure 8. Typical air conditions leaving the peanuts during the drying stage in the closed-air system.

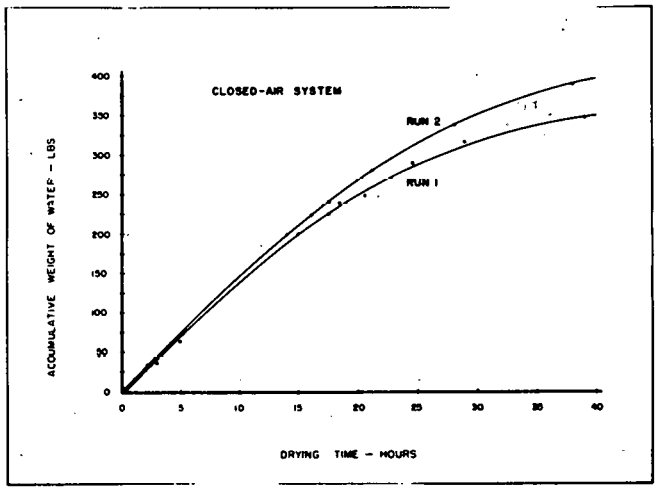

Figure 9. Accumulative weight of water condensed and drained from the evaporator coil during drying.

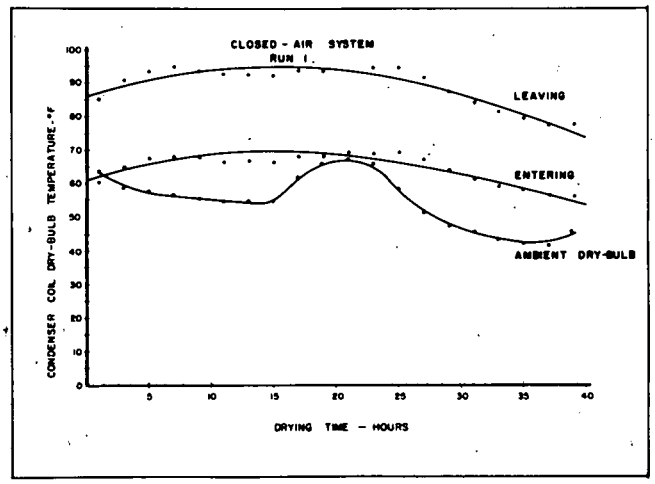

Figure 10. Dry-bulb temperatures entering and leaving the evaporator coil during Run 1.

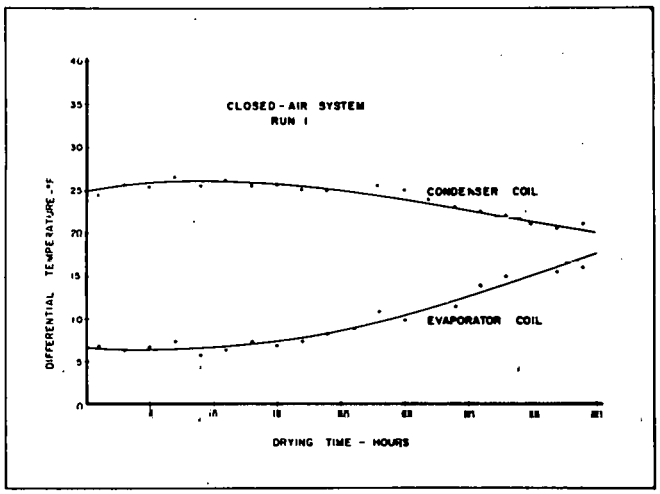

Figure 11. Changes in air temperature across the condenser and evaporator coils during Run 1.

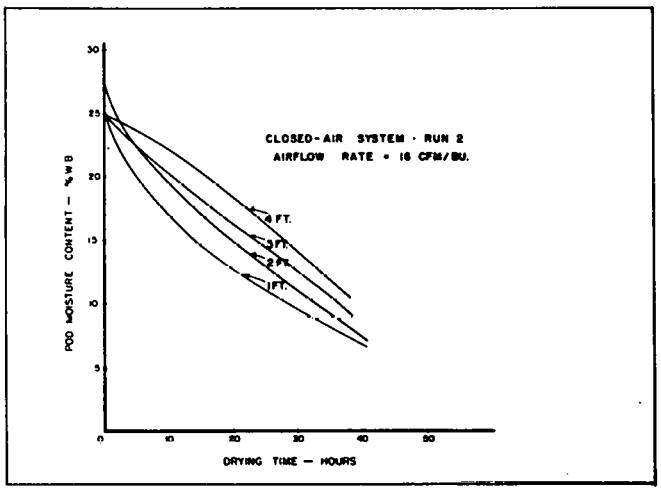

Figure 12. Typical moisture loss versus drying time curves for closed-air system.

The overall drying rates based on the average moisture content throughout the peanuts was 0.34 and 0.44 percentage points per hr. for Test Runs 1 and 2, respectively. The relationships of the moisture contents of pods located at the top of the dryer with drying time are given in Figure 13.

System Efficiency

A summary of the data collected on the energy requirements and efficiencies to dry approximately one ton of wet peanuts is listed in Table 1. The total energy consumed in removing 345.5 lbs. of water in Run 1 was 139 kwh. A plot of the accumulative input energy is given in Figure 14. The peak total power was approximately 3400 watts while the power required to drive the compressor averaged about 2300 watts during the test. The average capacity of the system was 25,369 BTUH with an average energy efficiency ratio (EER) in BTUH/watt of 11.1. This EER was calculated for the refrigeration system only. It is assumed in this report that the same fan requirements exist regardless of the source of heat. A total of 135 kwh were consumed to dry peanuts during Run 2. The compressor required 91.5 kwh of this total and had an average capacity and EER of 24,874 BTUH and 10.3, respectively.

Spot-checking the performance of the system during the test runs revealed a fluctuation in the heat capacity of the system from 19,398 to 28,640 BTUH, Figure 15. This fluctuation was due to the operation of the auxiliary condenser coil which was used to maintain the design dry-bulb temperature. The auxiliary coil fan cycle varied with the condition of the system and outside temperatures. The on-cycle averaged 1.4 minutes and varied from 1.6 to 1.87 minutes during both test runs. The off-cycle varied from 2.39 to 5.15 minutes with an average of 3.51 minutes. This cycle produced a temperature cycle of approximately 7°F and a condenser coil capacity range from 20,503 to 27,188 BTUH. The corresponding change in the heating EER due to the auxiliary coil was from 8.5 to 11.3. Figure 16 shows the heating EER at different times during the tests.

The average coefficient of performance (COP) of the heat pump was 3.25 during Run 1 and 3.02 during Run 2. The maximum and minimum COP was 3.43 and 2.37, respectively. The maximum theoretical COP of the heat pump operating on the vapor-compression cycle can be calculated from the following equation (8):

$$COP = \frac{T_c}{T_c - T_s}$$

where T_s = evaporator temperature, °F absolute
T_c = condenser temperature, °F absolute

Based on the average conditions encountered in this research, the maximum theoretical COP of the closed-air system for drying peanuts using the vapor-compression cycle was 42 and 48 for Runs 1 and 2, respectively.

The typical vapor compression refrigeration cycle during the closed-air system test is plotted on the pressure-enthalpy diagram in Figure 17. Point A represents the state at which the liquid refrigerant entered the expansion valve. At the time these data were collected, point A was well into the sub-cooled region. The liquid is expanded at a constant enthalpy through the expansion valve to point B. The change in enthalpy from points B to C represents the cooling obtained in the evaporator coil. The portion of the line which lies to the right of the saturated vapor line is the degree of superheating which was occurring. The line CD indicates compression at constant entropy across the compressor. From points D to A is the enthalpy change across the condenser coil.

The actual refrigerant cycle in Figure 17 conforms as well as could be expected to the non-ideal cycle. It shows the normal subcooling and superheating and, to a small degree, the pressure loss in the high and low side piping. The system was not instrumented in such a manner to record the deviations caused by the pressure loss in the compressor valves.

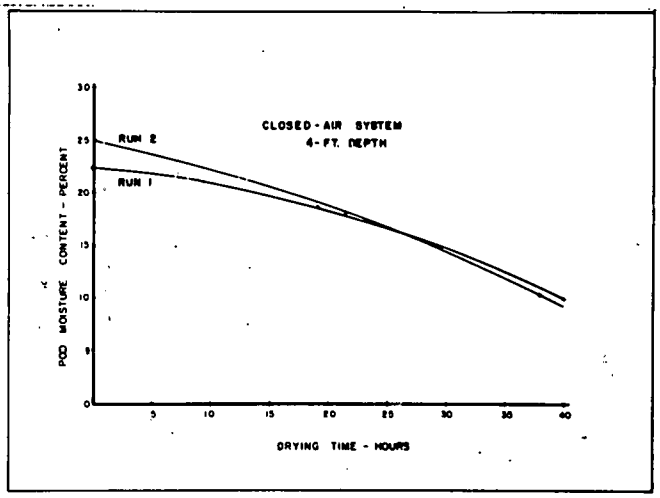

Figure 13. Pod moisture content of peanuts located near the top of the dryer during the drying process.

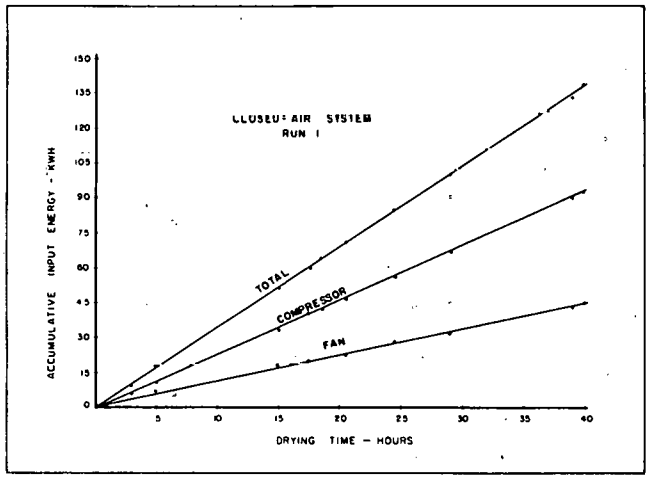

Figure 14. Accumulative input energy to the closed-air system during drying.

Table 1. Energy requirements for drying approximately one ton of wet peanuts with a closed-air system using a vapor-compression cycle.

	Average Pod Moisture Content - % Initial	- Final	Initial Weight of Peanuts	Drying Time hrs.	Water Removed lbs.	Energy Consumed - kwh Total	Fan	Compressor	Energy per lb. Water Removed kwh/lb Total	Compressor	Average Performance of Condenser Coil Capacity BTUH	EER
Run 1	22.7	9.1	2,060	40	345.5	139	47	92	0.40	0.27	25,369	11.1
Run 2	25.5	8.7	2,260	38	387.75	135	43.5	91.5	0.35	0.24	24,874	10.3

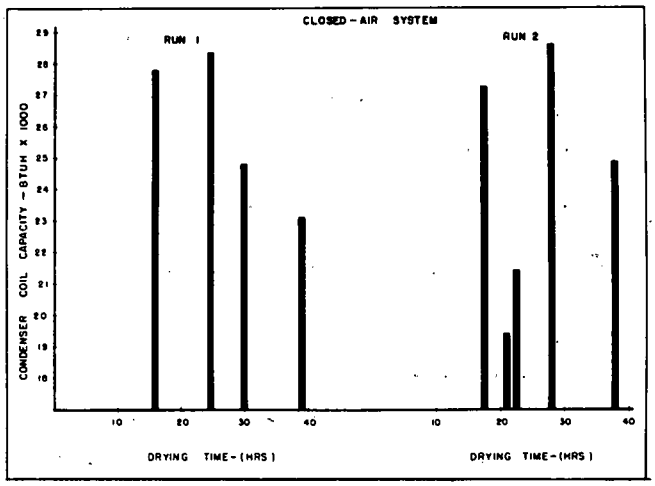

Figure 15. Condenser coil heating capacity at different times during the drying period.

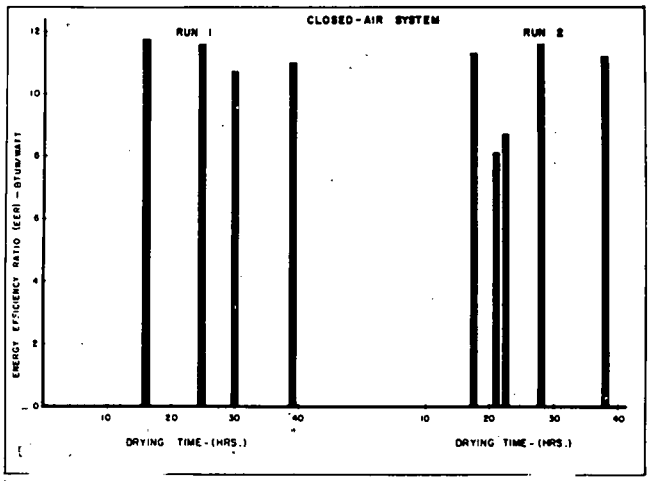

Figure 16. Heating energy efficiency ratio of refrigeration equipment at different times during the drying period.

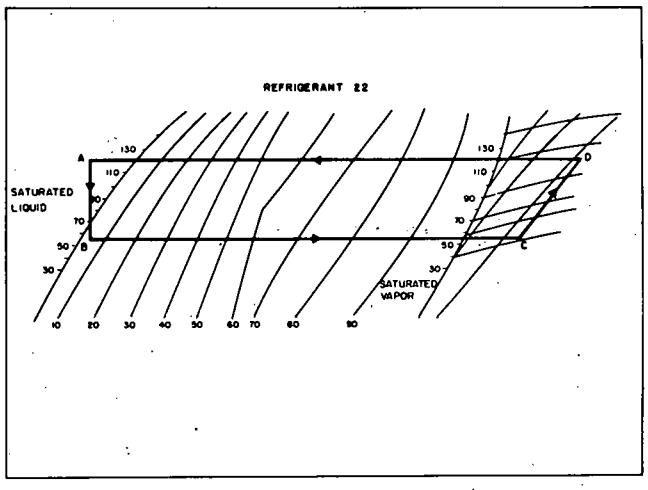

Figure 17. Typical vapor compression refrigeration cycle during closed-air system test.

Product Quality

The purpose of any mechanical drying operation for peanuts is the preservation of quality. Percents of sound splits and damage were used as a measure of quality for these tests, Table 2. Comparative results indicated that the peanuts dried in the closed-air system were of equal quality to those dried by other methods. Air-dried check samples were used for both test runs. Run 1 also had a check dryer of equal size operating under conventional supplemental heat procedures. Run 2 utilized this check dryer as a continuous heated air dryer operating with an average temperature rise above ambient of 18°F.

Damage figures listed in Table 2 represent the damage found throughout the dryer. This damage was determined by the Federal-State Inspection Service and was determined immediately after drying. Results show that the closed-air system was at least equally effective as the check samples. Run 2 resulted in no damage compared to 1 percent for the check dryer while the closed-air system and check dryer in Run 1 both had 1 percent damage.

Samples were taken from the bottom and top of the test bins during unloading. These samples were stored in an environmentally controlled room in order to equalize the moisture contents before shelling tests were conducted. Results found in Table 2 show that the closed-air system did not cause any significant increase on the sound splits during shelling. The air-dried check sample during Run 1 had 1.2 percent splits compared to an average of 1.1 and 0.9 for the closed-air system and check dryer, respectively. All three figures would round off to 1 percent on the grade sheet. The air-dried check sample for Run 2 had only 0.6 percent splits. The closed-air system resulted in an average of 1.7 percent splits while the check dryer had 1.5 percent. Run 2 percentages would round off to 1 and 2 percent and are unimportant since the grower is allowed 4 percent splits before any price deductions occur.

These comparative split percentages are very important when correlated to the drying rates. Increased drying rates in the closed-air system did not have the normal increase in splits due to rapid drying. The peanuts in the closed-air system in Run 1 dried 66 percent faster than the conventionally operated check dryer. A 48 percent increase was observed in Run 2 when compared to a dryer which had continuous heat.

Solar Energy

The basic interest of ERDA in the support of this research centered around the use of solar energy for drying peanuts. The conversion of solar energy into usable energy for peanut drying could theoretically be accomplished through the use of a solar-powered refrigeration machine. This machine would be incorporated with the closed-air system to furnish heated air for drying. A basic closed-air system utilizing a solar-powered refrigeration cycle is shown in Figure 18. The solar radiation would be used to heat water which would activate the generator of an absorption-type unit. This in turn would provide the heating and cooling for the closed-air system through heating and cooling coils located in the air stream.

The equipment requirements for this type of dryer utilizing solar radiation are discussed in this paper in order to give the reader a feeling for the potential of absorption units under this application. No brand names will be used or data referenced. The data presented in the following discussion represent the best estimates at the present time and were arrived at by searching available product literature, advertisements and personal conversations with manufacturer representatives.

The selection of the absorption refrigeration unit used in the closed-air system must be based on the cooling capacity. Even though the required enthalpy change for heating and cooling are theoretically the same in the closed-air system, the heat capacity of the absorption unit is much greater than the cooling capacity. This is similar to that found in the vapor-compression unit except it is of a much larger magnitude. For all practical purposes the heat rejected by the absorption unit will be equal to the cooling capacity plus the heat input to the unit. To maintain control of the closed-air system during

Table 2. Effect of the closed-air system on product quality.

Treatment	Damage - Percent	Sound Splits - Percent	Moisture Content During Shelling - Percent
Run 1			
Air-dried check	-	1.2	9.4
Closed-air system	1		
Bottom of dryer		1.4	9.6
Top of dryer		0.8	9.9
Check dryer using supplemental heat procedures	1		
Bottom of dryer		2.4	10.1
Top of dryer		0.6	10.0
Run 2			
Air-dried check	-	0.6	10.2
Closed-air system	0		
Bottom of dryer		2.2	9.7
Top of dryer		1.2	10.1
Check dryer using continuous heat with ΔT = 18°F	1		
Bottom of dryer		2.2	9.5
Top of dryer		0.8	10.0

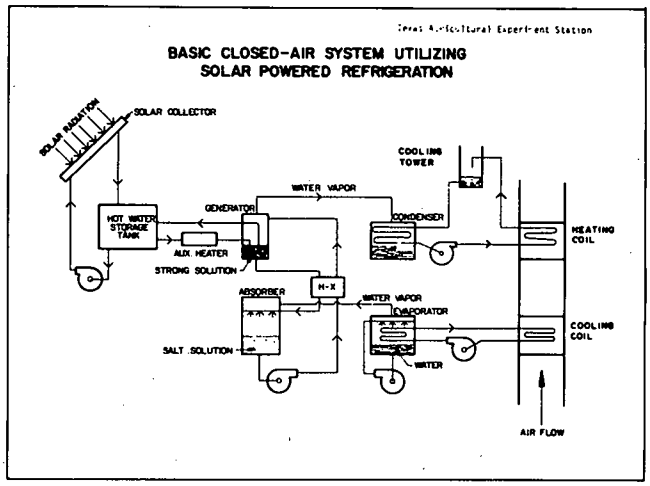

Figure 18. Closed-air system utilizing solar powered refrigeration.

operation, some provision must be utilized to exhaust the excess heat from the system. The most practical way appears to be with an external cooling tower piped in series with the closed-air system heating coil, Figure 18. In a commercial 3-ton absorption unit this excess heat will be approximately 50,000 BTUH, depending upon the conditions the system is operating under.

It is difficult to discuss the economics of the solar-powered refrigeration unit in the closed-air system because of limitations on unit capacity availability. There are only two sizes available in the capacity range required for peanut drying. These sizes are 3- and 25-ton units. Extrapolating the data presented in the report estimates a capacity requirement of about 10 tons to dry an average size load of peanuts. This would require at least three 3-ton units priced at $2,750 each.

The small commercial absorption units discussed above operate at a COP of around 0.72 and require a water temperature of 195°F. This is the temperature which must be produced by the solar collectors. The recommended collector area is 850 sq. ft. for each 3-ton unit. Larger areas would be required if storage was added to the system in order to be able to operate at night or under cloudy skies.

The capacity of an auxiliary heater to insure sufficient input heat to the absorption unit depends on the quantity of solar energy available. A typical clear day in the North Texas peanut producing area is shown in Figure 19. The total daily solar insolations received during the drying tests are given in Figure 20. Test Run 1 was started late on November 3 and continued until the morning of November 5. Run 2 started the night of November 9 and ended the morning of November 11. The daily insolations for November 5 to 8 are averages from a single total reading. However, each inclusive day making up the total measured insolation was similar.

Summary

This report presents the final results of a 3-year development program which determined the equipment requirements and engineering design procedures for utilizing a closed-air system in peanut dryers. These tests were performed in the North Texas peanut production area at the Texas A&M University Research and Extension Center at Stephenville.

The closed-air system was incorporated in a peanut dryer which consisted of a 4 ft. x 4 ft. x 8 ft. plywood bin interconnected with the necessary vapor compression refrigeration equipment to dry 1-ton loads of wet peanuts. All loads of peanuts used in these tests were harvested and handled in the conventional manner so that the only difference in the final product was the method of drying.

The results of these tests confirm that the theoretical principle of the closed-air system is valid and that this system can be used for drying peanuts. A refrigeration compressor with a nominal rating of 1-1/2 tons was used to dry 1-ton loads of peanuts having an average initial pod moisture content of 24 percent (wet basis). These loads were dried to below 10 percent pod moisture content in an average time of less than 40 hrs. The average heat capacity of the condenser coil of the refrigeration unit was around 25,000 BTUH with an average energy efficiency ratio (EER) of 10.7 BTUH per watt input.

The closed-air system required an auxiliary condensing coil to maintain control of the system near the design conditions. The particular coil used for this purpose during these tests caused a 7°F swing in the dry-bulb temperature entering the peanuts. Also, the air conditions produced by the closed-air system were influenced to a certain extent by ambient temperatures. Whenever the outside temperature was below about 50°F the air temperature entering the peanuts decreased below the design temperature. This is not considered to be a major problem, however, since this influence can be controlled by restricting heat losses from the drying bin.

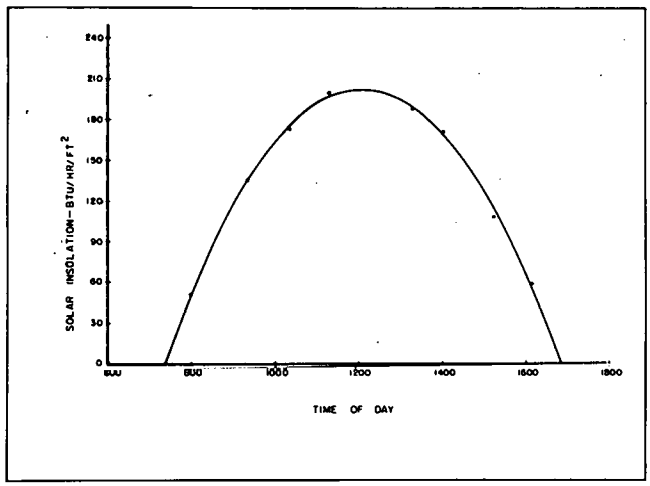

Figure 19. Solar insolation during typical clear day in the North Texas peanut production area.

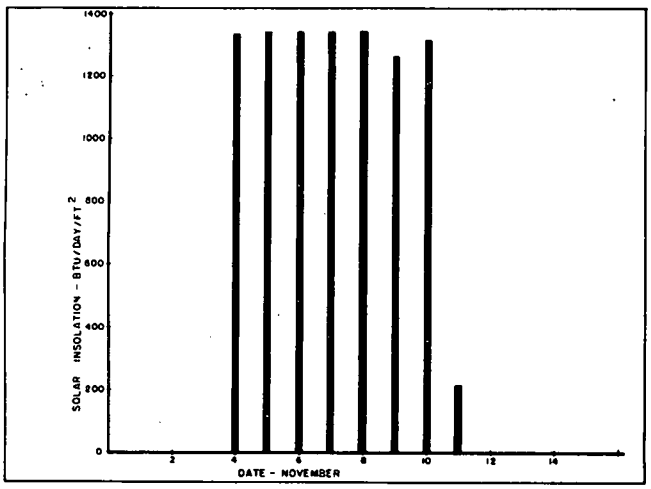

Figure 20. Total daily solar insolation received during the drying tests.

Analyses of grading results showed that the peanuts dried in the closed-air system were of equal quality to peanuts dried under present conventional procedures. The percent damaged kernels in dryers operating under conventional methods averaged 1 percent compared to 0.5 percent for peanuts dried in the closed-air system.

The use of solar radiation to supply the energy for a dryer operating as a closed-air system is discussed in the report. Data showing the typical insolation in this peanut-producing area of the State during the harvest period are presented as well as the suggested collector area required for commercial absorption refrigeration units.

References

1. Coble, C. G. and W. A. LePori. Energy consumption, conservation and projected needs for Texas Agriculture. Report S/D-12, Special Project B, Governor's Energy Advisory Council. December 1974.

2. Becker, C. F. and J. S. Boyd. Availability of Solar Energy. Agricultural Engineering 42(6):302-305. 1961.

3. Henderson, S. M. and C. V. Khe. Performance of a Matrix Solar Collector for Heating Air. American Society of Agricultural Engineers, Paper No. 75-3005. June 1975.

4. _____ Handbook of Air Conditioning System Design. McGraw-Hill Book Company. 1965.

5. White, G. M. and G. W. Isaacs. Solar-Power Cooling for Livestock Shelters. Agricultural Engineering 42(11):612-615, 621. 1961.

6. Flikke, A. M., et al. Grain Drying by Heat Pump. Agricultural Engineering, pp. 592-597. August 1957.

7. Ayers, D. L., et al. Use of a heat pump to conserve energy in grain drying. American Society of Agricultural Engineers, Paper No. 76-3519. December 1976

8. _____ ASHREA Guide and Data Book, Fundamentals and Equipment. American Society of Heating, Refrigerating and Air-Conditioning Engineers. Page 796. 1961.

Acknowledgements

The authors wish to acknowledge the following organizations for their support of this research:

1. Energy Research and Development Administration for their financial support during the final year of this research program.
2. Texas Power and Light Company for its financial and personnel support.
3. Lennox Industries, Inc. for its technical assistance and gift of specific equipment.
4. Sporlan Valve Company for its technical assistance and gift of components.
5. Erath County Electric Cooperative for its donation of personnel and equipment to wire the test installations.
6. Tecumseh Products Company for its technical assistance.

SOLAR DRYING OF HAY: OPEN CHAMBER DRYER DESIGN

by

B. L. Bledsoe
Professor
Agricultural Engineering Department
The University of Tennessee
Knoxville, Tennessee 37901

Large hay packages (big round bales and rectangular stacks) can be formed and transported with greater capacity (metric tons per hour) than conventional bales. If these packages could be formed from high moisture hay (at least 35 percent wet basis) and dried economically using solar heated air, one-day hay harvesting might become a reality even in the humid southeastern region of the United States.

The objective was to develop and evaluate means for applying energy gathered by simple, low-cost solar collectors to drying large packages of high moisture hay. Equipment developed was to be applicable to existing hay storage structures where possible.

Previous Work

A "solar heat absorber", consisting of a 55.7 m^2 false metal roof constructed over an existing barn roof was evaluated at the West Tennessee Agricultural Experiment Station in the late thirties (Weaver and Wylier, 1939). The absorber raised the temperature of outside air as much as 12°C while the relative humidity was lowered 33 percent when air was drawn under its surface at a rate of 85 m^3/min (1.5m^3/min per m^2 absorber surface) before being forced through loose hay in a barn mow. Further trials were recommended to demonstrate the value of the solar absorber to barn hay drying.

Conventional bales of hay have been successfully dried using solar heated air at less cost than with comparable drying using an oil-fired air heater (Williams, 1961). The collector had an absorber surface area of 139.4 m^2 consisting of 6 mil black polyethylene film. Air moved over the top side only of the film and was contained beneath a 4 mil clear cover film spaced 0.3 m above the absorber surface. Daily collector efficiency was about 33 percent.

An open-construction drying chamber for large roll bales was built by a dairyman in New York State (Successful Farming, 1975). He used a natural gas burner to heat the drying air to temperatures between 34 and 38°C and forced the heated air through roll bales set on end over 0.61 m diameter ducts. Density of the bales dried was only about 96 kg/m^3. Tightly rolled bales of hay have a density ranging from 160 to 224 kg/m^3.

Design

An open chamber design was chosen to readily disperse moisture-laden air coming from the hay packages and to keep construction simple and economical. The large hay packages were supported by the metal frames of the floor-duct air-discharge ports. The frames were fastened to concrete foundations. Port flanges, 50.8 mm in height, were built to penetrate into the hay packages to form a seal for directing air into the package.

Two types of structures were selected for collecting available solar energy: (1) the shed roof of an existing hay storage structure (bare plate collector), and (2) a free-standing, covered suspended-plate collector constructed near the existing barn.

Construction

The shed of a gambrel-type barn, common throughout the southeast, was remodeled to form the open chamber dryer. It was designed to accommodate both low-density stacks and low- and high-density rolls of hay. It had capacity to dry two stacks and five rolls of hay (about 5.5 metric tons) simultaneously. The shed roof was oriented south 27 degrees east and was inclined 16 degrees from the horizontal. It was used as the bare plate collector and had a surface area of 47.6 m^2. Latitude of the barn location was 36 degrees north. The roof material consisted of weathered, corrugated aluminum sheets. Half the surface was painted black (Glidden 908 flat black enamel over galvanized primer) while the most severely weathered half was left as found to evaluate the effect of surface finish on collector performance. A portion of the weathered half of the roof, about one-eighth of the surface, required new roofing panels before the chamber was complete. Plywood sheets, 6.4 mm thick, were nailed beneath the roof rafters to form 20 ducts for air flow, one between every pair of rafters, under the roof surface. Each duct was 102 mm x 559 mm in cross-section. Wood strips of 19 mm x 38 mm cross-section were nailed over joints of the plywood panels after caulking the joints with a silicone base sealant (G.E. 1200 construction sealant).

The free-standing, suspended-plate collector with an absorber surface area of 27.9 m^2 was constructed facing due south and was positioned southeast of the barn to avoid shadows throughout the day. Its location required a 21.3 m length of 0.46 m inside diameter wire reinforced tubing (Peabody ABC mine duct) to convey the heated air from the collector to the fan chamber. A portion of the duct was laid in a trench over which a wooden bridge was built to allow transport of the hay packages to and from the drying chamber. A plan view of the drying chamber and the collectors is shown in Figure 1.

The free-standing collector was patterned after one used for drying grain at Iowa State University (Kranzler, Bern, and Kline, 1975). Black 6 mil polyethylene film was the absorber surface. Air moved through the spaces above and below the absorber surface (Figure 2) to be heated for drying hay. The top cover consisted of 6-mil Monsanto 602 greenhouse film and was supported by wooden spars 0.61 m apart. The collector inclination was 28 degrees from the horizontal. Calculation of weighted average daily solar intensity, as a function of inclination angle and latitude (ASHRAE, 1972), indicated the 28 degree angle would be satisfactory for optimum energy collection.

The air delivery system was designed to have a nominal flow rate of 16 m^3/min per metric ton of hay (Hall, 1957). Duct cross-sectional areas were proportioned to give air velocities between 3 and 5 m per sec. A 0.46 m diameter tube-axle fan (Aerovent Model 7-18992-DW) provided the air flow. It could deliver 105 m^3/min of air at a static pressure of 625 Pa. and was powered by a 2.3 kW electric motor.

Dimensional relationship of the floor ducts, fan, fan plenum, and vertical duct are shown in Figure 3. Cross-sectional views of the floor ducts are shown in Figures 4 and 5. To provide an escape for any surface water that might enter the drying chamber, perforated plastic drain line was laid in an excavation down the center of the shed floor, and the excavation was filled with gravel. Concrete foundations to support the frames of the air discharge ports were placed, and the plywood floor ducts were fastened to the metal frames of the ports. Metal spacer blocks were positioned inside the plywood ducts to provide a solid connection between the foundation and the port frames where required (Figure 4).

Air flow from the roof collector came to the fan plenum by way of a variable cross-section header duct and a vertical "down" duct (Figure 6). A sliding plate valve in the vertical duct controlled flow of air from the roof collector. A variable opening shutter in the vertical duct allowed flow of ambient air into the fan plenum to control drying air temperature when desired. The shutter was operated by a proportional motor actuated by a dual bulb controller (Honeywell Model T991B-1037). The shutter could be opened to a stationary position for use of ambient air only for drying when desired. Air flow from the mine duct leading to the outdoor collector was controlled by a rotary plate valve in the fan plenum. The floor duct was connected to the fan through smooth transition geometry to keep air flow resistance to a minimum.

Instrumentation

A scanner-logger system with 90 channels for input signals printed dryer variables each hour. Copper-constantan thermocouples sensed dry bulb temperatures, and thermocouples within water saturated, aspirated wicks sensed wet bulb temperatures. Total solar radiation (direct and diffuse) received on a horizontal surface was detected by a 50 junction Eppley pyranometer (180° Weather Bureau type). Its output was plotted continuously by a strip chart recorder. Air velocity at various points in the delivery ducts and in the collectors was measured with a Thermo Systems, Inc. Model 1610-12 hot wire anemometer connected to a digital voltmeter for readout. Static pressures were measured with an inclined tube manometer.

Dryer Evaluation

Preliminary drying experiments with the open chamber dryer were performed in November and December, 1976. Three groups of high density roll bales, five in each group, were dried (Table 1). The bales were rolled from weedy fescue hay.

Accuracy of weight and moisture content data was not within the desired range of ± 2½% of true values; further tests will be required to verify the responses noted. However, results indicate that rolls of high density dried more slowly than less dense rolls, as happens with conventional bales (Wood and Parker, 1971). Greater air flow rates were observed through the less dense rolls when rolls of unequal density were dried simultaneously. Continuous operation of the fan (24 hours per day) caused redeposit of moisture in the hay packages at night.

With both the roof and the free-standing suspended-plate collectors connected to the fan inlet, mean air flow was 88.5 m^3/min from the roof collector and 34.3 m^3/min from the suspended-plate collector. Static pressure drop through the outdoor collector and the mine duct was 104 Pa. Static pressure drop through the roof collector, header duct, and vertical duct was 65 Pa.

Air velocity distribution in the roof collector ducts is shown in Figure 7. Velocity measurements were made at three equally spaced locations across each duct at a location about 0.5 m from the intersection of the roof ducts with the header duct. Interference within each duct to air flow by rafters at the juncture of the shed roof with the gambrel roof of the barn is clearly shown. Variation in velocity from duct to duct also occurred and was greatest (by a factor of 9.4) between ducts 11 and 20.

The mean temperature of air exiting from the various roof ducts might be expected to vary inversely with mean velocity, but this relationship did not hold (Table 2). Since rough lumber was used in the original construction of the barn and shed, duct cross-sectional dimensions were not completely uniform. The decking boards that supported the aluminum roofing also were not uniformly spaced across the roof surface. These boards were 25 mm thick by 152 mm wide and comprised an area of 27.9 m^2. They could affect heat storage and transfer to air flowing in the various roof ducts.

Evaluation of Solar Collectors

The amount of solar energy striking a horizontal surface at the dryer location for each day of the drying experiments was determined by integrating the instantaneous radiation recorded by the pyranometer. Polynomial equations relating tilted to horizontal surface incident radiation (Becker and Boyd, 1957) for the given latitude and date were then applied to calculate the energy available for the suspended-plate collector. These equations and a correction factor to account for the effect of the roof collector orientation of south 27 degrees east (Duffie and Beckman, 1974) were applied to calculate the energy available to the roof collector.

The available solar energy actually imparted to air moving through the collectors was determined from the change in enthalpy of the air. Daily mean wet- and dry-bulb air temperatures at the entrance and the exit of each collector were computed. These temperatures then were used as input parameters to a computer program (Wilhelm, 1976) which calculated change in enthalpy and mean specific volume of the heated air. With these values and the mean flow rate of air through the collectors known, the energy added by the collector was calculated with the following equation:

$$\Delta E = \frac{H_2 - H_1}{v} \times Q \times \frac{60 \text{ min}}{1 \text{ hr}} \times T \times \frac{1}{A} \times \frac{1 \text{ MJ}}{10^6 \text{ J}}$$

where

ΔE = collected energy, megajoules per m^2 - day
H_2 = heated air enthalpy, J per kg of dry air
H_1 = ambient air enthalpy, J per kg of dry air
v = heated air specific volume, m^3 per kg of dry air
Q = flow rate of heated air, m^3 per min
T = number of hours for accumulating solar energy per day
A = surface area of the collector, m^2

Then collector efficiency = $\frac{\text{collected energy}}{\text{available energy}} \times 100$

A summary of the collector efficiencies during the preliminary drying experiments is given in Table 3. Heat loss from the mine duct connecting the suspended-plate collector to the fan plenum was widely variable during the hay-curing period. This heat loss was to both ambient air and to the soil. The variations in ambient air temperature and in air temperatures at the exit of the collectors during the curing period are given in Table 4.

The mean efficiency of the painted half of the roof collector was 48.2 percent, compared to 42.4 percent for the unpainted half. The unpainted portion of the roof was less efficient in absorbing solar energy, but about one-eighth of its surface was comprised of new roof panels. Had the entire surface been of weathered roofing, its performance could have been near that of the black-painted roof surface.

Structural Revisions

Two structural failures occurred with the suspended-plate collector. Some of the softwood spars supporting the cover film absorbed moisture and buckled soon after the collector began operating. The use of 9.5 mm x 31.8 mm cross-section oak spars to replace the smaller softwood spars corrected the problem.

Low temperatures during the winter of 1976-77 contracted the black absorber film such that a longitudinal tear developed. Substitution of "three

vee" aluminum roofing (painted flat black over a primer coat) for the plastic film absorber surface corrected this failure. The corrugations of the roofing panels also provided for turbulent air flow through the collector.

Variable openings were constructed for the roof collector ducts with inlet area inversely proportioned to previous-measured mean air velocity. This change should provide more uniform air flow through the roof collector.

The revised open chamber dryer and collectors are shown in Figure 8. The photograph shows three types of hay packages being dried during extensive evaluation experiments begun in May, 1977.

Summary

An open-chamber dryer using solar heated air from two collectors (roof and free-standing suspended-plate) was designed, constructed and evaluated in drying late growth fescue hay in large round bales. The dryer performed satisfactorily during the November-December trial period. The mean drying rate was 1.3 percentage points of moisture (wet basis) per metric ton of dry matter-day for periods of operation of 4 days or more. However, volume of air flow through individual bales varied with bale density, and operation of the air system at night redeposited moisture in the hay; this practice was stopped late in the experiments.

Overall mean efficiency of the roof collector was 45 percent, compared to 66 percent for the free-standing, suspended-plate collector. Extensive heat loss occurred from the duct between the suspended-plate collector and the system fan such that mean overall suspended-plate collector-and-duct efficiency was only 34 percent, compared to 38 percent for the roof collector-and-duct efficiency.

Volume of air flow within the ducts under the roof collector varied across the width of the roof. The cross-sectional areas of openings admitting inlet air to the ducts were revised to give a more uniform air flow.

The softwood spars supporting the suspended-plate collector cover failed and required replacement with oak spars of greater cross-sectional dimensions. The 6-mil black polyethylene absorber sheet split from contraction stresses induced by the cold winter temperatures. It was replaced by corrugated aluminum panels painted black.

References Cited

1. ASHRAE Handbook of Fundamentals. 1972. American Society of Heating, Refrigerating and Air Conditioning Engineers, Inc., New York, Chapter 22, Tables 3 and 4.

2. Becker, Clarence F. and James S. Boyd. 1957. Solar radiation availability on surfaces in the United States as affected by season, orientation, latitude, altitude, and cloudiness. Solar Energy 1(1): 13-21.

3. Duffie, John A. and William A. Beckman. 1975. Solar energy thermal processes. John Wiley and Sons, New York. Chapter 3.

4. Hall, Carl W. 1957. Drying farm crops. Edward Brothers, Inc. Ann Arbor, Michigan.

5. Kranzler, Glenn, C. J. Bern and G. L. Kline. 1975. Grain drying with supplemental solar heat. ASAE Annual Meeting, Davis, California, Paper No. 75-3001.

6. Successful Farming. 1975. I tailored big bales to my dairy system. 73(7): D2-D4.

References Cited (cont'd.)

7. Weaver, J. W. and C. E. Wylie. 1939. Drying hay in the barn and testing its feeding value. Bulletin No. 170. Tennessee Agricultural Experiment Station, Knoxville, Tennessee.

8. Wilhelm, L. R. 1976. Numerical calculation of psychrometric properties in SI units. Transactions of the ASAE 19(2)8: 318-321, 325.

9. Williams, Larry G. 1961. Application of solar energy to hay and corn drying (a progress report). ASAE Pacific Northwest Section Meeting, Boise, Idaho, unnumbered paper.

10. Wood, J. B. M. and J. Parker. 1971. "Respiration during the drying of hay." J. Agric. Engr. Res. 16(3): 179-191.

TABLE 1. Summary of drying experiments during preliminary evaluation of the open chamber dryer.

Exp. No.	Time Period	Management	Metric Tons of Hay (wet wt/dry wt)	Mean Bale Density (wet basis) kg m^3	Mean Initial Moisture Content (wet basis) %	Mean Final Moisture Content (wet basis) %	Drying Rate % w.b./metric ton dry matter-day
1	1400 hrs, 4 Nov 76 to 2000 hrs, 6 Nov 76 (2.25 days)	Continuous fan operation; air pulled from both roof and free standing collectors	2.9/1.9	144-192	34.1	31.6	0.2
2	1800 hrs, 9 Nov 76 to 2000 hrs, 13 Nov 76 (4.1 days)	Continuous fan operation; air pulled from both roof and free standing collectors	1.6/1.2	88-144	22.1	15.1	1.4
3	1600 hrs, 18 Nov 76 to 1600 hrs 24 Nov 76 (6 days)	Continuous fan operation; air pulled from both roof and free standing collectors	2.4/1.5	112-192	35.5		
	1600 hrs 24 Nov 76 to 1100 hrs, 30 Nov 76	System shut down					
	1100 hrs, 30 Nov 76 to 1600 hrs, 3 Dec 76 (3.2 days)	Fan operated from 0800 to 1600 hrs daily; air pulled from free standing collector only				17.4	1.3 overall

TABLE 2. Variation of air temperature with air velocity for roof ducts.

Quantity	Duct Number 2	5	8	13	16	19
Mean Velocity, m/sec	0.5	1.0	1.6	1.9	1.0	0.5
Mean Temperature at Time of Velocity Reading (1700 hrs), °C	7.5	7.4	7.5	6.7	7.5	7.6
Mean Temperature for Day, °C	11.3	11.5	10.9	11.9	11.6	11.9
Range of Temperatures for Day, °C	0.2-20.1	1.0-21.8	1.1-20.9	1.9-22.2	1.5-21.7	0.9-21.8

Measurements taken November 11, 19, 23, 1976.

Velocity ratio of air in ducts 11 and 20 = $\frac{2.669}{0.284}$ = 9.4

TABLE 3. Efficiencies of suspended-plate and roof solar collectors with available energy for the indicated curing days in 1976.

Date and Time Interval of Operation	Suspended-plate Solar Energy Available to Collector (Mj/day)	Collector Efficiency %	Collector and Duct Efficiency %	Roof Solar Energy Available to Collector (Mj/day)	Collector Efficiency %	Collector and Duct Efficiency %
11-6 (10 hrs)	19.5	81.1	33.0	16.5	76.9	29.7
11-10 (12 hrs)	17.2	-	38.9	14.5	44.8	43.9
11-11 (10 hrs)	9.6	64.2	51.3	8.1	56.2	44.8
11-12 (11 hrs)	8.0	55.4	36.3	6.7	32.5	30.2
11-13 (12 hrs)	14.3	62.5	35.9	12.0	32.6	29.9
11-19 (11 hrs)	14.2	59.4	29.1	11.8	39.2	37.6
11-20 (11 hrs)	7.4	52.6	28.8	6.2	46.5	43.9
11-21 (9 hrs)	13.4	62.9	30.8	11.2	36.6	31.5
11-22 (8 hrs)	12.8	67.5	28.4	10.6	41.8	41.7
11-23 (9 hrs)	18.1	67.3	34.1	15.0	42.2	39.1
11-24 (9 hrs)	13.8	81.6	23.6	11.4	50.1	48.3
Means		65.5	33.7		45.4	38.2

Mean air flow through suspended-plate collector = 1.23 m^3/min - m^2 collector area.
Mean air flow through roof collector = 1.86 m^3/min - m^2 collector area.

TABLE 4. Temperature means and ranges for ambient and heated air during the indicated curing days in 1976.

Date	Hours of Operation	Temperatures °C									
		Ambient Air		Suspended-plate				Roof			
				Collector Only		Collector and Duct		Collector Only		Collector and Duct	
		Mean	Range	Mean	Range	Mean	Range	Mean	Range	Mean	Range
11- 6	10	8.81	0.6→12.1	29.06	2.7→46.0	10.02	6.0→12.7	13.50	8.3→17.2	-	-0.3→12.4
11-10	12	14.54	10.2→17.2	22.34	8.3→33.0	19.14	8.8→26.1	17.28	10.1→22.5	16.93	10.2→21.7
11-11	10	7.09	0.3→10.3	12.32	2.0→19.8	10.94	1.7→16.8	10.47	1.5→19.1	10.03	1.3→14.2
11-12	11	2.41	0.9→ 3.6	5.42	0.8→12.4	4.60	0.9→ 9.6	5.74	0.8→ 7.1	3.52	0.8→ 6.6
11-13	12	1.59	-4.1→ 4.5	8.11	-6.2→19.2	6.47	-5.7→14.9	4.27	-5.5→ 9.1	3.94	-5.3→ 8.6
11-19	11	14.29	5.4→17.2	21.01	8.0→33.8	18.18	7.2→26.9	16.42	7.1→21.9	16.08	6.9→21.0
11-20	11	10.20	5.9→12.2	12.48	5.4→17.6	11.69	5.4→15.3	11.35	5.8→14.1	11.11	5.8→13.6
11-21	9	7.49	4.9→ 9.7	14.49	2.8→25.8	11.43	3.5→18.6	9.47	3.9→14.3	8.88	2.9→13.9
11-22	8	2.38	0.6→ 4.2	10.39	5.2→14.6	7.32	5.4→10.8	5.86	4.0→ 8.4	5.53	3.3→ 7.9
11-23	9	3.53	0.8→ 5.9	16.74	-12.6→31.0	12.60	0.6→20.2	8.97	2.0→13.3	8.19	1.4→11.9
11-24	9	9.54	5.3→11.9	18.46	6.6→28.2	13.34	2.6→20.6	11.98	5.7→15.0	11.53	5.6→14.1

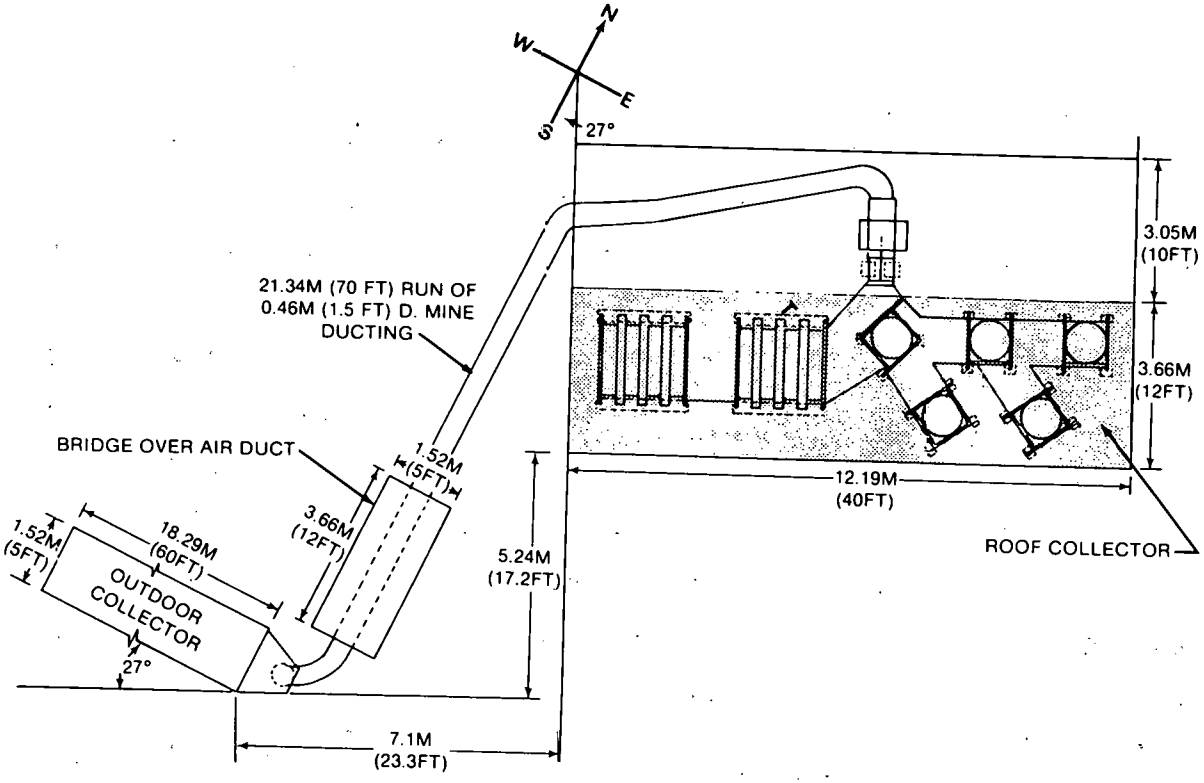

Figure 1. Plan view of the solar drying chamber and the associated collectors.

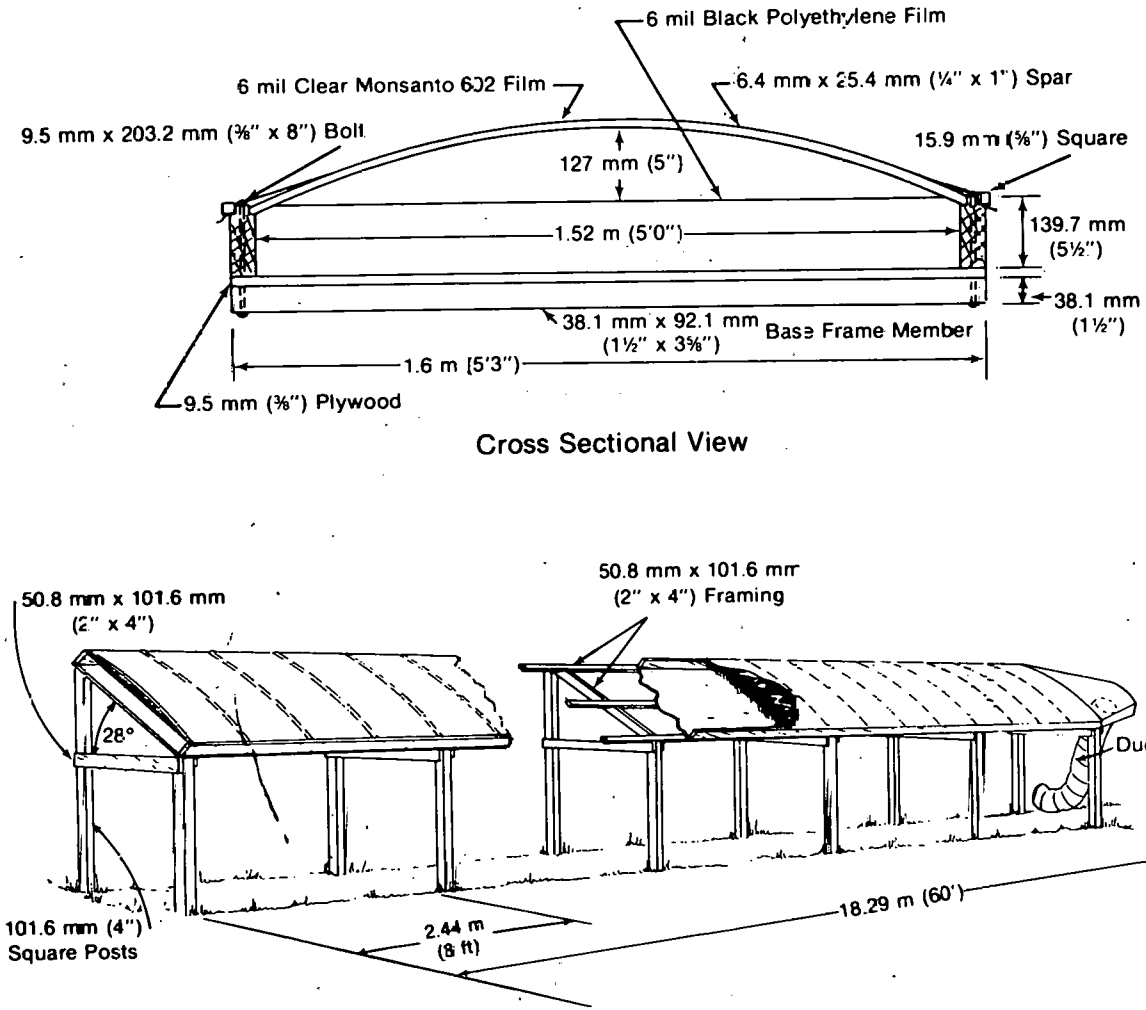

Figure 2. Construction details of the free standing suspended film collector.

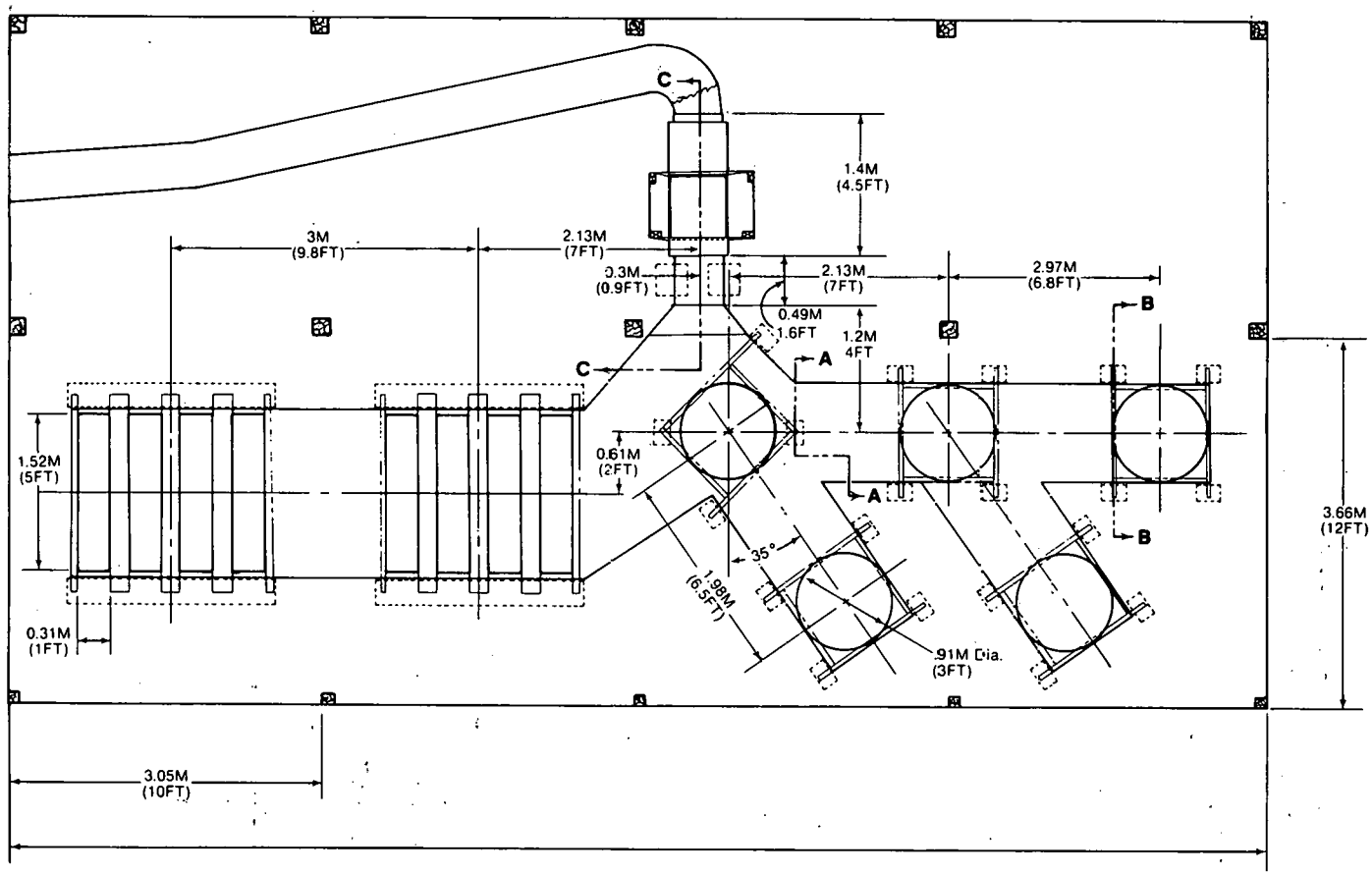

Figure 3. Plan view of the drying chamber.

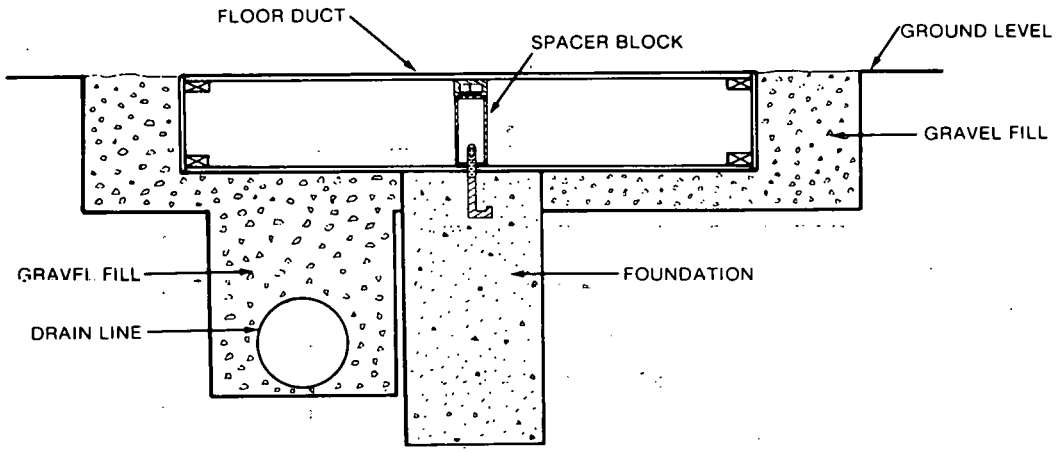

SECTION **A-A**

Figure 4. Sectional view of a floor duct in the drying chamber showing a metal spacer block between the port frame and the duct base sheet and foundation.

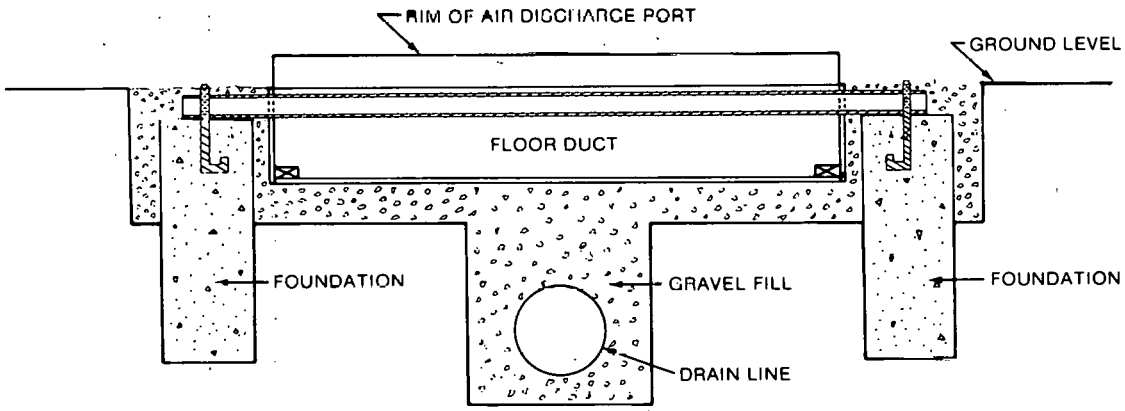

SECTION **B-B**

Figure 5. Sectional view of a floor duct showing the rim of the air discharge port. The rim presses into the base of hay packages to form a seal and direct air into the package.

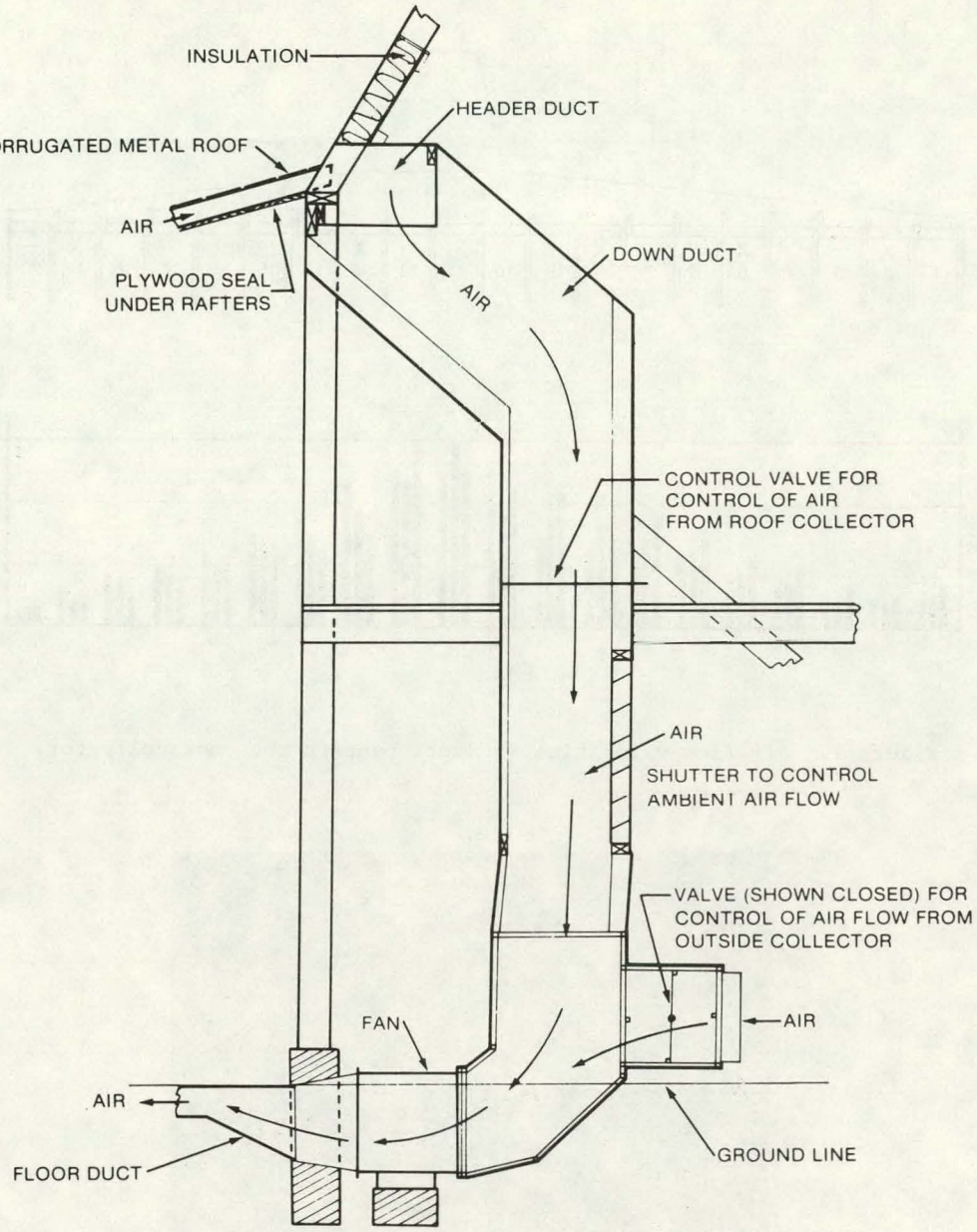

SECTION **C-C**

Figure 6. Sectional view of vertical duct, fan plenum, fan, and transition to floor duct.

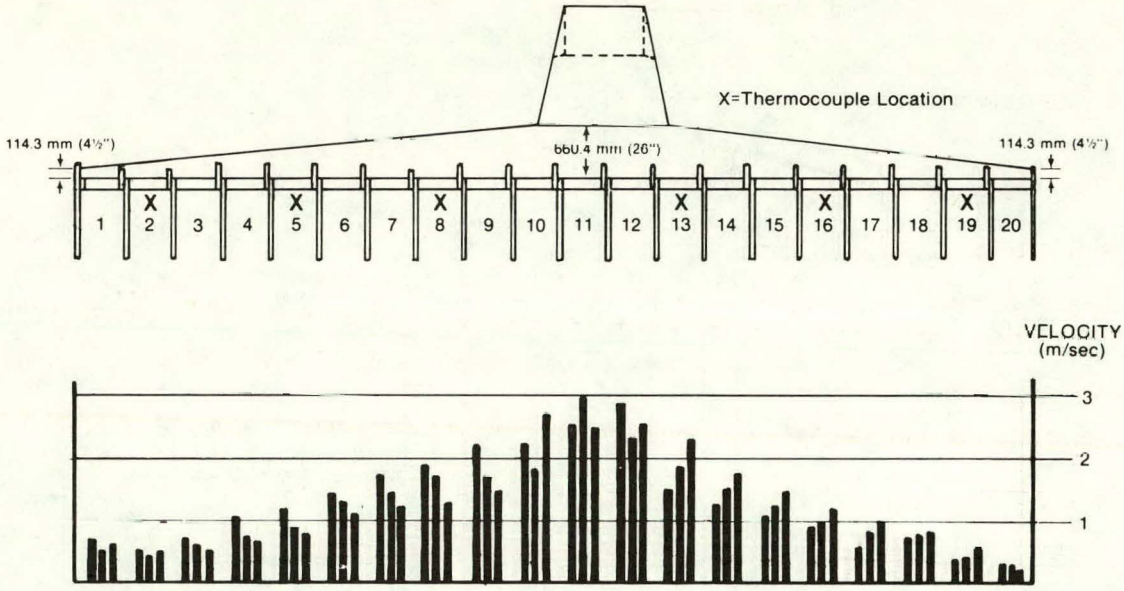

Figure 7. Air flow velocities in ducts beneath the roof collector.

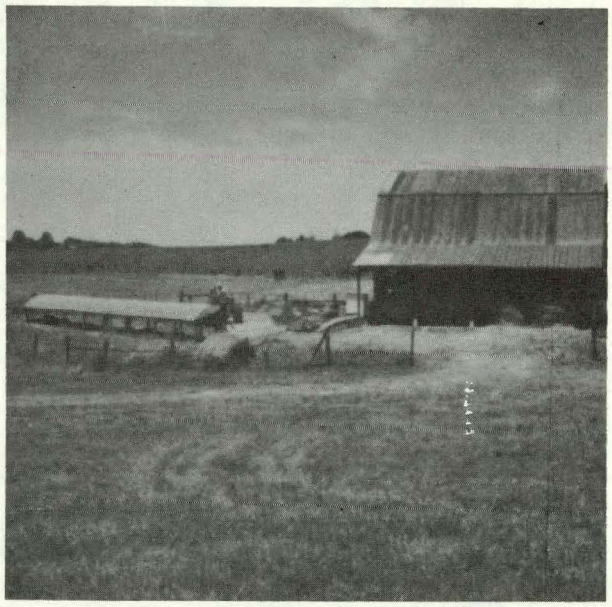

Figure 8. Overall view of drying chamber and collectors during 1977 evaluation experiments.

SOLAR DRYING OF HAY IN BIG PACKAGES

by

Z. A. Henry
Associate Professor
Agricultural Engineering Department
The University of Tennessee
Knoxville, Tennessee 37901

The application of solar energy to drying large hay packages can be correctly evaluated only if consideration is given to the mechanism of drying within the package. The objective of this investigation was to evaluate the drying mechanism within the large hay package in a system where the air movement was restricted only by the package itself (open-drying-chamber construction).

PROCEDURE

The solar collector and drying chamber system for this study have been described by Bledsoe (1977). The system provided for simultaneous drying of five large round bales and two stacks (approximately 500 kg each for the bales and 900 kg each for the stacks), in an open drying chamber where the large hay packages were placed over an open grillwork mounted in the ducts of the forced air system (Figure 1). The system was designed for a minimum air flow rate of 16 m^3 per minute per metric ton of hay (Hall, 1957).

Dry- and wet-bulb temperatures and air volume of air flow were measured in the plenum under the bales, dry-bulb and dew-point temperatures were measured at the center of the bales, and dry bulb temperature only was measured at top of the bales. A special lithium-chloride, heated-electrical hygrometer designed and constructed for this experiment was used for measurement of psychrometric properties at the center of the bale (Eller, 1977).

Three tests, each of which included five high-density, high-moisture roll bales of late growth fescue, were conducted on the following dates in the fall of 1976: (1) November 4-6; (2) November 9-13; and (3) November 18-24, and November 30 to December 3. Lack of labor and inclement weather caused the experiment to be interrupted during the third test. Stacks were not used in this experiment; therefore, the duct to this area of the drying chamber was blocked. A moisture sample for each bale (combined cored subsamples from top, center and bottom) was obtained periodically during the drying period of each day.

RESULTS

The adverse conditions of late fall weather affected the experiment. Not only were drying conditions unfavorable, but data collection was hampered. Tests one and two provided excellent temperature and isolation data for late fall conditions and also excellent data for bale internal conditions. The data from test three were not as good due to inclement weather and especially because freezing temperatures affected the wet-bulb measurements. Therefore, only limited data are presented from the third test. Data from bale 5 of test one are presented as representative of the drying experiment. At the ambient temperatures existing for this experiment the respiration heat was negligible (Wilkerson and Hall, 1966).

Relative humidities of ambient and heated air reached a difference as great as 30 percentage points at the time of greatest difference between ambient and heated air temperatures (Figure 2). A spread in ambient and heated air temperatures of approximately 16 C occurred at various times during the second test. However, the temperature differences between heated air and ambient air never exceeded 4 C in the first test. Increases in vapor pressure at the center of the bale (Figure 3) coincided with the times of highest temperature and lowest relative humidity of the drying air (times of greatest drying potential). The difference in heated and ambient air vapor pressures can be attributed to measurement error primarily as a result of the positioning of the sensing element with respect to the collector inlet.

Each of the bale center relative humidity curves provided a slightly different perspective of moisture removal from the hay bale; however, the basic trend is represented by Figure 2. The bale center relative humidity started at 85 percent and generally declined throughout the cure with the exception of a sharp increase from 0600 to 1000 hours on November 6. The increase occurred at the point when heated air temperature increased suddenly which caused moisture to be removed from the bottom of the bale and the vapor at the center of the bale to rise (Figure 3). After the sudden rise in bale-center relative humidity, it began to drop due to the movement of the moisture up through the bale. Data from all bales showed a general decline in the bale center relative humidity from the beginning of the cures to the end. This indicated a decline in hay moisture content, which was substantiated by the data of Table 1.

Figure 2 shows that during the daylight hours, when solar radiation was being received, the drying air temperature decreased as it moved through the bale. During periods of no solar radiation the relative temperatures below the bale, at the bale center, and at the bale top shifted, with the air temperature at the center of the bale being highest and the temperature at the top of the bale remaining lowest. Thus, the heated-air temperature was between the top and center bale temperatures. The temperature at the top of the bale was lower than ambient during most of the drying period with the effect being especially evident during the daylight hours. This, in addition to high moisture conditions (detectable by feel) at the top of the bale, indicated that evaporative cooling was occurring, and some moisture removed from the lower part of the bale was being deposited at the top.

Data for a four-hour period selected for bale 5 of test one (Table 2) were used to determine the amount of moisture removed from a representative bale in a given period of time. The assumption was made that the air was saturated at the top of the bale since free moisture was observed to continually exist there. By using the humidity ratio differences of heated, bale center and bale top air (Table 2) with an average air flow rate of 18.8 m^3 per minute through the bale an estimated 16.8 kg of water was removed from the bottom portion of the bale in the four-hour period with at least 3.2 kg being redeposited in the bale. Thus, only 13.6 kg of water exited the bale. This conclusion was supported by lower air temperatures and detectable high moisture conditions at the top of the bale as previously discussed. The 13.6 kg of water removed from the bale represented a substantial drying rate. However, since the temperature of the air entering the bale was between the center-bale and top-bale temperatures for periods of no solar radiation, it can be assumed that some moisture was being released from the air to the hay during this period. Freezing temperatures prevented data collection which may have verified this. Partial verification may be obtained by examination of oscillating moisture content values (Table 1). Also the data from bale 5 of test one showed a moisture loss of 5.3 percentage points during the drying period. For an approximate bale weight of 500 kg, this would mean a total moisture loss of 26.5 kg, or 8.8 kg net moisture loss per day. Thus, for the specified case, much of the moisture removed during the drying period of the day was apparently regained during the cold damp night hours.

TABLE 1. Wet basis moisture content at the beginning of each cure and at the end of each subsequent curing day.

DATE	Bales 1	2	3	4	5	Avg.
			Test One			
11/04/76	35.7	32.7	34.5	35.9	33.1	34.1
11/05/76	30.9	31.4	29.7	33.6	30.4	31.2
11/06/76	31.9	32.2	32.2	34.0	27.8	31.62
			Test Two			
11/09/76	21.5	20.5	21.4	20.6	21.8	21.2
11/10/76	18.6	17.4	18.1	20.1	18.2	18.4
11/11/76	14.2	20.4	15.3	16.5	14.5	16.2
11/12/76	15.0	16.5	18.0	18.3	16.8	17.0
11/13/76	14.5	17.6	13.2	15.5	14.2	15.1
			Test Three			
11/18/76	25.6	37.9	43.1	32.5	39.7	35.5
11/19/76	21.9	35.9	41.8	30.5	41.3	34.3
11/20/76	23.0	36.9	31.6	33.1	39.3	32.8
11/21/76	20.1	28.9	36.7	32.0	38.1	31.2
11/22/76	19.6	20.9	42.4	30.3	37.1	30.1
11/23/76	24.2	31.5	31.5	26.8	36.7	30.1
11/24/76	17.1	33.1	31.3	29.4	28.6	27.9

The nature of the experiment did not permit the hay to be dried to optimum moisture level for storage; however, the three drying zones described by Wood and Parker (1971) were evident.

SUMMARY

Five high-density roll bales were dried in three separate tests in the late fall of 1976 using the combined heat from a roof collector and a suspended-plate collector. The drying reduced the wet-basis moisture content of hay (initially at about 35 percent) by approximately 5 percentage points. However, the total drying during inclement weather did not give sufficient reduction for long-term storage. Psychrometric properties of air inside the bale showed that a drying condition existed as the drying potential of the air increased in the daylight hours; but, as air was passed through the bale during the night hours, moisture was deposited within the bale.

REFERENCES

Bledsoe, B. L. 1977. Solar Drying of Hay: Open Chamber Dryer Design. Solar Crop Drying Conference, North Carolina State University, Raleigh, North Carolina. June 30, 1977.

Eller, D. D. 1977. Evaluation of Solar Hay Drying and Collector Efficiency. Unpublished Master of Science Thesis. University of Tennessee, Knoxville, Tennessee.

Hall, C. W. 1957. Drying Farm Crops. Edward Brothers, Inc., Ann Arbor, Michigan.

Wilkinson, R. H., and C. W. Hall. 1966. Respiration Heat of Harvested Forage. Transactions of the ASAE. 9(3):424-427.

Wood, J. G. M., and J. Parker. 1971. Respiration During the Drying of Hay. Journal of Agricultural Engineering Research. 16(3):179-191.

TABLE 2. Heated air, bale-center air, and bale-top air data for bale 5 of test one for a four-hour period of November 6, 1976.

	Heated Air			Bale-Center Air			Bale-Top Air		
Time*	Dry Bulb Temp- C	Wet Bulb Temp. C	Humidity Ratio kg/kg Dry Air	Dry Bulb Temp. C	Dew Point Temp. C	Humidity Ratio kg/kg Dry Air	Dry Bulb Temp. C	Relative Humidity Percent	Humidity Ratio kg/kg Dry Air
1200	10.2	4.8	0.00313	7.4	5.6	0.00563	3.8	100**	0.00496
1300	12.0	5.3	0.00279	8.0	6.0	0.00579	4.3	100**	0.00514
1400	11.6	5.2	0.00287	8.4	6.1	0.00584	4.7	100**	0.00529
1500	12.9	5.8	0.00283	8.7	6.5	0.00600	5.1	100**	0.00544

*Twenty-four hour clock.

**The assumption was made that saturation existed at the top of the bale as evidenced by the continual wet condition of the hay at this level.

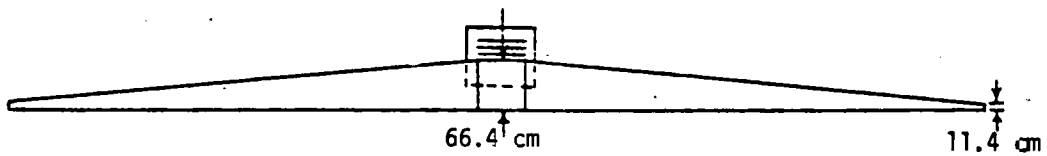

Top view of header duct

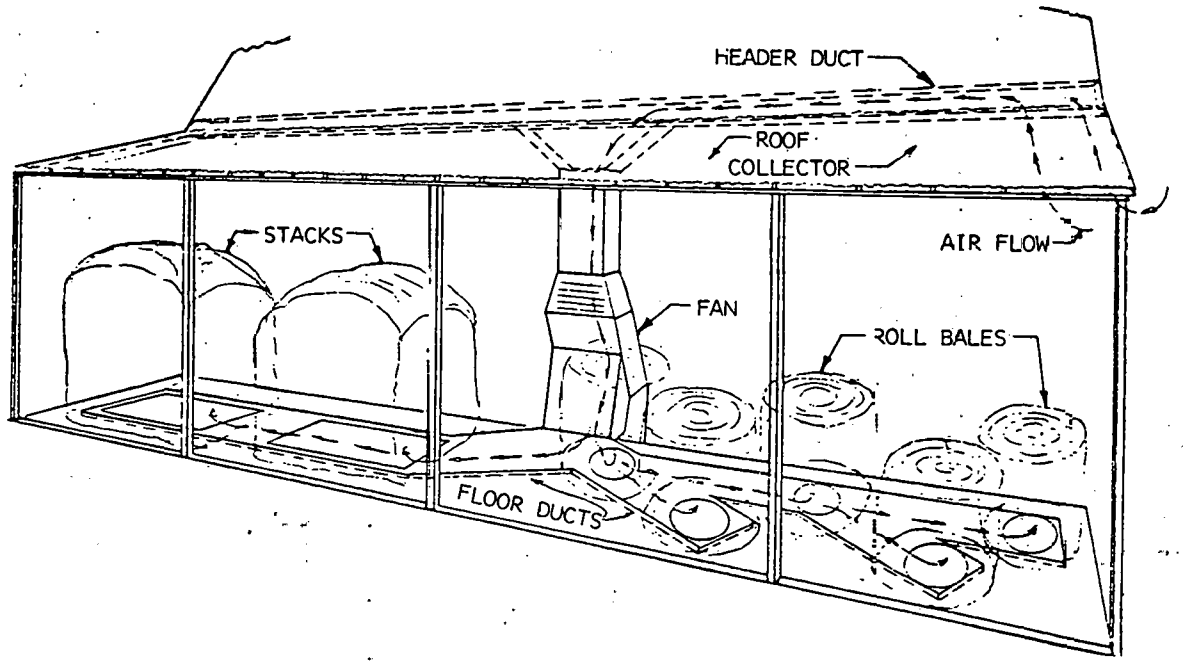

FIGURE 1. Details of the drying chamber.

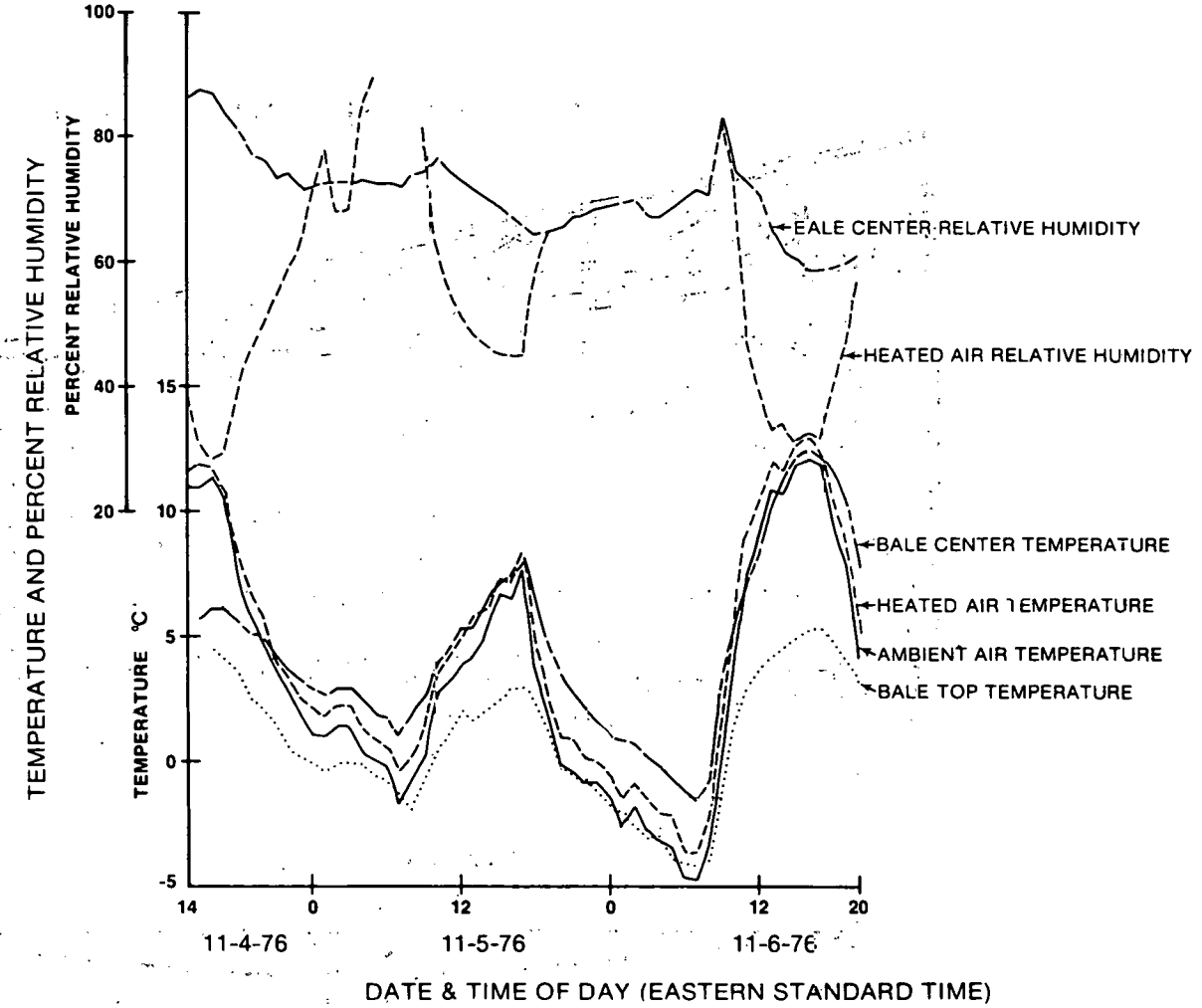

FIGURE 2. Ambient, heated, bale-top, and bale-center air temperatures, and relative humidities of heated and bale-center air for bale 5 of test one.

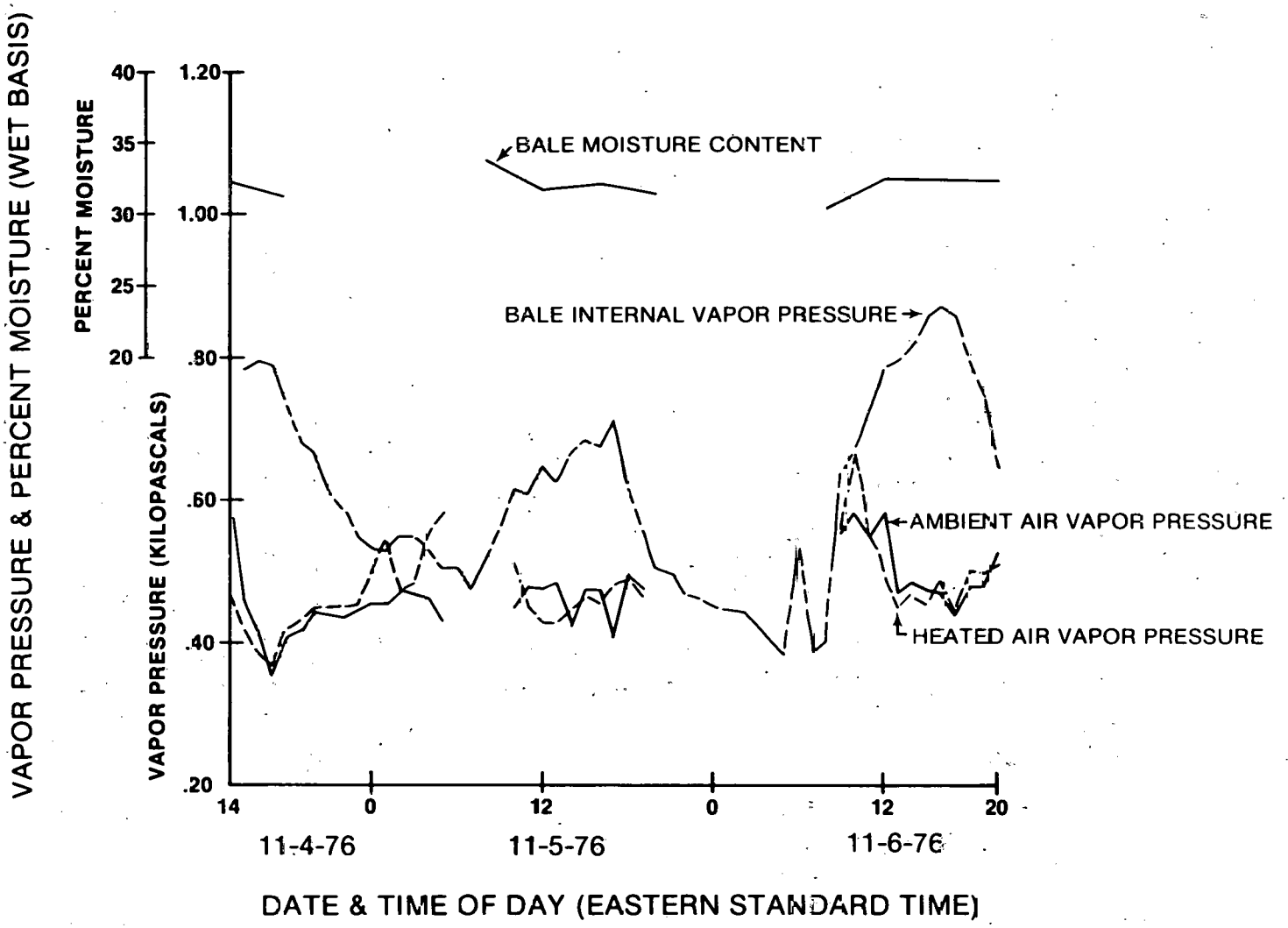

FIGURE 3. Vapor pressure of ambient, heated, and bale-center air and bale moisture content for bale 5 of test one.

CURING BURLEY TOBACCO WITH SOLAR ENERGY [1/]

by

Linus R. Walton, Wiley H. Henson, Jr., Samuel G. McNeill,
John N. Walker, B. F. Parker, and Joe M. Bunn

Agricultural Engineer, ARS, USDA; Agricultural Engineer,
ARS, USDA; Agricultural Engineer; Professor
and Chairman; Professor; and Associate Professor,
Agricultural Engineering Dept., University of Kentucky,
Lexington, Ky. 40506

INTRODUCTION

Adverse weather conditions during curing of burley tobacco lowers the quality of the cured leaf. Hamon (1954) set the average loss in value to the crop at 12 percent, based on field observations. He further indicated that approximately half of this loss could be prevented by the timely use of supplemental heat to raise temperature and lower relative humidity during sustained periods of high humidity. The recommended amount of supplemental heat for the conventional burley barn is approximately 145,000 J/s-ha (200,000 Btu/hr-A). Duncan (1976) reported that producers have used as much as 2800 liters/ha (300 gal/A) of LP gas in the new, two-tier, forced-ventilation barn. Curing burley tobacco with solar energy would alleviate the burley producers' dependence on fossil fuels as his heat source.

A two-stage solar curing system consisting of solar field curing and curing in a solar barn is being developed. An experiment (Walton, et al., 1976) conducted during the 1975 curing season established that with 2 days of solar field curing during cool weather, the market price of the tobacco was as much as $0.10/lb higher than that of tobacco cured in a conventional curing barn. During solar field curing, drying rate was reduced and yellowing rate increased, both of which are beneficial in alleviating damage to quality from overdrying of burley tobacco. It was concluded that the producer should leave his tobacco in the field for 2 days of solar field curing during cool dry weather.

This paper reports the initial research effort by the Agricultural Research Service, U. S. Department of Agriculture [2/] and the University of Kentucky to develop a solar curing structure for burley tobacco. The specific objective of the research was to experimentally evaluate the capabilities of four forced-ventilation curing chambers to reduce high relative humidity during curing:

1. A conventional, two-tier chamber with conventional metal roof.
2. A transmitting-roof chamber with a fiberglass roof.
3. A chamber with a solar collector (referred to later as the noncharging collector) and no storage.

1/ The investigation reported in this paper (No. 77-2-67) is in connection with a joint project of the Southern Region, Agricultural Research Service, U. S. Department of Agriculture, and the Agricultural Experiment Station, College of Agriculture, University of Kentucky, and is published with the approval of the Director of the Station.

2/ This research was funded in part by the Energy Research and Development Administration.

4. A chamber with a solar collector (referred to later as the charging collector) and rockbed storage.

For maximum effectiveness, the relative humidity within the facility should be in the 65 to 70% range. The solar curing facility should have the capability to overcome the underdrying of burley tobacco which occurs when the relative humidity is above 70% (Walton et al., 1973). The greatest danger, therefore, occurs during rainy periods.

EXPERIMENTAL METHODS

A solar curing facility consisting of the four forced-ventilation curing chambers was designed and built during 1976 and was used to cure burley tobacco in the fall. The first chamber was a conventional chamber with a metal roof designed to simulate the two-tier forced ventilation barn developed at the University of Kentucky (Bunn, et al., 1973). A fan was used to continually blow fresh air through the tobacco at a velocity of 4.57 m/min (15 ft/min). This chamber has no capability to modify the curing environment and was used as a standard of comparison for the other chambers.

The transmitting-roof chamber had a fiberglass roof that transmitted solar energy directly into the chamber. The tobacco and interior surfaces of the chamber absorbed the solar energy transmitted through the roof. Heat was then transferred to the air by convection. The temperature and relative humidity of the air was modified only during the day and then in proportion to the solar radiation intensity.

The solar chamber without storage used heat from a flat plate air heating collector to provide daily temperature and relative humidity modification within the solar-collector-no-storage-chamber during the daylight hours. The premise for including the chambers with the transmitting roof and the collector without heat storage was to facilitate good curing during intermittent rainy and sunny weather with minimal cost. In addition, the daily application of heat would aid in curing tightly packed tobacco in a forced-ventilation system.

We designed one chamber with solar collector and rockbed with the capability to store heat over a period of several days which would then be available for withdrawal over a period of several days during the cure without replenishment. The solar-collector-rockbed-storage chamber was the only chamber capable of providing environmental modification during prolonged rainy periods.

The chambers were 1.13 m (3.71 ft) wide, 3.35 m (11 ft) long, and 4.27 m (14 ft) high. Individual fans continually moved fresh air vertically downward through the tobacco at 4.18 to 4.45 m/min (13.7 to 14.6 ft/min). The solar curing facility is shown in Figure 1.

The solar collectors were flat plate collectors built as part of the roof. They were constructed at an angle of 30° from the horizontal for optimum operation during the curing months of August, September, and October (Barfield, Hill, and Walker 1975). They had a single fiberglass cover. In the charging collector, 4.36 m^3/min (154 cfm) of air was circulated between the abosrber plate and another plate placed 2.54 cm (1 in.) below the absorber plate. In the noncharging collector, 2.04 m^3/min (72 cfm) of air was circulated beneath the absorber plate in a channel that was 4.45 cm (1.75 in.) deep. The backs of both collectors were insulated with 8.9 cm (3.5 in.) of standard fiberglass insulation. The length of each collector was about 10.36 m (34 ft). The surface areas of the charging and noncharging collectors were 8.27 m^2 (89.0 ft^2) and 6.32 m^2 (68.0 ft^2), respectively.

Inlet and outlet temperatures of the air flowing through the collectors were determined by use of thermocouples. Solar radiation was determined by use of a pyrheliometer placed in a plane parallel to that of the collector. The average efficiency was calculated for each collector for selected days.

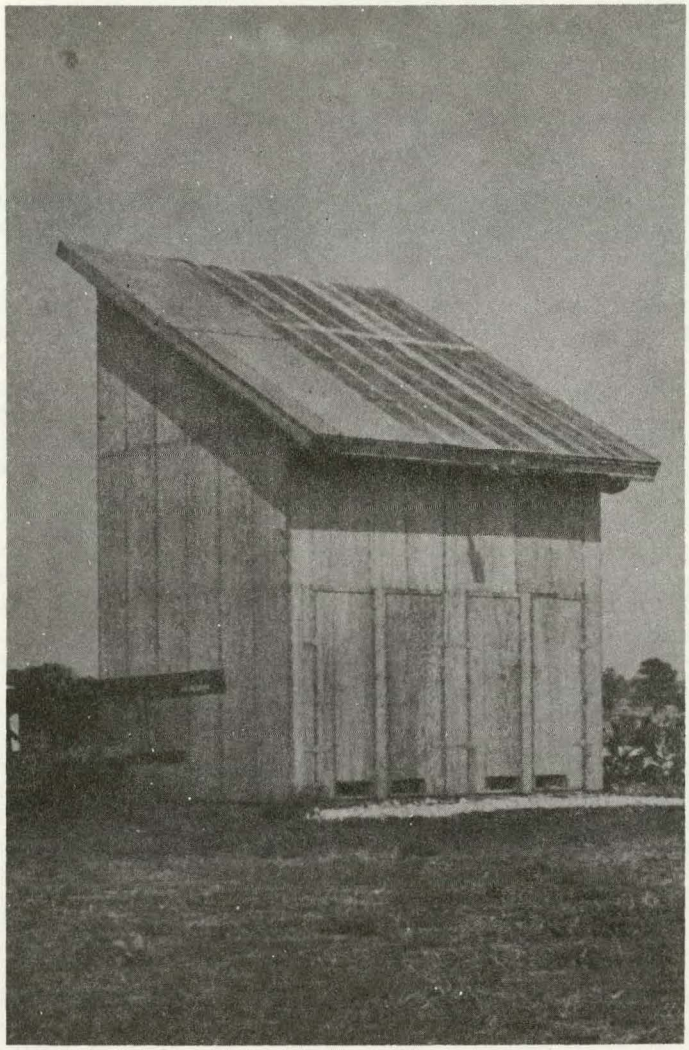

Figure 1. An experimental solar curing facility for burley tobacco consisting of four forced-ventilation curing chambers.

A concrete retaining wall, six blocks high, was laid in an excavation made for the rockbed. The retaining wall also served as the foundation of the building. Entrance and exit plenums were formed by laying an additional concrete block wall that was 0.5 m (1.5 ft) from each end wall. The blocks were laid on their sides (holes horizontal) up to the top of the rockbed to permit air movement through the bed.

The rockbed used in these tests consisted of 9.7 tonnes (10.7 tons) of limestone rock ranging in diameter from 1.27 cm (0.5 in.) to 7.5 cm (3.0 in.). The average equivalent spherical diameter was 2.67 cm (1.05 in.). The rockbed was 3.66 m (12 ft) long and was located beneath the curing structure. The cross sectional dimensions were 2.24 m (6.33 ft) wide and 0.76 m (2.5 ft) deep. The rockbed was insulated with 5.08 cm (2 in.) of styrofoam. About 0.46 m (1.5 ft) of soil was placed over the rockbed.

Twenty-five pairs of thermocouples were placed in the rockbed to form a 5 x 5 matrix from boundary-to-boundary along the length and depth of the rockbed. The paired themocouples were in a vertical plane containing the centerline of the rockbed. Of each pair of thermocouples, one was imbedded in the center of a rock and the corresponding one was placed in the air adjacent to the rock. We suspended the latter thermocouple on a string that was centered in a conduit which was placed vertically in the rockbed. Air moved freely over the thermocouple through slots ir the conduit.

The airflow system through the charging collector and rockbed was a closed-loop system with positive pressure through the collectors. Air passed through the collector, through the rockbed, and then back to the collector in a closed loop. The superficial air velocity in the rockbed, based on empty cross-sectional area was 2.6 m/min (8.4 ft/min) during charging. For discharging, outside air was blown through the rockbed in the reverse direction of charging and mixed with the fresh air being blown through the curing chambers. The airflow rates for discharge were 4.0 m^3/min (142 cfm) from 1400 to 0200 hr and 3.0 m^3/min (106 cfm) from 0200 to 1400 hr. We produced the lower airflow rate by opening the duct system during discharge so that the chamber fan could draw a portion of its fresh air intake through the rockbed. The higher airflow rate was produced by a fan.

We manually controlled the operation of the charging and discharging of the rockbed. The fan moving air to the collector and on through the rockbed was on a timeclock which in turn was connected to a manual switch. On days when we could expect collector outlet temperatures above 38°C (100°F), fan operations were controlled by the timeclock. The timeclock was turned off on cloudy days and then turned on the next suitable day. Discharging of the rockbed was also controlled by timeclock, with the fan operating for a set number of hours each day. We discharged the rockbed only during prolonged rainy periods. Therefore, temperature and relative humidity of the solar-collector-rockbed-storage chamber were modified only during such periods.

We monitored the temperature and relative humidity of the air as it passed through the tobacco to evaluate the ability of each chamber to modify the curing environment. Dry- and wet-bulb thermocouples were placed above, midway through, and below the tobacco. The dry-bulb and wet-bulb temperatures were recorded hourly. The average daily temperatures and relative humidities given in this paper were averages of the even hour values of temperature and relative humidity throughout the day.

The tobacco (160 sticks, 6 plants to the stick) was cut and left in the field for 2 days of solar field curing before being placed two tiers deep in the curing chambers.

The curing chamber with solar collector and rockbed storage was tested during two periods of high humidity during curing. The rockbed was not fully charged before harvest because of late completion of the curing facilities; therefore, we used electric heat to supplement the heat from the rockbed during the first discharging period. The percentage of the total heat supplied by the rockbed was calculated from the temperature of the air leaving the rockbed and the temperature of the air leaving the electric heating section. To fully charge the rockbed before the second high-humidity period, we used electric heat during a 4-day charging period to boost the charging hours from 1030-1700 hr. to 800-1800 hr. The electric heat was thermostatically controlled to boost the collector output to 38°C (100°F) only when the collector outlet temperature fell below that value. The rockbed supplied all of the heat and was discharged continuously during the second high humidity period, which lasted 4 days.

RESULTS AND DISCUSSION

Fall weather in Kentucky during 1976 was well above average for curing high quality burley tobacco. The need for environmental modification was less than usual. However, we were successful in evaluating the ability of each chamber to modify the environment. Figure 2 shows the performance of the charging and non-charging collectors for one day during the cure. The maximum rise in temperature was 30.5°C (55°F) and 32.8°C (59°F) for the charging and noncharging collectors, respectively. The effect of scattered clouds can be seen at 1400 hr. The result was a 11-12°C (20-21°F) reduction in outlet temperature. Peak temperatures were maintained from 1200 to 1400 hr. The collector efficiencies for the charging and non-charging collectors were 42.0% and 27.7%, respectively. The higher efficiency of the charging collector was attributed to its shallower airflow channel and its higher airflow rate.

Table 1 shows a comparison of the average temprature and relative humidity in the solar chamber without storage, in the transmitting-roof chamber, and in the conventional chamber during 4 days of curing. The chamber with the solar collector without storage performed slightly better than the chamber with transmitting roof. The maximum average daily humidity was five percentage points lower in both the chamber with transmitting roof and the chamber with solar collector without storage than in the conventional chamber. The maximum daily humidity reduction was 5%. The environmental modification was slight, but occurred on a daily basis during dry weather. We observed that the tobacco in both the solar chamber without storage and the transmitting-roof chamber was curing noticeably faster than the tobacco in the conventional chamber. The benefits derived from the solar chamber without storage and the transmitting-roof chamber during dry periods when the mean daily humidity was above 70% and during intermittent rainy and sunny weather were not sufficient to warrant their further consideration, especially when coupled with their inability to provide relief during prolonged rainy periods. However, with the solar chamber with storage, heat could be supplied whenever it was needed.

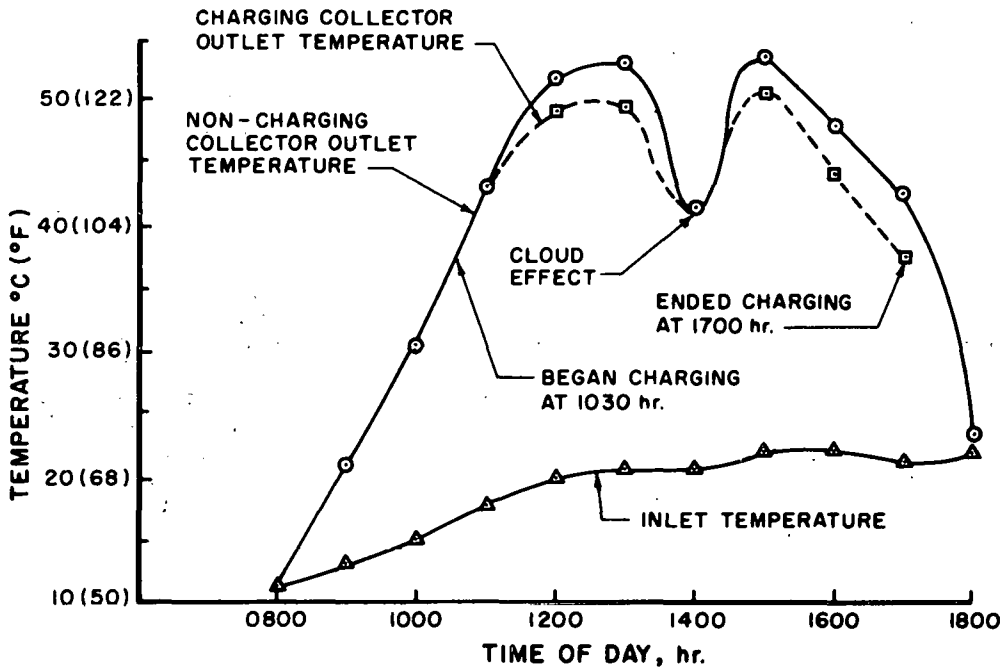

Figure 2. Inlet and outlet temperatures of the charging and non-charging collector on a selected day.

Table 1. Comparison of average temperature and relative humidity in the solar chamber without storage, in the transmitting roof chamber, and in the conventional chamber during 4 days of tobacco curing.

	Solar chamber without storage			Transmitting roof Chamber			Conventional chamber		
	Temp, °C	(°F)	RH,%	Temp, °C	(°F)	RH,%	Temp, °C	(°F)	RH,%
Day 1	18.9	(66.0)	68	18.9	(66.0)	70	17.8	(64.0)	72
Day 2	12.9	(55.3)	72	12.6	(54.6)	72	11.7	(53.1)	77
Day 3	13.4	(56.2)	71	13.0	(55.4)	71	12.3	(54.1)	75
Day 4	16.11	(61.0)	65	15.4	(59.7)	66	14.6	(58.3)	70

Figures 3 and 4 show the temperature profiles along the centerline of the rockbed during 4-day periods of charging and discharging, respectively. The profiles designated day 1 through 4 in Figure 3 are the temperature profiles at 1800 hr, after the end of the charging period each day. During charging, a temperature gradient developed along the entire length of the rockbed.

Factors that contributed to the temperature gradient were:

1. The relatively large rock produced a larger temperature transition zone (the portion of the rockbed in which temperature changes take place) than would have been produced by smaller rock.

2. Heat was conducted from the hot rock to adjacent cooler rock.

3. Heat was lost from the rockbed to the surroundings during the night, particularly, heat loss at the entrance to the rockbed adjacent to the plenum.

We observed that the length of the transition zone was much smaller than the length of the rockbed during the initial stages of charging. We also observed conduction of heat along the bed during only one night of charging. A comparison of the temperature profile at 1800 hr, when charging had ended (profile designated day 4 in Figure 3), with the temperature profile at 0600 hr the next morning(initial profile of Figure 4) shows the effect of heat loss. The heat loss caused a flattening of the temperature profile. We concluded, as did Close et al. (1968),that the intermittent nature of the operation -- with its relatively short period of charging and relatively long period of noncharging, the latter period being the one during which heat losses alter the temperature profile, -- was the dominant factor in producing the temperature gradient along the entire length of the rockbed.

The average rock temperature when the rockbed was fully charged was considerably lower than the average collector outlet temperature. We found two reasons. First, the air temperature entering the rock during charging was lower than the average collector outlet temperature because of duct and plenum heat losses and heat absorbed by the concrete block before the air reached the rock. The second reason for the average rock temperature being lower than the average collector temperature was the previously discussed temperature gradient in the rockbed caused by heat losses during noncharging periods.

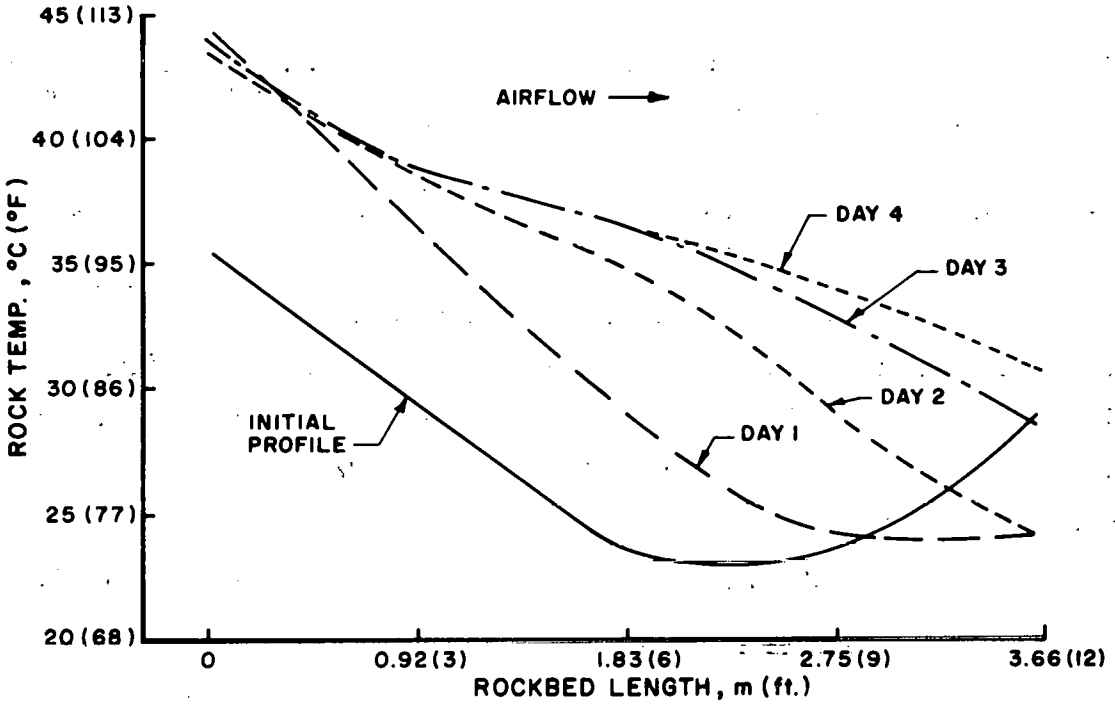

Figure 3. Temperature profiles in rockbed during charging.

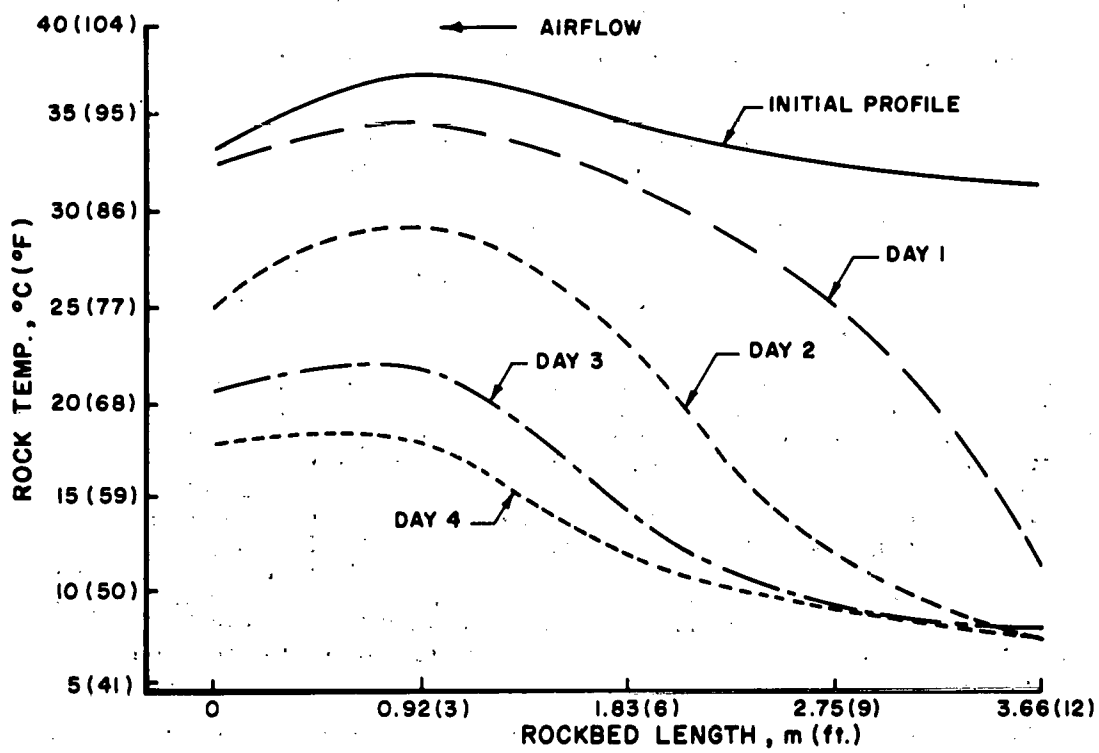

Figure 4. Temperature profiles in rockbed during discharge.

The temperature profiles designated as day 1 through 4 in Figure 4 are the temperature profiles at 2400 hr each day. The rockbed temperature gradient caused the outlet air temperature of the rockbed (operating temperature of the rockbed) to decline continuously during discharging. Thus, the heat was withdrawn at a temperature well below the average collector outlet temperature.

The average temperature and relative humidity in the conventional chamber and the solar chamber,during which heat withdrawn from the rockbed of the solar chamber was supplemented by electric heat,are shown in Table 2. The percentage of the total heat supplied by the rockbed ranged from 51 to 77 percent. Day 4 showed a much higher percentage of total heat from the rockbed because of one good day of charging between days 3 and 4. (The discharging period in Table 2 was not the same discharging period as depicted in Figure 4.) The relative humidity in the solar chamber with storage averaged 25 to 33% lower than the relative humidity in the conventional chamber. We bypassed the 65 to 70% relative humidity range in the solar chamber by adding too much electric heat during the first 3 days. As it turned out, the rockbed by itself could have lowered the relative humidity to near the 70% level.

Table 2. Comparison of average temperature and relative humidity, in the conventional chamber and the solar chamber during which heat withdrawn from the rockbed of the solar chamber was supplemented by electric heat.

	Solar chamber with storage			Conventional chamber			Percentage of total-heat supplied by rock bed
	Temp, °C	(°F)	RH,%	Temp,°C	(°F)	RH,%	Percent
Day 1	20.6	(69.0)	62	15.2	(59.4)	87	60
Day 2	19.9	(67.9)	60	13.8	(56.9)	91	56
Day 3	15.4	(59.8)	51	9.2	(48.5)	84	51
Day 4 *	12.8	(55.0)	65	8.4	(47.1)	90	77

* Storage was charged 1 day between days 3 and 4.

The average temperature and relative humidity within the conventional chamber and the solar chamber with the rockbed supplying all the heat during a 4-day rainy period during which the rockbed supplied all of the heat are shown in Table 3. (The discharge period covered in Table 3 was the same as that shown in Figure 4.) The rockbed supplied enough heat to bring the relative humidity within the desired 65-70% range for the first 3 days. We ran low on heat on the fourth day and were unable to attain the desired humidity level. Yet the 75% relative humidity average on day 4 was 10 percentage points lower than that in the conventional chamber. Approximately one-fourth of the heat was supplied by the concrete block foundation and soil. But such was not unexpected, since the foundation weight was one-half that of the rock. Even though edge effects are greater for a small rockbed than a large one, apparently some heat can be withdrawn from the surroundings of an underground rockbed.

The performance of the solar collector with rockbed storage system was quite satisfactory since it provided sufficient heat for a 3-day period. During the first 3 days, the rockbed supplied an average of 281 J/m^2-s (89 Btu/hr-ft^2). A 15.6°C (60°F) and 90% ambient environment would require 379 J/m^2-s (120 Btu/hr-ft^2)

Table 3. Comparison of average temperature and relative humidity within the conventional chamber and the solar chamber during heat withdrawal from rockbed during a 4-day rainy period.

	Solar chamber with storage			Conventional chamber		
	Temp, °C	(°F)	RH,%	Temp, °C	(°F)	RH,%
Day 1	13.1	(55.5)	67	10.2	(50.3)	81
Day 2	8.9	(48.1)	68	5.3	(41.5)	91
Day 3	8.4	(47.1)	68	5.7	(42.2)	86
Day 4	6.2	(43.2)	75	4.1	(39.4)	85

to lower the relative humidity to the desired level. Thus, more heat may be required for higher ambient temperatures, possibly endangering the ability of the present system to maintain the desired environment on the third day. Still, from an environmental modification standpoint, the solar chamber with rockbed-storage was superior to the solar chamber without storage and the transmitting-roof chamber in that it provided heat during critical periods.

SUMMARY AND CONCLUSIONS

A solar curing structure consisting of four forced-ventilation curing chambers was used to cure burley tobacco during the fall of 1976. The objective was to use solar heat to reduce high relative humidity during curing. One chamber was a conventional, two-tier chamber with metal roof, one had a fiber-glass roof for transmitting solar radiation directly into the chamber, one had a solar collector without storage, and one had a solar collector and rockbed storage. The maximum average daily relative humidity was five percentage points lower in both the chamber with transmitting roof and the chamber with solar collector without storage as compared to the conventional chamber. The solar collector with rockbed system supplied enough heat to maintain the desired 65-70% relative humidity for 3 of 4 days of rainy weather.

Our conclusions were as follows:

1. The solar chamber with rockbed storage was superior to the solar chamber without storage and to the chamber with transmitting roof because it provided heat during critical periods of high humidity.

2. A rockbed can be used for thermal storage to supply heat for 3 days of curing without replenishment.

3. A tapered temperature gradient forms from front to back of a rockbed because of heat conduction along the bed and heat loss caused by the intermittent nature of the operation.

4. A solar curing facility with a 3- to 4-day heat supply stored in the rockbed should provide the capability to prevent a substantial portion of crop-value losses that might otherwise be sustained during periods of high humidity.

REFERENCES

1. Barfield, B. J., Hill, J., and J. N. Walker. 1975. Solar radiation on sloping surfaces in Kentucky. Progress Report 208, University of Kentucky, College of Agriculture, Agricultural Experiment Station. 16 pages.

2. Bunn, J. M., G. A. Duncan, W. H. Henson, Jr., and L. R. Walton. 1973. Environmental design of new burley curing barn. Tobacco Science 17: 1 - 5.

3. Close, D. J., R V . Dunkle, and K. A. Robeson. 1968. Design and Performance of a thermal storage air conditioning system. Mechanical and Chemical Engineering Transactions, Australia. MC4(1): 45-54.

4. Duncan, G. A. 1976. Private comminication.

5. Hamon, W. R. 1954. Weather and burley tobacco curing. U. S. Weather Service Report, Washington, D. C., 28 pages.

6. Walton, L. R., W. H.Henson, Jr., and J. M. Bunn, 1973. Effect of environment during curing on the quality of burley tobacco: II. Effect of high humidity curing on support price. Tobacco Science 17: 25-27.

7. Walton, L. R., W. H. Henson, Jr., J. N. Walker, and J. M. Bunn. 1976. Using solar energy to cure burley tobacco. Final Report covering period from July 1, 1975 to June 30, 1976. 23 pages. Energy Research and Development Administration, ARS-USDA sponsored solar energy use in drying crops other than grain.

SOLAR-ENERGY UTILIZATION USING GREENHOUSE BULK CURING AND DRYING SYSTEM

by

B.K. Huang, Professor
C.G. Bowers, Jr., Research Assistant
Department of Biological and Agricultural Engineering
North Carolina State University
Raleigh, N.C. 27607

ABSTRACT

The greenhouse bulk curing system utilizes solar energy as a first priority energy source to cure tobacco in the summer months and to grow greenhouse crops and tobacco seedlings the remainder of the year. A 30-40 percent fuel savings was achieved during the past two tobacco curing seasons (summer, 1975, 1976) using solar energy in this system as compared to a conventional bulk curing barn. Klancho flowers were grown in the winter, 1975-76, with excellent results and an estimated 10-15 percent fuel savings. Tobacco transplants were produced on multiple layers for automatic transplanting with germination rates of 95-97% for various layers.

Computer modeling and analysis for design optimization of the solar barn for maximum solar energy utilization and minimum fossil-fuel and electrical energy consumption are under development. Thermal-electrical systems analogies were applied to study temperature responses of the solar collectors under time-varying solar radiation and ambient air temperatures. Simulation results conformed well with the field data for various stages of curing.

Introduction

Solar energy is a primary energy source for agricultural production. Photosynthesis for food production and field drying for processing agricultural materials are two important, natural uses of solar energy. Substitution of solar energy for fossil-fuel energy has only been seriously considered as a viable alternative within the last three or four years. The low cost and abundance of fossil-fuel energy coupled with the high cost and output variability of solar energy systems have resulted in an energy and economic situation which did not require the development of alternative energy sources. The "energy crisis" has reversed this trend for all phases of the energy situation - production, research, conservation, application, etc.

Much of the basic studies on solar energy collectors and their possible application were done over 10 years ago (3,12,15,21,22). Intensive research efforts to develop practical, efficient and economical equipment and technology for solar energy have come only in the last couple of years. Most of the current studies for agricultural application involve an air preheating solar collector which is to be used either in the drying of agricultural materials or the heating of greenhouses. Significant energy savings have been achieved by several investigators (16,17,19) in grain drying by retrofitting solar collectors to grain bins. Energy research programs in greenhouses are concentrating on solar energy collection and storage with emphasis also being placed on minimizing the loss of solar and fossil-fuel heat energy (5,8,19,22). Solar heated air has been used in peanut drying (4).

The greenhouse bulk curing and drying system was developed by Huang et al (1,2,6,12 13,14) to utilize solar energy year-around as either a tobacco curing and drying facility or as a plant growth facility. Being basically a greenhouse type structure, it is an inherent solar energy collector. In a plant growth configuration the system uses solar energy to heat the structure for fuel savings and to

photosynthesize plants for food and plant production in a controlled environment. With the addition of solar absorbers and curing equipment, solar energy is used to cure tobacco. This multi-purpose structure is designed for year-around use by the farmer for agricultural production and year-around solar energy utilization.

Tobacco Curing Operation of Greenhouse Bulk Curing Solar Barn

The greenhouse bulk curing system is a greenhouse which accommodates a solar energy bulk curing module during tobacco curing. The system, shown in Figure 1, consists of a combination curing/growth room with facilities for curing tobacco or growing plants, furnace room with heating unit, auxiliary fan and appropriate air flow plenums, gravel energy storage system consisting of gravel and corrugated slotted ducts, top air duct with shutters and side openings for air flow control, side vents for air intake or exhaust, and portable frames to support plants or tobacco.

For tobacco curing, heat absorbers are added to the sides and tops of the portable frames to form a bulk curing module within the greenhouse (Figure 2a&b). Solar energy is absorbed and transferred to air which is moved over these black surfaces by the auxiliary and/or furnace fan(s). This preheated air is used either for curing or storage, depending upon curing requirements. Outside air enters the structure for preheating either from the front shutter or side vents (Figure 1a), depending upon the available solar energy and curing energy requirements. The openings in top air duct and bottom gravel air ducts cause the air flow to be uniform over the absorber surfaces.

Motorized shutters in the front, rear, and rear bottom of the top air duct control the flow of preheated air. The side vents are also motorized. The preheated air for energy storage or for curing can then be easily controlled for optimum energy utilization as required by the curing stage and available solar energy. Fresh air is pulled in from either the top or sides of the structure to optimize the solar energy collection, storage, and utilization.

Solar energy utilization tests were conducted during July, August and September, 1975 and 1976 in the Central Crops Station structure (Figure 1). Five complete cures were made each year in the greenhouse solar curing barn, and five were made in a conventional bulk curing barn used as a control. Curing procedures, discussed below, were approximately the same in each barn with minor variations as required by the individual cures.

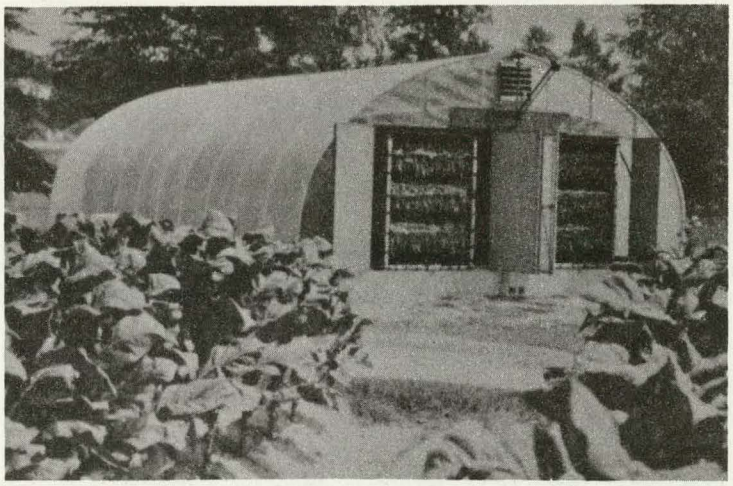

Figure 1. Greenhouse bulk curing system during summer, 1976.

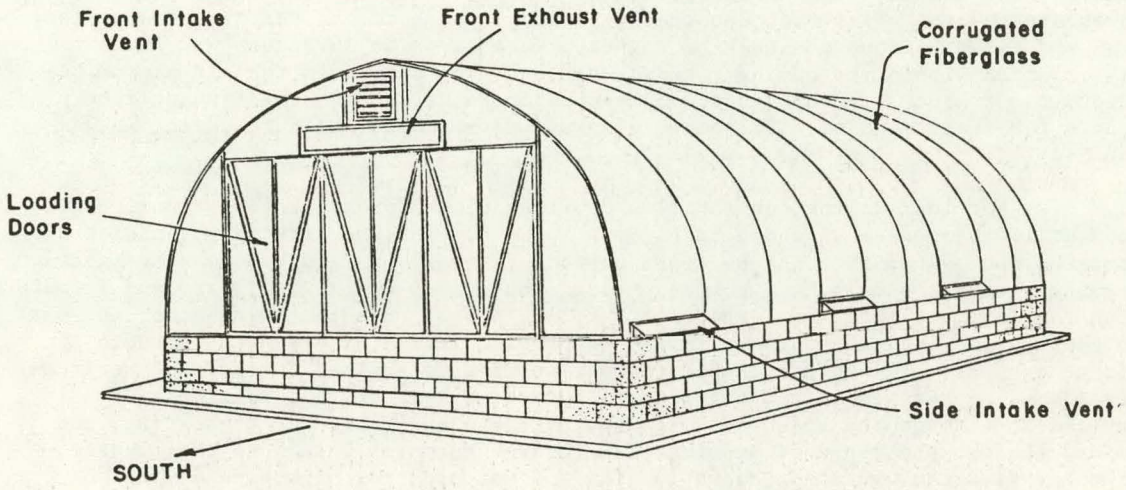

(a)

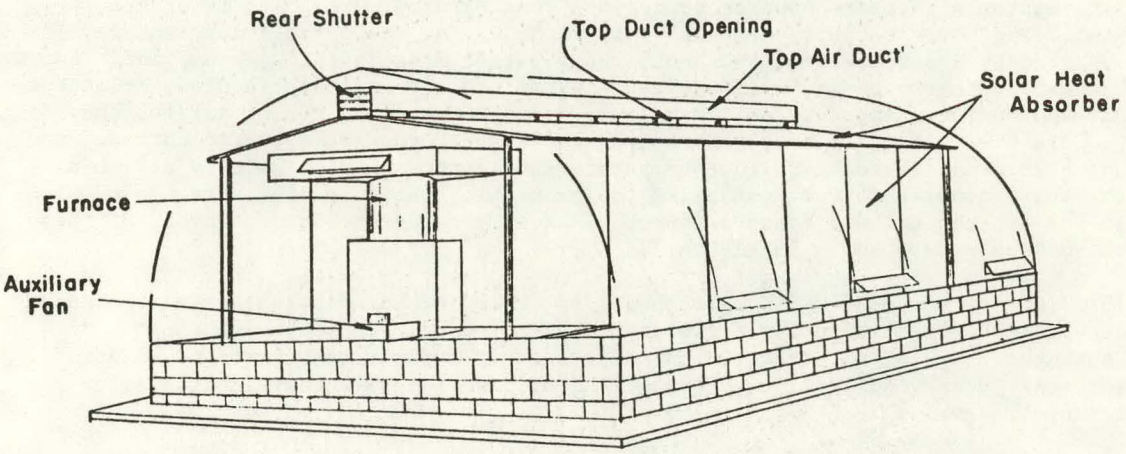

(b)

Figure 2. Greenhouse bulk curing system: (a) front view and (b) rear view.

The general curing procedure was as follows:

(1) Bulk racks were filled in the field and placed in the barn.

(2) The furnace was fired and a typical bulk curing schedule followed for temperature and air ventilation rate. The temperature curing schedule generally consisted of two-three days yellowing at 32-35°C, three days of leaf drying with the air temperature being advanced from 32°C to 76°C at 1 to 1.5°C per hour, and one day of stem drying at 76°C. During leaf drying, the temperature was maintained at certain levels as determined by tobacco conditions. The air ventilation rate was usually 10 percent or less for yellowing, gradually increased during initial leaf drying until it was about 30-40 percent for temperatures of 54 to 60°C, then gradually reduced during later stages of leaf drying, and held at 10 percent or less intake during stem drying.

For the solar curing barn, air preheated by either the absorber or the gravel was used as intake to the furnace during both day and night operation as shown in Figures 3-6 and as discussed below.

(1) The daytime yellowing configuration used to store solar energy in the gravel (Figure 3) was a closed loop circulation of the air over the heat absorbers, through the gravel to the auxiliary gravel fan and then through the top duct for recirculation. If the system temperature was resulting in a tobacco temperature above 38°C, outside air was brought into the system through the front shutter, preheated by the solar heat absorbers, pulled through the gravel by the auxiliary fan and exhausted out the back of the structure as shown in Figure 4. The air circulation within the curing room was through the furnace to the air plenum beneath the tobacco, up through the bulk tobacco racks, and to the furnace return doors for recirculation. If some drying was to be done, the furnace intake was opened slightly.

(2) For leaf drying the air flow configurations for solar energy collection and utilization were as shown in Figures 5 and 6. For the first day, outside air entered the system through the front shutter as shown in Figure 5, was preheated by the absorber panels, was pulled through the gravel by the auxiliary and furnace fan for movement into the furnace intake, was pushed through the tobacco, and was either pulled into the furnace intake for recirculation or exhausted through the front exhaust. The furnace intake damper setting determined the percent recirculation. For the second and third days of daytime leaf drying, outside air was pulled in through the side vents, passed over the absorbers for preheating, and moved through the top duct and into the furnace room for intake to the furnace. The air flow configuration shown in Figure 5 was used for nighttime drying.

(3) For the stem drying stage, outside air was provided as shown in Figure 6 for daytime drying and as in Figure 5 for nighttime drying.

Instrumentation for monitoring the test conditions and variables consisted of a data system with thermocouples to measure temperature, multipoint recorders for monitoring these sensors, a strip chart recorder for monitoring radiation levels measured by a pyranometer, and an LP gas meter to measure fuel consumption. Copper constantan thermocouples were used to measure ambient air temperatures, collector-air and-surface temperatures, gravel air temperatures, and curing air/tobacco temperatures. For air temperatures, shielded thermocouples measured both dry and wet bulb temperatures. Surface temperature measurements were made by attaching the thermocouples to the surface of the material. Thermocouples were placed within the tobacco rack to measure tobacco bulk temperatures. The locations of these thermocouples are shown in Figure 7.

Solar energy was used by the greenhouse solar curing barn to supplement the energy requirement for bulk curing of tobacco. Data for one complete cure, August 26 - September 2, 1976, is presented and discussed as typical results to be expected for solar energy collection, storage, and utilization by the greenhouse solar curing system.

Incident solar radiation collected by the upper and lower solar collector sections (Figure 7), resulted in absorber surface temperature of 82° to 97°C on clear sunny days when the sun was approximately perpendicular to the absorber surfaces.

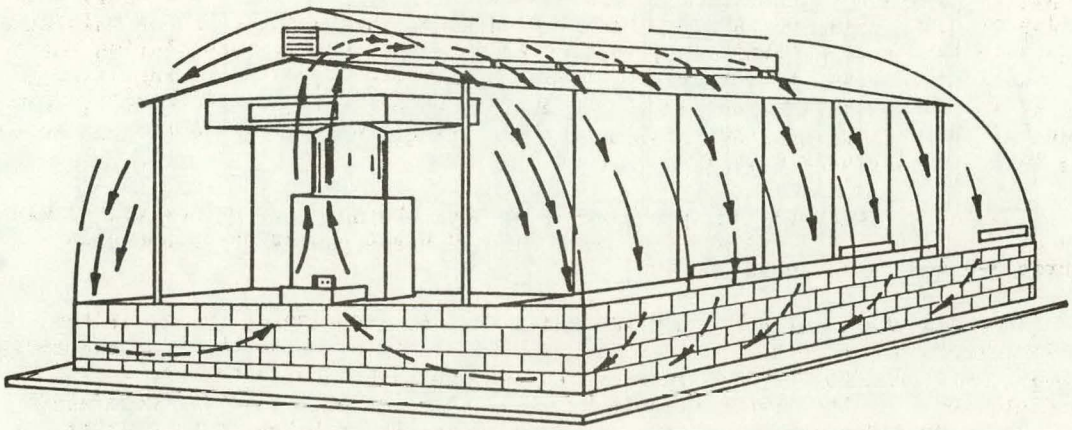

Figure 3. Air flow configuration for closed-loop energy storage during yellowing stage.

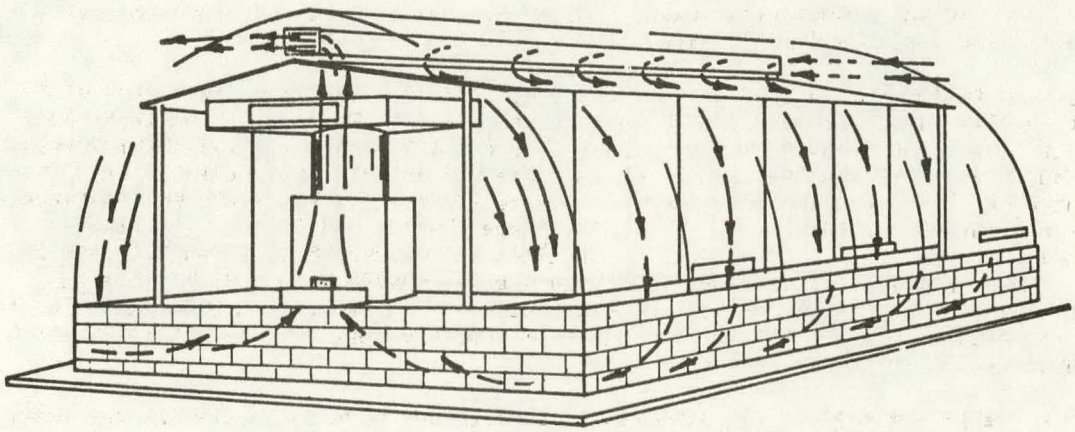

Figure 4. Air flow configuration for open-ended energy storage during yellowing stage.

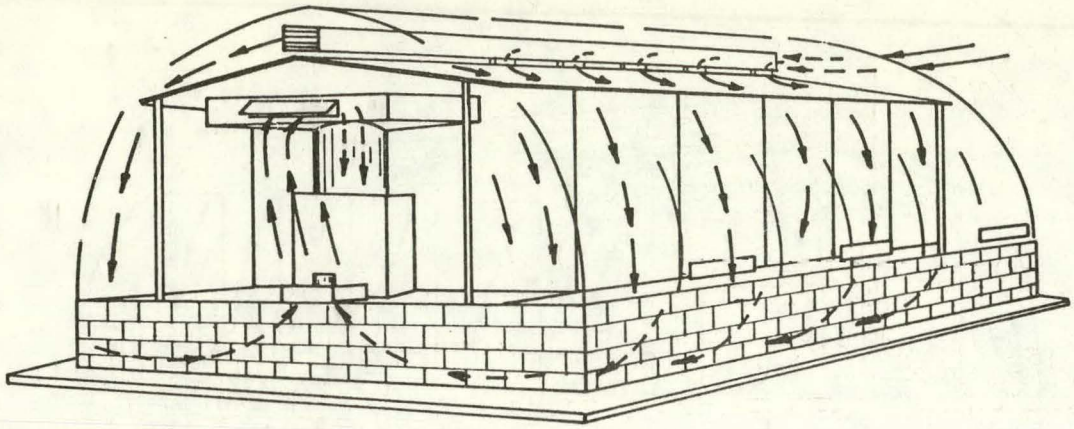

Figure 5. Air flow configuration for energy storage and supplemental heating of furnace air during initial leaf drying stage.

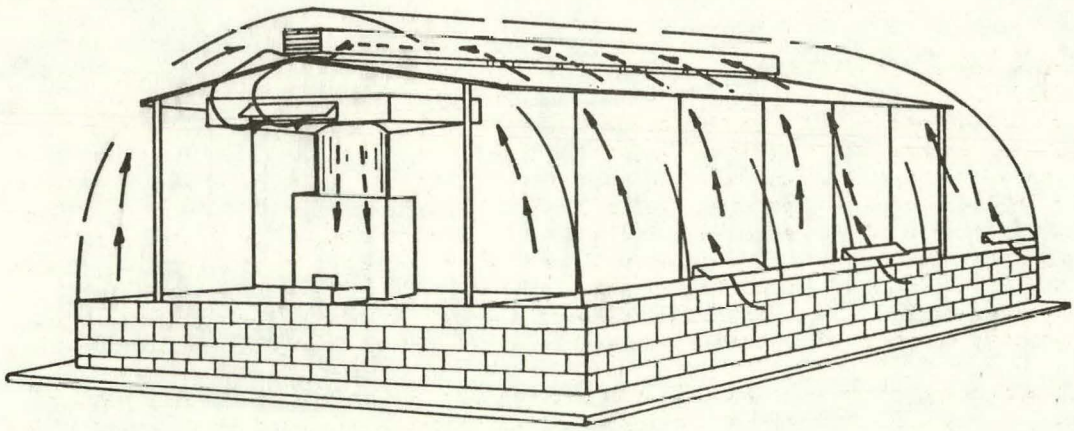

Figure 6. Air flow configuration for preheating furnace air intake during final leaf and stem drying stage.

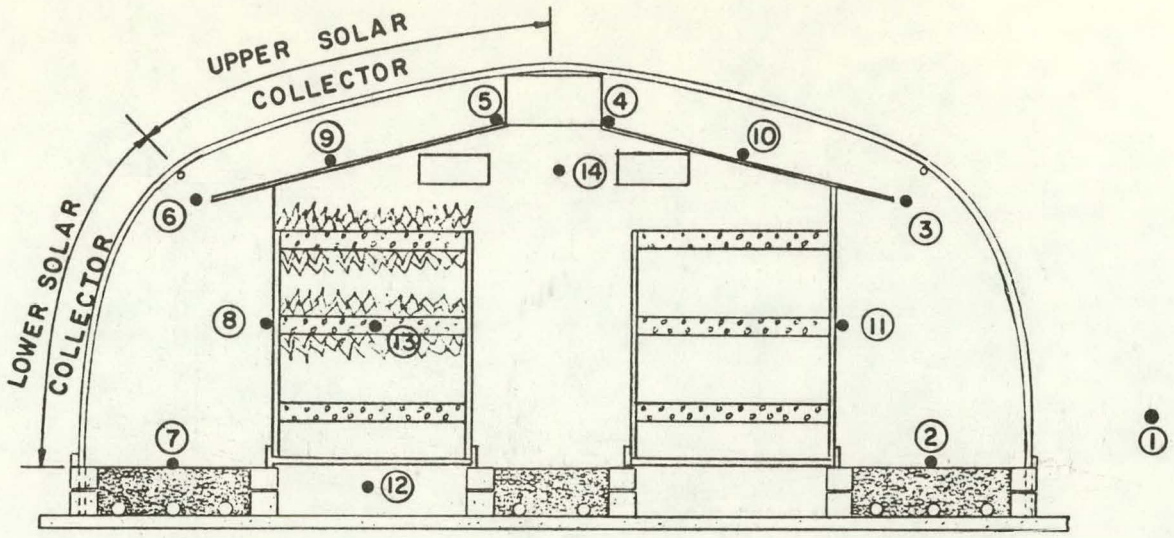

(1) Outside air temperature (DB)
(2) Gravel surface air temperature (East)
(3) Midway collector air temperature (East)
(4) Top collector air temperature (East)
(5) Top collector air temperature (West)
(6) Midway collector air temperature (West)
(7) Gravel surface air temperature (West)
(8) Vertical absorber surface temperature (West)
(9) Sloped absorber surface temperature (West)
(10) Sloped absorber surface temperature (East)
(11) Vertical absorber surface temperature (East)
(12) Curing air temperature beneath tobacco
(13) Tobacco temperature within rack
(14) Curing room temperature

Figure 7. Cross-sectional view of greenhouse bulk curing system showing locations of thermocouples.

Figure 8 shows the absorber temperatures for the west side, lower and upper collectors. The temperature decreases on August 27 and 28 were caused by changing the yellowing stage, air flow configuration for energy storage from closed loop (Figure 3) to open-ended (Figure 4) circulation. Energy collection and storage for the solar barn on these days were causing the tobacco temperature to increase above 38°C, an upper temperature limit for "safe" yellowing. The air flow configuration was changed to decrease this build-up. Design changes to increase the storage capacity and air flow rates will enable the greenhouse solar curing system to more efficiently store collected solar energy. Then, the exhausting of the temperature build-up will not be necessary; it will be stored for nighttime use. The daytime temperature decrease on August 29 was caused by a thunderstorm.

The temperature difference between the outside air and the top collector air, shown in Figure 9, represents the degree of air heating produced by the west side, solar collector sections (Similar results were achieved on the east side). The air temperature differential across the two collector sections varied from a minimum of 18°C on August 29 to a maximum of 43°C on September 1, excluding the low collector air temperature on August 29 caused by the thunderstorm. The air ventilation rates for drying on these days were approximately 40 and 10 percent respectively which corresponded to center-line collector velocities of 0.11 and 0.02 meters per second respectively. Radiation levels on these days, and also for the entire cure, were approximately the same with peak day, total hemispherical

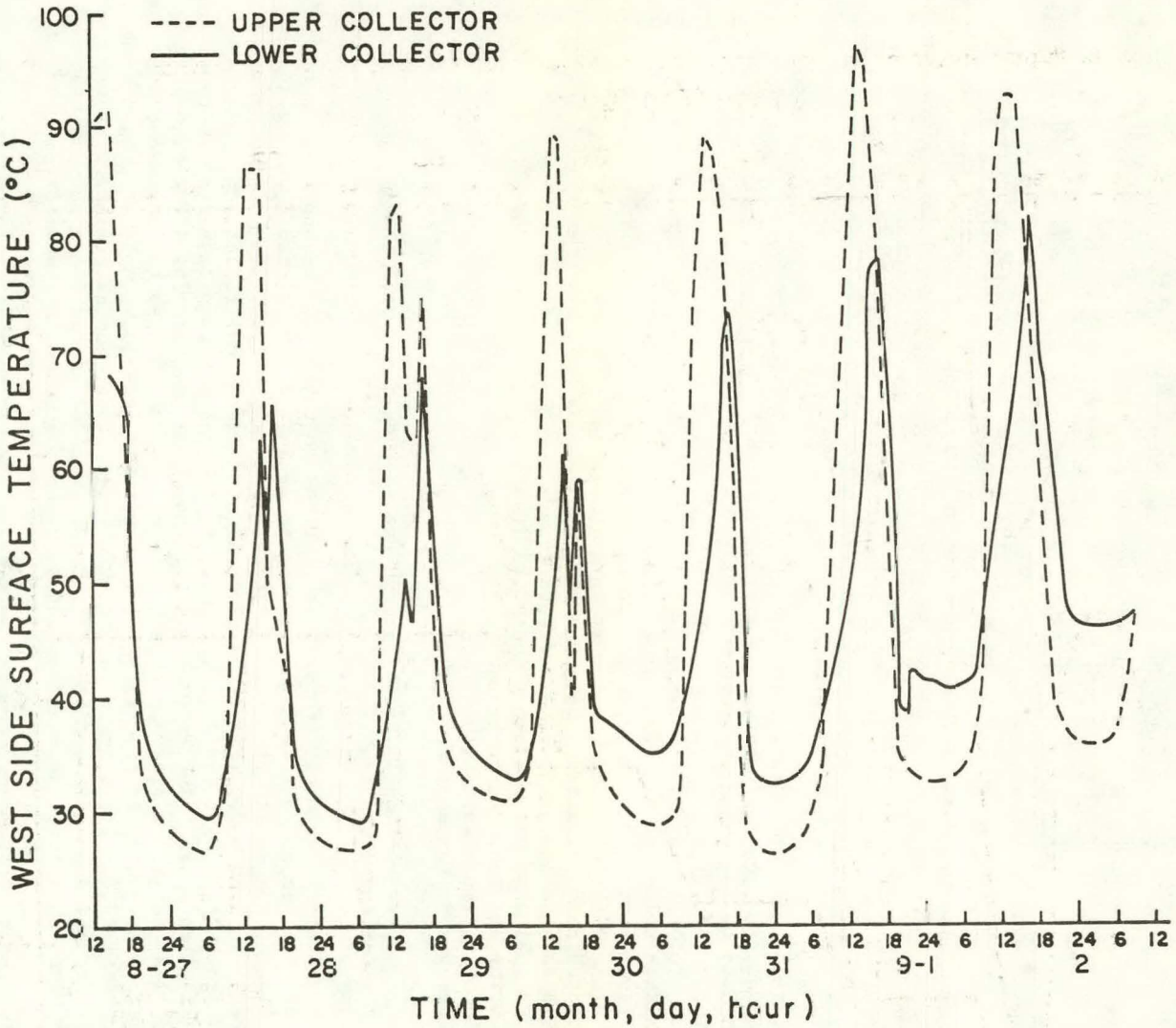

Figure 8. Absorber surface temperatures during one complete cure.

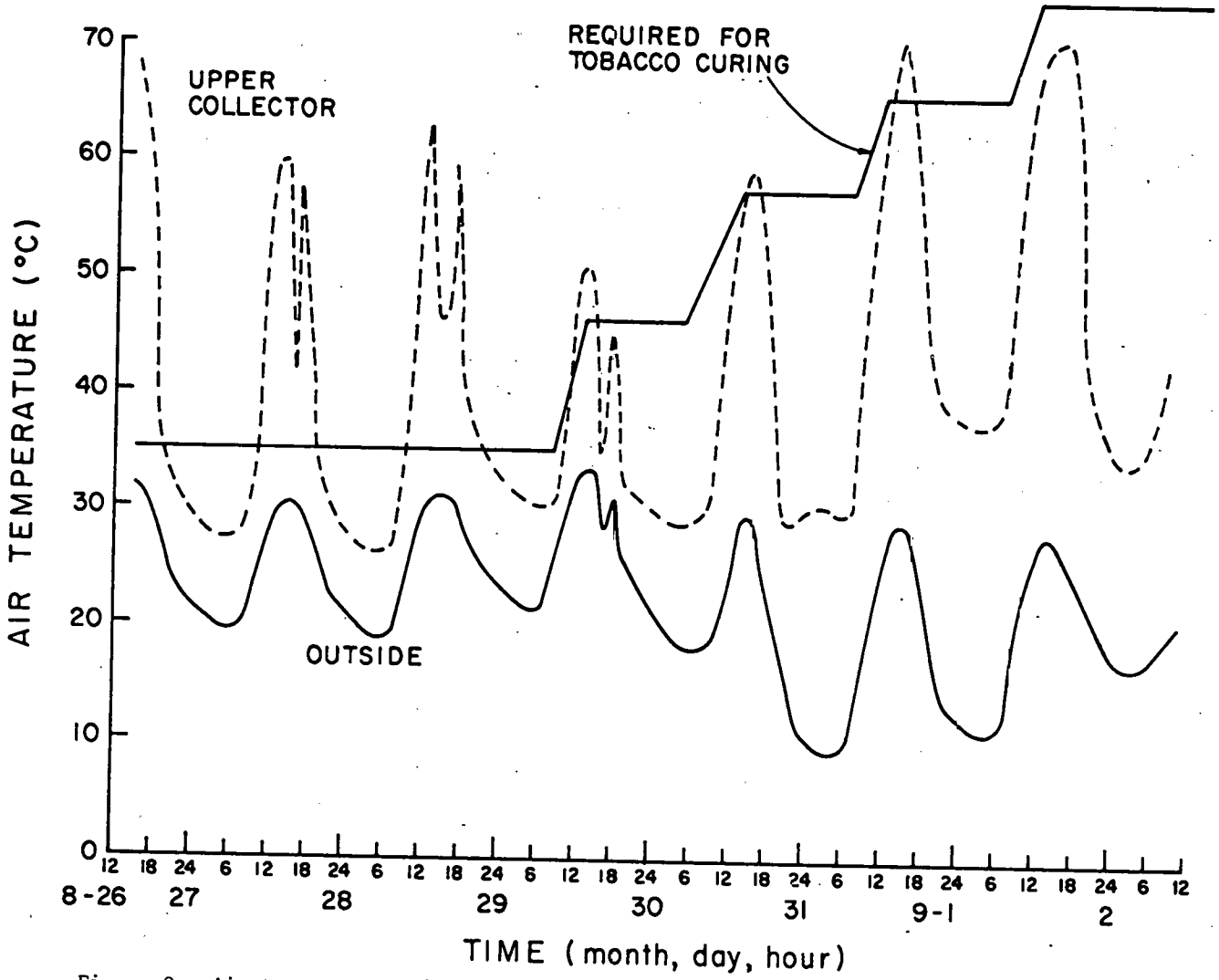

Figure 9. Air temperatures involved in tobacco curing with greenhouse solar curing system.

radiation being about 875 watts per square meter. The higher collector air temperatures achieved at the beginning and end of the cure occurred when air movement through the collector section was less than 0.02 meters per second.

The difference between the outside air temperature and the required tobacco curing temperature (Figure 9) is indicative of the total energy that must be supplied for curing. The energy that was supplied from fossil-fuel energy is represented by the temperature difference between the collector air and curing air. As shown by the curves of Figure 9, the energy requirement above that supplied by solar collection occurred mainly at night.

The overall fuel savings achieved by the greenhouse solar curing system as compared to a conventional bulk curing barn was 30 percent for the five cures in 1976. The average LP fuel consumed in gallons per pound of cured (and ordered) tobacco was 0.075 for the solar barn and 0.107 for the conventional bulk barn. The curing time, fuel consumption, tobaccos used, and fuel saving per cure are given in Table 1. The fuel savings for the individual cures varied from a low of 7 percent for the second cure to a high of 40 percent for the fifth cure. The low fuel saving for the second cure of the solar barn was caused by two days of rain and three cool nights, temperatures of 15° and 18°C, which occurred during the peak energy requirement for leaf and stem drying in the solar barn. The conventional bulk barn's second cure had been started two days before the solar barn's second cure, and leaf drying was almost completed prior to this cool weather.

Table 1. Tobacco cures for greenhouse solar curing barn and conventional bulk barn

Conventional Bulk Curing Barn			Greenhouse Solar Curing System			
Curing Time (days)	Fuel used (gal/lb tobacco)	Primings/ varieties	Curing Time (days)	Fuel used (gal/lb tobacco)	Primings/ varieties	Fuel Savings (%)
8	0.148	First primings for G-28, Coker 319 and plot tobacco	7.3	0.120	First primings for G-28	19
7	0.111	Second primings for G-28 and plot tobacco	7	0.103	Second primings for G-28	7
6	0.094	Third primings for plot tobacco	8.2	0.066	Third primings for G-28	30
7	0.092	Fourth primings for Coker 319	6.7	0.057	Fourth primings for Coker 319 & G-28	38
7	0.094	Top of stalk for plot tobacco	7	0.056	Top of stalk for Coker 319, G-28 and plot tobacco	40
Average	0.107	-	-	0.075	-	30

Computer Simulation Analysis of Thermal Behavior of Tobacco Curing in Solar Barn

In order to further optimize the design of solar barn, it is necessary to investigate its thermal behavior. Computer simulation analysis representing the system and boundary conditions by a thermal circuit would provide powerful techniques for studying the thermal behavior of a complex heat transfer system. Analogous electrical circuits can be developed to represent the three modes of heat transfer - conduction, convection and radiation - within the solar drying system. Electrical analogies to a thermal system are given in Table 2.

Table 2. Analogies in thermal and electrical systems

Thermal System	Electrical System
Temperature T	Voltage
Heat Flow Q	Current
Thermal Capacitance C	Capacitance
Thermal Conductivity K	Conductance
Thermal Resistance R	Resistance

Conduction:

The heat transfer in a medium by conduction can be expressed as:

$$Q = -KA \frac{dT}{dX} \tag{1}$$

where
- Q = heat flow rate (heat flux)(Btu/hr)
- K = thermal conductivity (Btu/hr ft ^{o}F)
- A = cross-sectional area perpendicular to the heat flow (ft^2)
- $\frac{dT}{dX}$ = temperature gradient (^{o}F/ft), or the rate of temperature T change with respect to distance X in the direction of heat flow

Consider the steady-state heat flow through a conductor of length L, cross-sectional area A, and assume K is independent of T. Eq. (1) can be rewritten as:

$$Q = KA \frac{T_1 - T_2}{L} \tag{2}$$

The thermal resistance R, which is analogous to electrical resistance, can then be expressed by:

$$R = \frac{L}{KA} \left(\frac{^{o}F}{Btu/hr}\right) \tag{3}$$

Thermal capacity, or the heat necessary to cause unit change in temperature of the mass, may be defined as:

$$C = \frac{Q}{T_f - T_i} = \frac{\int_{T_i}^{T_f} C_p \gamma dT}{T_f - T_i} \tag{4}$$

where
- Q = thermal energy required to raise the temperature of a given mass from T_i to T_f
- C_p = specific heat capacity (Btu/lb ^{o}F)
- γ = density (lb/ft^3)
- T_i = initial temperature (^{o}F)
- T_f = final temperature (^{o}F)

If C_p and γ are constant over the temperature interval considered or if appropriate mean values of these quantities are used, Eq. (4) may be written as:

$$C = C_p \gamma V (Btu/^{o}F) \tag{5}$$

where
- V = volume of the mass (ft^3)

Convection:

The heat transfer between air and a solid surface can be expressed as:

$$Q_c = h_c A (T_s - T_a) \tag{6}$$

where
- Q_c = rate of heat flow (Btu/hr)
- h_c = convection coefficient (Btu/hr ft^2 ^{o}F)
- A = cross-sectional area perpendicular to heat flow (ft^2)

T_s = temperature of the surface (^oF)
T_a = temperature of the air (^oF)

The convection thermal resistance R_c can then be expressed as:

$$R_c = \frac{1}{h_c A} \left(\frac{^oF}{Btu/hr}\right) \tag{7}$$

Radiation:

Radiation exchange occurs through a separating space between objects as a result of their temperatures. If an enclosure has m surface and all surfaces are gray and opaque, diffuse and uniform in temperature, and their reflective and emissive properties are constant over all surfaces, the net energy exchange at a particular surface boundary (i) may then be expressed as (10,18).

$$(q_{net})_i = \frac{A_i \epsilon_i}{1-\epsilon_i} [R_i - (E_b)_i]$$

$$= \frac{R_i - (E_b)_i}{\frac{1-\epsilon_i}{A_i \epsilon_i}} \tag{8}$$

where q_{net} = net energy exchange (Btu/ft^2hr)
R = radiosity or total radiation which leaves a surface per unit time and per unit area (Btu/ft^2hr)
E_b = blackbody emissive power (Btu/ft^2hr)
ϵ = emissivity of a surface
A = area of a surface (ft^2)

In Eq. (8), $\frac{1-\epsilon}{A\epsilon}$ is considered as "surface resistance" to radiation heat transfer. The net energy can also be expressed as:

$$(q_{net})_i = \sum_{n=1}^{m} F_{in} A_i (R_n - R_i)$$

$$= \sum_{n=1}^{m} \frac{R_n - R_i}{\frac{1}{F_{in} A_i}} \tag{9}$$

where F_{in} = shape factor or fraction of energy leaving surface in which reaches surface n

$F_{in}A_i = F_{ni}A_n$ (by the law of reciprocity)

The term $\frac{1}{F_{in}A_i}$ is considered as "space resistance" to radiation heat transfer.

From Eqs. (8) and (9) an energy balance at R_i for radiation at the i^{th} surface would result in

$$\frac{R_i - (E_b)_i}{\frac{1-\epsilon_i}{A_i \epsilon_i}} = \sum_{n=1}^{m} \frac{R_n - R_i}{\frac{1}{A_i F_{in}}} \tag{10}$$

An equation similar to Eq. (10) may be written for each of the (m) surfaces resulting in a closed resistance network representing the system of (m) radiating surfaces. Figure 10a shows the thermal network of radiation at the i^{th} surface, in which E_b and R are proportional to the fourth power of their absolute temperatures. In order to use such a network in the thermal circuit representing the conduction paths of a heat transfer system, it is desirable to adjust the resistors so that a first power temperature potential at each of the (E_b) nodes would result in the same heat or current flow through all of the resistors. In order to

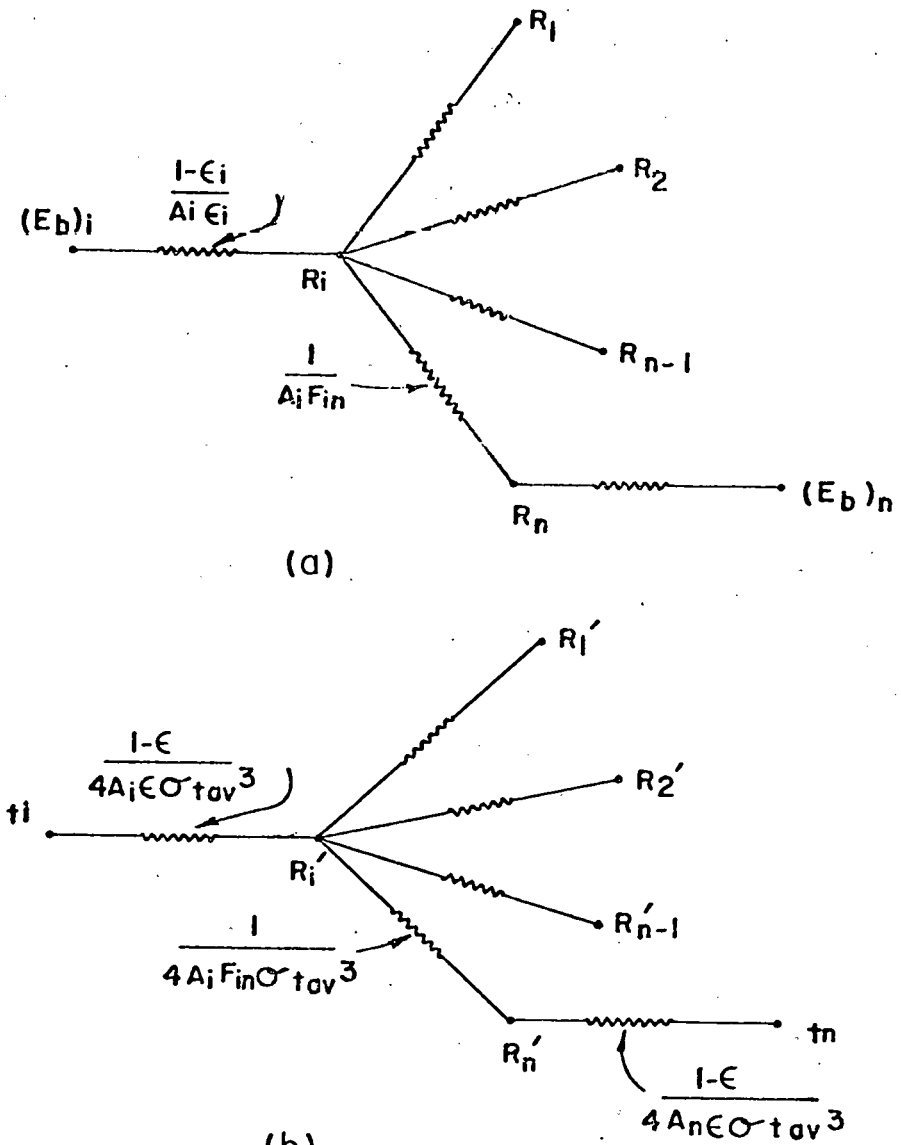

Figure 10. Radiation thermal network.

determine the proper adjustment of each resistor, consider a path through the network between $(E_b)_i$ and $(E_b)_n$ or:

$$\frac{t_i - t_n}{NR} = \frac{(E_b)_i - (E_b)_n}{R} \tag{11}$$

where R = sum of all resistors between $(E_b)_i$ and $(E_b)_n$

N = adjustment in resistance to linearize the potential

t_i and t_n = absolute temperatures at i and n surface respectively.

Since $(E_b)_i = \sigma t_i^4$ and $(E_b)_n = \sigma t_n^4$, where σ is the Stefan-Boltzmann constant, Eq. (11) can then be written as:

$$N = \frac{t_i - t_n}{\sigma(t_i^4 - t_n^4)} \tag{12}$$

A good approximation for small differences in temperature is:

$$t_i^4 - t_n^4 = 4t_{av}^3 (t_i - t_n)$$

Then,

$$N = \frac{1}{4\sigma t_{av}^3} \tag{13}$$

and the network shown in Figure 10a may be replaced by a network with linearized potentials shown in Figure 10b.

Circuit Analogy and Results:

To describe the heat transfer in the greenhouse bulk curing system using thermal circuit analysis, some simplifying assumptions were made concerning the collector, air flow, and heat flow direction. The structure is shown schematically in Figure 11. It is directed North and South longitudinally and is symmetrical with respect to East and West. There are four solar collectors (S.C.) - the east-side upper S.C., the east-side lower solar collector, the west-side upper S.C., and the west-side lower S.C. Thermal energy transfer through all structural elements is considered to be unidirectional and perpendicular to the long dimension. All lumped thermal properties are considered to be constant over the temperature range encountered, and the space temperature is considered uniform at any instant. The net long wave radiation between the outer fiberglass wall and the surroundings is assumed to be small and can be included in the convection heat transfer.

The thermal circuits representing the upper solar collector (Figure 12) and lower solar collector (Figure 13) are shown in Figures 14 and 15 respectively. The ratios and units of analogous electrical and thermal parameters chosen for this thermal circuit study are given in Table 3.

Table 3. Ratios and units of analogous electrical and thermal parameters

Quantity	Units		Scale Factors	
	Thermal	Electrical	Ratio	Value
Time	hrs	sec	$\frac{\theta_e}{\theta_t}$	2
Capacity	$\frac{\text{Kcal}}{^oC}$	Farads	$\frac{C_t}{C_e}$	4×10^6
Resistance	$\frac{^oC}{\text{Kcal/hr}}$	Ohms	$\frac{R_e}{R_t}$	8×10^6
Potential	^oC	Volts	$\frac{E}{T}$	1
Rate of Energy Transfer	$\frac{\text{Kcal}}{\text{hr}}$	$\frac{\text{Coulombs}}{\text{sec}}$ or Amperes	$\frac{Q}{I}$	8×10^6

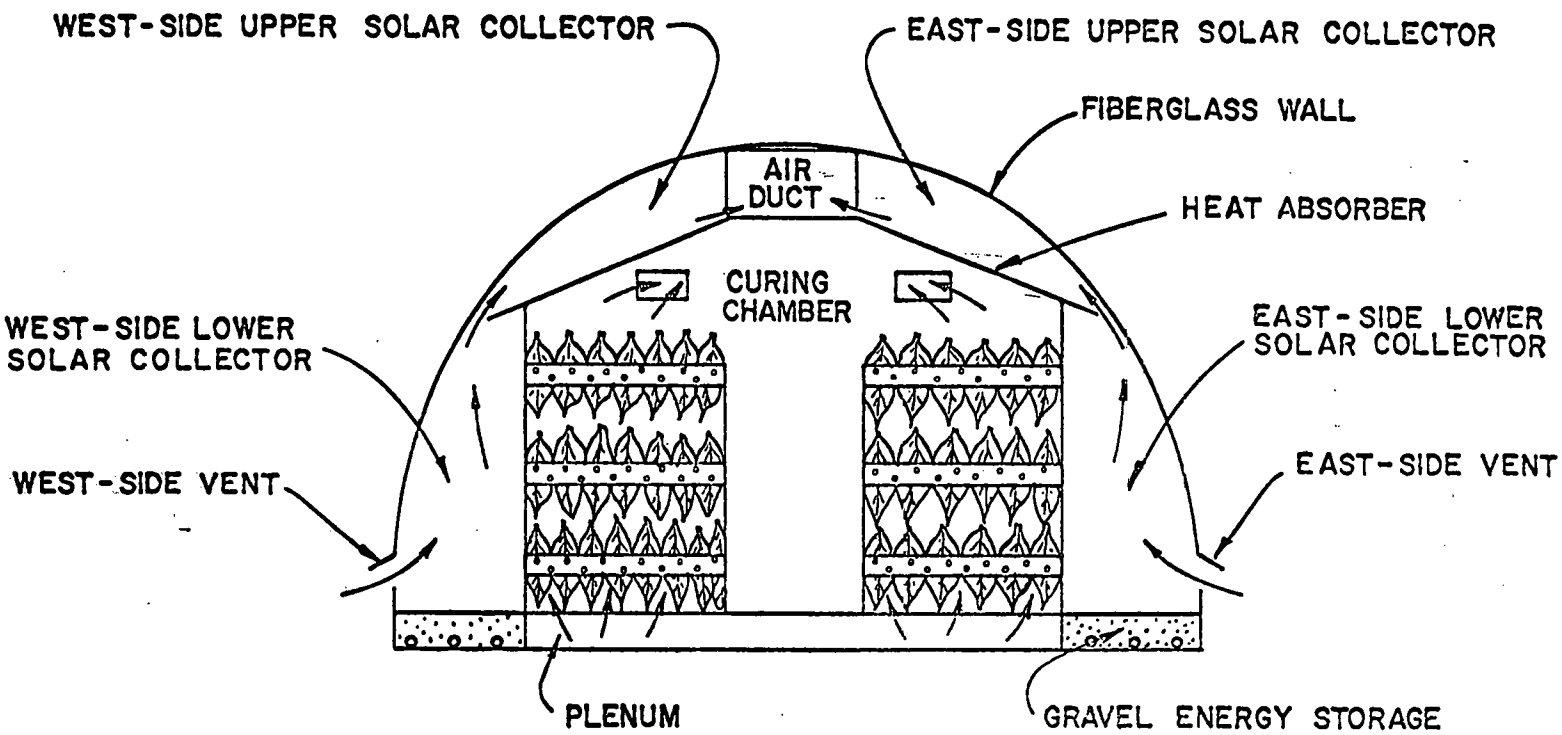

Figure 11. Schematic cross-sectional view of greenhouse bulk curing solar barn.

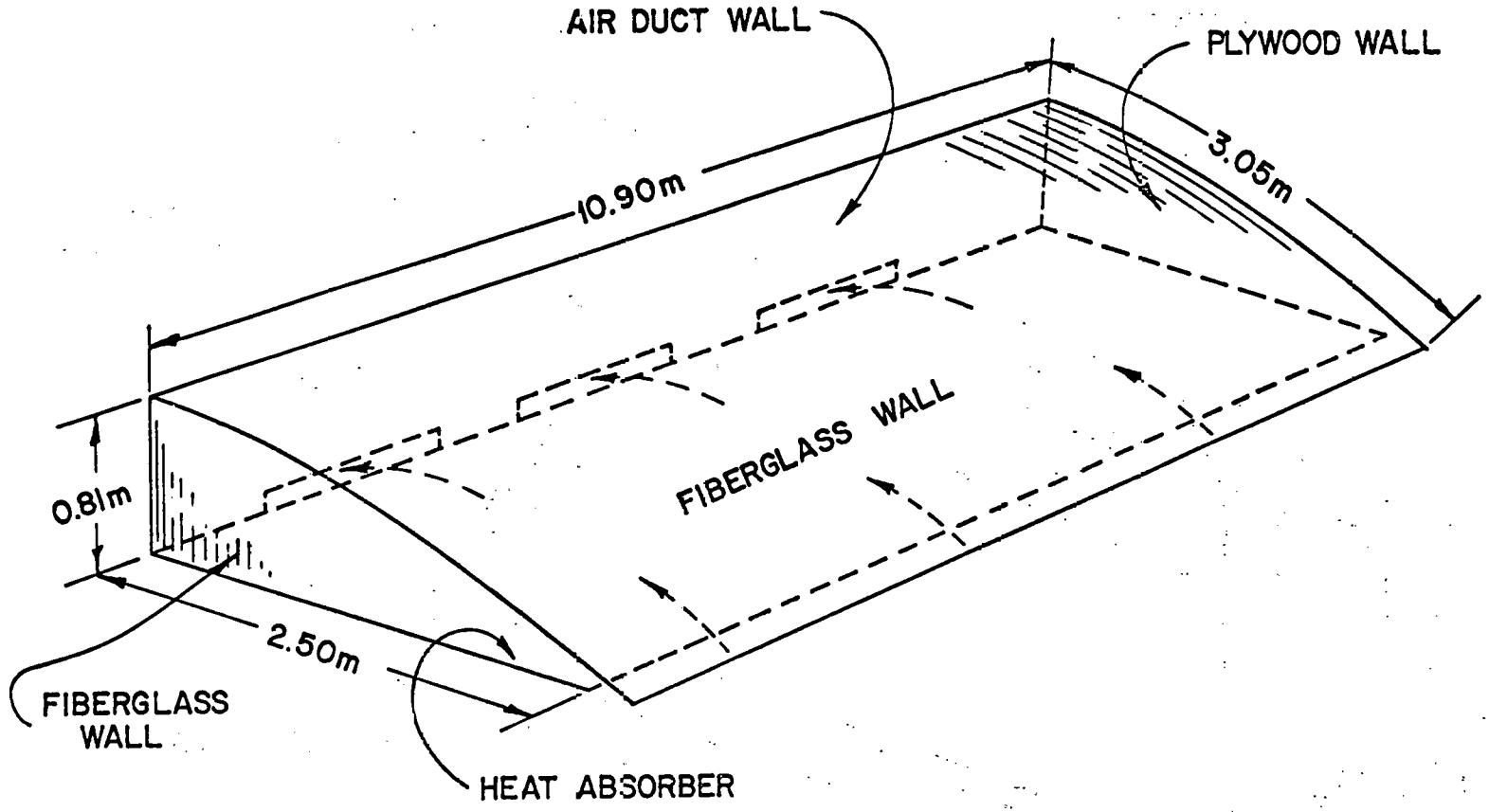

Figure 12. Schematic diagram and dimensions of upper solar collector.

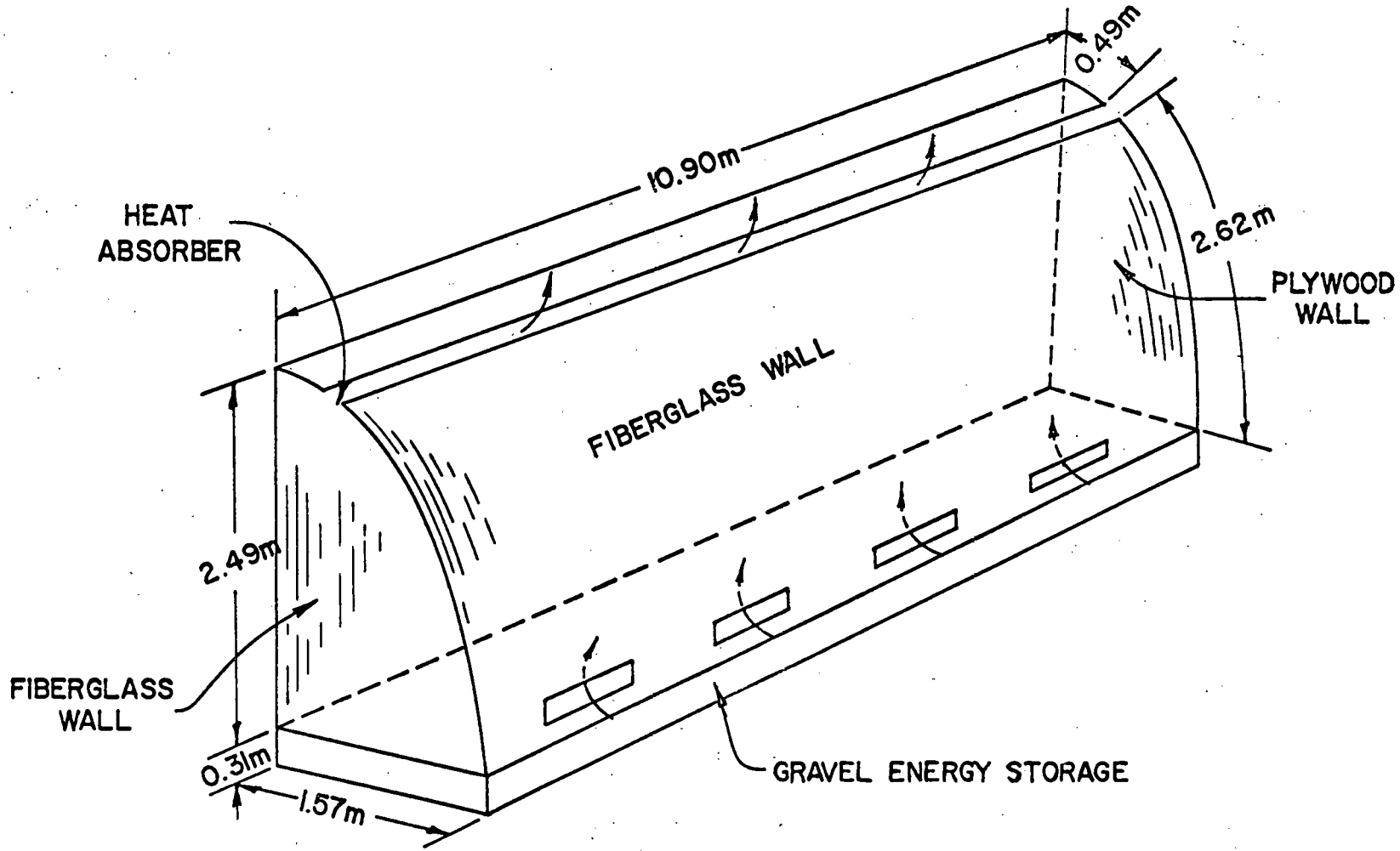

Figure 13. Schematic diagram and dimensions of lower solar collector.

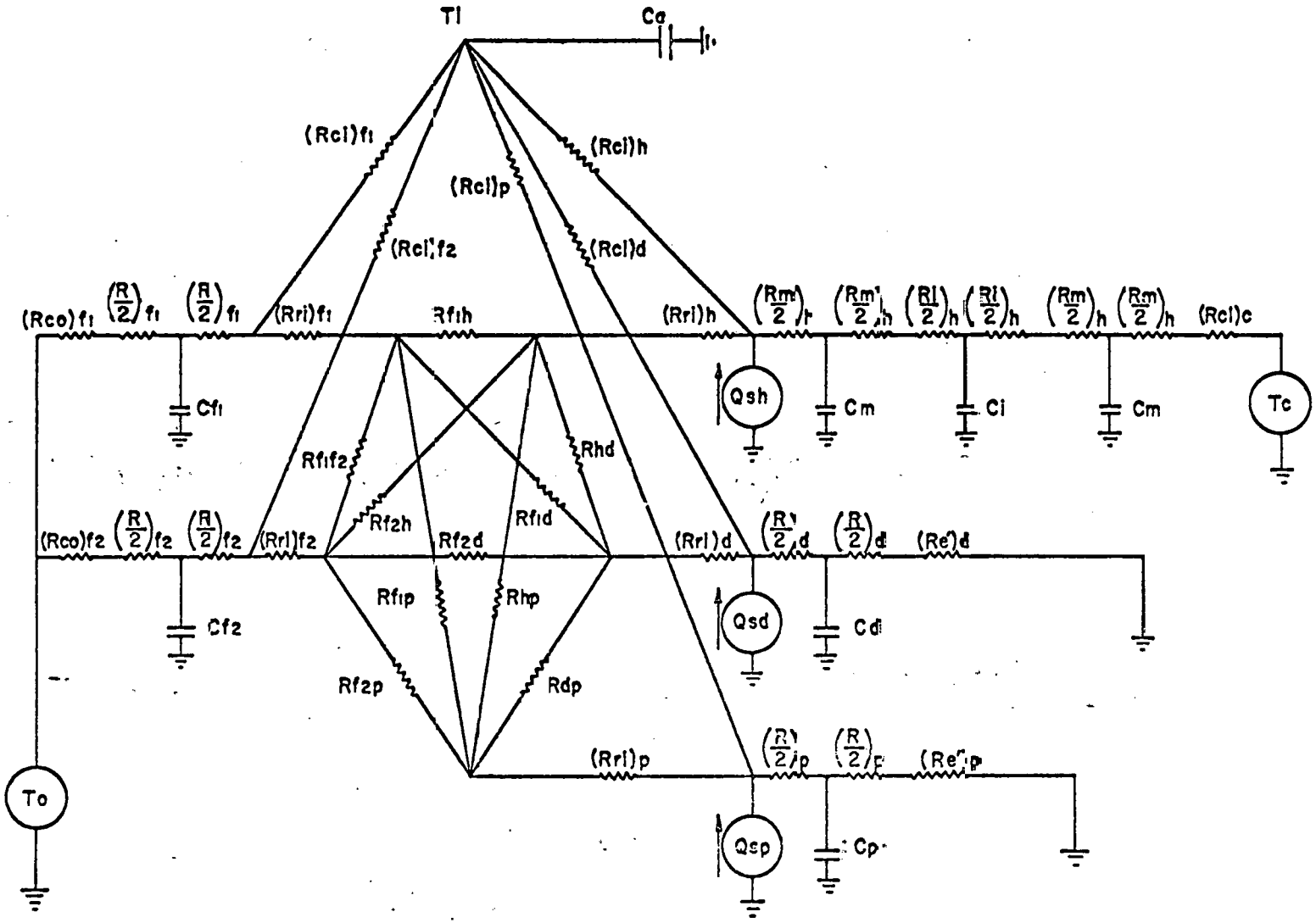

Figure 14. Thermal circuit representing upper solar collector.

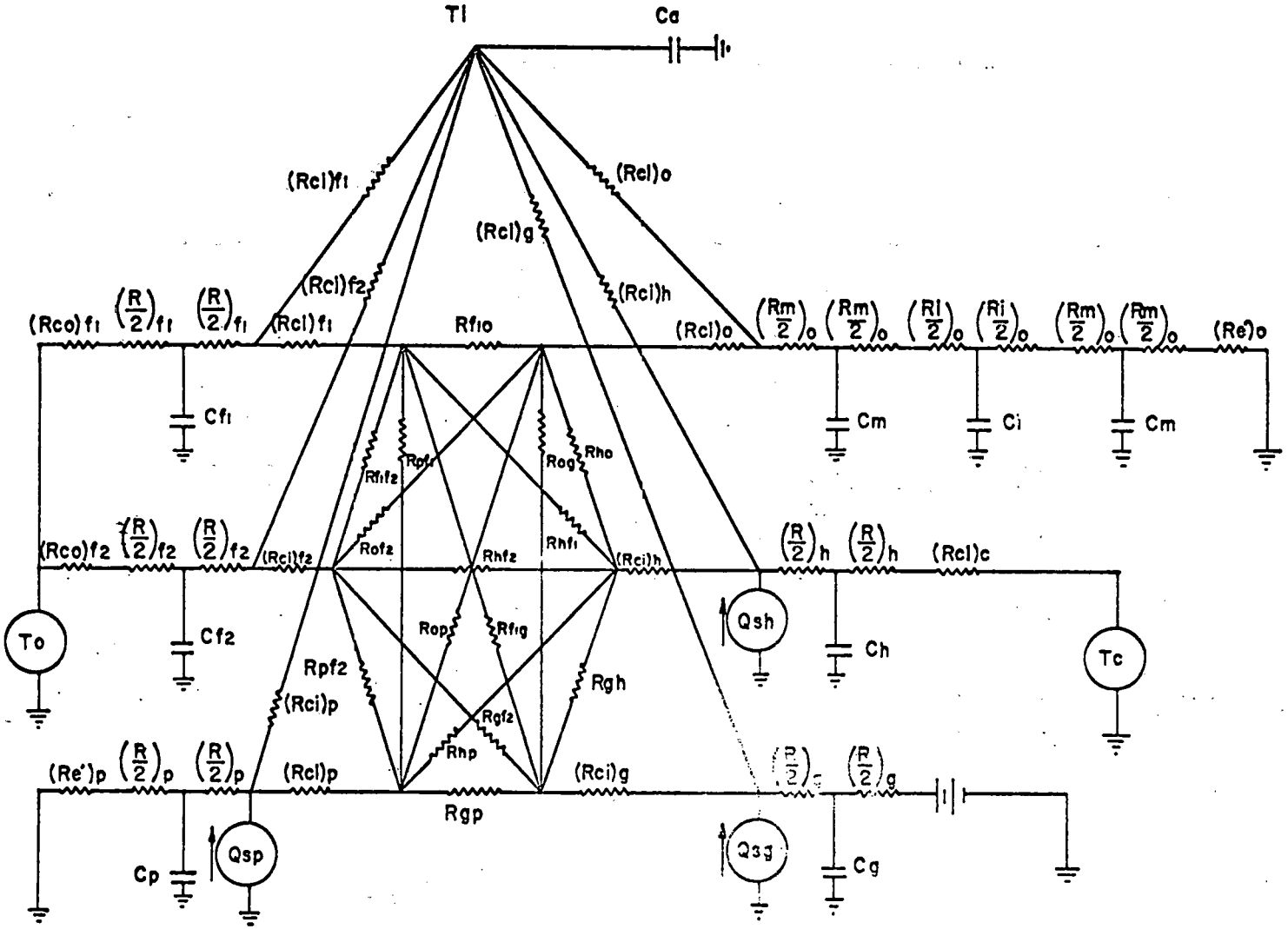

Figure 15. Thermal circuit representing lower solar collector.

The symbols used in Figures 14 and 15 and Table 3 are defined as follows:

Symbols		Subscripts	
R	= conduction resistance	f_1	= tilted fiberglass wall
R_{co}	= outside convection resistance	f_2	= vertical fiberglass wall
R_{ci}	= inside convection resistance	h	= heat absorber
R_{ri}	= inside 'surface' radiation resistance	d	= top air duct
R_{xy}	= inside 'space' radiation resistance	g	= gravel energy storage
C	= capacitor	p	= plywood wall
T_i	= inside air temperature	m	= aluminum foil
T^o	= outside air temperature	i	= insulating material
T^c	= air temperature of curing chamber	a	= air space
Q_s	= solar radiation input	e	= electrical circuit element
R_e	= insulation resistance (5500×10^3 ohms)	t	= thermal circuit element
θ	= time	o	= overhang
E	= constant electrical potential	c	= curing chamber
T	= temperature		
Q	= heat flux		
I	= electric current		

Results of the thermal circuit analogy for one day (Aug. 17, 1976) will be presented as representative of the simulation analysis. Determination of parameters used in the circuit are discussed below. The thermal properties of materials used in the solar collectors are given in Table 4. From these values, the thermal conduction path resistor and capacitors for the walls of the solar collectors were calculated and are given in Table 5. With the inside air velocity of the solar collector being approximately 1 m/sec which results in heat transfer being mainly by free convection, the inside convection coefficients h_c were estimated based on free convection. The values are given in Table 6. The convection resistances of the collectors were then calculated from the h_c values of Table 6. These are given in Table 7. The outside convection coefficient was estimated at 6.71 kcal/hr $m^2{}^oC$ for Aug. 17, 1976 based on the equation 14 given below (9) and the measured outside air velocity of 2.0-3.0 m/sec.

$$h_c = 0.053 + 0.746\mu_o \qquad (14)$$

where h_c is in cal/hr $m^2{}^oC$
μ_o is outside wind velocity in m/hr.

An average surface temperature of 318^oK (45^oC) was used in the evaluation of the network radiation within the solar collector. A summary of network resistances is given in Table 8. The average air flow rate inside the solar collector was recorded as 33.98 m^3/min, which is equivalent to 146.9×10^{-6} farad.

Table 4. Thermal properties of materials used

Material	Thermal Conductivity K Btu/(hr)(ft)(^oF)	Heat Capacity C_p Btu/(lb)(^oF)	Mass Density γ (lb/cu ft)
Douglas Fir Wood (1/2")	0.065	0.5	34
Aluminum	118	0.214	169
Urethane Foam Insulation Board (1/2")	0.01	0.35	2.0
Fiberglass (0.04")	0.02	0.2	~90
Iron Plate (1/16")	34	0.11	490
Gravel	0.42	0.22	120
Air	0.016	0.24	0.072

Table 5. Values of solar collector wall conduction path resistors and capacitors

		Conduction Resistance ($R \times 10^3$ ohms)	Capacitor ($C \times 10^{-6}$ farads)
Upper Solar Collector	Heat Absorber (h)		
	Aluminum Foil (m)	0.08×10^{-3}	0.20
	Insulation Board (i)	246.4	1.00
	Tilted Fiberglass Wall (f_1)	8.2	2.55
	Vertical Fiberglass Wall (f_2)	168.2	0.12
	Air Duct Wall (d)	0.028	3.17
	Plywood Wall (p)	638.7	1.47
Lower Solar Collector	Heat Absorber (h)	38.4	24.50
	Overhang (o)		
	Aluminum Foil (m)	0.4×10^{-3}	0.04
	Insulation Board (i)	1266.0	0.19
	Tilted Fiberglass Wall (f_1)	9.6	2.18
	Vertical Fiberglass Wall (f_2)	83.8	0.25
	Plywood Wall (p)	318.4	2.95
	Gravel Energy Storage (g)	1321.2	601.9

Table 6. Inside convection coefficients of solar collectors: (Unit-Kcal/hr m^2 ^oC)

	Upper Solar Collector	Lower Solar Collector
Heat absorber	3.66	2.71
Tilted fiberglass wall	2.31	2.00
Vertical fiberglass wall	1.99	1.99
Plywood wall	2.28	2.28
Air duct wall	2.71	-
Overhang	-	2.31
Gravel energy storage	-	2.91
Curing chamber	2.00	2.00

Table 7. Convection resistances for solar collectors

		Outside Convection Resistance ($R_{co} \times 10^3$ ohms)	Inside Convection Resistance ($R_{ci} \times 10^3$ ohms)
Upper Solar Collector	Heat Absorber (h)	-	79.5
	Tilted Fiberglass Wall (f_1)	35.5	102.9
	Vertical Fiberglass Wall (f_2)	728.1	2451.3
	Air Duct Wall (d)	-	331.6
	Plywood Wall (p)	-	2139.4
	Curing Chamber (c)	-	145.5

Table 7. Cont'd

		Outside Convection Resistance (R_{co} x 10^3 ohms)	Inside Convection Resistance (R_{ci} x 10^3 ohms)
Lower Solar Collector	Heat Absorber (h)	-	108.1
	Tilted Fiberglass Wall (f_1)	41.5	138.9
	Vertical Fiberglass Wall (f_2)	362.9	1221.9
	Plywood Wall (p)	-	1066.5
	Gravel Energy Storage (g)	-	159.0
	Overhang (o)	-	647.3
	Curing Chamber (c)	-	146.4

Table 8. Inside radiation exchange network resistances (R x 10^3 ohms)

Upper Solar Collector	$(R_{ri})_{f1}$	2.0	R_{f1h}	52.4	R_{f1d}	237.6
	$(R_{ri})_{f2}$	40.7	R_{hd}	385.3	R_{f2h}	2090.9
	$(R_{ri})_h$	2.4	R_{dp}	5526.0	R_{f1p}	1256.9
	$(R_{ri})_d$	7.5	R_{f2p}	96707.0	R_{hp}	2307.7
	$(R_{ri})_p$	40.7	R_{f1f2}	1641.1	R_{f2d}	5526.1
Lower Solar Collector	$(R_{fi})_{f1}$	2.4	R_{f1f2}	986.9	R_{f20}	5780.3
	$(R_{ri})_{f2}$	21.3	R_{f1h}	77.3	R_{f2g}	1926.8
	$(R_{ri})_h$	2.6	R_{f10}	4622.2	R_{f2p}	40462.0
	$(R_{ri})_o$	13.1	R_{f1g}	144.4	R_{ho}	609.1
	$(R_{ri})_g$	4.1	R_{f1p}	1155.6	R_{hg}	211.9
	$(R_{ri})_p$	21.3	R_{f2h}	1305.2	R_{hp}	2436.3
	R_{gp}	2566.4	R_{og}	549.9	R_{op}	8294.1

The PCAP (Princeton Circuit Analysis Program) computer programs for the solar collectors were developed based on the thermal circuits (Figures 14 and 15), input ambient air potential (Figure 16), and solar radiation input evaluated from Figure 17. The simulation results that were obtained are shown in Figure 16. The curves show that the predicted solar heated air temperature is in good agreement with the measured temperature. Some phase delay is shown between measured and predicted values since a large capacitor was used to simulate the moving air. The peak value of the predicted temperature curve lags that of the measured one by approximately 1 hour but can be adjusted by modifying the program.

Greenhouse Operation of Greenhouse Bulk Curing Solar Barn

During greenhouse operation the solar absorbers and portable frames used in tobacco curing are removed, and appropriate greenhouse equipment for growing plants is moved into the structure. The temperature, humidity and watering are automatically regulated to provide a controlled environment for optimum plant production. When more solar energy is available than is needed to heat the greenhouse

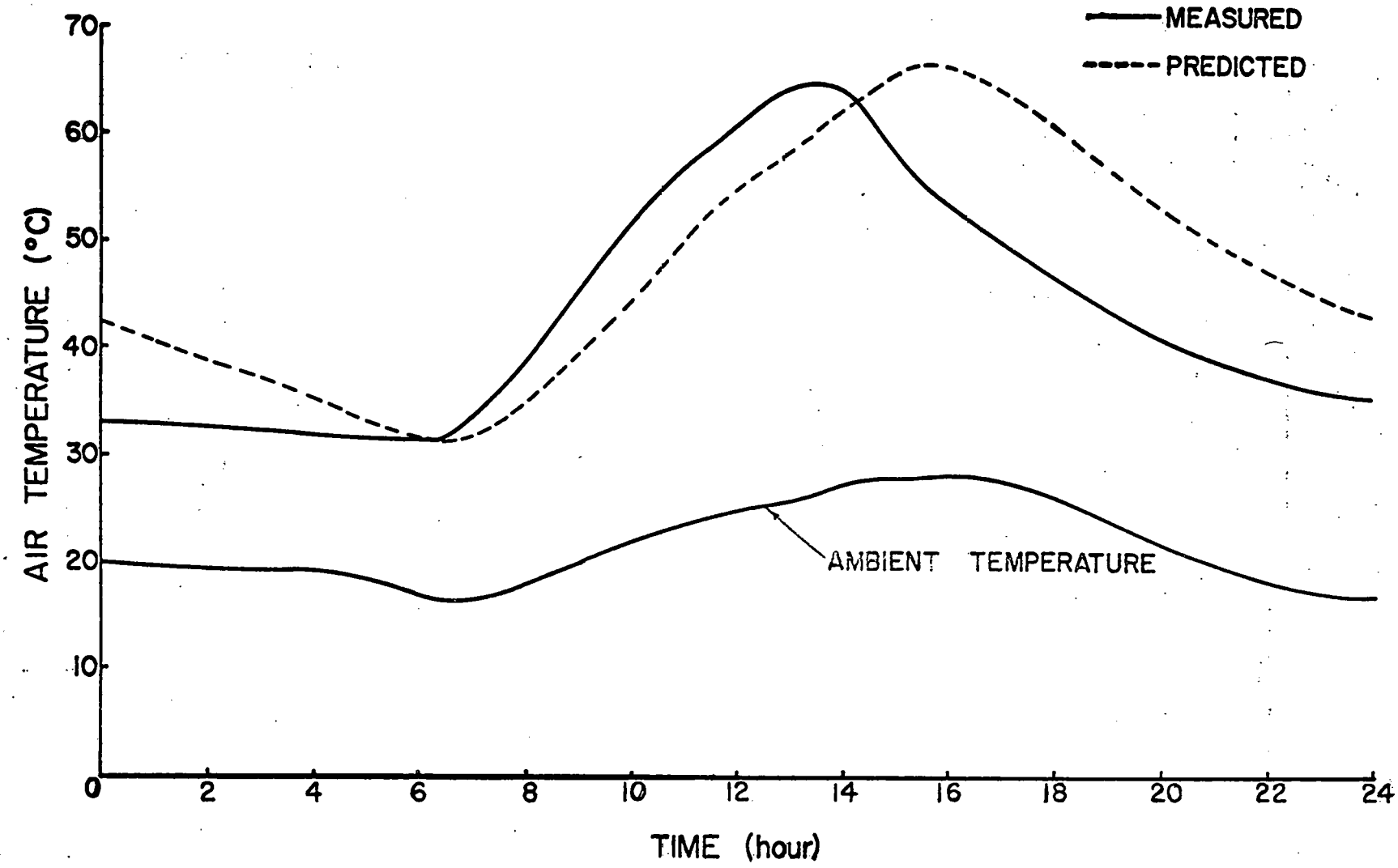

Figure 16. Predicted and measured temperatures of east-side upper solar collector (Aug. 17, 1976).

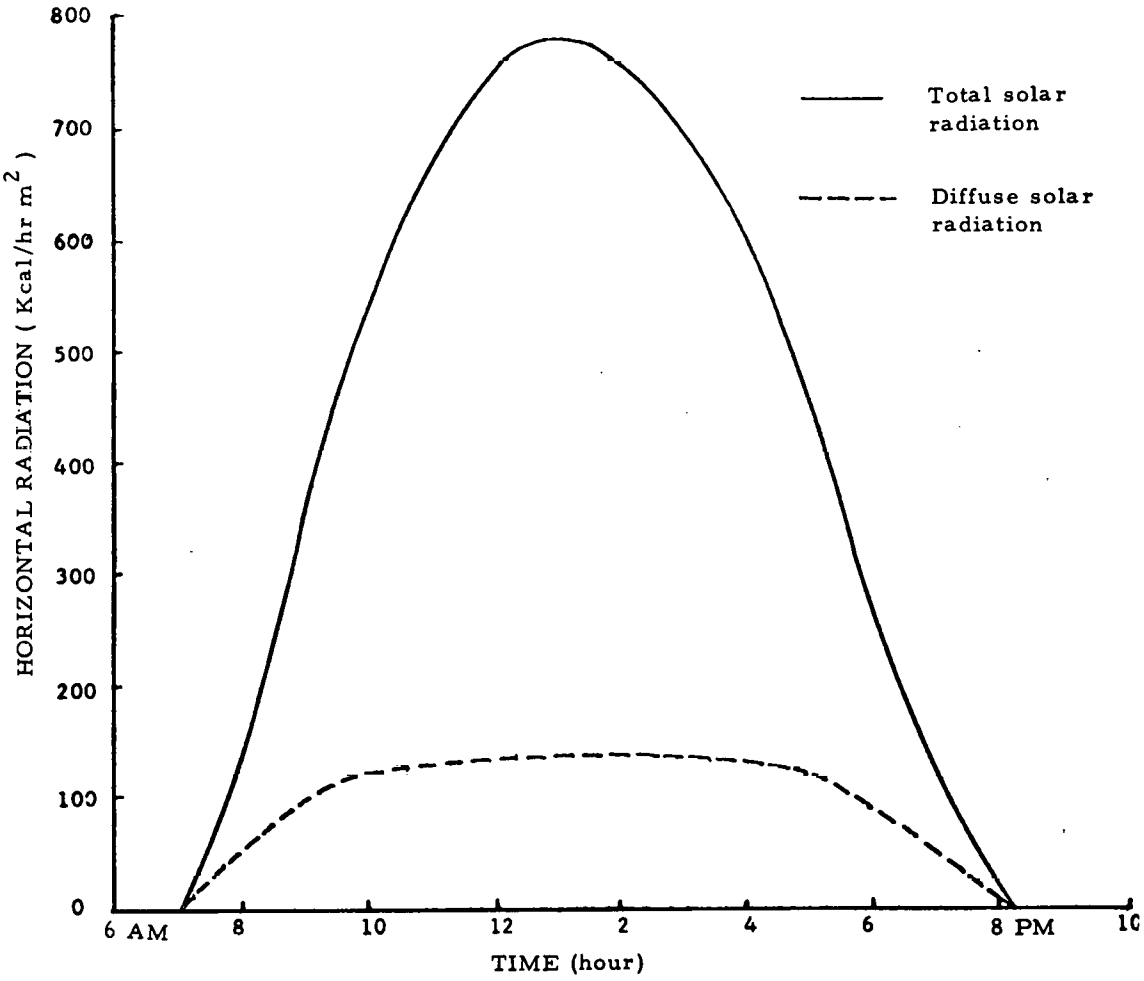

Figure 17. Observed solar radiation on horizontal surface (Aug. 17, 1976).

during the daytime, it is stored in the gravel to reduce the neating requirement at night.

Crop Production:

The structure was converted to the greenhouse mode of operation in October, 1975 (22). A crop of Klanchoe flowers in 13 cm pots were grown in it from November 20, 1975 to March 18, 1976 (Figure 19). The automatic temperature and watering controls combined with efficient utilization of available solar energy produced an excellent crop of flowers. A second crop, patio tomatoes in 13 cm pots, was added February 18, 1976. The tomatoes were arranged in 9 blocks (two plants each) down the length of the house and 4 blocks across the house. The Klanchoes were removed March 3, 1976 and measured for height, width, and fresh weight. The tomatoes were removed March 18, 1976 and the dry weights were measured. Neither the Klanchoe nor the tomatoes exhibited any significant block effects in any of the measured variables. This indicates that the system did not adversely affect growth uniformity. It was estimated that a flowering crop such as the Klanchoes would provide between $700 to $800 income in a 4 month growing period.

Temperature gradients and running times were used to calculate the energy supplied by the heater Q_h, the energy stored in the rock beds Q_s, and the energy vented to the outside Q_v. These quantities are shown in Tables 9 and 10 for two 6-day periods in January. Table 9 represents a particularly severe period and Table 10 a more moderate one. The energy recovered from the rock beds were not included in these tables because neither the heat conducted into the greenhouse nor that lost to the outside environment were monitored during this initial study.

A limitation in analyzing the data in Tables 9 and 10 is the lack of information about the total energy lost from the structure during a given period. A transient analysis to determine this information would require, among other things, knowledge of wind speed and cloud cover, variables which were not monitored during this study. An approximation of the total heat loss during a 24-hr period can be made, however, by noting that the energy stored within a given period was always depleted within that same 24-hr period and that the thermal capacitance of the structure, excluding the rock beds and furnace room, was small. This allows the total heat lost during a 24-hr period to be estimated by the sum of the energy stored in the rock beds and the energy supplied by the heater. Thus, the energy stored during each of the two periods considered becomes 7.7% and 15.9%, respectively, of the total estimated heat loss of the structure.

Table 9. Energy stored and vented versus energy supplied by the auxiliary heater for the period January 1-6, 1976.

Date	Q_h [1] (GJ)	Q_s (GJ)	Q_v (GJ)	Ambient Low (^oC)	Degree Days [2]
January 1	0.42	0.13	0.037	6.8	8.0
January 2	0.55	0.13	0.057	-2.2	11.8
January 3	0.62	0.0	0.0	3.7	6.6
January 4	0.85	0.10	0.0	-0.7	14.8
January 5	1.13	0.04	0.0	-13.1	21.0
January 6	1.21	0.00	0.0	-12.4	19.8
Totals	4.78	0.40	0.094		82.0

[1] Based on 20.4 kJ/l net heating value for L.P. gas

[2] Calculated using a 15.6°C base

A feeling for the potential capability of the system is indicated by adding Q_s and Q_v and comparing this to the total estimated heat loss. For the period of January 10-15, as much as 26% of the total estimated heat loss could have been supplied if the rock beds had been large enough to collect all of the available solar energy. Undoubtedly the data for February and March will show an even stronger trend in this direction.

Figure 18. Greenhouse bulk curing system during greenhouse operation for growing flowers.

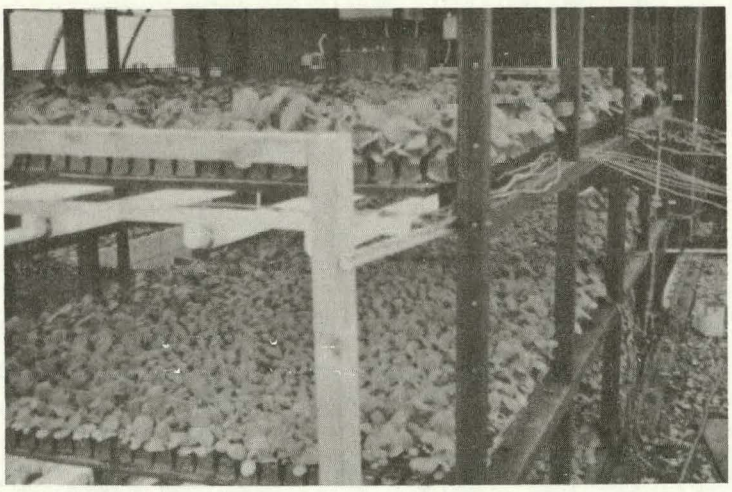

Figure 19. Tobacco transplant production in greenhouse bulk curing system.

Table 10. Energy collected and vented versus energy supplied by the auxiliary heater for the period January 10-15, 1976.

Date	Q_h[1] (GJ)	Q_s (GJ)	Q_v (GJ)	Ambient Low (°C)	Degree Days[2]
January 10	0.86	0.16	0.0	-10.3	18.7
January 11	0.78	0.0	0.0	-4.4	12.1
January 12	0.61	0.13	0.10	-3.4	12.3
January 13	0.49	0.07	0.0	-4.4	9.0
January 14	0.28	0.14	0.18	5.7	7.7
January 15	0.63	0.19	0.16		13.7
Totals	3.65	0.69	0.44		73.5

[1] Based on 20.4 kJ/l net heating value for L.P. gas

[2] Calculated using a 15.6°C base

Table 11 provides a slightly different look at the data. Here, Q_s and Q_v are shown with Q_p, the total energy incident upon horizontal and vertical surfaces with areas equal to the greenhouse floor and north wall respectively. Q_p was calculated, using the method of Liu and Jordan (14) from the total daily radiation on a horizontal surface obtained by numerically integrating the solar insolation curve. A total diffuse to direct ratio of 0.2 was assumed along with an albedo factor of 0.2. The daily efficiencies N_s and N_{s+v} were calculated from

$$N_s = Q_s/Q_p, \tag{15}$$

Table 11. Daily collection and storage efficiencies versus Φ and Δt for the period January 10-15, 1976.

Date	Q_s (GJ)	Q_v (GJ)	Q_p (GJ)	N_s (%)	N_{s+v} (%)	Φ[1]	Δt (°C)
January 10	0.16	0.0	1.26	12.9	12.9	4	17.1
January 11	0.0	0.0	.85	0.0	0.0	6	15.8
January 12	0.13	0.10	1.47	9.1	16.0	2	21.8
January 13	0.07	0.0	.88	8.0	8.0	6	11.6
January 14	0.14	0.18	1.40	10.2	23.0	1	14.6
January 15	0.19	0.16	1.38	13.6	25.0	2	11.3

[1] Relative form factor for solar insolation curve

and

$$N_{s+v} = (Q_s + Q_v)/Q_p. \tag{16}$$

The values of N_{s+v} compare quite favorably with daily efficiencies given by Close (7) for good quality solar air heaters (25% to 50%).

The variations in N_{s+v} in Table 11 can be explained by the following discussion. For a given structure or collector, the daily efficiency varies inversely with the difference in air temperature (inside vs. outside), solar declination angle, frequency of fluctuation of solar insolation, and wind speed. Temperature difference, frequency of fluctuation, and wind speed are stochastic variables, while declination angle is a function of the time of year. Unfortunately, wind speed was not monitored during this study. However, Table 11 does include a relative form factor Φ, which describes the smoothness of the solar insolation curve for that day, and Δt, which is the temperature difference between inside and outside taken at 2:00 pm. The factor Φ varies from 1 for a smooth curve to 10 for a rapidly fluctuating one. Examination of Table 11 shows that the highest values of N_{s+v} occurred at the lowest values of Φ and Δt and that increasing Φ or Δt generally decreased N_{s+v}. The exception was on January 11 when a moderate Φ and Δt produced a zero efficiency. This more than likely resulted from higher than normal wind conditions which probably caused the heat loss to be greater than the 15.8°C would indicate. For two periods in January, approximately 8% and 16% of

the total estimated heat loss of the structure was collected and stored. If the storage beds had been large enough to store the energy exhausted through ventilation, the potential savings could have been as high as 26% for a period when lows of -4°C were experienced. Undoubtedly this percentage would have been larger in February and March, when solar insolation values are higher. Nevertheless, a potential energy reduction of 26% in January indicates that a significant fuel savings can be achieved without having to resort to the more expensive conventional solar collection systems.

Tobacco Transplant Production:

The greenhouse was set up for tobacco transplant production in Spring 1976 and 1977 (Figure 19). Portable frames were placed in the greenhouse. Each frame had four layers consisting of perforated sheet metal covered frames that slide in on the same spacing (approximately 25 inches) as the bulk tobacco racks. An automated misting system was installed on each layer to provide a fine misting for approximately 30 seconds per 30 minutes during daylight hours. During the 1977 tests, artificial lighting was added as shown in Figure 19. Temperatures in the greenhouse were maintained between 72°F minium and 85°F maximum during the day and 65°F minimum at night.

The tobacco seedling, growing and handling trays were seeded using a spraghum peat moss mixture. The mixture was almost saturated prior to being placed in the trays. Once the trays were seeded, they were placed on three layers of the portable frames.

Seedling emergence began approximately 8 to 9 days after seeding. Germination rates of 95-97% were obtained on each layer. During the 1976 tests uniform growth occurred through the third week at which the seedlings were damaged by over-fertilization. Also during 1976 light level variation between layers and within each layer contributed to the non-uniform growth. The light levels varied from approximately 1500-2000 foot candles on the top layer to 500-100 foot candles in the middle and bottom layers. This lighting difficulty was solved in 1977 by adding artificial lighting to the middle and bottom layers. Uniform transplants were produced in 1977.

Tobacco transplant production can be achieved using multiple layer growing with appropriate lighting and watering system. Uniform tranplants can be produced in 6 to 8 weeks.

References

1. Bowers, C.G., B.K. Huang, and D.H. Willits. 1976. Improving solar energy collection, storage, and air flow control in greenhouse solar curing barn. ASAE Paper No. 76-3548.
2. Bowers, C.G., B.K. Huang, and C.F. Abrams, Jr. 1975. Solar energy utilization in a bulk curing/greenhouse system. ASAE Paper No. 75-3504.
3. Buelow, F.H. 1962. Corrugated solar heat collectors for crop drying. Sun at Work, 4th Quarter, 1962, p. 8.
4. Butler, J.L. and J.M. Troeger. 1975. Application of solar energy for peanut drying and curing. ASAE Paper No. 75-3505.
5. Chandra, P. and M.G. Britton. 1976. Predicting the effects of orientation and insulation on greenhouse environment. ASAE Paper No. 76-4008.
6. Chang, H.S. and B.K. Huang. 1976. Simulation of thermal behavior of tobacco curing in solar barn. ASAE Paper No. 76-3549.
7. Close, D.J. 1963. Solar air heaters for low and moderate temperature application. Solar Energy, 7(3):117-124.
8. Duncan, G.A., O.J. Loewer, Jr. and D.G. Colliver. 1976. Simulation of solar energy availability, utilization, and storage in greenhouses. ASAE Paper No. 76-4010.
9. Hodges, C.N., et al. 1966. Solar distillation utilizing multiple-effect humidification. Final Report. The University of Arizona Solar Energy Laboratory of the Institute of Atmospheric Physics.
10. Holman, J.P. 1972. Heat transfer. McGraw-Hill Book Co., New York, N.Y.
11. Hottel, H.C. and B.B. Woertz. 1941. The performance of flat-plate solar-heat collectors. Trans. ASME:91-104.

12. Huang, B.K. and C.G. Bowers, Jr. 1976. Immediate solar-energy utilization using greenhouse bulk curing and drying system. Final Report PTP74-17622. 71p.
13. Huang, B.K. and H.S. Chang. 1976. Circuit simulation analysis of heat transfer effect in solar drying. ASAE Paper No. 76-3019.
14. Huang, B.K., C.F. Abrams, L.L. Coats, and C.G. Bowers. 1975. Development of greenhouse bulk drying system for solar energy utilization and plantbed mechanization. ASAE Paper No. 75-1018.
15. Liu, B.Y.H. and R.C. Jordan. 1963. The long-term average performance of flat-plate solar-energy collectors. Solar Energy 7(2):53-74.
16. Morey, R.V. and W.W. Nelson. 1975. Field evaluation of a solar energy grain drying system. ASAE Paper No. 75-3515.
17. Morrison, D.W. 1975. Bare plate solar collector grain drying bin. ASAE Paper No. 75-3513.
18. Ozisik, M.N. 1973. Radiative transfer and interactions with conduction and convection. John Wiley and Sons, Inc., New York, N.Y.
19. Peterson, W.H. and M.A. Hellickson. 1976. Solar-electric drying of corn in South Dakota. Trans. ASAE 19(2):349-353.
20. Short, T.H., P.C. Badger, and W.L. Roller. 1976. OARDC's solar-heated greenhouse. Ag. Eng. Journal 57(7):30-32.
21. Whillier, A. 1964. Performance of black-painted solar air heater of conventional design. Solar Energy 8(1):31-37.
22. Whillier, A. 1963. Plastic covers for solar collectors. Solar Energy 7(3):148-151.
23. Willits, D.H., C.G. Bowers, Jr., P.V. Nelson, and B.K. Huang. 1976. A solar energy storage system for greenhouse. ASAE Paper No. 76-3507.

☆U.S. GOVERNMENT PRINTING OFFICE:1978 -740 -306/4414 REGION NO. 4